8-30-2018

Performance Evaluation of Shear Connectors Embedded in Ultra-High Performance Concrete as Part of a Bridge Repair Method

Dominic Kruszewski
University of Connecticut - Storrs, dominic.kruszewski@uconn.edu

Performance Evaluation of Shear Connectors Embedded in Ultra-High Performance Concrete as Part of a Bridge Repair Method

Dominic Kruszewski, PhD

University of Connecticut, 2018

Corrosion is one of the most dominant forms of deterioration in steel bridge girders. U.S. federal and state agencies spend billions of dollars annually on bridge rehabilitation as a direct result of corrosion. Even with these efforts, approximately $125 billion is needed to address the current backlog of structures in need of repair. Over time, corrosion leads to section loss of critical load bearing components, hindering the structural integrity of the bridge. To strengthen weakened girders ends with section loss, a structurally efficient repair option has been developed. In this repair, headed shear studs are welded to the intact portion of the web plate just above the bearing. The studs are encased in a panel of Ultra-High Performance Concrete (UHPC), which is cast to the bottom flange. This creates an alternate load path to omit the weakened web plate, transferring the forces through the studs and into the UHPC panels.

However, the success of the proposed repair hinges on the interaction between the headed studs and UHPC cast and therefore must be thoroughly assessed. In this study, a five-phase approach is deployed to better understand the critical load-transfer mechanism as part of this repair. First, an extensive series of push-out tests was conducted to evaluate the mechanical behavior of the headed studs when welded on thin web plates and embedded in UHPC. Next, design considerations such as eccentric loading, cover for studs, concrete embedment variations, concrete curing conditions, and welding are evaluated to aid engineers during field implementation. The third phase consisted of a high-fidelity finite element analysis to validate the experimental results. Further design parameters such as eccentric loading and stud-diameter-to-web-thickness ratios for various limit states were evaluated. In the fourth phase, a corrosion investigation was conducted to assess the durability of the headed studs when embedded in UHPC. Finally, alternate shear connectors such as threaded rods and UHPC dowels are evaluated experimentally to provide flexibility to the designer as an alternative option to headed studs. The results of this work are used to facilitate the field implementation of the proposed repair method by addressing critical design parameters.

Performance Evaluation of Shear Connectors Embedded in Ultra-High Performance Concrete as Part of a Novel Bridge Repair Method

Dominic Kruszewski

B.A., University of Connecticut, 2014

M.S., University of Connecticut, 2016

A Dissertation

Submitted in Partial Fulfillment of the

Requirements for the Degree of

Doctor of Philosophy

at the

University of Connecticut

2018

APPROVAL PAGE

Doctor of Philosophy Dissertation

Performance Evaluation of Shear Connectors Embedded in Ultra-High Performance Concrete as Part of a Novel Bridge Repair Method

Presented by

Dominic Kruszewski, B.S., M.S.

Major Advisor

_____

Arash E. Zaghi

Major Advisor

_____

Kay Wille

Associate Advisor

_____

Jeongho Kim

Associate Advisor

_____

Wei Zhang

University of Connecticut
2018

ACKNOWLEDGEMENTS

First, I would like to thank my advisors, Dr. Arash E. Zaghi and Dr. Kay Wille, for their guidance and unwavering support throughout my studies. Their advising reached me on more than just an academic level. They helped shape the man I am today through many insightful conversations about my work, my life, and even broader topics. I owe a lot to my advisors for encouraging my transformation throughout these past few years.

I would also like to thank my advisory committee members, Dr. Jeongho Kim and Dr. Wei Zhang, for their guidance and advice throughout my work. Their unique insight and exceptional ability to convey engineering concepts allowed me to bolster the quality of my work.

Next, I would like to thank all of my friends and colleagues who have made this journey possible. From my officemates, to the graduate students working in this lab, to the specialists in the machine shop and the front office of the department. Being a graduate student may seem like a solo adventure, but success is driven and created through the teamwork of many people from all areas.

Finally, I would like to thank my family for making this possible. This includes my mother, Alex, my father, Alex, my brother, Kasper, and even my dogs, Rex, Cici, and Lola, and my cat Kobe. My family has been my rock during these past few years and they have always encouraged me to work hard and follow my dreams, no matter how hard the path may seem. I would like to thank my beautiful girlfriend, Lauren, who inspired me to work harder and provided incredible patience and support throughout the hardest of times. I could not have done it without you all. Thank you.

TABLE OF CONTENTS

Chapter 1

Push-Out Behavior of Headed Shear Studs Welded on Thin Plates and Embedded in UHPC

INTRODUCTION

Deterioration of steel bridge girders is a pressing issue facing today's infrastructure. The 2017 ASCE Infrastructure Report Card indicates that approximately 15% of the 56,000 structurally deficient bridges in the United States suffer from corrosion damage [1]. Corrosion damage is particularly significant in bridges with expansion joints at the piers or abutments (Fig. 1). Faulty expansion joints permit water and deicing chemicals to leak through to the superstructure which induces corrosion at the girder end [2]. A significant reduction in bearing capacity may occur if corrosion reduces the thickness of the web plate near the bearing region [3, 4]. The current repair procedure to remedy girders with section loss is costly, time-consuming and labor intensive. The method involves jacking the superstructure, removing the corroded section of steel, welding in new steel, and lowering the superstructure back into place [5].

Fig. 1. Corrosion at Girder End

A novel repair method for deteriorated bridge girders has been proposed to improve the current procedure [6]. The proposed method involves welding headed shear studs to the intact portion of the web outside of the corrosion damaged portion with reduced area. A panel of ultra-high performance concrete (UHPC) is cast over the bottom flange to cover the damaged area and embed

the welded shear studs. The UHPC cast creates a force-transfer path to enhance the bearing capacity of the weakened end. A schematic of the proposed repair is shown in Fig. 2. The procedure does not require jacking of the superstructure, which significantly reduces the cost of the repair. As the studs are welded to localized portions of the girder, minimal cleaning of the surface is required.

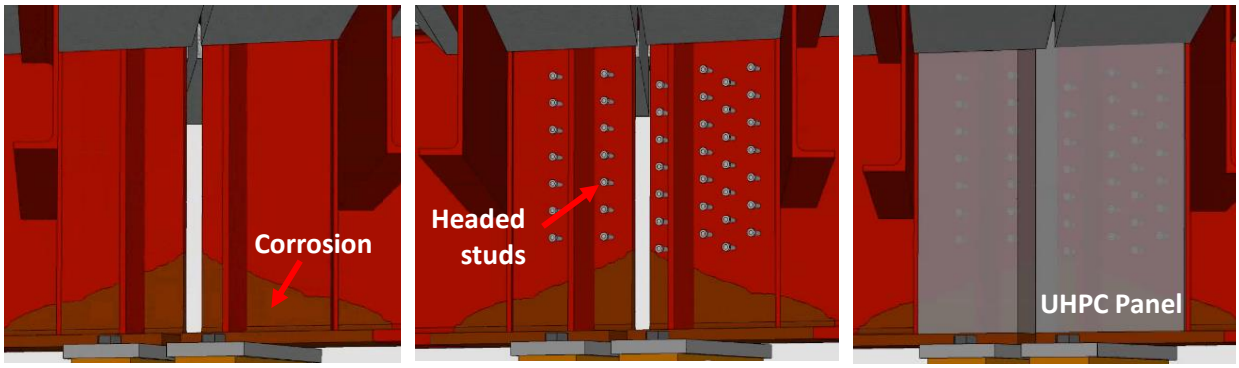

a) Corrosion at Girder Ends b) Studs Welded to Intact Web c) Cast UHPC Panel

Fig. 2. Concept of Proposed UHPC Repair

The headed shear studs play a critical role in transferring the bearing forces from the web to the UHPC panel. Therefore, this study focuses on investigating their performance as part of the proposed repair. First, the studs' capacity welded onto thin plates is validated since the webs of bridge girders are typically thinner than 10 mm. Second, because the arrangement of the studs may vary based on the available surface area on the web plate, the effect of tight spacing and staggered position is assessed. Lastly, the weldability of the new studs to an older steel material with different metallurgical properties must be examined. To investigate these parameters, push-out experiments were conducted with headed shear studs embedded in UHPC and welded to 9.5-mm thick web plates that were salvaged from the old Pearl Harbor Memorial Bridge (Connecticut, U.S.A.) which was constructed in 1958. Three stud diameters, several stud layouts, and different compressive

strengths of UHPC were evaluated. A total of 13 push-out experiments were conducted to evaluate these parameters. A unique loading protocol was adopted to reduce the demand on the thin web plate. The force was applied onto the flanges of the section, through the web, and finally to the studs which were embedded in UHPC. The experimental capacities generated from the tests were compared to those proposed by other researchers. It was shown that headed studs welded to a thin web plate achieve full capacity without imposing damage to the base web plate or UHPC panels. Based on the tests, an existing stud capacity formulation was refined for predicting the shear strength of headed studs embedded in UHPC.

PERFORMANCE OF HEADED STUDS IN UHPC

The behavior of headed studs embedded in conventional concrete has been widely studied and is well known. When studs are embedded in regular-strength concrete with a compressive strength of 20 MPa, the failure mode is governed by conical failure of the surrounding concrete with partial yielding of the stud [7]. When headed studs are embedded in ultra-high performance concrete (UHPC) and loaded in shear, their mechanical behavior differs from when they are embedded in conventional concrete. Push-out experiments have been conducted to compare the performance of headed studs embedded in regular- and high-strength concrete, and UHPC [8]. It was concluded that studs embedded in regular-strength concrete exhibit higher ductility than when embedded in a high-strength one and UHPC. Another study found that the shear capacities generated by 16- and 22-mm diameter studs embedded in UHPC were consistently higher than those outlined by AASHTO and Eurocode-4 [9]. It has also been observed that headed studs with a diameter of 22 mm embedded in UHPC fail via stud fracture when spaced at twice the stud

diameter [10]. Even with a cover less than 25 mm, the failure mode of headed studs embedded in UHPC is still governed by stud shank failure [11]. Fatigue performance of headed studs in UHPC was also evaluated; it was found that when studs are embedded in UHPC, their expected fatigue life is longer than those embedded in regular strength concrete (RSC). Experimental evaluation of demountable headed stud shear connectors in UHPC was conducted [13]. It was found that a stud aspect ratio less than 1.5 resulted in UHPC breakout; for larger aspect ratios, stud fracture was the governing failure mode. These studies all generate a common observation that the failure mechanism of studs embedded in UHPC is typically stud shank failure with little or no damage to the UHPC.

Another unique advantage of studs embedded in UHPC involves the presence of a weld collar which provides an increase in shear capacity when loaded in shear [14]. The weld collar is formed at the base of the stud during the welding process (Fig. 3). Its diameter is slightly larger than the stud shank because of the shape of the ferrule that contains the molten pool of metal during welding.

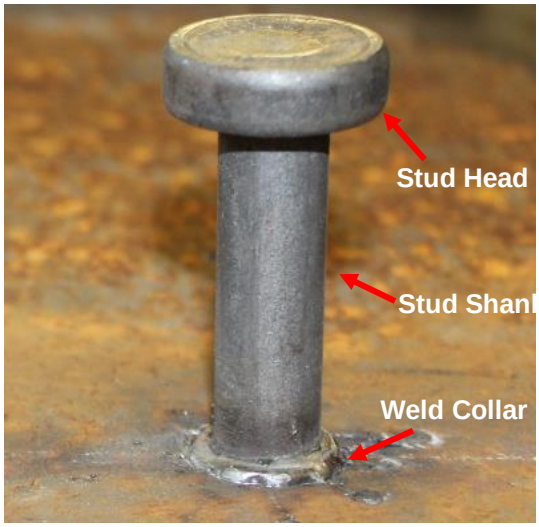

Fig. 3. Typical Headed Stud After Welding Process

This observation is particularly prevalent in studs embedded in concrete with a higher compressive strength. If the concrete is strong enough to resist micro-cracking at the weld collar interface, the weld collar will bear onto an area with a slightly larger diameter. To account for the bearing contribution of the weld collar, a formula for predicting the shear strength of headed studs embedded in high-strength concrete (f'c > 90 MPa) was derived as the following:

$$P_u = A_{sc} f_{su} + \eta f_{cu} d_{wc} l_{wc} \quad (1)$$

, where A_{sc} is the area of the stud shank, f_{su} is the ultimate tensile capacity of the stud, f_{cu} is the compressive strength of the concrete, d_{wc} is the diameter of the weld collar, l_{wc} is the height of the weld collar, and η is an empirical factor typically taken as 2.5 for UHPC.

Although formulations have been proposed for headed studs embedded in UHPC by several researchers [12, 14], these equations are based on tests conducted with studs welded to the flange of a new steel shape. The flange thickness in these experiments was at least 12 mm. When considering the proposed repair, it is important to validate the studs' capacity when welded to plates thinner than 12 mm. Furthermore, it is important to understand the mechanical and metallurgical properties of an old substrate material since the proposed repair targets older bridges. US specifications for structural steel in 1958 called for Type A373-58T steel with a minimum yield strength and ultimate strength of 220 MPa and 400 MPa, respectively [15]. These mechanical properties differ from the material specified for modern construction, such as Type A992 with a minimum yield and tensile strength of 345 MPa and 450 MPa, respectively [16]. In addition, the weldability of new studs to an older material with different metallurgical properties must be assessed to ensure full capacity of the studs can be expected for this repair.

FABRICATION OF PUSH-OUT SAMPLES

A total of 13 push-out samples were fabricated to confirm the feasibility of the proposed repair method and quantify individual stud shear capacity. To obtain results relevant to the repair, rolled steel girders were salvaged from an old bridge which was erected in 1958. The base steel section was fabricated by cutting the salvaged girders into approximately 300-mm long sections. The headed shear studs were welded to the web of the section using a stud gun to adhere to common construction practices (Fig. 4a, b). Steel forms were pressed against the web of the section so that UHPC panels could be cast (Fig. 4c, d). The symbol H_S defines the height of the stud as outlined in Table 1. Foam sheeting was used to separate the UHPC panels under the web. This allowed the panels to behave separately during the experiment without the web bearing onto the UHPC. The final geometry and layout of the push-out specimens is illustrated in Fig. 5.

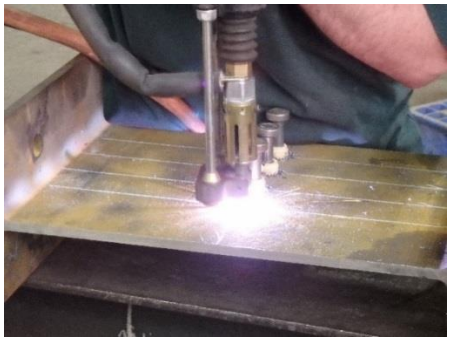

a) Welding of Studs Using Stud Gun

b) Beam With Studs Welded

c) Forms Pressed Against Web for Casting

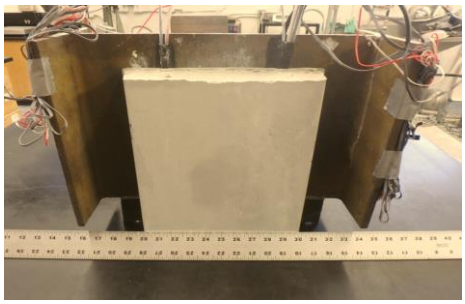

d) Completed Push-Out Specimen

Fig. 4. Fabrication of Push-Out Specimens

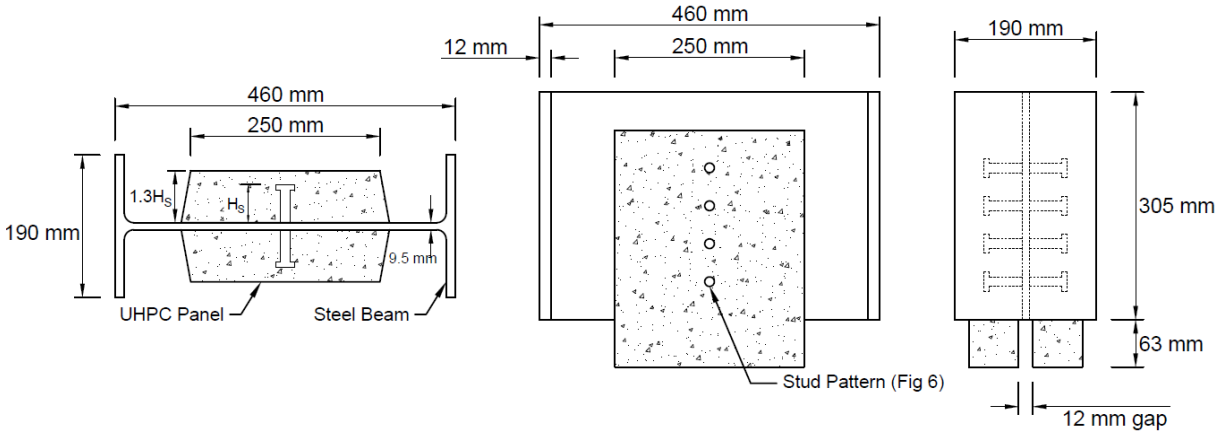

a) Plan b) Elevation c) Cross Section

Fig. 5. Geometry of Completed Push-Out Specimen

The parameters studied include a) stud diameter, b) stud layout, c) stud spacing, and d) UHPC compressive strength. These were selected to address the potential design options that may be considered for field installation. For example, a tightly spaced, staggered pattern may be favorable when a limited surface area is available for welding. Larger diameter studs may also be an option when a higher capacity is needed. Further, it is important to understand the influence of the UHPC compressive strength if it does not develop in the field as expected.

Fig. 6 shows the layouts of the stud arrangements. The symbols S_V and S_H represent vertical spacing and horizontal spacing respectively from the center of the studs. Pattern A is a single column of four studs on each side (eight in total) spaced at four times the diameter of the stud (4db); Pattern B is similar to the benchmark but with a vertical stagger between the two sides; Pattern C contains a vertical and horizontal stagger with vertical and horizontal spacing of 2db; Pattern D is a single column of two studs with larger diameters (16 mm and 19 mm) welded symmetrically on each side of the web; and Pattern E contains four studs welded in two rows and

two columns and spaced at 4db. All spacing is considered center-to-center from the stud shank. The dimensions of the UHPC panels were kept constant in all specimens.

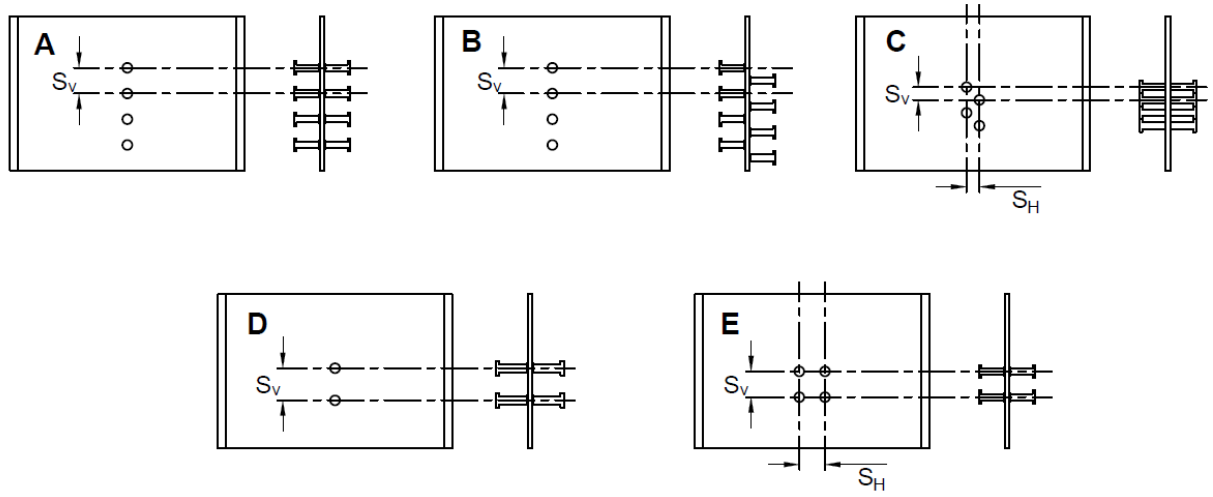

Fig. 6. Stud Patterns

Table 1 summarizes the tests conducted in this study. The specimen identification format is as follows: D (diameter of stud shank) (stud batch series) S (number of studs) – (stud pattern) (sample identification number). Three different stud shank diameters of 12, 16, and 19 mm were examined. The batch series letter ("a" or "b") refers to the batch of headed shear studs used as outlined in the Material Properties section. Five batches with varying mechanical properties were used for the experimental specimens (two for 12 mm studs, one for 16 mm, and two for 19 mm). The stud pattern refers to the layout of the studs as shown in Fig. 6. For example, sample D12aS8-A2 contains eight headed studs with a 12 mm diameter from batch "a". The studs are welded according to stud pattern A. The specimen is designated as sample number 2.

Table 1. Summary of Experiments

Specimen ID	f'c (MPa)	Stud Diam. (mm)	H_S	S_V	S_H
D12aS8-A1	131	12	4db	4db	--
D12aS8-A2	114	12	4db	3db	--
D12bS8-A3	145	12	4db	4db	--
D12aS8-A4	193	12	4db	4db	--
D12aS4-A5	158	12	4db	4db	--
D12bS8-A6	165	12	4db	4db	--
D12bS8-A7	180	12	4db	4db	--
D12aS8-B1	145	12	4db	4db	--
D12aS8-C1	117	12	4db	2db	2db
D16aS4-D1	110	16	4db	4db	--
D19aS4-D2	141	19	2.7db	4db	--
D19aS4-D3	141	19	4db	4db	--
D12aS8-E1	134	12	4db	4db	4db

EXPERIMENTAL METHODOLOGY

All samples were tested using a 1800-kN hydraulic load frame. Each push-out specimen was mounted such that the UHPC panels were resting on a 250-mm diameter spherical bearing to account for small rotations due to imperfections in the sample. To prevent local buckling of the web, the loading was applied onto the beam through the flanges (Fig. 7). This was accomplished by utilizing a hole in the top platen intended for fixtures, which omitted the web of the section. The forces were transferred from the flanges to the web, and finally to the studs which were embedded in the UHPC panels. This experimental setup ensured the studs were loaded in shear,

similar to how they would be loaded when applied to a bridge. The bottom of the UHPC panels were not fixed which allowed for lateral spreading throughout the test.

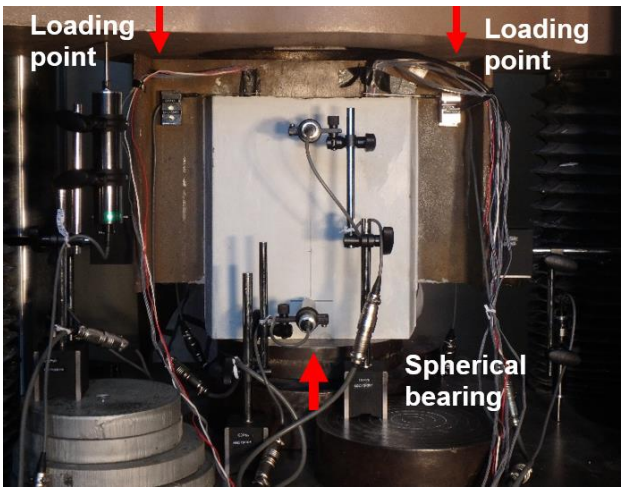

Fig. 7. Instrumented Specimen for Push-Out Experiments

The push-out experiments were conducted using a cyclic loading protocol. A schematic of the loading protocol is shown in Fig. 8.The four initial load steps were conducted using force control at a loading rate of 2.2 kN/s. Each sample was loaded to 15%, 30%, 45% and 60% of its theoretical capacity as outlined by AASHTO [17]. After each step, the specimen was unloaded back to 4.5 kN. After the first four cycles, the sample was loaded with increments of 0.4 mm per cycle using displacement control at a loading rate of 0.004 mm/s until failure.

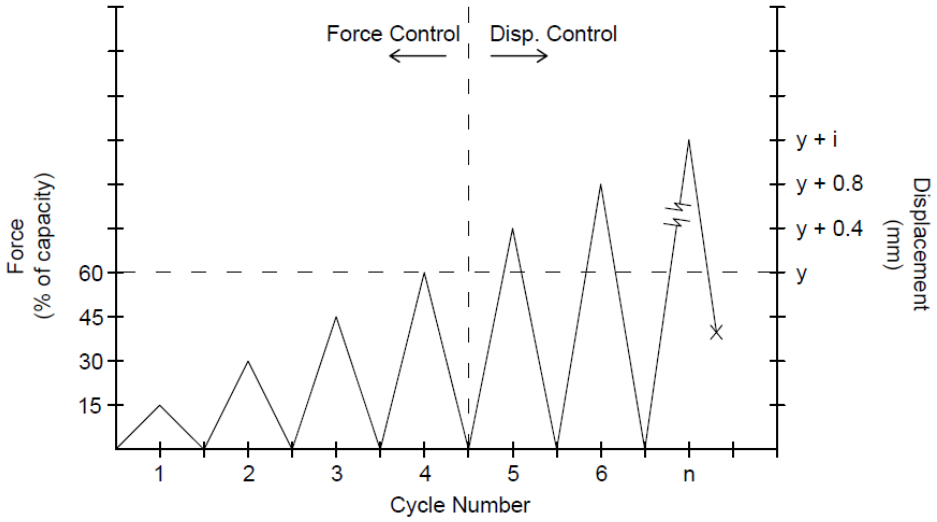

Fig. 8. Loading Protocol for Push-Out Experiments

INSTRUMENTATION

Several different sensors were used to measure slippage, strains on the web, strain in studs, and global deformations. Uniaxial strain gauges were embedded inside the stud shanks to capture axial strains. A hole with a diameter of 2 mm was drilled at the center to approximately 80% of the length of the stud from its head. A high-strength epoxy was injected into the hole until it was filled and free of air voids. The specialized uniaxial strain gauges were embedded into the epoxy-filled hole such that the tip of the gauge remained 2 mm away from the bottom of the drilled hole (Fig. 9a). Biaxial strain gauges were installed onto the web plate above the weld collar (Fig. 9b). These were installed to observe the strain values on the compressed portion of the web plate and to capture any possible yielding of the web.

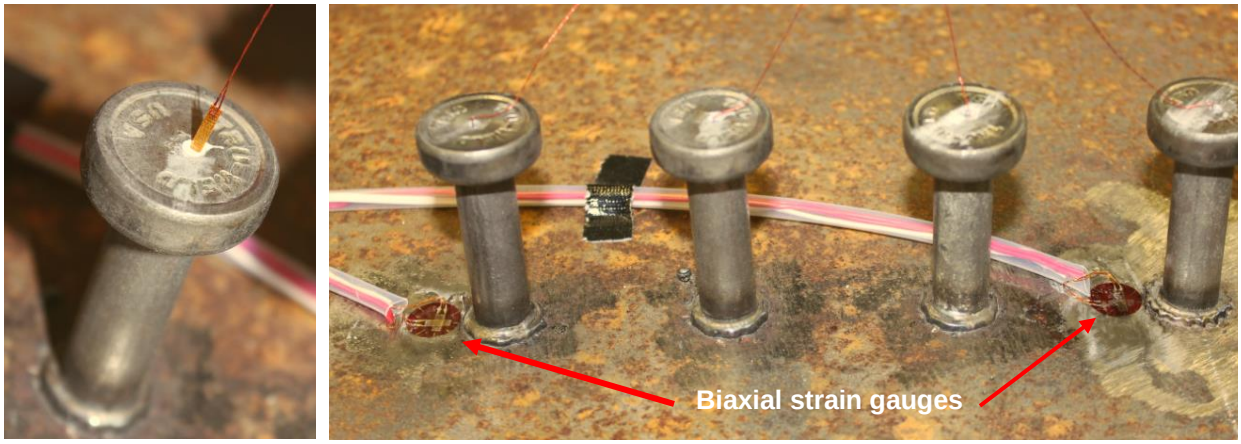

a) Stud Gauges b) Biaxial Strain Gauges Attached at the Base of the Studs

Fig. 9. Uniaxial and Biaxial Strain Gauges for Load Transfer Behavior

Four cantilever-type slip displacement transducers were attached to the web plate using high-strength magnets. These sensors extended onto the UHPC panels to record the relative displacement, i.e. slip, between the web and the UHPC. Based on this displacement, stiffness and ductility of the system may be determined. Seven displacement transducers were used to observe global displacements throughout testing. Two sensors were installed on the left and right flanges of the beam to capture the movement of the steel section. These sensors were used to monitor any possible rotations. Two displacement transducers were installed on each UHPC panel to capture out-of-plane movements. Each sensor was placed along the centerline approximately 65 mm from the top and bottom of the UHPC panel. Finally, a displacement sensor was placed at the top platen to monitor the machine displacement. An overview of the global instrumentation is shown in Fig. 10.

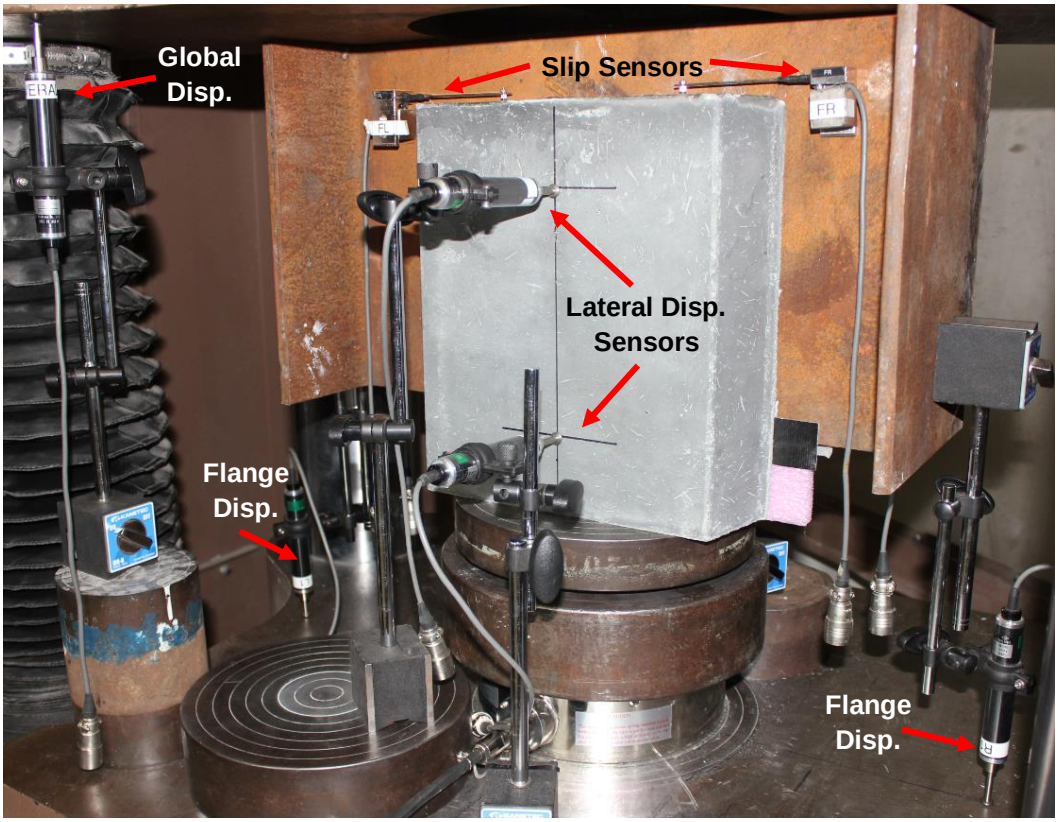

Fig. 10. Overview of Global Instrumentation

MATERIAL PROPERTIES

UHPC is defined as a cementitious composite material made of optimized granular constituents and a water to cementitious materials ratio less than 0.25 [18]. The commercially available UHPC, Ductal JS1212 by Lafarge-Holcim, was used for all experiments. This mix design was selected due to its high early-age strength gain. It is specified to achieve a compressive strength of 83-MPa in 12 hours at 49°C curing. This feature is particularly advantageous to the proposed repair because it enables the opening of a bridge in a short time after casting. The UHPC mix is composed of a premix powder containing a mixture of cement, silica fume, ground quartz, and sand, three admixtures, and high-strength steel fibers. The admixtures include two types of

high range water reducers (HRWR) as well as a non-chloride based accelerator. The steel fibers are 0.2 mm in diameter and 12 mm long with a minimum specified tensile strength of 2,000 MPa. The fiber content is 2% by volume. The composition by weight is shown in Table 2.

Table 2. Composition of the UHPC Mix

Component	% by weight
Premix	86.6
Water	5.1
HRWR 1	0.7
HRWR 2	0.5
Accelerator	0.9
Steel Fibers	6.2

Fig. 11a shows a spread test which was conducted as a quality control measure of the workability of the UHPC. A typical spread for this mix is 250 mm. The mix was accepted if the spread of each UHPC mix was 250±12 mm. Twelve cylinders (75 x 150 mm) were cast from each mix for compressive strength testing. These cylinders were tested at 12 hrs, 24 hrs, and 3, 7, 14, 21 and 28 days. Fig. 11b shows the compressive strength gain including periods up to 60 days.

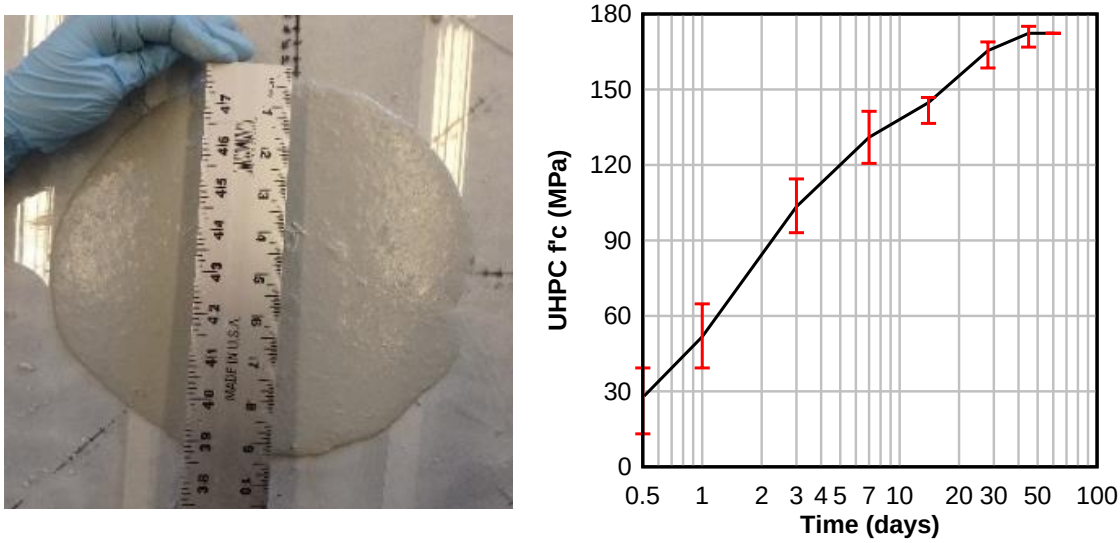

(a) Spread Test of UHPC (b) Strength Gain Over Time

Fig. 11. Quality Control for Ductal JS1212

To evaluate the mechanical properties of the steel beam sections, 6 coupons were fabricated in accordance with ASTM E8 [19]. For the studs, due to their size and geometry, custom coupons were fabricated by removing the head of the stud and machining the stud shank into a flat coupon. The middle of the shank was further machined to produce a circular throat with a diameter of 7 mm. The throat length was 3 times longer than the throat diameter to reduce triaxiality effects. Five various stud batches were used in this experimental program. Two batches were used for studs with a 12-mm diameter, one batch for studs with a 16-mm diameter, and two batches for studs with a 19-mm diameter. All the steel samples were tested in uniaxial tension in accordance with ASTM E8 until rupture (Fig. 12). Table 3 shows a summary yield and ultimate stress values.

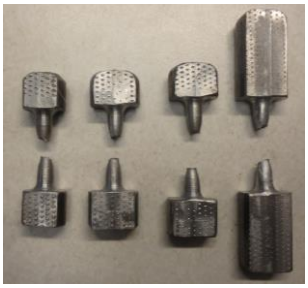

Fig. 12. Ruptured Stud Coupons

Table 3. Summary of Mechanical Properties of Steel Material

Steel Series	Yield Stress, F_y (MPa)	Ultimate Stress, F_u (MPa)
Beam Section	286.1	448.2
D12a	404.0	484.0
D12b	426.1	545.4
D16a	387.5	502.6
D19a	419.9	489.5
D19b	422.6	503.0

RESULTS AND DISCUSSION

The failure mode for all specimens was governed by shear rupture of the stud shank at the interface of the weld collar and stud shank. The weld collar remained almost intact on the web plate and the entire stud remained embedded in the UHPC panel (Fig. 13). A thin wedge of the UHPC sheared off due to bearing action of the weld collar. All the stud patterns failed in a similar manner (Fig. 14).

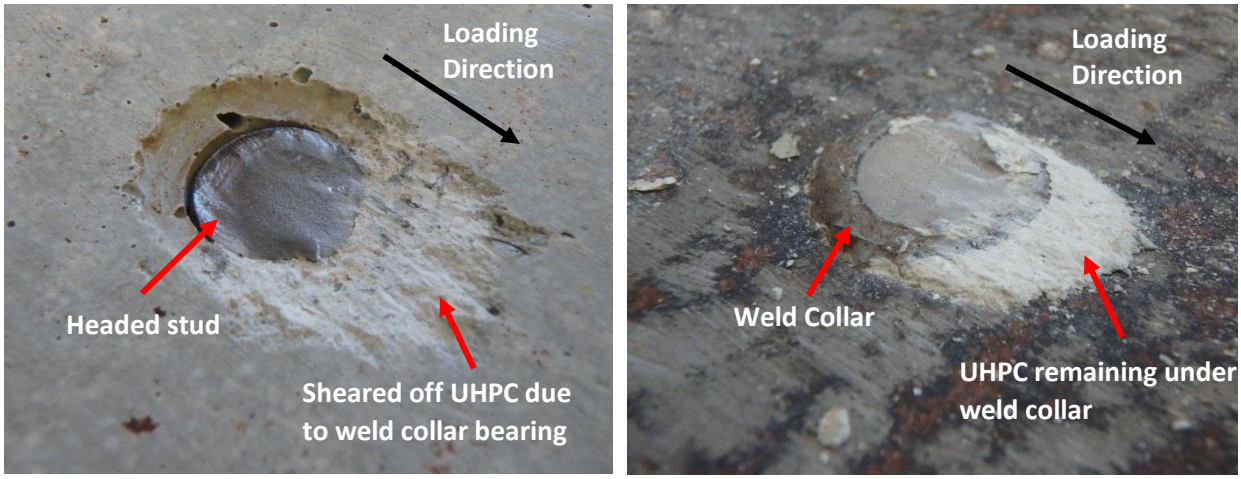

(a) Stud Embedded in UHPC After Failure

(b) Weld collar remaining on web plate

Fig. 13. Typical Shear Failure Mode of Headed Studs Embedded in UHPC

Stud Patter	Base Steel Section	UHPC Panel
A		
B		
C		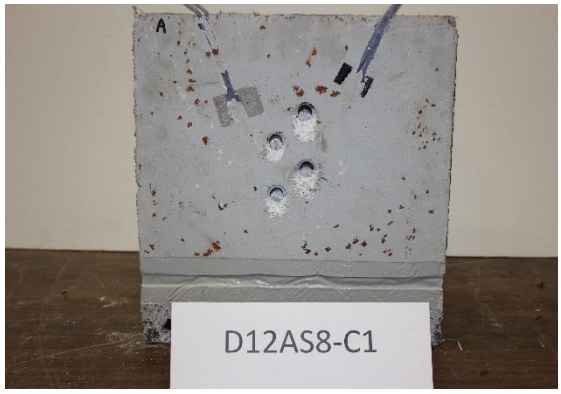

D

E

Fig. 14. Summary of Failed Samples for All Stud Arrangements

Values of elastic shear stiffness (k_e), yield slip (δ_y), maximum slip (δ_u), yield force (P_y), experimental capacity (P_u), and the weld collar bearing force (P_{wc}) at experimental capacity were recorded for all specimens. Elastic shear stiffness (ke) was calculated using the slope of the force vs. slip curve up to one-third of the overall load bearing capacity [20]. The slip is defined as the relative displacement between the UHPC panel and the web plate. The maximum and residual slip at loading cycle i is denoted by $\delta_{i,max}$ and $\delta_{i,res}$, respectively. Four slip sensors were used to monitor the relative displacement between the steel beam and the UHPC panel. The average value is presented for all data herein. Figure 15 shows a typical force-slip relationship. The yield slip and yield force were generated by a 0.1 mm offset from the origin shown by the blue offset line as shown in Fig. 15. The offset was extended with a slope of 220-, 365- and 400 kN/mm for the 12-,

16- and 19 mm studs to capture the yield point for various stud diameters with different ultimate capacities. The slopes varied according to the elastic stiffness of each respective diameter. The force per stud was calculated as the total bearing force resisted by the specimen divided by the number of studs. The bearing contribution of the weld collar (P_{wc}) was calculated by subtracting the contribution of the stud shank ($A_{sc}F_u$) from the total experimental capacity of the stud. Table 4 shows a summary of the test results.

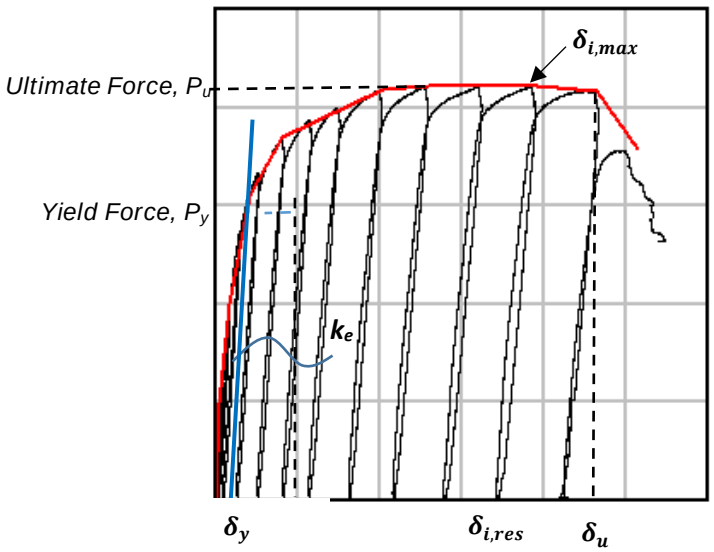

Fig. 15. Parameters for Typical Force vs. Slip Curve

Table 4. Summary of Experimental Results

Specimen ID	f'c	k_e	δ_y	δ_u	P_y	P_u	P_{WC}	P_{WC}/P_u
Unit	MPa	kN/mm	mm	mm	kN	kN/stud	kN/stud	%
D12aS8-A1	131	181.5	0.330	4.65	41.5	66.7	8.43	8.15
D12aS8-A2	114	167.4	0.380	5.86	40.3	62.3	1.54	1.59
D12bS8-A3	145	228.5	0.241	4.47	52.5	69.8	5.41	5.00
D12aS8-A4	193	273.2	0.193	3.25	51.4	70.7	14.64	13.35
D12aS4-A5	159	200.2	0.305	5.91	51.6	66.7	8.43	8.15
D12bS8-A6	179	260.4	0.229	3.43	53.1	73.8	7.42	6.49
D12bS8-A7	166	240.7	0.231	3.46	50.3	70.5	6.38	5.84
D12aS8-B1	145	297.2	0.264	5.15	52.1	68.5	3.34	3.15
D12aS8-C1	117	201.3	0.293	4.71	47.9	62.3	1.54	1.59
D16S4-D1	110	363.9	0.344	4.42	84.7	101.4	3.07	1.96
D19aS4-D2	141	391.4	0.312	6.78	105.0	144.6	7.92	3.54
D19aS4-D3	141	405.9	0.267	4.84	107.6	150.3	10.80	4.63
D12aS8-E1	134	150.7	0.351	5.08	51.6	65.4	6.36	6.28

Fig. 16a shows the backbone force vs. slip curves for all samples. Slip is an important parameter for shear connections because it reveals the stiffness and ductility of the system. The 12-, 16- and 19-mm diameter studs generated an average capacity of 68.2, 101.4 and 147.7 kN/stud, respectively. The studs exhibit ductile behavior as they sustain the loading over an average slip of 4.60, 4.42 and 5.81 mm for the 12-, 16-, and 19-mm studs, respectively. However, these slip capacities do not satisfy the ductility requirements of 6 mm as outlined in Eurocode-4 [21]. On average, the weld collar attributed for 5.4% of the shear resistance for all samples. However, it was observed that the contribution of the weld collar varied for different UHPC

strengths. For example, when the UHPC compressive strength was 114 MPa, the weld collar was only responsible for 1.6% of the stud capacity. However, for a compressive strength of 193 MPa, the weld collar attributed for 13.3% of the capacity. This is further shown in Fig. 16b which shows the normalized shear strength of a single stud as a function of compressive strength of UHPC. The graph is normalized because of the various diameters and material strengths of the studs. It is shown that as the compressive strength of the UHPC increases, the shear strength of the headed stud also increases. When the UHPC compressive strength increases from 114 to 193 MPa, the shear strength increases by approximately 14%. This may be due to less micro-cracking at the interface between the weld collar and the UHPC. At higher compressive strengths, the intact UHPC provides more resistance to the bearing action of the weld collar. This effect may also be pronounced further for larger weld collars with more available surface area. This means that the overall shear resistance of the stud is dependent on the UHPC which engages the weld collar more effectively at higher compressive strengths.

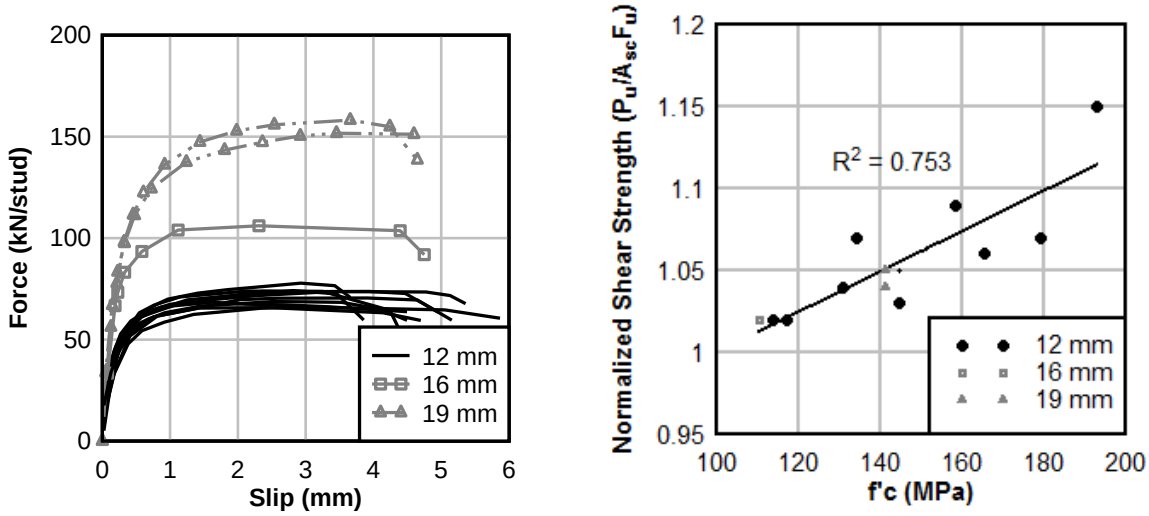

a) Force vs. Slip Summary b) Strength of Stud vs. UHPC f'c

Fig. 16. Ultimate Strength of Headed Studs

To further understand the influence of the UHPC compressive strength, the slip at the yield point was studied (Fig. 17). The trend line suggests that the slip at yield decreases as the UHPC compressive strength increases. When the UHPC compressive strength increased from 114 MPa to 193 MPa, the yield slip decreases from 0.380 mm to 0.193 mm, respectively. This may be due to less localized cracking near the weld collar, which results in a more efficient shear connection between the stud and the UHPC. A higher strength UHPC may resist micro-cracking in the elastic range which allows the material to contain the studs more effectively. This behavior reduces flexure of the stud and promotes shear deformation, resulting in a stiffer system.

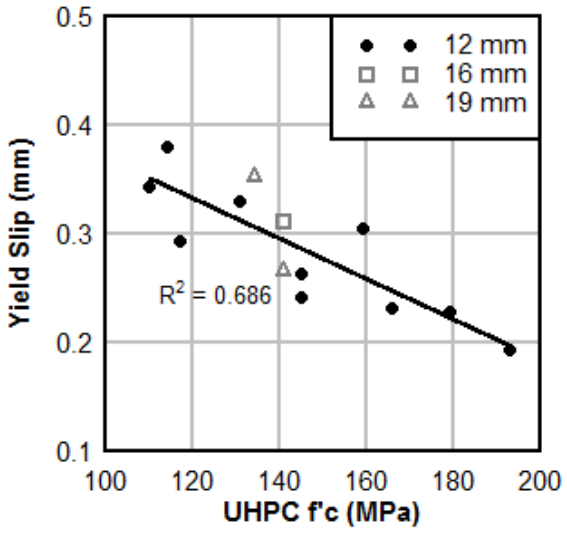

Fig. 17. Slip at Yield Point vs. UHPC Compressive Strength

Fig. 18 illustrates the relationship between residual slip and maximum slip experienced by the system during loading and unloading cycles. This graph provides information regarding the systems' ability to recover from the induced displacement. Maximum slip is defined as the slip experienced by the system at each cycle *i*. Residual slip is defined as the slip of the system when

the sample has been unloaded from cycle *i*. Typically, residual displacement can be considered plastic displacement. In this graph, a slope approaching 0 represents an elastic system (i.e. no residual displacement). If the slope of the curve approaches 1, it indicates that the system has experienced plastic deformation. The figure shows that the system is in the elastic range when maximum slip is less than ~0.3 mm. After this point, the slope of the curve increases to approximately 0.89 mm/mm, suggesting more damage accumulation between the studs and the UHPC. From here, damage accumulation is constant as characterized by the linear shape of the curve.

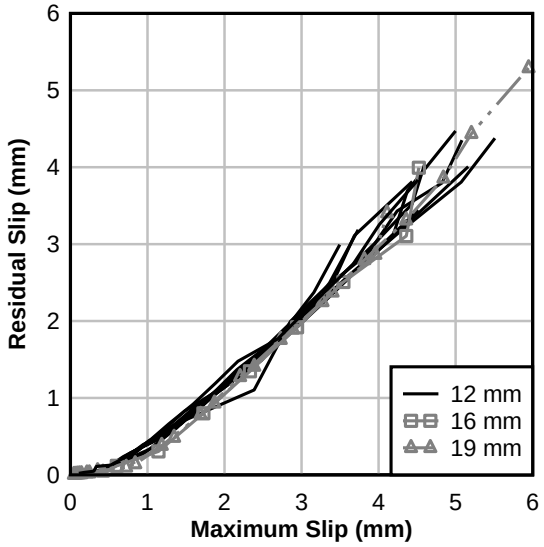

Fig. 18. Residual Slip vs. Maximum Slip

Damage initiation is an important parameter when studying the load-transfer behavior between the headed studs and the UHPC. Understanding the source and progression of damage can provide information to further optimize the shear connection. Damage was captured by comparing the stiffness at each loading cycle (k_i) against the elastic stiffness (k_e). The stiffness at

each cyclic loading (k_i) is defined using the change in slope between the residual slip and maximum slip at each cycle. A damage variable of 0 indicates that the connection behaves elastically since the system experiences no residual displacement. A damage variable of 1 indicates that the connection has no stiffness remaining and is thus fully damaged or ruptured. The damage variable, D_i, is calculated using the following expression:

$$D_i = 1 - \frac{k_i}{k_e} \quad (2)$$

Fig. 19 illustrates the damage initiation and reduction in stiffness of a single stud. In general, over 50% damage was experienced by all samples before a slip of 1 mm. This may be due to a combination of micro-cracking of the UHPC and yielding of the studs. At larger slip ranges (i.e. more than 1 mm), the damage curve flattens, indicating less damage accumulation when the studs begin to undergo shear deformation. This is because the change in stiffness is minimal in the plastic region due to strain hardening of the stud material. The minimum and maximum damage variable prior to rupture is 0.61 (sample D19S4-D2) and 0.96 (sample D12S8-A3), respectively. Several factors may contribute to the variation in damage: a) higher UHPC strengths generate more resistance to micro-cracking and thus less damage, b) less UHPC cover provides smaller resistance to tensile splitting and thus more damage, and c) poor quality weld collars may lead to more residual slip as the efficiency of the connection is debilitated. Sample D12S8-A3 showed the highest damage because of the reduced spacing between studs (3db). The reduced spacing may have caused overlapping of the bearing regions of the studs inducing higher compressive demands on the UHPC. No clear trend was observed in damage initiation when comparing the stud arrangement or stud diameter.

Post-yield stiffness is defined as the stiffness of the stud at each cycle *i* after yielding is observed. Stiffness measurements were calculated by recording the slope of the force-slip curve at each loading cycle. This stiffness was divided by the number of studs to calculate the theoretical stiffness of one stud. For studs with a diameter of 12, 16 and 19 mm, the stiffness per stud decreased by 27.2, 28.8, and 19% respectively. The benchmark stud arrangement (A) generated a consistently higher stiffness than samples with staggered stud arrangements (B, C, E). The studs with larger diameters generated a higher stiffness due to their ability to carry higher forces over the same slip range.

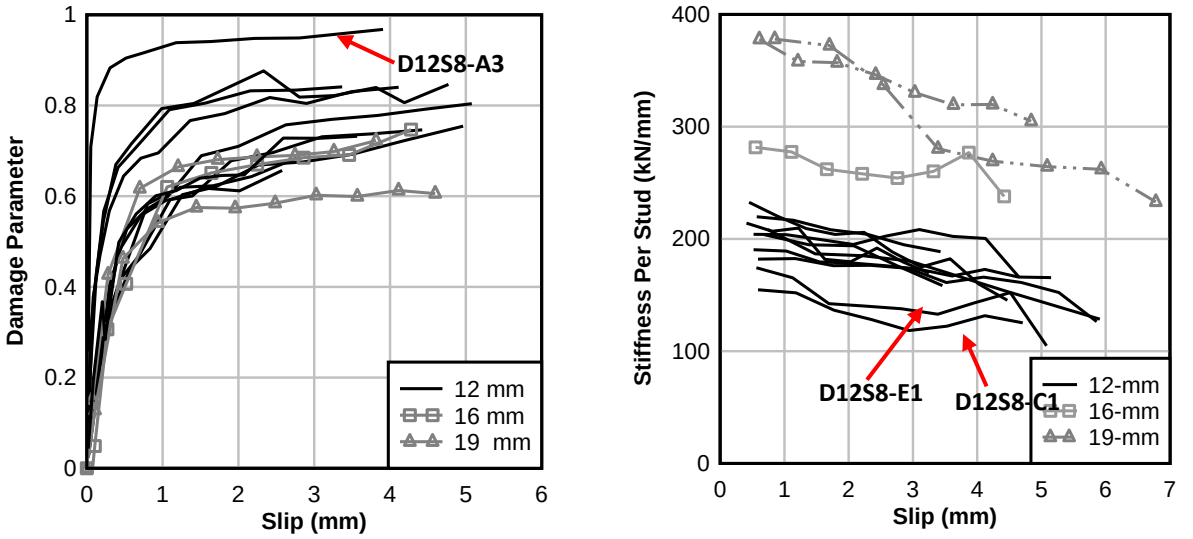

a) Damage Initiation b) Reduction in Stiffness After Yielding

Fig. 19. Damage Initiation and Stiffness Reduction

Since the headed studs are welded onto a thinner plate than traditionally used in push-out tests, understanding the demands on the web plate is critical when considering the proposed repair. If the web plate experiences excessive strain and/or yielding, the proposed repair may not be

favorable as additional damage to the structure must be avoided. Fig. 20 shows the strain transfer between the stud and adjacent web plate onto which it was welded. In Fig. 20a, the loading and unloading cycles are shown in dashed gray and the generated backbone curve is shown solid black. Fig. 20b shows the backbone curves for all samples tested. The stud strains shown are axial, as shear strain in the studs is difficult to capture during testing. When initial loads are applied to the system, the web and studs act in unison to resist the demands in the elastic range. Once the studs reached their yield strength, the web no longer experiences additional strain; instead, the demand is fully transferred to the studs. The flattening of the strain curve at higher cycles indicates this behavior. The studs continue to deform until they rupture in shear. Each sample tested in this series showed comparable stud strains, indicating no significant shear lag effects. The average detachment of the UHPC panel due to axial elongation of the studs is 1.01 mm.

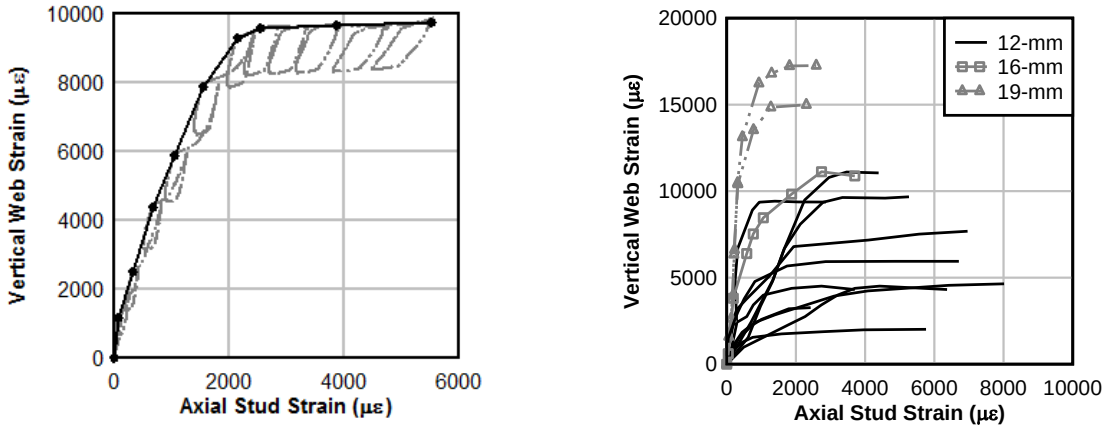

a) Typical Strain Transfer with Cyclic Loading

b) Backbone of Strain Transfer for All Samples

Fig. 20. Transfer of Strain Between Web and Headed Shear Studs

Another important parameter of interest regarding the proposed repair is the effect of various stud diameters. Welding larger studs may be favorable when a larger capacity is needed and little surface area is available on the web plate. Fig. 21 illustrates the relationship between web

strains generated adjacent to the stud as a function of stud diameter. The trend indicates that the strain experienced by the web is larger as the stud diameter increases. On average, the studs with a diameter of 12, 16 and 19 mm generated a strain of 6,950, 9,800 and 16,200 με respectively. The 12-mm studs generated a larger deviation in web strain due to a variety of stud layouts tested. For example, a sample with vertical stagger (layout B) experienced larger vertical web strains, approximately 13,000 με, than a sample with no stagger (layout A) which experienced approximately 9400-με. However no significant deterioration in capacity was observed when comparing the stud arrangements. These results indicate that headed studs up to a diameter of 19 mm can be welded on web plates with a thickness of 9.5 mm, validating the feasibility of the repair.

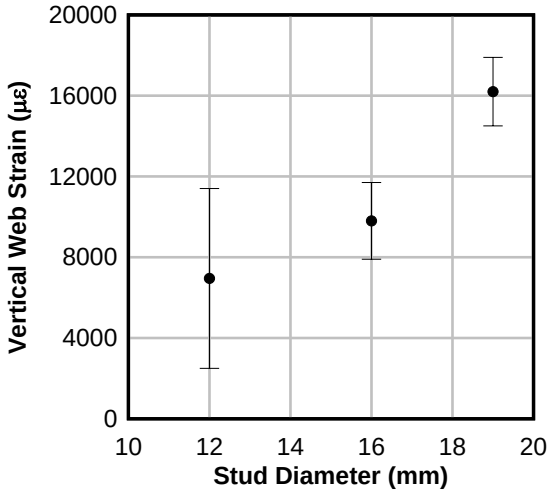

Fig. 21. Web Strain vs. Stud Diameter

CAPACITY OF HEADED STUDS IN UHPC

Equation (1) proposes that the capacity of a headed shear stud embedded in UHPC is the sum of the shear resistance generated by the area of the stud shank ($A_{sc}F_u$) and the bearing

resistance generated between the weld collar and the UHPC panel ($\eta f'_c d_{wc} l_{wc}$). The results generated through this experimental program confirm that the weld collar plays a significant role in the shear capacity of a headed stud. However, the weld collar contribution may vary based on the weld quality and geometry of the collar. Headed studs are typically welded using a stud gun; a manual process which can produce varying weld collar shapes (Fig. 22). Therefore, it is important to identify the quality of the weld collar since it was found to play such a critical role in the load bearing capacity of the stud.

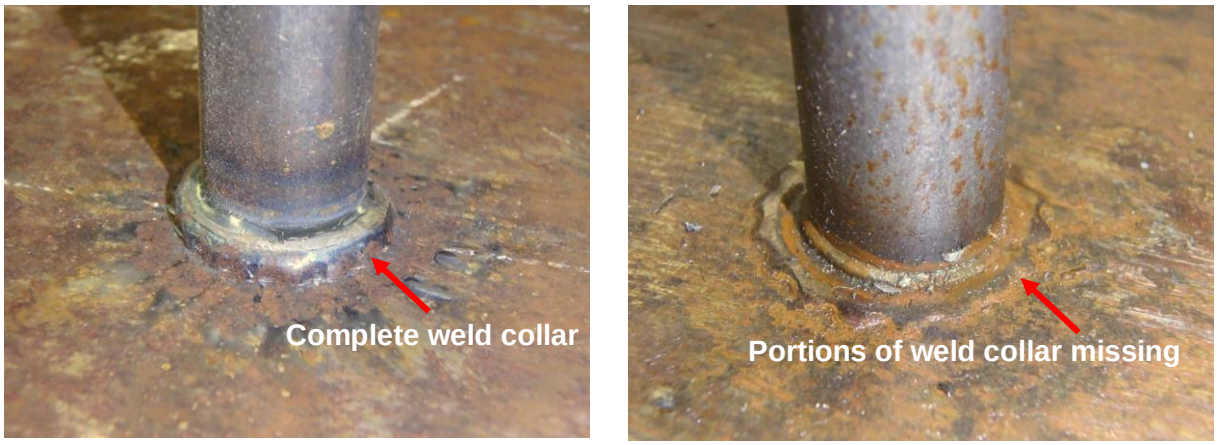

(a) Good Quality Weld Collar (b) Poor Quality Weld Collar

Fig. 22. Variation in Weld Collar Geometry

An effort was made to improve the current stud capacity formulation derived in Equation (1) to include variations in the weld collar. Diameter and height measurements of 128 weld collars were recorded for studs with diameters of 12, 16, and 19 mm. Each weld collar was measured at four locations along its circumference using a digital caliper. The measurements indicate that the average weld collar diameter and height is $1.44d_b$ ($\sigma = 0.035$) and $0.14d_b$ ($\sigma = 0.005$), respectively.

Since a limited number of samples were available, a Monte Carlo simulation was conducted to assess a statistical range of weld collar sizes using the data obtained from the measurements. From these simulations, the diameter and height of the weld collar was generated with a 95% confidence interval. Normalized by the diameter of the stud shank, these parameters were used to modify Equation (1) as follows:

$$Pu = A_{sc}F_u + 0.16\eta f'_c \, {d_b}^2 \qquad (3)$$

where A_{sc} is the area of the stud shank, F_u is the ultimate tensile strength of the stud, f'_c is the compressive strength of UHPC, and d_b is the nominal diameter of the stud shank. Various researchers have attempted to quantify a value for the empirical factor η: Hegger et al. (2006) suggested that η = 1.5 and Kim et al. (2015) proposed η = 2.5. However, the results generated from this experimental program suggest that a single value for η cannot be assumed because the back-calculated value is dependent on the UHPC strength (Fig. 23). The experimental results generated in this program were used to calibrate the η. From the outlined experimental program, η was quantified as a function of UHPC compressive strength shown by Equation (4) where β is a unitless factor taken as 0.0119 (MPa) or 0.0822 (ksi).

$$\eta = \beta f'_c - 0.983 \qquad (4)$$

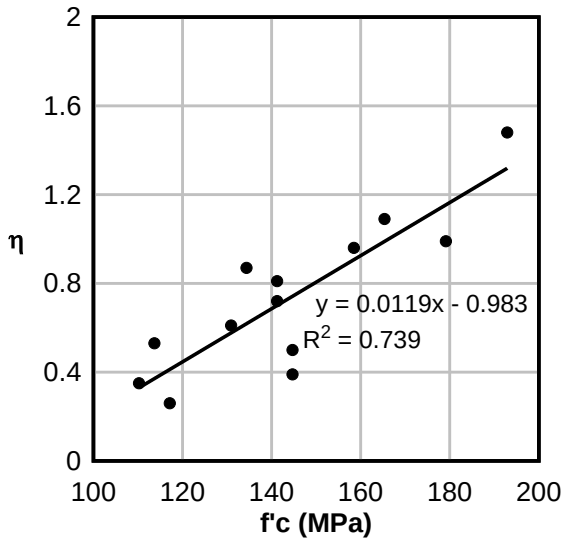

Fig. 23. Empirical Factor η vs UHPC f'c

Table 5 compares the experimental capacities generated in this program against various design codes [17, 21, 22] and the formulation developed by [14]. The results show that design codes are conservative with the capacities calculated. However, the formulations outlined by these codes may not consider studs embedded in UHPC and therefore, may need to be revised when this material is incorporated. In addition, it should be noted that codes such EC-4 incorporate a 5% characteristic fractile number which should be considered in the comparison. When the experimental capacities are compared against Equation (1), good agreement is generated when η = 1.5 (97% agreement). However, when η = 2.5, the formulation over-predicts the shear capacity by an average of 9%, suggesting that this value may be too high. When the comparison is made against the proposed equation (3) good agreement is achieved within an average of 1%.

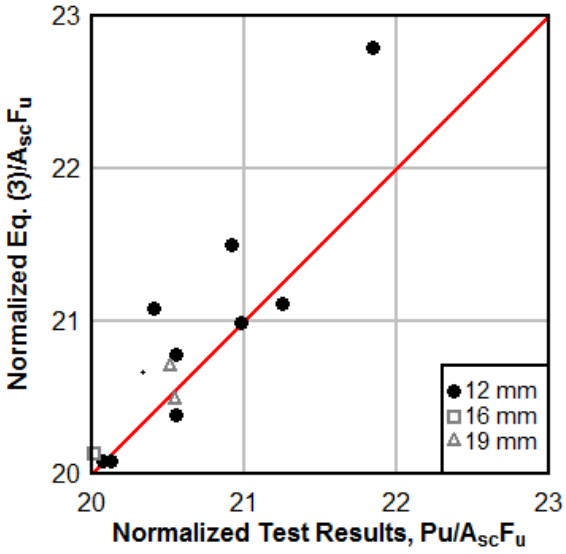

Fig. 24. Normalized Comparison of Results

Table 5. Design Code Comparison

Specimen ID	f'c (MPa)	P_u (kN)	P_u/AASHTO	P_u/EC-4	P_u/CSD	P_u/Eq (1) $\eta = 1.5$	P_u/Eq (1) $\eta = 2.5$	P_u/Eq (3)
D12S8-A1	131	66.7	1.09	1.36	1.34	0.98	0.91	0.99
D12S8-A2	114	62.3	1.02	1.27	1.26	0.97	0.94	1.00
D12S8-A3	145	69.8	1.14	1.42	1.41	0.98	0.85	0.99
D12S8-A4	193	70.7	1.16	1.44	1.43	1.00	0.92	0.96
D12S4-A5	159	66.7	1.09	1.36	1.34	0.96	0.89	0.98
D12S8-A6	179	73.8	1.21	1.51	1.49	0.98	0.92	1.00
D12S8-A7	166	70.5	1.15	1.49	1.42	0.99	0.94	1.00
D12S8-B1	145	68.5	1.12	1.40	1.39	0.98	0.90	1.00
D12S8-C1	117	62.3	1.02	1.27	1.26	0.97	0.91	1.00
D16S4-D1	110	101.4	1.06	1.32	1.31	0.97	0.92	0.99
D19S4-D2	141	144.6	1.05	1.31	1.30	0.97	0.93	1.00
D19S4-D3	141	150.3	1.09	1.36	1.35	1.00	0.95	0.99
D12S8-E1	134	65.4	1.07	1.33	1.32	0.96	0.89	0.97
Average			1.10	1.37	1.36	0.97	0.91	0.99

CONCLUSIONS

A novel bridge repair method has been proposed for bridge girders suffering from section loss due to corrosion at the bearing. The repair involves welding headed shear studs to intact portion of the web plate and embedding them in UHPC. Push-out tests were conducted to validate the capacity of the studs when embedded in UHPC and welded to a 9.5 mm thick web plate. The following conclusions are derived:

1. The experimental results validate the full plastic capacity of the studs was achieved even when the studs were welded to a 9.5-mm thick web plate. The stud layouts tested did not have a significant effect on the load bearing capacity.
2. It was observed that a higher compressive strength (f'_c) of the UHPC resulted in a higher shear capacity of the headed stud due to bearing action of the weld collar. When the UHPC compressive strength increases from 114 MPa to 193 MPa, a 13% increase in stud shear capacity is observed.
3. When a higher UHPC compressive strength was used, the yield slip and ultimate slip decreased. This indicated that the composite connection loses ductility at higher compressive strengths. This may be because a higher strength UHPC confines the stud more effectively and minimizes flexure of the stud shank.
4. A cyclic loading protocol revealed the extent of damage in the composite connection. In the elastic range, there was little or no damage to the UHPC or studs. After the studs yield, larger residual slip was experienced due to shear deformation of the studs, indicating that the connection was largely governed by the material strength of the studs.

5. The strain transfer between the web and headed studs was observed. In the elastic range, the web plate experienced larger axial strains until the studs reached their yield strength. Upon stud yielding, they began to deform extensively in shear with some longitudinal flexural deformation until shear failure of the stud shank. After the studs yield, additional strain accumulation in the web is minimal.
6. The experiments revealed that the shear capacity of a headed stud was consistently higher than the predicted capacities provided by design codes. The experimental results were 2-21% higher than AASHTO's design strength and 27-43% higher than EC-4 and CSD (when design fractile numbers are incorporated).
7. An existing capacity formulation was refined to better quantify the shear capacity of a headed stud embedded in UHPC. The formulation is applicable for various UHPC strengths and considers potential weld collar imperfections with a 95% confidence interval. The refined formula estimated the experimental stud capacity with good agreement.

REFERENCES

1. ASCE (2017). “2017 Report Card for America’s Infrastructure.” American Society of Civil Engineers. www.asce.org
2. Shi, X., Fay, L., Yang, Z., Nguyen, T. A., and Liu, Y. (2009). "Corrosion of Deicers to Metals in Transportation Infrastructure: Introduction and Recent Developments." *Corrosion reviews*, 27(1-2), pp23-52.
3. Ahn, J.-H., Kainuma, S., and Kim, I.-T. (2013). "Shear Failure Behaviors of a Web Panel with Local Corrosion Depending on Web Boundary Conditions." *Thin-Walled Structures*, 73, 302-317.’
4. Zmetra, K., McMullen, K., Zaghi, A.E., Wille, K. (2017). “Experimental Study of UHPC Repair for Corrosion-Damaged Steel Girder Ends.” Journal of Bridge Engineering, 22(8).
5. Rossow, M. (2003). "FHWA Bridge Maintenance: Superstructure." Continuing Education and Development, Inc., Federal Highway Association.
6. Zaghi, A.E., Wille, K., Zmetra, K., and McMullen, K. (2015). "Repair of Steel Beam/Girder Ends with Ultra High Strength Concrete (Phase I)." Connecticut Department of Transportation. University of Connecticut. SPR-2282 (Report #CT-2282-F-15-2).
7. Lam, D., and Ellobody, E. (2005). “Behavior of headed shear stud shear connectors in composite beam”. Journal of Structural Engineering” ASCE, 131(1): pp96-107.
8. Hegger, J., Rauscher, S., Goralski, C. (2004). “Push-Out Tests on Headed Studs Embedded in UHPC.” *Proc., International Symposium on Ultra High Performance Concrete*, Kassel, Germany, vol 3, pp 425-434.
9. Kim, J.S., Park, S.H., Joh, C.K., Choi, E.S. (2013). “Push-Out Test on Shear Connectors Embedded in UHPC.” Applied Mechanics and Materials, vol. 351-352, pp50-54.

10. Cui, Y., Luo, Y., Nakashima, M. (2013). "Development of steel beam-to-column connections using SFRCC slabs." Engineering Structures, vol. 52, pp 545-557.
11. Kim, J.S., Kwark, J., Joh, C., Yoo, S.W., Lee, K.C. (2015) "Headed stud shear connector for thin ultrahigh-performance concrete bridge deck." Journal of Constructional Steel Research, 108(1), 23-30.
12. Cao, J., Shao, X., Deng, L., Gan, Y. (2017) "Static and Fatigue Behavior of Short-Headed Studs Embedded in a Thin Ultrahigh-Performance Concrete Layer". Journal of Bridge Engineering, 22(5).
13. Wang, J.Y., Guo, J., Jia, L., Chen, S., Dong, Y. (2017) "Push-out tests of demountable headed stud shear connectors in steel-UHPC composite structures". Composite Structures, accepted manuscript.
14. Hegger, J., Sedlacek, G., Döinghaus, P., Trumpf, H., and Eligehausen, R. (2006) "Studies on the ductility of shear connectors when using high-strength steel and high-strength concrete." *Proc., International Symposium on Connections between Steel and Concrete*, University of Stuttgart, 1025-1045.
15. Brockenbrough (2002). "AISC Rehabilitation and Retrofit Guide – A Reference for Historic Shapes and Specifications". American Institute of Steel Construction (AISC), Pittsburgh, PA.
16. AISC (2011). "Steel Construction Manual," American Institute of Steel Construction, 14th Edition.
17. AASHTO (2012). *AASHTO LRFD Bridge Design Specifications,* American Association of State Highway and Transportation Officials, Washington, DC 20001.

18. FHWA (2011). “Ultra-High Performance Concrete”. Report No. FHWA-HRT-11-038, Federal Highway Adminstration, McLean, VA.
19. ASTM E8 (2016). “Standard Test Methods for Tension Testing of Metallic Materials”. ASTM International, West Conshohocken, PA, 2016. www.astm.org
20. JSSC (Japan Society of Civil Engineers). (2002). *Guidelines for performance-based design of steel-concrete hybrid structures*, Tokyo.
21. Eurocode-4 (2004). "Design of Composite Steel and Concrete Structures." European Committee for Standardization., Brussels, Belgium.
22. MHURDOC (Ministry of Housing and Urban-Rural Development of China). (2013). “Code for design of steel and concrete composite bridges (GB 50917-2013), China Planning Press, Beijing (in Chinese).

Chapter 2

Design Considerations for Headed Shear Studs Embedded in UHPC as Part of a Novel Bridge Repair Method

Introduction

There is a growing need for more efficient and effective repair methods to rehabilitate the rapidly deteriorating infrastructure. To improve the efficiency of repairing deteriorated bridge girders with section loss at the ends, a new repair method has been proposed, in which headed shear studs are embedded in ultra-high performance concrete (UHPC) [1]. UHPC is the ideal candidate material for this repair because of its flowability, excellent corrosion resistance, superior tensile capacity. No additional reinforcement is needed other than the steel fibers present in the mix. Additionally, studies have shown that headed studs exhibit superior fatigue performance when embedded in UHPC compared to regular strength concrete (RSC) [2]. In this repair, the headed shear studs are welded to the non-corroded portion of the web plate near the bearing region and encased in a panel of UHPC. This panel of UHPC extends down to the bottom flange, enabling a force transfer mechanism to alleviate the weakened web (Fig. 1).

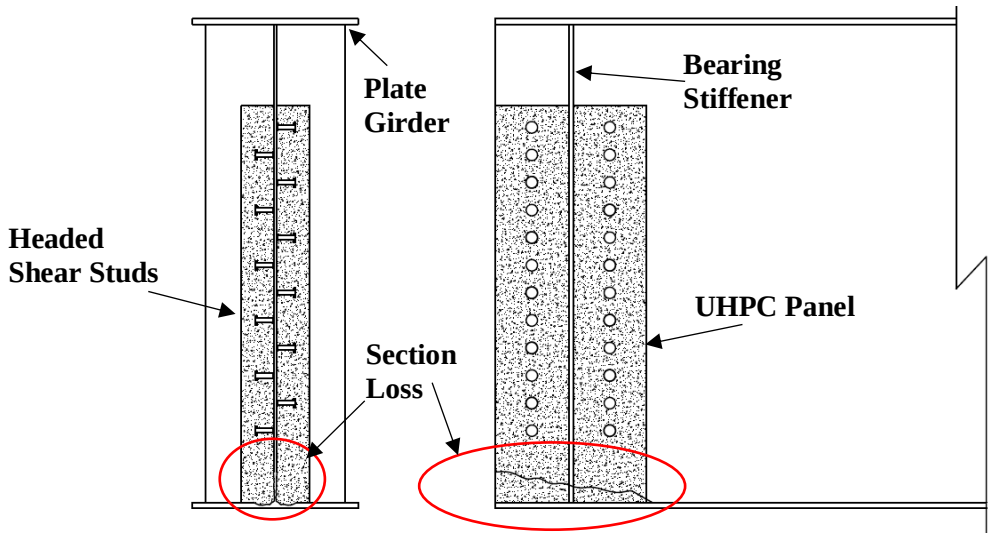

a) Cross section b) Elevation view

Fig 1. Schematic of Proposed Repair Concept

It is estimated that there is a backlog of approximately $123 billion in bridge rehabilitation projects in the United States [3]. The current procedure to repair damaged girder ends is expensive, time consuming, difficult to implement, and leads to bridge closures. First, the superstructure must be jacked to relieve the dead load from the affected portion of the girder. This procedure is costly and sensitive, as improper jacking can result in bridge collapse, serious structural damage to the components, injury to workers, or traffic accidents [4]. Next, the damaged section of the steel must be cut out so that a new section can be welded into place. Lead abatement may be necessary if the girder was treated with a lead-based paint. After the damaged portion is removed, a new section of steel is carefully welded into place such that the girder remains straight and upright. Finally, the superstructure is lowered back into place. While this repair procedure is commonly accepted as the standard protocol for repairing corroded girders, there is a growing need for an alternative method which decreases the time needed for lane closures, minimizes cost, and improves the effectiveness of the repair.

Corrosion is one of the most prevalent issues facing steel superstructures. A typical expansion joint for new construction in small-span bridges lasts less than 15 years [5]. However, leakage of the joints can occur prior to the expected lifespan of the joint, exposing the superstructure to water and deicing chemicals. Additional inhibitors that induce corrosion in steel girders include high temperature, salt concentration in the air, presence of sulfur oxides, and wind velocity [6]. Exposure to these hazards may cause significant corrosion of the load-bearing components (Fig. 2). Experimental studies have been conducted to evaluate the bearing capacity of steel girders with section loss due to corrosion near the bearing region [7]. The studies revealed

that a 70% section loss in the web and flange area decreased the bearing capacity of the girder by 76%. When corrosion damage is present in the web and stiffener, the failure mode shifts from buckling of the web plate to local crippling at the reduced region [8].

Fig. 2. Corrosion at girder end

The proposed repair method utilizing headed studs and UHPC has been proven as a viable option to restore the bearing capacity of a weakened girder. Experiments were performed with one-third scale bridge girders to validate this concept [9]. The results showed that the capacity of a damaged steel girder increased by approximately 25% compared to the undamaged section when the proposed repair was applied. When the damaged girder was tested, high levels of axial strain concentrations were observed at the reduced section of the web plate. However, when the UHPC repair was implemented, these strains were drastically lowered and instead transferred to the UHPC, demonstrating the success of the repair. A critical component of the proposed repair is the interaction between the web plate, the headed shear studs, and the UHPC panel. A study was

conducted by the authors to examine the performance of headed shear studs welded onto 9.5-mm thick web plates. Parameters such as stud diameter, stud spacing, stud arrangement, and UHPC compressive strength were assessed [10]. The results showed that when studs are embedded in UHPC, stud shank failure always governs, with no damage to the UHPC. These results were consistent for all patterns tested, including vertical stagger, horizontal and vertical stagger, and tight spacing.

Although experimental studies have proven that this repair method is a promising alternative to the current repair procedure, design parameters must be established to ensure proper application and longevity of the repair. In this research, push-out experiments were designed to evaluate potential design parameters that may be considered by the bridge owner. Factors studied include a) eccentric loading, b) concrete variations, c) clear and side cover, d) welding/surface preparation, and e) presence of vibration while curing. The results from each push-out test are compared against the baseline sample, which represents typical behavior of headed studs embedded in UHPC. The data obtained from the tests was used to provide design recommendations for implementing the proposed repair method in the field.

Review of Prior Studies

Extensive literature exists on the shear capacity of headed shear studs. However, there is still a need for validation of the proposed parameters as part of the UHPC repair. No data was found on the performance of headed studs when subjected to a combination of shear and in-plane torsion. This scenario may be relevant in the field when there is a moment applied to the stud group. Therefore, the effect of eccentric loading must be studied, as it is currently unknown. The

influence of concrete embedment material has been more commonly studied. Lam et al. [11] reported that when conducting push-out tests using regular strength concrete (RSC) with a compressive strength of 20 MPa, the failure mechanism was governed by conical failure of the surrounding concrete with partial yielding of the stud. When studs are embedded in higher strength concrete, larger capacities are generated with a failure mode resulting in stud shank rupture [12]. It was found that the stiffness and deformability of headed studs embedded in RSC is also dependent on the concrete strength [13]. When studs are embedded in UHPC, a spacing of 3.5 stud diameters (d_b) generates at least 90% of the shear strength of a single stud, while in RSC a spacing of $6d_b$ is required [14]. However, transverse reinforcement is necessary for RSC panels, as the tensile resistance of concrete is insufficient to accommodate the splitting forces generated by the studs [15]. In the context of the UHPC repair, bridge owners may opt for an alternative embedment material and therefore experiments must be performed to validate their use.

Another important design parameter for the proposed repair is clear and side cover of the studs. Due to the nature of the repair, the studs may be welded close to the end of the girder or adjacent to a bearing stiffener. Therefore, minimum clear distance and cover must be established. A study has shown that a UHPC cover of 25 mm is sufficient to generate full capacity of the studs (i.e. stud shank failure) [16]. However, no studies have evaluated side cover or minimum clear distance to the edge of the concrete.

Due to the nature of the repair, the effect of the welding surface must be examined. He et al. [17] investigated the effect of interface bond between UHPC and steel by applying a grease to separate the two surfaces. It was found that the bond provides a significant increase in capacity of the shear connection. However, most push-out experiments in prior studies consist of studs welded

onto a surface with mill scale. During field implementation, it is expected that the welding surface will consist of weathered steel with surface rust. In addition, a protective paint coating may be present. Another parameter regarding weldability is the effect of the weld collar during shooting of studs. It is known that the presence of a weld collar at the base of the stud increases its shear capacity due to its bearing action onto the UHPC [18]. However, a special welding ferrule is needed to shoot the headed studs onto a vertically oriented web plate. Therefore, a further understanding of surface preparation and weldability is needed as part of the proposed repair.

Finally, the effect of UHPC curing must be studied. The influence of structural vibrations must be examined to determine if any detrimental effects are generated. In addition, since the proposed repair aims to minimize lane closures, a specialized UHPC mix design containing accelerators may be used to generate rapid strength gain. No literature was found on the influence of concrete curing under the presence of vibration or on the performance of headed studs when embedded in a UHPC with accelerated curing. This study will address these issues to develop field installation guidelines as part of the proposed repair.

Experimental Program

The experimental program consists of a series of 16 push-out experiments. Each experiment was designed to evaluate a parameter of interest. Fig. 3 shows the geometry of a typical push-out sample. The benchmark specimen consists of eight headed shear studs welded to a 9.5-mm thick web plate of a salvaged bridge girder. The studs are 12 mm in diameter and 50 mm long, spaced at 50 mm (4db) center-to-center [19]. The benchmark was designed to reflect the typical behavior of headed shear studs embedded in UHPC (i.e. stud shank failure) while ensuring other

design criteria such as shear yielding or bearing of the web plate were satisfied. The studs were embedded in a concrete slab, such that two separate panels were created on each side of the web. A 12-mm gap was maintained between the panels below the web to allow the steel section to move during the experiment without bearing on concrete. Table 1 summarizes the tested samples. The following design categories were evaluated: a) eccentric loading on studs, b) concrete variations, c) clear and side cover of studs, d) welding and surface preparation, and e) effect of traffic vibration during curing of UHPC.

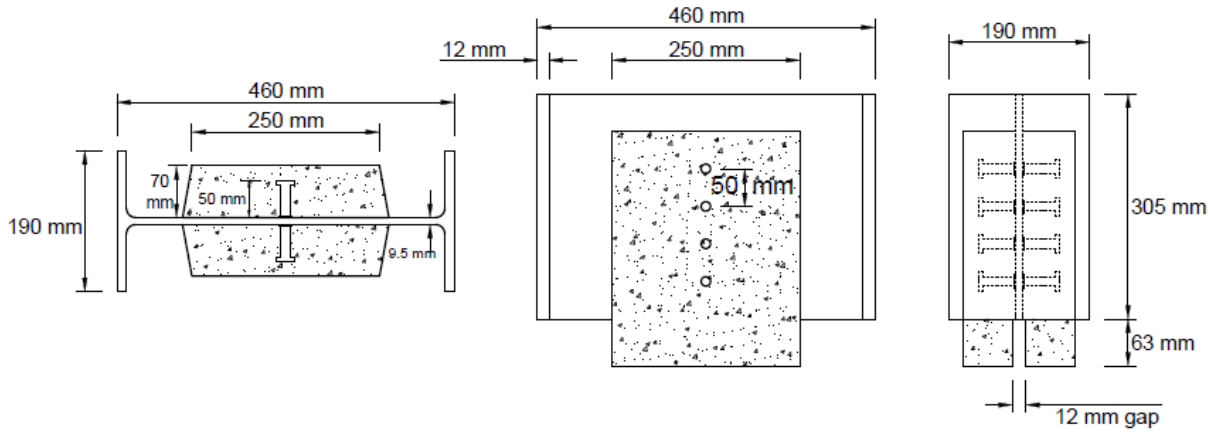

Fig. 3. Overview of benchmark push-out specimen

Table 1. Summary of push-out specimens

Design Category	Specimen ID	Concrete Mix	f'c (MPa)	Reinf.	Clear Cover (mm)	Side Cover (mm)	Eccentricity (mm)
Baseline	Baseline	UHPC-A	131	Fibers (2%)	19	125	0
Eccentricity	100mm_Ecc.	UHPC-A	134	Fibers (2%)	19	125	100
	50mm_Ecc	UHPC-A	128	Fibers (2%)	19	125	50
Concrete Variations	Unreinf. HSC	HSC	55	None	19	125	0
	Reinf. HSC	HSC	55	Steel Bars	19	125	0
	UHPC-A_Heat	UHPC-A	97	Fibers (2%)	19	125	0
	UHPC-B	UHPC-B	131	None	19	125	0
	UHPC-C	UHPC-C	176	Fibers (2%)	19	125	0
	UHPC-D	UHPC-D	148	Fibers (1%)	19	125	0
Cover	Side-Cov_25mm	UHPC-A	148	Fibers (2%)	14	25	0
	Side-Cov_50mm	UHPC-A	134	Fibers (2%)	14	50	0
	Clear-Cov_6mm	UHPC-A	145	Fibers (2%)	6	125	0
Welding/Surf. Prep	Paint	UHPC-A	137	Fibers (2%)	19	125	0
	Unbonded	UHPC-A	149	Fibers (2%)	19	125	0
	V. Ferrule	UHPC-A	148	Fibers (2%)	19	125	0
Vibration	Vibration	UHPC-A	145	Fibers (2%)	19	125	0

Experimental Setup and Loading Protocol

The experimental setup and loading protocol was consistent for all samples. The push-out specimen was tested using an 1800-kN compressive testing machine with an MTS Controller [20]. Each sample was mounted such that the concrete panels were resting on a 250-mm spherical bearing. The loading was applied from the top platen of the machine to the flanges of the steel section to prevent local buckling of the web. The applied force was resisted by the studs, which were embedded in the concrete panels. Fig. 4 shows the experimental setup. Each push-out experiment was conducted using a series of cyclic loadings to understand the damage development. For the first four steps, the sample was loaded in increments of 15% of its theoretical capacity and unloaded to 4.5 kN. These increments were applied to observe the behavior of the

studs in the elastic region. The specimen was unloaded to 4.5 kN to prevent disengaging of the sample. After unloading from 60% capacity, displacement control was used to continue the cycles in the plastic region with a similar load rate until the sample failed.

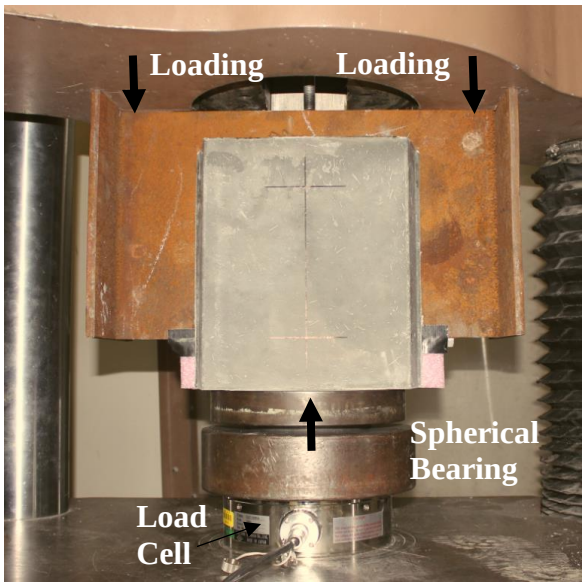

Fig. 4. Experimental setup for push-out test

Material Properties

The headed studs and base steel section were tested to extract the stress vs. strain characteristics. To make coupons out of the studs, the stud head was removed, and the stud shank was machined into a dog-bone shape. The base steel section was simply cut and machined into larger dog bones as outlined in ASTM E8 [21]. The coupons were tested in uniaxial tension at a strain rate of 0.015 mm/mm/min. For the headed studs, strain was captured using a high-elongation strain gauge, which was installed in the throat of the coupon. Since the beam section coupons were larger, an extensometer was used with a measurement length of 100 mm. The stress vs. strain responses are shown in Fig. 5.

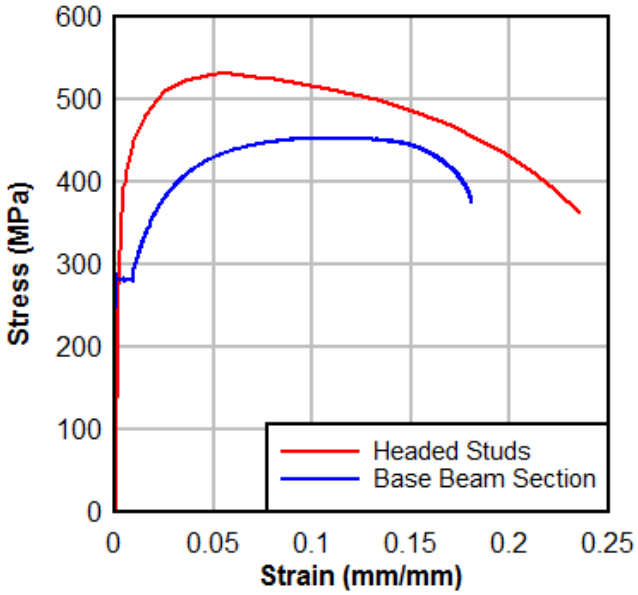

Fig. 5. Typical uniaxial tensile behavior for steel materials

The four UHPC mix designs used in these experiments are produced by Lafarge Holcim [22]. The first, and most commonly used, mix in this series is commercially available as Ductal JS1212 (UHPC-A), a UHPC mix tailored for accelerated strength development [23]. UHPC-A consists of a premix powder (a blend of cement, silica fume, silica powder, and sand), water, two high-range water reducers (HRWR), an early age accelerator, and high-strength steel fibers (2% by volume). The steel fibers are 0.2 mm in diameter and 12 mm long, specified for a minimum tensile strength of 2,000 MPa. UHPC-B is the same mix design as UHPC-A, but does not contain fibers. UHPC-C is commercially available as Ductal JS1000 and is similar to UHPC-A without accelerated strength development. UHPC-D is the same mix design as UHPC-A, except the fiber content is reduced to 1% by volume. The high-strength concrete (HSC) mix consists of cement, fine aggregate able to pass through a 10-mm sieve, water, and super plasticizer. The water-to-

cement ratio for this mix is 0.41. The composition by weight for all concrete materials is shown in Table 2.

Table 2. Concrete compositions

(a) UHPC				
% by Weight				
Batch	UHPC-A	UHPC-B	UHPC-C	UHPC-D
Premix	86.6	92.32	87.5	89.4
Water	5.1	5.44	5.1	5.3
HRWR1	0.7	0.75	1.2	0.7
HRWR2	0.5	0.53	0	0.5
Accelerator	0.9	0.96	0	0.9
Steel Fibers	6.2	0	4.4	3.2
28-Day f'_c (MPa)	149	131	176	148

(b) HSC	
% by Weight	
Batch	HSC
Water	16.9
Cement	40.7
Fine Agg.	42.2
HRWR1	0.027
28-Day f'_c (MPa)	55

Push-Out Specimens

Eccentric Loading on Studs

When the repair method is implemented on a bridge, it is possible that the headed studs may experience eccentric loading or an induced moment. To validate the performance under these conditions, two samples were fabricated with a stud offset (e) of 50 mm and 100 mm from the center of the web plate (Fig. 6). The UHPC panels were cast in the middle of the web plate similar to the benchmark specimen. Since the UHPC panels were centered and the studs were offset, a moment was introduced onto the studs. Rotation of the panels was allowed through the spherical bearing during testing.

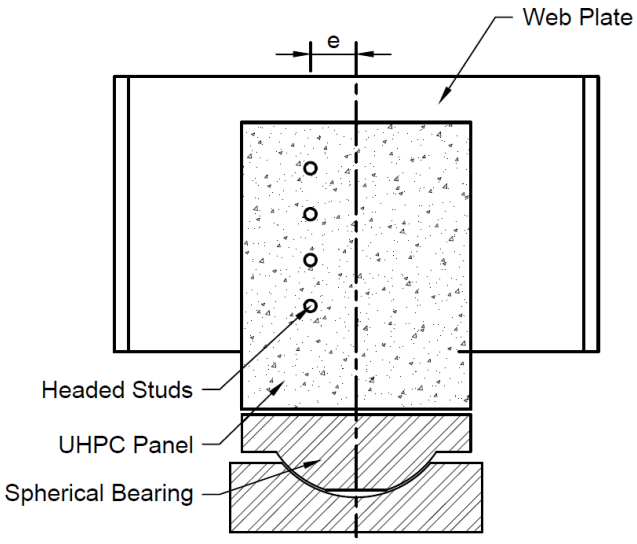

Fig. 6. Overview of eccentric sample

Concrete Variations

Cost is the main driving factor behind embedding the headed studs in a material other than UHPC. UHPC is a cementitious, concrete material that has a minimum specified compressive strength of 150 MPa with specified durability, tensile ductility and toughness requirements; fibers are generally included to achieve specified requirements [24]. Although UHPC exhibits excellent mechanical properties, it is approximately 20 times more expensive than conventional concrete due to the proprietary nature, increased quality control, and high cost of materials. Further, the fibers that are responsible for accommodating tensile forces in the UHPC account for up to 63% of its cost [25]. Bridge owners may opt for a cheaper material, such as HSC, UHPC without fibers, or a less expensive UHPC, in an effort to reduce the repair cost.

To validate the use of these concrete materials, four push-out samples were fabricated with studs embedded in: a) unreinforced HSC, b) reinforced HSC, c) UHPC-A_Heat, d) UHPC-B (no

fibers), e) UHPC-C (increased setting time), and f) UHPC-D (1% fiber volume fraction). Each sample contains the benchmark geometry as shown in Fig. 4. For the reinforced HSC sample, a reinforcement cage was placed into the panels. The reinforcement cage was fabricated by splicing several #3 bars with 90° hooks on each end with sufficient development length. The #3 bars were chosen because of the tight constraints in the concrete panel. The reinforcement was placed with a 32-mm offset from the web such that the cage was resting 6 mm below the stud head. To investigate the efficiency of the setup, the geometry of the concrete panels was kept consistent for all samples. A schematic of the reinforced HSC specimen is shown in Fig. 7.

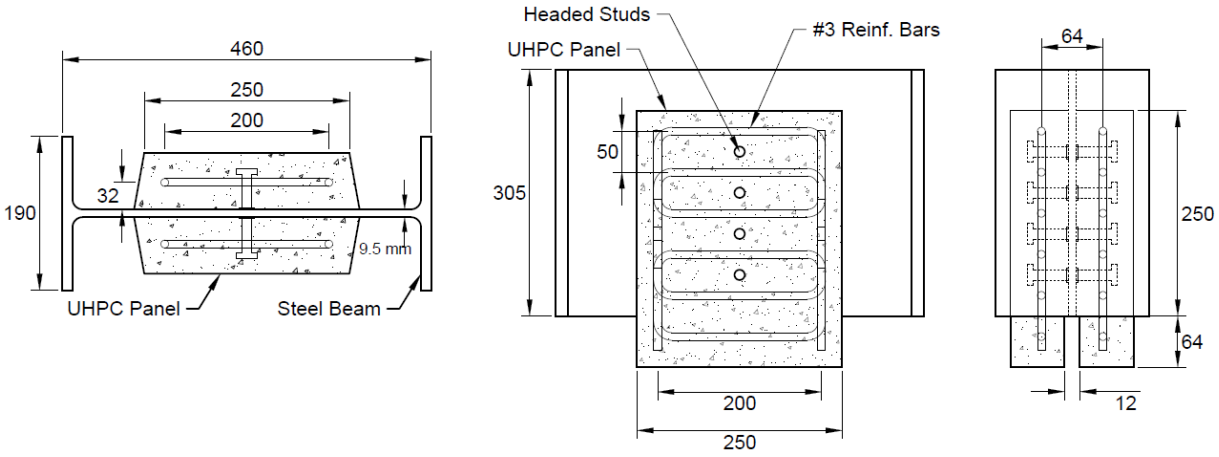

a) Plan view b) Elevation c) Cross section

Fig. 7. Schematic of reinforced HSC sample with rebar cage

Cover of Studs in UHPC

Cover is one of the most critical aspects of embedding steel components in concrete. Clear cover is important in reinforced concrete structures to a) ensure that corrosion does not penetrate through the concrete and expose the reinforcement to chlorides, b) to act as a fire protection coating, and c) to prevent blow-out or spalling of the concrete due to flexural action of the reinforcement. Side cover is essential to ensure that enough concrete material is present to allow the forces generated from the reinforcement to develop into the concrete without disturbing their load path. Three push-out samples were tested to investigate the stud performance with a side cover of 25 mm and 50 mm from the center of the stud shank (Fig. 8). To fabricate the side cover sample, precast UHPC panels were created with an opening in the center to contain the studs. The openings for the 25-mm and 50-mm side cover samples were 50 mm x 64 mm and 100 mm x 64 mm, respectively. Here, the clear cover for the studs was 14 mm. The panels were pressed against the web plate of the steel beam such that the opening surrounded the studs. Next, UHPC was poured into the openings of the precast panels to create a column of studs embedded in UHPC with the dimensions of the respective opening. The purpose of the precast panels was two-fold: 1) they served as formwork for the inner core of the UHPC and 2) they acted as stabilizing elements during testing. Due to the weak bond between the precast panels and the inner core, the inner core acted independently, allowing for evaluation of the side cover. To evaluate clear cover, custom forms were fabricated and placed against the web plate such that two independent UHPC panels were created with a similar geometry to the benchmark. This time, the panels were approximately 56 mm instead of 70 mm thick to provide a clear cover of 6 mm.

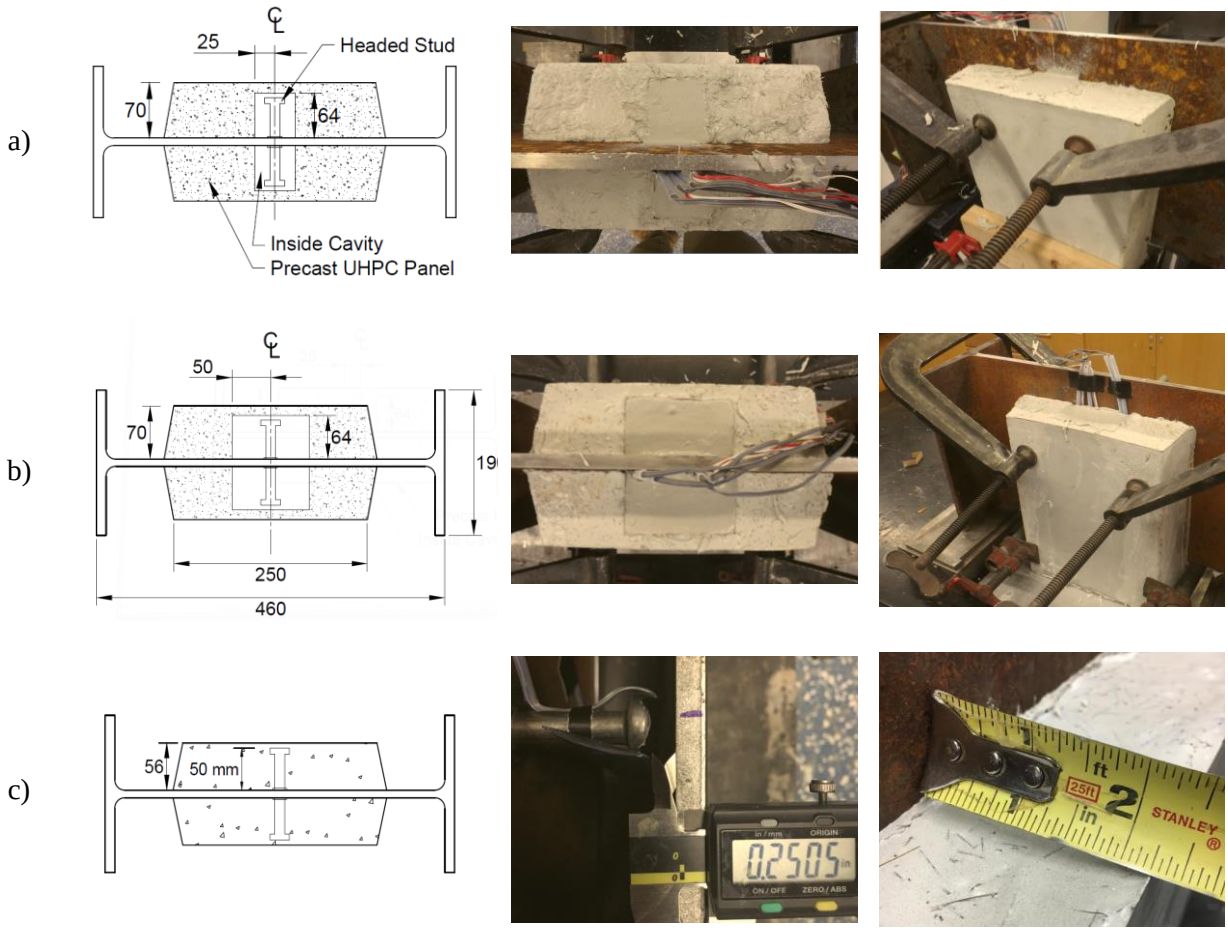

Fig. 8. Specimens for UHPC cover: a) 25-mm side cover, b) 50-mm side cover, c) 6-mm clear cover

Welding/Surface Preparation

The most common and efficient method of welding headed shear studs is using a stud gun. First, the stud is loaded into the chuck of the stud gun. Next, a ceramic or clay ferrule is placed at the tip. The stud is positioned at the desired location with the ferrule in touch with the base material. During the welding process, a current is sent through the stud, which creates an arc, melting the stud and parent material at the interface. Then, the stud is rapidly lifted off the base material and

plunged back into the pool of molten metal. The ferrule acts as a form to contain the pool of metal until it hardens. The welding process is illustrated in Fig. 9.

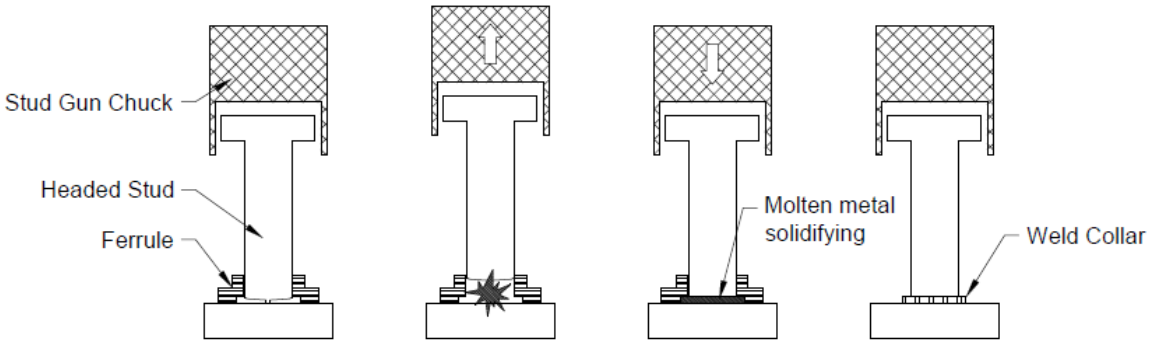

Fig. 9. Procedure for shooting headed studs

The shape of the weld collar is dependent on the geometry of the ferrule and the induced current. The geometry of the ferrule may vary based on the orientation of the welding surface. A ferrule for horizontal surfaces is typically circular with small openings along its perimeter to allow for some discharge of the molten metal (Fig. 10a). A ferrule for vertical applications is completed closed along half of its perimeter to prevent leakage during the hardening process (Fig. 10b). Naturally, these two ferrules will produce weld collars of varying shapes. All specimens in this study were welded using a ferrule for horizontal welding applications. Since the proposed repair entails welding studs onto a vertically oriented surface, a push-out specimen was tested with studs welded using vertical-surface ferrules to validate their performance.

a) Horizontal surface ferrule

b) Vertical surface ferrule

Fig. 10. Ferrule types for welding orientation

The effect of surface preparation of the web plate is another parameter that is evaluated as part of the proposed bridge repair. Avoiding or minimizing removal of the existing protective paint from the girder may result in significant savings of time and cost. Therefore, two push-out specimens were designed to investigate the effect of surface bond. One sample contained a web plate coated with a two-part epoxy-based paint specified for cathodic protection of steel bridge girders [27]. An attempt was made to weld the headed shear studs directly onto the painted surface. However, the layer of paint prevented proper formation of the weld arc, which produced an inadequate weld collar. Therefore, a sample was fabricated with the paint locally scraped off at the locations where studs were expected to be welded (Fig. 11a). The studs were successfully welded in the desired locations and a benchmark sample was cast. Another specimen was designed to investigate the "unbonded" state between the UHPC panels and the web plate. To prevent bonding, the web plate was covered with a layer of paraffin prior to casting (Fig. 11b). The solidified paraffin ensured no contamination to the UHPC mix.

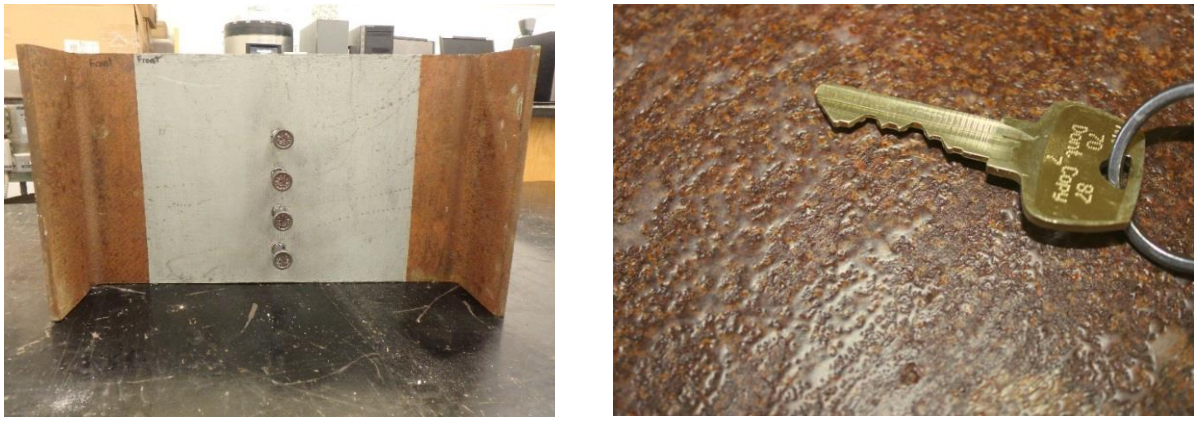

a) Painted web plate b) Unbonded web plate using paraffin

Fig. 11. Ferrule types for welding orientation

Curing of UHPC

A unique advantage of the proposed repair is quickness and ease of installation. To further reduce the implementation time, a high early-age strength UHPC is used to generate a high bearing capacity shortly after casting. To validate the strength gain at early age, a push-out sample was cast with UHPC-A and cured in a heat chamber at 49°C for 12 hours (Fig. 12a). After 12 hours of heat curing, the specimen was removed from the chamber and immediately installed in the machine for testing. Compressive strength gain was recorded as a function of curing time (Fig. 12b), reaching approximately 97 MPa after 12 hours of curing.

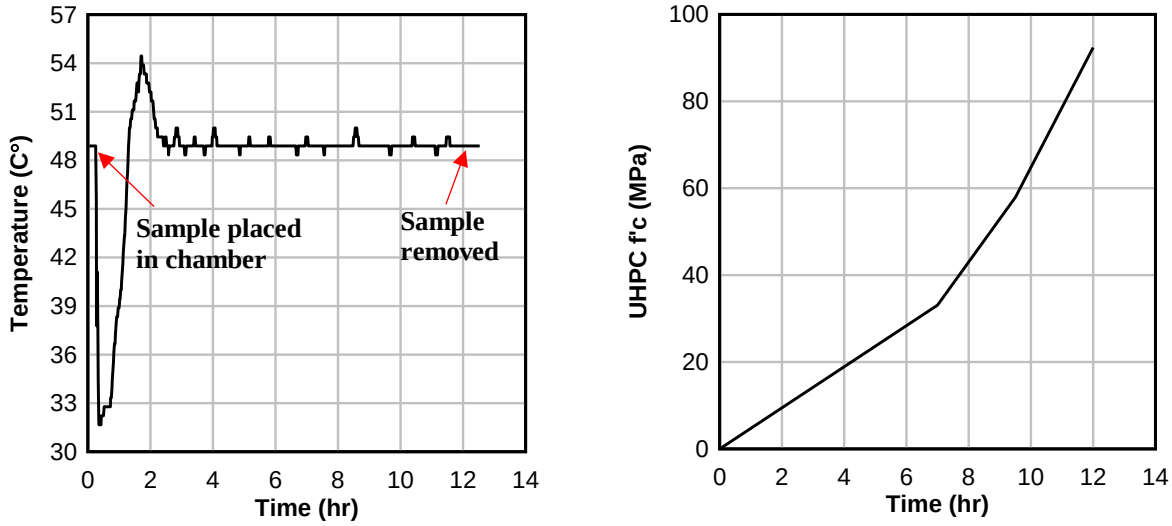

a) Temperature of UHPC during heat curing b) Strength gain vs time

Fig. 12. Heat curing of UHPC-A

Another investigation parameter of interest is the effect of vibration on the stud-UHPC performance. To adhere to the physical scenario that may be expected in the field, vehicular vibration data was collected from an in-service bridge composed of a rolled steel girder superstructure with steel bearings. First, accelerometers were placed at the top flange of the girder near the bearing region. Acceleration data was collected as vehicles of various classes crossed the expansion joint. Since the bridge was skewed, each vehicle produced four distinct peaks of acceleration which represent each tire driving over the expansion joint (Fig. 13a). Next, the accelerations were replicated using an LDS V408 electro-dynamic mass shaker with a frequency range up to 9 KHz [26]. Acceleration time histories from 16 different vehicles were used. The accelerations were induced onto the steel beam by attaching the mass shaker to an adapter plate, which was welded to the beam. The data was sent from the computer, through an amplifier, and finally to the mass shaker which was mounted on top of the sample (Fig. 13b). Another accelerometer was attached to the beam to ensure that the accelerations induced on the beam were

representative of those found in the field. The mass shaker induced the vibration onto the steel beam for 3 hours after casting.

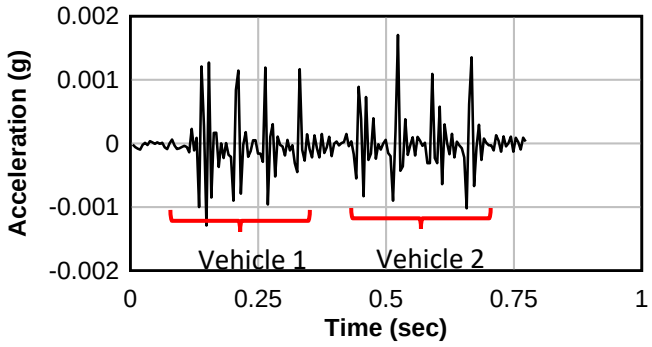

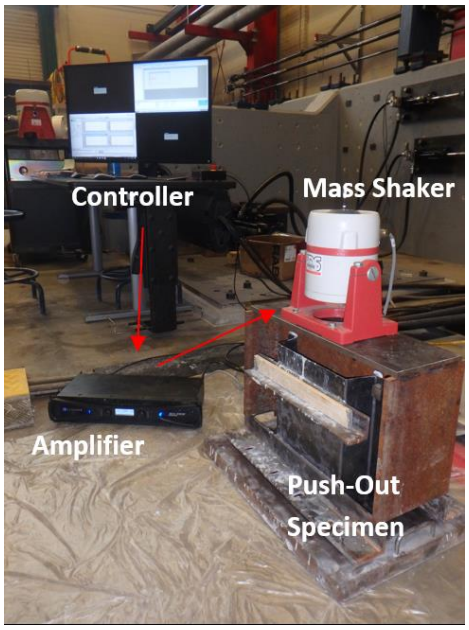

a) Time history of acceleration data b) Casting of UHPC during vibration

Fig. 13. Simulation of truck vibration

Results and Discussion

The results from each push-out experiment were compared against the benchmark sample to determine the effect of each parameter. Values such as elastic shear stiffness, yield slip, ultimate slip, yield force and ultimate force per stud as defined in [9] are shown in Fig. 14. Elastic shear stiffness, an important parameter in the design of composite structures, was calculated using the slope of the secant line of the force-slip curve until one-third of the overall force of the stud [17]. The yield point was computed by extending a line with a 0.1-mm offset from the origin at a slope of 220 kN/mm. The yield slip and yield force were computed at the point of intersection between the extended line and the force-slip curve. The ultimate slip was recorded just prior to rupture of

the stud shank. The ultimate force per stud was calculated as the maximum load bearing capacity of the sample divided by the number of studs. The per-stud capacity of each specimen was normalized by the capacity of the benchmark sample as comparison. The results are shown in Table 3.

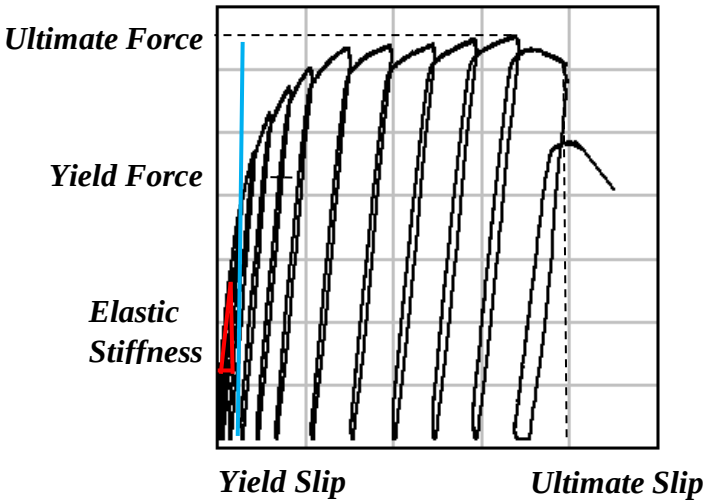

Fig. 14. Sample force vs. slip curve with cycles

Table 3. Summary of experimental results

Specimen ID	f'c	Elastic Stiffness	Yield Slip	Yield Force	Ultimate Slip	Ultimate Force	Pu/Baseline
Unit	MPa	(kN/mm)	(mm)	(kN)	(mm)	(kN/stud)	kN/kN
Baseline	131	216	0.32	46.8	4.97	67.5	1.00
100mm_Ecc.	134	64.0	0.15	9.53	---*	22.1	0.33
50mm_Ecc	128	122	0.26	33.4	14.6	62.7	0.93
Unreinf. HSC	55	173	0.25	33.3	0.98	46.1	0.68
Reinf. HSC	55	175	0.28	36.6	9.44	47.1	0.70
UHPC-A_Heat	97	232	0.31	45.3	4.73	68.2	1.01
UHPC-B	131	167	0.31	44.4	2.50	51.6	0.77
UHPC-C	176	199	0.45	52.9	3.93	72.7	1.08
UHPC-D	148	208	0.40	52.1	4.69	75.6	1.12
Side-Cov_25mm	148	120	0.18	16.6	7.51	46.6	0.69
Side-Cov_50mm	134	127	0.41	37.8	6.37	68.4	0.91
Clear-Cov_6mm	145	233	0.23	49.1	4.95	69.6	1.03
Paint	137	165	0.29	41.1	4.48	65.2	0.97
Unbonded	149	147	0.41	44.2	4.92	73.8	1.09
V. Ferrule	137	228	0.61	71.2	5.22	80.3	1.19
Vibration	148	173	0.28	47.7	4.64	77.7	1.15

Eccentric Loading on Studs

The average stud capacities for the samples with an eccentricity of 50 mm and 100 mm, 62.7 kN and 22.14 kN respectively, were significantly lower compared to the benchmark of 67.5 kN. Fig. 15a shows the force vs. slip relationship for both samples. In Fig. 15a, the black curves show the average slip, which is observed in the middle of the UHPC panels. Much less slip is experienced at the corner of the UHPC panels closest to the studs. Due to the rotational effect, the opposite corner experienced much larger slip, as illustrated by the blue and green lines for the respective 50-mm and 100-mm eccentric samples. Fig. 15b shows that the ultimate slip (approximately 6 mm) experienced at the centerline of the studs is comparable to the benchmark sample.

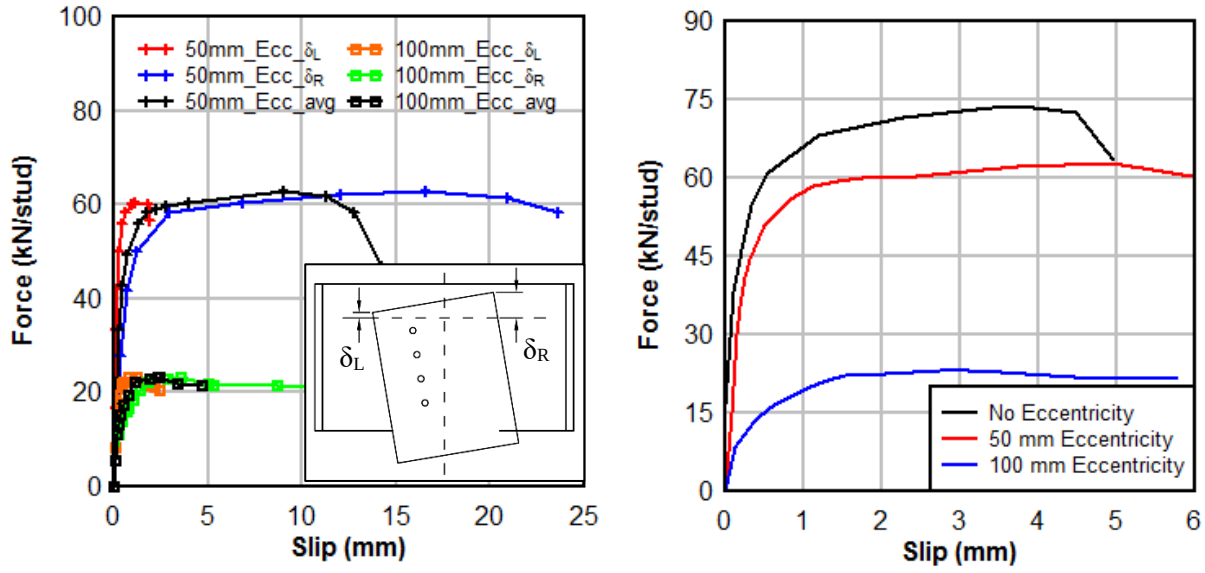

a) Slip measured at corners of panel b) Slip measured at center line of studs

Fig. 15. Force vs. slip behavior for eccentrically loaded studs

Fig. 16 shows the force vs. rotation relationship for the 50-mm eccentric sample, which illustrates the loading sequence on each group of studs. Fig. 16 shows that the rotation is minimal in the elastic stage (i.e. rotations less than 1°). An increase in force leads to an increase of rotation and thus displaces the outside studs more than the inside studs. Here, the outside studs are defined as the top and bottom-most studs and the inside studs are the two middle studs (closest to the center). At point A, the outside studs yield, which reduces the rotational stiffness. At point B, the inside studs yield, further reducing the stiffness. Point C indicates rupture of the outside studs. This becomes apparent as the capacity of the system is significantly lower at the next cycle. Finally, the two inside studs rupture at point D.

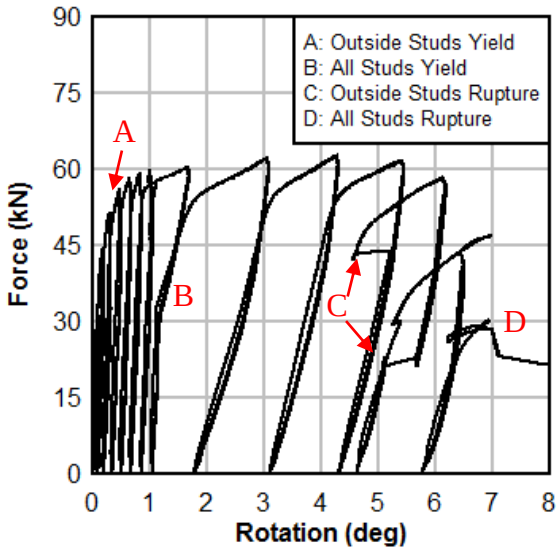

Fig 16: Yielding and rupture sequence of studs

The sequence of stud rupture is further analyzed through the instantaneous center of rotation (ICR) method. The instantaneous center of rotation method is applicable to this scenario because it accounts for translation and rotation of the stud group, whereas elastic analyses account for only one or the other. In this case, two force components act on the studs: 1) an upward (longitudinal) component that balances the reaction force and 2) an angled component balancing the induced moment. The studs rotate around their ICR, which is a distance e' away from the center of gravity (CG) of the stud group (Fig. 17).

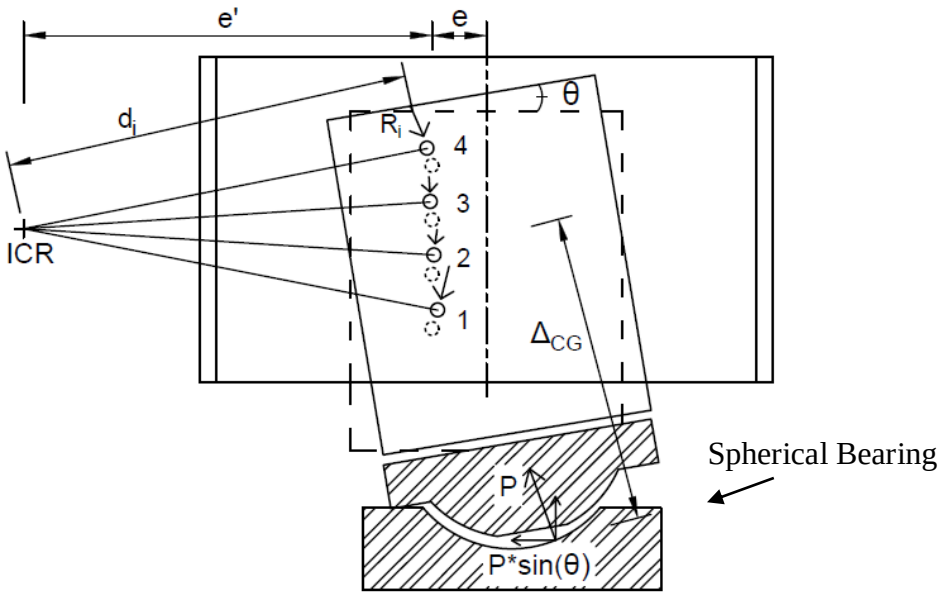

Fig 17. Schematic for instantaneous center of rotation (ICR) calculation

Throughout the loading sequence, the studs resist the loading according to their distance to the ICR of the system. Since the inner studs are closer to the ICR, they will experience smaller displacements and thus smaller forces. The ultimate shear force that one 12-mm stud can resist is dependent on the experimental force vs. slip curve generated by the benchmark sample (Fig. 18). The following equation for the load-deformation relationship of a single bolt was adopted to create the closed-form equation for the force-slip relationship of a single 12-mm stud:

$$R_i = Pu(1 - e^{-\alpha\delta})^{\beta} \qquad (1)$$

, where i is the stud designation, Pu is the ultimate shear capacity of one stud (assumed as the benchmark stud capacity from Table 3) and δ is the slip experienced by the stud. For presentation of calculations, the studs were labeled in chronological order assuming the bottom-most stud is "stud 1" and so on. Curve fitting was used to calibrate the empirical factors α and β

which control the shape of the curve. It was found that a value of -2.143 and 0.6251 for α and β, respectively, generate good agreement with the experimental curve for 12-mm studs.

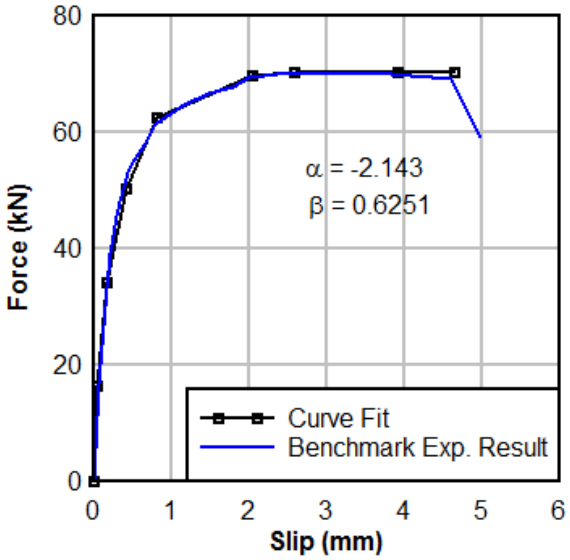

Fig 18. Curve fitting of force-slip relationship for one single 12-mm stud

To calculate the theoretical slip of each stud, it was assumed that each stud experiences a slip proportional to the ratio of its distance from the ICR (d_i) to the largest distance in the stud group (d_{max}). That ratio was multiplied by the maximum slip of one single stud (5.00 mm) to generate the theoretical resultant slip of each stud (δ_i). Next, equation (1) was used to generate the resultant force (R_i) experienced by that stud. In addition, the horizontal force component generated from the spherical bearing ($P \cdot \sin(\theta)$) must be added since it contributes to the moment resistance of the stud group. Finally, the total load-bearing capacity of the stud group can be predicted using the following formula:

$$P_{total} = \frac{P \sin(\theta)\, \Delta_{CG} + \sum R_i d_i}{e' + e} \qquad (2)$$

, where P is the resultant load-bearing force, α is the angle of panel rotation, Δ_{CG} is the distance between the CG of the stud group and the location of the reaction force, R_i is the resultant force generated by each stud, d_i is the distance of each stud from the ICR, e is the eccentricity of the studs from the centerline of the loading, and e' is the distance from the centerline of the studs to the ICR. In this scenario, it was found that the ICR was approximately 114 mm from the CG of the stud group. The results of the calculations are presented below.

Table 4. Calculations for ICR method

50 mm Eccentricity (Exp. Capacity for Stud Group: 250.8 kN)													
Stud	Location CG		Location ICR		d_i	δ_i	R_i	R_i*d_i	ΣR_i*d_i	$P\sin(\theta)\Delta_{CG}$	$\frac{P\sin(\theta)\Delta_{CG}+\sum R_i d_i}{e'+e}$	$\sum\frac{R_i*x_i}{d_i}$	ICR
	x	y	x_i	y_i									
	mm	mm	mm	mm	mm	mm	kN	kN*mm	kN*mm	kN*mm	kN	kN	mm
1	0	76.2	114	76.2	137.1	5.00	70.00	9599	35548	6161.8	253.1	253.0	114
2	0	-25.4	114	-25.4	116.8	4.26	70.00	8176					
3	0	-25.4	114	-25.4	116.8	4.26	70.00	8176					
4	0	-76.2	114	-76.2	137.1	5.00	70.00	9599					

100 mm Eccentricity (Exp. Capacity for Stud Group: 88.4 kN)													
Stud	Location CG		Location ICR		d_i	δ_i	R_i	R_i*d_i	ΣR_i*d_i	$P\sin(\theta)\Delta_{CG}$	$\frac{P\sin(\theta)\Delta_{CG}+\sum R_i d_i}{e'+e}$	$\sum\frac{R_i*x_i}{d_i}$	ICR
	x	y	x_i	y_i									
	mm	mm	mm	mm	mm	mm	kN	kN*mm	kN*mm	kN*mm	kN	kN	mm
1	0	76.2	25.5	76.2	80.35	0.50	56.03	4502	12227	431.1	99.6	99.0	25.5
2	0	-25.4	25.5	-25.4	35.99	0.22	44.78	1612					
3	0	-25.4	25.5	-25.4	35.99	0.22	44.78	1612					
4	0	-76.2	25.5	-76.2	80.35	0.50	56.03	4502					

The iterative procedure outlined through the ICR method shows reasonable agreement to the experimental results obtained from the push-out tests when the location of the ICR is converged such that the resultant force generated from the studs equals the vertical resultant force. After several iterations, the location of the ICR was found to be at a distance of 114 mm and 25.5 mm from the centerline of the studs for the 50 mm and 100 mm eccentricities, respectively. This

correlates to a theoretical capacity of 253 kN and 99.6 kN for the respective stud groups. These predicted capacities are comparable to the experimental forces of 250 kN (50 mm eccentricity) and 88.4 kN (100 mm eccentricity). A larger discrepancy is observed when a higher eccentricity is introduced, possibly due to the boundary conditions having a more significant effect at higher rotations.

To further validate the use of the ICR method, the directional shear planes generated by the weld collars were analyzed. Since the ICR provided a reasonable estimate of the experimental capacity, the resultant vector of each stud should correlate with the normal projection of the weld collar shear planes. Fig. 19 shows the failed push-out specimen with an emphasis on the failure plane at the UHPC panel. The weld shear planes generated on the UHPC panel from the weld collars are shown in Fig 19b. Using computer-aided drafting, the ICR was drawn to scale, with the failed specimen containing a 50-mm eccentricity (the 100-mm eccentric sample was not analyzed as the spherical bearing reached its displacement limit at higher rotations). Lines were extended to the center of each stud to compare the angles between the shear planes generated by the weld collars and the ones theoretically calculated using the ICR method. The top and bottommost studs exhibit a more skewed shear plane, whereas the two inner studs show a failure plane that is more parallel to the loading direction. It is observed that the calculated ICR shows a reasonable projection of the weld collars when extending a normal line from the center of the studs.

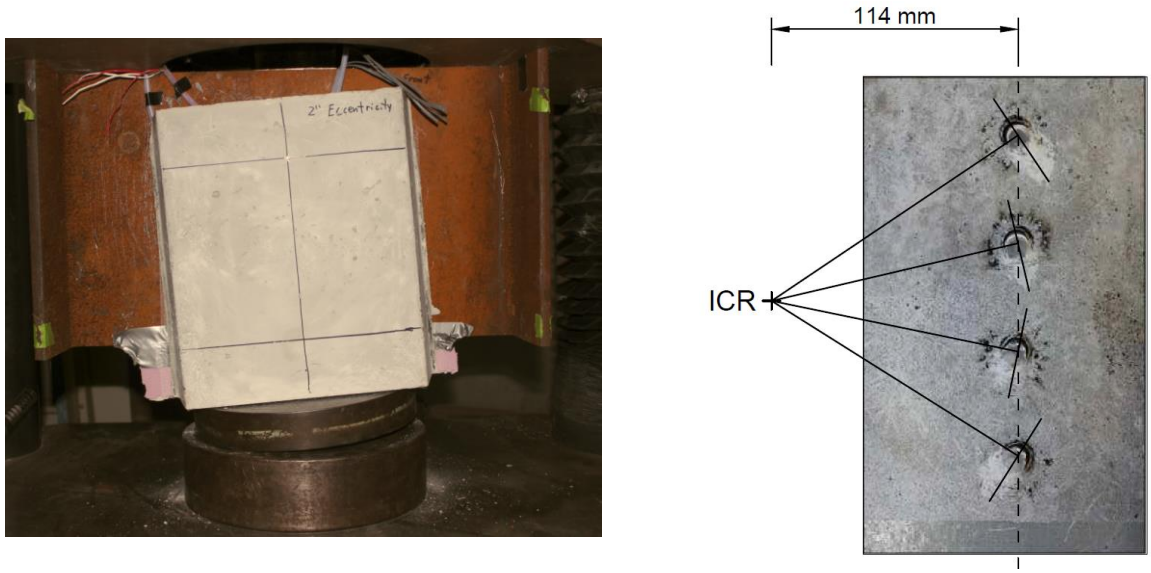

a) Failure of 50-mm eccentric sample b) Shear planes from weld collars

Fig. 19. Failed eccentric sample and UHPC panel interface

5.2. Concrete Variations

Stud shear capacity and shear ductility have been defined as the two design criteria required for an acceptable repair parameter. The strength criterion here is based on the minimum design capacity as outlined by AASHTO (66 kN for a 12 mm diameter stud). The ductility criterion is based on the minimum expected slip achieved by the benchmark sample. Eurocode-4 specifies a minimum slip of 6 mm for a connection to be classified as "ductile" [27]. However, it is known that headed studs in UHPC do not satisfy that criteria because of the stiffness and strength of the UHPC, which does not crush to generate flexure of the studs. Therefore, the ductility criterion in this study is defined as sustaining 90% of the capacity over a slip range of 4 mm. Since the outlined criteria demand sufficient strength over a relatively large slip range (i.e. plastification of the headed studs), a ductile failure mode is required for a parameter of interest to be accepted.

Fig. 20 shows the force vs. slip summary for all concrete variations tested, including the benchmark sample for comparison. The samples with unreinforced high-strength concrete (HSC) panels exhibited a brittle failure mode via longitudinal panel splitting due to the transverse tensile force component at the headed studs [28]. This resulted in a stud capacity of 46.1 kN/stud, a maximum slip of 0.72 mm and thus, did not satisfy the strength and ductility criteria. A similar result was achieved from the sample containing UHPC panels with no continuous reinforcement or fiber reinforcement (UHPC-B). This sample generated a capacity of 51.6 kN/stud, a maximum slip of 0.94 mm prior to failure and therefore, did not satisfy the strength and ductility criteria. The reinforced HSC showed significantly improved ductility (slip of 9.44 mm), as the reinforcement in the panels allowed tensile stress transfer across the splitting cracks. Local crushing and separation of concrete was the governing failure mode, due to insufficient concrete cover and crowded reinforcement arrangement. Therefore, the strength criterion (66 kN/stud) was not satisfied here.

All samples with fiber-reinforced UHPC panels generated acceptable strength and ductility. When an alternative mix design (UHPC-C) is used with a 2% fiber fraction, the ultimate capacity is 72.7 kN/stud with a corresponding ultimate slip of 3.93 mm. UHPC-D, which contained fiber-reinforced UHPC panels with a 1% fiber fraction, also generated sufficient strength and ductility (75.6 kN/stud and 4.69 mm respectively). These results indicate that the presence of fibers is crucial to accommodating the splitting forces generated in the panel. All failed samples are presented in Fig. 21.

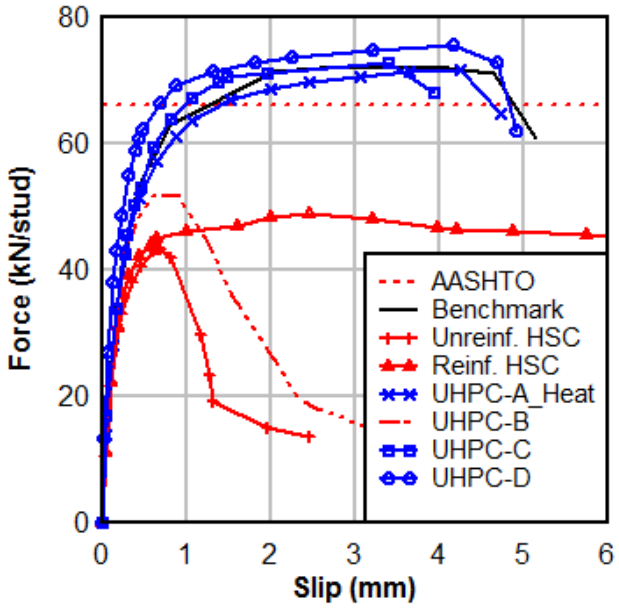

Fig. 20. Force vs slip summary for concrete variations

a)

b)

c)

d)

e)

f)

Fig. 21. Failed specimens: a) Unreinforced HSC, b) Reinforced HSC, c) UHPC-B, d) UHPC-A_Heat, e) UHPC-C and f) UHPC-D

The strain demand on the web plate varied significantly based on the type of concrete material used. When unreinforced HSC or UHPC is used, the maximum web strain is 1,040 με and 1,700 με, respectively. However, when a fiber reinforced UHPC with a 2% fiber content is used, the maximum strain in the web plate increases to 9250 με. The web plate experiences this strain just prior to yielding of the studs. Once the studs yield, little to no additional strain accumulation is observed in the web (Fig. 22a). However, there is no mechanism in the unreinforced samples to accommodate the tensile splitting action in the concrete panels. The backbone curves for fiber-reinforced UHPC, unreinforced UHPC and unreinforced HSC are shown in Fig. 22b.

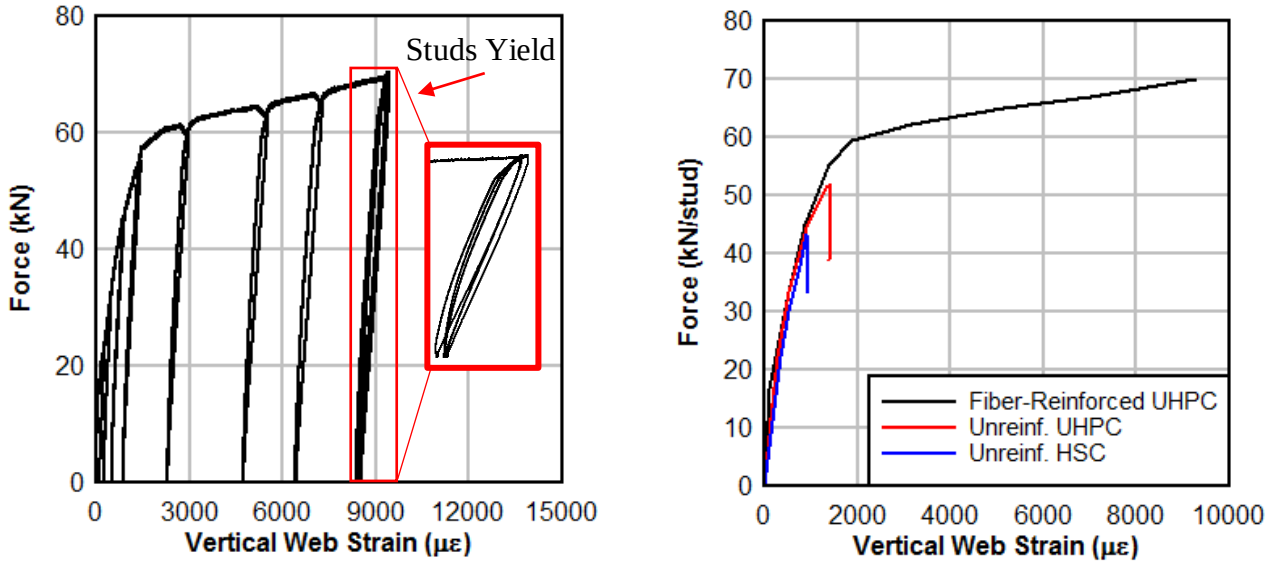

a) Strain accumulation in web plate for UHPC sample

b) Backbone strain accumulation for all samples

Fig. 22. Strain demand on web plate for studs embedded in UHPC

5.3. Cover of Studs in UHPC

The force vs. slip curves for all specimens used to evaluate cover are shown in Fig. 23. The figure shows that a 25-mm side cover does not generate adequate strength or ductility, as the

sample failed prematurely via UHPC splitting in the inner core (Fig. 24a). This is likely due to an inadequate area of UHPC to accommodate the tensile splitting generated from the studs. However, when a side cover of 50 mm is implemented, the splitting forces are resisted by the increased area of concrete which is sufficient enough to shift the failure mode to rupturing of the studs (Fig. 24b). When a clear cover of 6 mm was evaluated, full plastic capacity was achieved, as characterized by the consistent failure mechanism and by strength and ductility consistent with the benchmark sample (Fig. 24c).

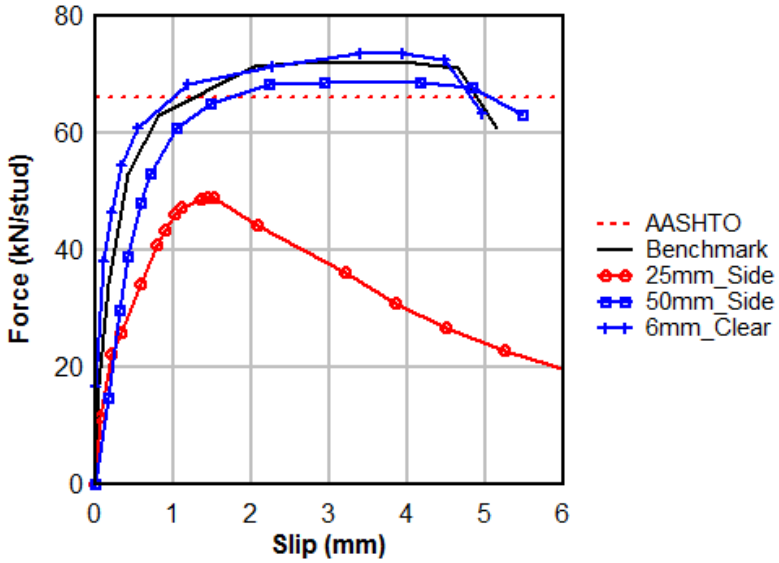

Fig. 23. Force vs. slip summary for cover evaluation

a)

b)

c)

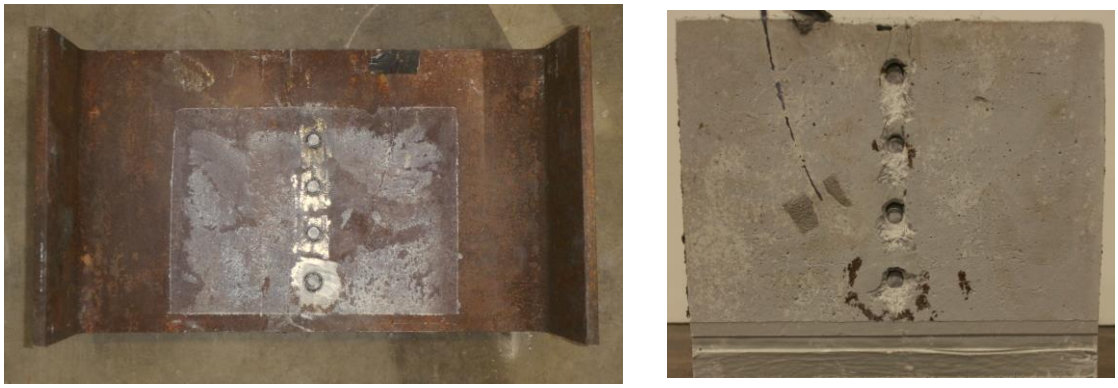

Fig. 24. Failed cover specimens: a) 25-mm side cover, b) 50-mm side cover, c) 6-mm clear cover

5.4. Welding/Surface Preparation

Fig. 25 shows the force vs. slip curve for the specimens designed to evaluate the effect of weldability and surface preparation. The studs which were welded with a ferrule for vertical applications generated a significantly higher capacity than all other samples, including the benchmark. This may be attributed to a significantly larger weld collar produced by the special ferrules. When a ferrule for horizontal applications is used, the weld collar diameter and height are approximately 1.40 and 0.14 times the diameter of the stud. However, the ferrule for vertical applications generated an average weld collar diameter and height of 1.42 and 0.22 times the diameter of the stud. This increase in weld collar geometry significantly increases the bearing area at the shear interface. For specimens which evaluated the effect of surface bond, no detrimental effects were observed when the web plate was "unbonded" from the UHPC with the applied wax coating. The strength and ductility performance of the unbonded sample is comparable to that of the benchmark. When a coating of paint was applied on the web plate, the force dropped slightly at later stages of shear deformation (beyond 3 mm).

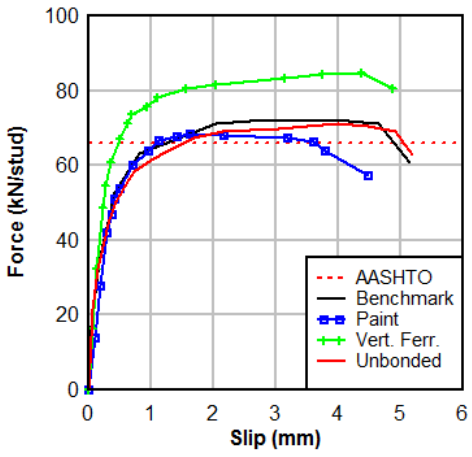

Fig. 25. Force vs. slip behavior for welding/surface preparation samples

5.5. Curing of UHPC

Fig. 26 shows the force vs. slip curve for the vibrated sample. It is observed that no loss in strength or ductility occurred due to the presence of vibration during UHPC curing. These results demonstrate the flexibility of the proposed repair method, as full plastic capacity of the studs can be achieved with as little as 12 hours of heat curing of the UHPC, if the mix design is appropriate. Additionally, the presented data proves that there are no detrimental effects from vibrations at the bearing region since full strength and ductility was achieved with no damage to the UHPC panels.

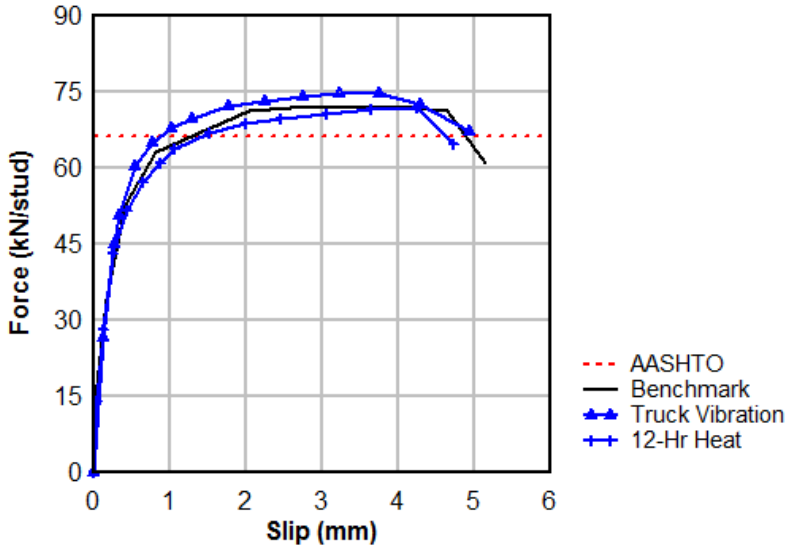

Fig. 26. Results for UHPC curing conditions

6. Conclusions

The following conclusions can be made from this study:

- When eccentric loading is applied to headed studs, their capacity decreases due to shear and moment interaction. An eccentricity of 50 mm and 100 mm generated a normalized stud capacity of 0.92 and 0.33 respectively compared to the benchmark sample.
- When a stud group is embedded in UHPC and eccentrically loaded, its capacity can be predicted using the instantaneous center of rotation (ICR) method. Using this iterative process, good agreement was achieved when comparing the theoretical capacity to the experimental results.
- The benchmark stud arrangement gained full capacity when the studs were embedded in fiber-reinforced UHPC containing a minimum fiber content of 1%, with no additional reinforcement.
- When studs are embedded in unreinforced HSC or UHPC, brittle failure of the concrete panels governs, with no ductility of the studs. When the studs are embedded in a small panel of reinforced HSC, concrete failure still governs but the studs exhibit yielding, and thus, more ductility. Neither of these materials are recommended for the proposed repair.
- If needed, alternative fiber-reinforced UHPC mix designs may be used to extend the workability time or promote high early-age strength development. The mix designs tested in this series show that full capacity was achieved in both scenarios.
- The experimental results indicate that a side cover of 50 mm is sufficient to develop acceptable stud capacity and ductility. A side cover of 25 mm resulted in failure of the

UHPC, due to a lack of tensile strength in the reduced width of the UHPC. Additionally, a clear cover of 6 mm is sufficient to achieve full plastic capacity of the studs.

- Shooting headed shear studs onto a painted steel surface does not produce a satisfactory connection. At minimum, the paint should be locally scraped off at the welding locations, such that the entire stud area is in contact with steel.
- During the welding process, using a ferrule designed for vertical shooting applications is acceptable, as full capacity was observed. The data shows that the capacity of the stud was significantly greater than the benchmark, likely because the larger weld collar produced by the ferrule generated a larger bearing surface at the shear interface.
- To mimic field conditions, vibrations were induced onto a push-out sample for three hours during curing of the UHPC. The experimental results revealed that no detrimental effects were caused from the induced vibrations.

REFERENCES

1. Zaghi, A.E., Wille, K., Zmetra, K., and McMullen, K. (2015). "Repair of Steel Beam/Girder Ends with Ultra High Strength Concrete (Phase I)." Connecticut Department of Transportation. University of Connecticut. SPR-2282 (Report #CT-2282-F-15-2).
2. Cao, J., Shao, X., Deng, L., Gan, Y. (2017) "Static and Fatigue Behavior of Short-Headed Studs Embedded in a Thin Ultrahigh-Performance Concrete Layer". Journal of Bridge Engineering, 22(5).
3. ASCE (2017). "Report card for America's Infrastructure." Infrastructure Advisory Council, American Society of Civil Engineers (ASCE), Reston, VA. https://www.infrastructurereportcard.org/
4. FLDOT (2011). "Bridge maintenance and repair handbook." Steel Beam & Girder Repair, Florida Department of Transportation (4.6). pp 78-83.
5. Milner, M.H. (2014. "Survey of past experience and state of the practice in the design and maintenance of small movement expansion joints in the Northeast". Transportation System Preservation Technical Services Program (TSP2). University of Delaware, Newark, DE. http://sites.udel.edu/dct/files/2013/10/Report-242-TSP2-Small-Movement-Expansion-Joints-2dzoc1e.pdf
6. Tamakoshi, T., Yoshida, Y., Sakai, Y., and Fukunga, S. (2006). "Analysis of damage occurring in steel plate girder bridges on national roads in Japan." Proc. 22nd US-Japan Bridge Engineering Workshop, Seattle, Washington, USA.
7. Zmetra, K. (2015). "Repair of Corrosion Damaged Steel Bridge Girder Ends by Encasement in Ultra-High Performance Concrete." Ph.D. Dissertation, University of Connecticut, Storrs, CT.

8. Khurram, N., Sasaki, E., Katsuchi, H., Yamada, H. (2014). "Experimental and numerical evaluation of bearing capacity of steel plate girder affected by end panel corrosion." International Journal of Steel Structures (14). pp. 659-676.
9. Zmetra, K., McMullen, K., Zaghi, A.E., Wille, K. (2017). "Experimental Study of UHPC Repair for Corrosion-Damaged Steel Girder Ends." Journal of Bridge Engineering, 22(8).
10. Kruszewski, D., Wille, K., Zaghi, A.E. (2018) "Push-Out Behavior of Headed Shear Studs Welded on Thin Plates and Embedded in UHPC." Engineering Structures, under review.
11. Lam, D., El-Lobody, E. (2005). "Behavior of Headed Stud Shear Connectors in Composite Beam." Journal of Structural Engineering 131(1). pp 96-107.
12. An, L., and Cederwall, K. (1996). "Push-out tests on studs in high strength and normal strength concrete." Journal of Constructional Steel Research, 36(1). pp 15 – 29.
13. Spremic, M., Markovic, Z., Veljkovic, M., Budjevac, D. (2013). "Push-Out Experiments of Headed Shear Studs in Group Arrangements." Advanced Steel Construction 9(2). pp 139 – 160.
14. Luo, Y., Hoki, K., Hayashi, K., Nakashima, M. (2016). "Behavior and Strength of Headed Stud-SFRCC Shear Connection. I: Experimental Study" Journal of Structural Engineering 142(2), ASCE.
15. Shim, C.S., Lee, P.G., Yoon, T.Y. (2004). "Static behavior of large stud shear connectors." Engineering Structures 26. pp 1853 – 1860.
16. Kim, J.S., Kwark, J., Joh, C., Yoo, S.W., Lee, K.C. (2015) "Headed stud shear connector for thin ultrahigh-performance concrete bridge deck." Journal of Constructional Steel Research, 108(1). pp 23 – 30.

17. He, S., Fang, Z., Mosallam, A. (2017). “Push-out tests for perfobond strip connectors with UHPC grout in the joints of steel-concrete hybrid bridge girders.” Engineering Structures 135. pp 177 – 190.
18. Hegger, J., Sedlacek, G., Döinghaus, P., Trumpf, H., and Eligehausen, R. (2006) "Studies on the ductility of shear connectors when using high-strength steel and high-strength concrete." Proc., International Symposium on Connections between Steel and Concrete, University of Stuttgart. pp 1025-1045.
19. AASHTO (2012). “AASHTO LRFD Bridge Design Specifications.” American Association of State Highway and Transportation Officials, Washington, DC 20001.
20. LaFarge Holcim, “Building materials, cement, aggregates and concrete.” LaFarge Holcim, 2018. https://www.lafargeholcim.com/
21. Ductal JS1212 (2016). “ JS1212 Rapid Strength Product Data Sheet”, Ductal, LaFarge Holcim.
22. MTS Systems Corporation (2014). “MTS FlexTest Controller Family.” 100-183-824b Datasheet, MTS Systems, Eden Prairie, MN, USA.
23. ASTM E8 (2016). “Standard Test Methods for Tension Testing of Metallic Materials”. ASTM International, West Conshohocken, PA, 2016. www.astm.org
24. ACI – 239 Committee in Ultra-High Performance Concrete, “Minutes of Committee Meeting October 2012”, ACI Annual Conference 2012, Toronto, ON, Canada.
25. Graybeal, B. (2013). “Development of Non-Proprietary Ultra-High Performance Concrete for Use in the Highway Bridge Sector”, Federal Highway Administration Report No. FHWA-HRT-13-100.

26. Bruel and Kjaer Sound and Vibration Measurements, “LDS V406 and V408 Shakers”, BP2399 Datasheet, 2012.
27. Luo, Y., Hoki, K., Hayashi, K., Nakashima, M. (2016). “Behavior and Strength of Headed Stud-SFRCC Shear Connection. II: Strength Evaluation” Journal of Structural Engineering 142(2), ASCE.
28. Eurocode-4 (2004). "Design of Composite Steel and Concrete Structures." European Committee for Standardization., Brussels, Belgium.

Chapter 3

Finite Element Study of Headed Shear Studs Embedded in UHPC

Introduction

A novel bridge repair method has been proposed to remediate bridge girders suffering from corrosion at the girder ends [1-4]. The method involves welding headed shear studs to the web plate of bridge girders near the bearing region where corrosion is present. Fig. 1 shows the schematic of this repair design. The studs are welded on the web directly above the bearing, omitting the region with section loss. Next, the studs are embedded in a panel of ultra-high performance concrete (UHPC) which extends to the bottom flange. The composite action between the headed studs and the UHPC develops an alternate load path for bearing forces.

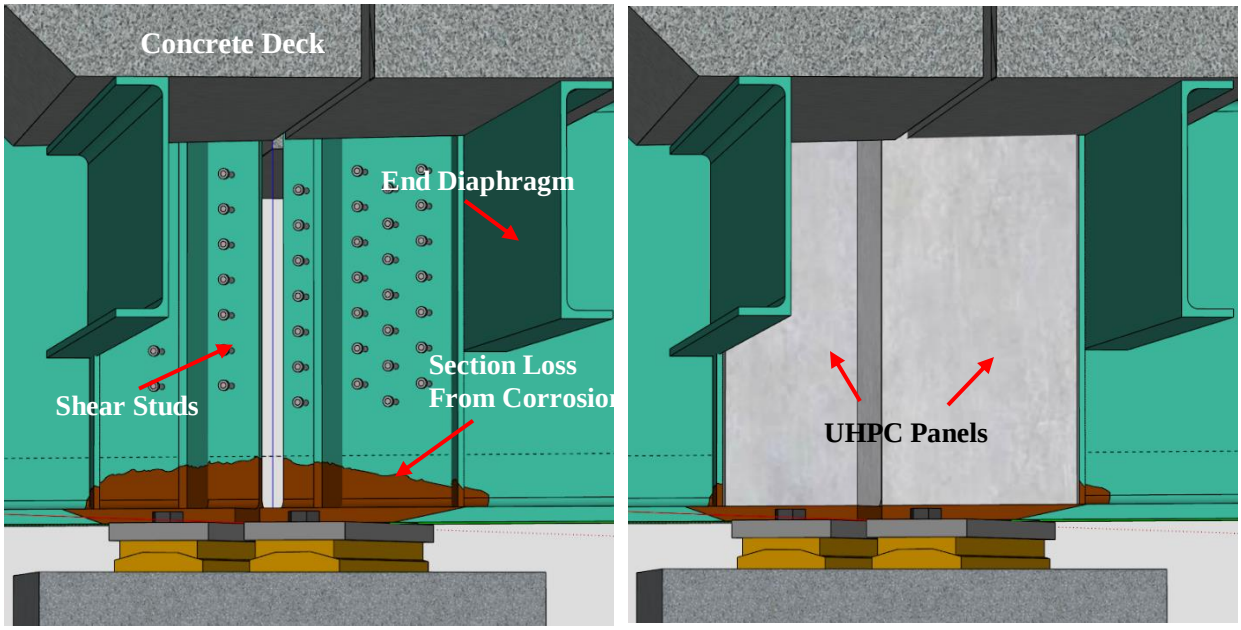

a) Studs welded to the web plate b) UHPC Cast

Fig. 1. Schematic of UHPC repair method

The diversity of girder end geometry and corrosion pattern requires different stud arrangements for different bridges. For bridges with no bearing stiffener with corrosion limited to the lower portion of the web, the stud layout is trivial. However, there may be situations where

studs need to be offset or larger stud diameters must be used to accommodate complex geometries due to limitations from stiffeners, connection plates, diaphragms, and the corrosion pattern. Experimental studies have been conducted to evaluate the performance of headed shear studs embedded in UHPC as part an extensive study supported by Connecticut Department of Transportation, USA [5]. The experimental results show that headed studs with a diameter of 12, 16 and 19 mm achieve full plastic shear capacity when they are welded onto a 9.5-mm thick web plate of a 55-year old salvaged beam girder and embedded in UHPC. Here, full plastic capacity is characterized as sustaining full strength of the headed stud in a ductile manner until shear rupture of the stud shank occurs at the interface near the weld collar. In addition to various diameters, several stud arrangements with different spacing were evaluated, yielding similar results. While a large number of push-out experiments have been performed to enhance understanding of the performance of studs in the context of this repair, there remains a significant need to complimentary analytical simulations to further the understanding of critical design parameters. This paper attempts to fill this knowledge gap by developing an experimentally validated finite element simulation method.

Several studies have been conducted relevant to finite element modeling of headed studs embedded in concrete. Xu et al. investigated the clustering of stud connectors with tight spacing and embedded in regular strength concrete (RSC) [6]. The simulations revealed that closely spaced stud groups generate a reduced shear stiffness and overall strength as the crushed concrete area distributed unevenly over the stud roots. Rocha et al. conducted simulations to investigate the influence of stud height to diameter ratio with RSC [7]. It was found that larger reductions in capacity are observed when a height to diameter ratio less than 4 is observed. These reduction factors are further magnified at weaker concrete strengths. When studs are embedded in high-

strength concrete (HSC) or UHPC, it is proven that the weld collar which is formed as a result of the welding process at the base of the stud, significantly boosts the shear capacity [8, 9]. Luo et al. conducted finite element simulations with headed studs embedded in high-strength steel fiber reinforced cementitious composites (SFRCC), concluding that the presence of a weld collar significantly improves the shear capacity of a stud [10]. As the concrete strength increased, the stud capacity also increased. However, the shear studs modeled in this study were embedded in high-strength concrete with a maximum compressive strength of 120 MPa. Therefore, the performance of 12-mm, 16-mm and 19-mm headed studs must be modeled when welded onto the web plate of an old steel girder and embedded in UHPC with a compressive strength of 170 MPa. In this work, the weld collar is explicitly modeled with interaction definitions to accurately replicate the experiments.

A critical aspect of the UHPC repair which must be analyzed in this study is the behavior of the web plate when the welded studs are loaded in shear. The significant portion of the literature on stud behavior in UHPC is concerned with composite deck connections where studs are welded to a thick top flange. However, web plates of bridge girders are typically less than 10-mm thick. Therefore, the bearing strength of the web plate close to the stud may be a limiting design parameter, particularly for large stud diameter-to-plate thickness ratios. Bouchair et al. conducted a parametric study of headed studs welded on flanges with various thicknesses [11]. It was found that when studs are welded onto a 5-mm thick flange, bearing failure of the flange governs the connection, preventing plastic deformations of the headed studs. However, their study focused on studs embedded in regular strength concrete (RSC). Further, the material properties of the base steel section resembled modern steel material. Therefore, the results cannot be applied to the repair where the studs will be welded onto old steel and embedded in UHPC.

This paper presents the results of finite element simulations, as part of the proposed repair method for deteriorated bridge girder ends. First, the experimental results from three stud diameters and two eccentric loadings are validated to confirm proper material model calibration. In addition to global force-slip relationships, local strains on the web plate adjacent to the studs are compared to the strain gauge data. Next, a parametric study is conducted to determine the relationship between stud diameter and web plate thickness to characterize web bearing and stud rupture limit states. Finally, the effect of eccentricity is studied by shifting the group of studs away from the centerline of the loading to induce a moment. An interaction formulation for in-plane torsion and direct shear is developed to predict the capacity of a stud group under an eccentric loading. The results are expected to inform the design of this novel repair. In addition, the details of the FE methodology may enable future studies on performance of headed studs in UHPC.

Overview of Push-Out Experiments

The comprehensive details of the experimental portion of the study has been presented by authors in Kruszewski et. al [5]. To familiarize the reader, a brief overview of the experiments that were used to validate the model is presented here. Because the FE model was used to investigate the effect of stud diameter-to-thickness ratio and interaction of in-plane torsion and direct shear, the model was required to be validated against experimental data obtained from specimens with different stud diameters and eccentric loading. To tailor the experiments to the repair, the headed shear studs were welded to a 9.5-mm thick web plate of an old and weathered steel girder section. The rolled girder was salvaged from a demolished bridge, which was originally built in 1958. This ensured that the material properties would reflect those which should be

anticipated during field installation. The studs were then embedded in a panel of UHPC such that a typical "push-out" specimen was fabricated.

A schematic of each push-out specimen is shown in Fig. 2. The first stud pattern (Fig. 2a) consists of eight headed shear studs with a diameter of 12 mm. They are welded symmetrically into one column of four studs spaced at 50 mm on each side of the web plate. Fig. 2b shows the stud arrangement for the 16 mm and 19 mm studs. For these diameters, two studs were welded symmetrically on each side of the web plate. The 16 mm and 19 mm studs are spaced at 64 mm and 75 mm, respectively. The stud spacing is based on the minimum spacing of 4 times the diameter of the stud, d_b, as specified by AASHTO bridge design specifications [12]. Fig. 2c and 2d show the two eccentric samples studied. The first sample contains the same stud arrangement as layout "A", but the studs are offset 50 mm from the centerline of the web plate. Fig. 2d shows an offset of 100 mm. In Fig. 2, S_v and H_s are the vertical spacing and height of the studs, respectively. Table 1 provides more details regarding the geometry of each specimen.

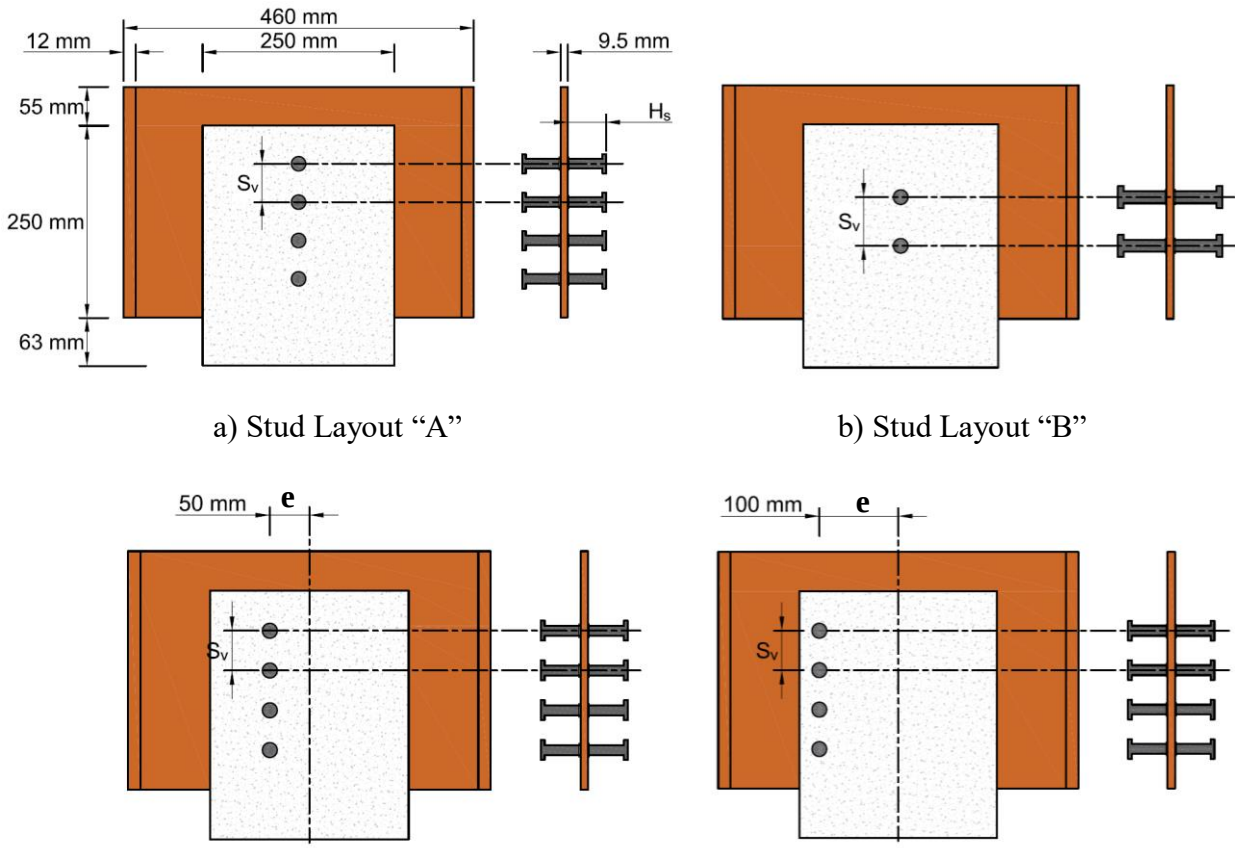

a) Stud Layout "A"

b) Stud Layout "B"

c) Stud Layout "C"

d) Stud Layout "D"

Fig. 2. Stud arrangements of specimens used for validation of FE models

Table 1. Summary of Experiments for Validation

Specimen ID	Stud Layout	Stud Diameter, d_b	H_S	S_V	Eccentricity, e
		(mm)	(mm)	(mm)	(mm)
D12_S8_A	A	12	50	50	0
D16_S4_B	B	16	54	64	0
D19_S4_B	B	19	75	75	0
D12_S8_C_e50	C	12	50	50	50
D12_S8_D_e100	D	12	50	50	100

The experiments were conducted using an 1,800 kN hydraulic load frame. Each sample was mounted and centered on a spherical bearing to account for any rotations due to imperfections.

To avoid excessive demands on the thin web plate, the sample was loaded from the flanges and a small portion of the web plate outside of the UHPC panel perimeter. This setup ensured that the headed studs were loaded in shear. Displacement transducers were mounted on the web plate via high strength magnets and extended to the UHPC panel to capture their relative displacement (i.e. slip). Strain gauges were installed on the web plate adjacent to the base of the studs to capture local strains. A schematic of the experimental setup is shown in Fig. 3.

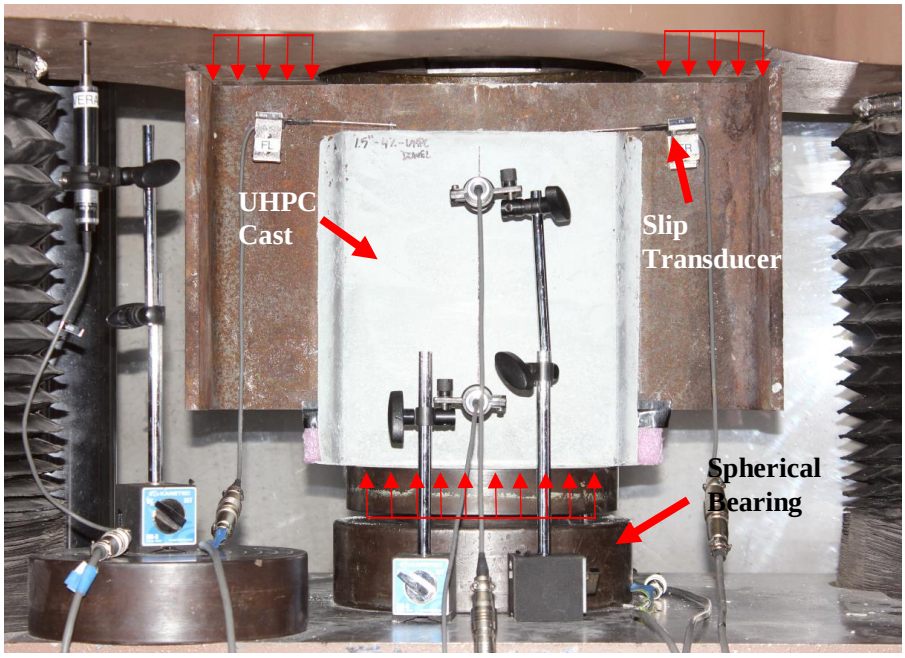

Fig. 3. Experimental setup of push-out test

Fig. 4 shows the experimental force vs. slip curves for all samples in this study. Slip is defined as the relative displacement between the steel beam and the UHPC panel. Slip was measured at the corners of the panels and interpolated such that the slip at the stud line was generated. The figure shows the capacity of one single stud, taken as the total load bearing capacity of the sample divided by the number of studs. The 12 mm, 16 mm and 19 mm studs generated a shear capacity of 73.8 kN, 104 kN and 146 kN respectively. The 50 mm and 100 mm eccentrically loaded samples achieved a respective stud capacity of 60.4 kN and 23.2 kN.

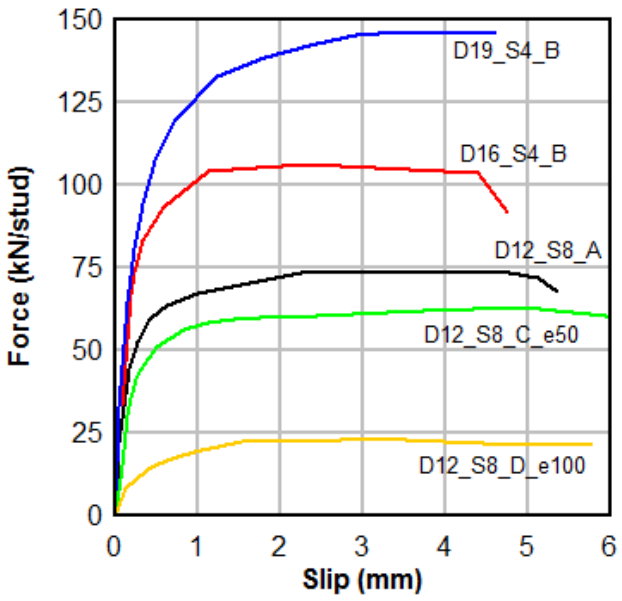

Fig. 4. Experimental force-slip curves

All samples failed via shear rupture of the stud shank except for the 100 mm eccentrically loaded sample, which was not loaded to failure due to excessive rotations of the UHPC panel. This failure occurs at the interface between the weld collar and the UHPC panel, as shown in Fig. 5. No damage is sustained to the UHPC panel except a small shear plane which was sliced off of the panel from sliding of the weld collar during rupture. Fig. 5c shows the centerline section cut of the UHPC panel after failure. It is observed that no interior damage to the UHPC panel was observed other than the weld collar plane. There is little evidence of flexure of the stud shank, as the UHPC constrains the studs such that only the localized region at the edge of the UHPC panel deforms.

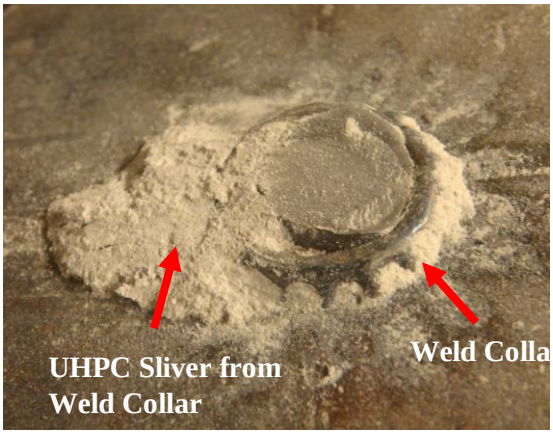

a) Web Plate Interface

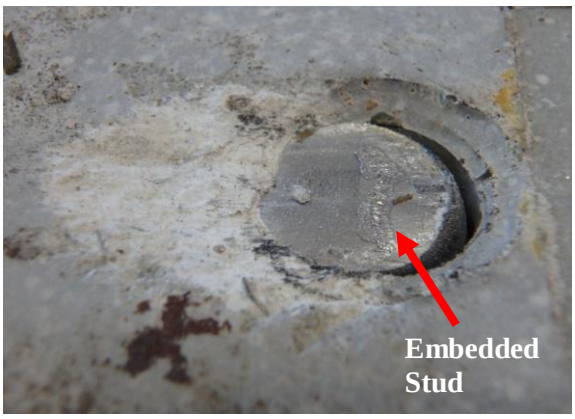

b) UHPC Panel Interface

c) Section Cut of UHPC Panel

Fig. 5. Experimental force-slip curves

Development and Validation of Finite Element Models

First, the experimental results presented in this study are validated to provide credibility to the finite element model before further parametric analyses are conducted. To simulate the experiments, ABAQUS/Explicit version 6.20 was used [13]. Material models were calibrated using stress-strain relationships obtained from testing the studs, web plate, and ultra-high performance concrete (UHPC). Next, the model was assembled with realistic geometry and contact

definitions to capture the essential load-transfer mechanisms. This section discusses the material inputs, damage model calibration, assembly of the finite element model geometry, and interaction details which were used to conduct the simulations. The results from each simulation were compared against the experimental data to provide credibility to the model inputs.

Material Models

Before assembling the global model of the push-out specimen, material models were calibrated by creating steel coupons for the beam section and studs and a cylinder specimen for the UHPC material. It is important to accurately model the material behavior of each component due to the nature of the repair. Since headed studs which are comprised of modern steel material are being welded to an old, weathered bridge girder and embedded in a new material such as UHPC, the materials must be carefully modeled to capture the correct failure mechanisms. The coupons were modeled with realistic geometry following a similar methodology to Pavlovic et al. [14]. The coupon test simulations were conducted with similar boundary conditions to the physical scenario such that reliable stress-strain relationship could be generated and then input into the global model.

Steel Material

Values for density and elastic properties were the same for the base beam section and headed studs. The density was assigned as 7833 kg/m^3. The modulus of elasticity and Poisson's ratio was 200,000 MPa and 0.3 respectively. The plastic material properties were assigned according to the experimental stress vs. strain curves which were extracted by testing coupons of each steel material. For the headed studs, small coupons were fabricated by removing the head of

the stud and machining a dog-bone shaped section with a reduced throat area (Fig. 4). The throat length was approximately 19 mm. Due to a small coupon size, the reduced area was machined to a diameter of 6.25 mm to avoid triaxiality effects during testing. A high-elongation strain gauge was used to extract the local strain in the necking region. After severe necking, machine displacement was used to complete the softening curve as it was assumed that further elongation after the onset of necking was applied only to the localized throat region. For the beam section, standard dog-bone coupons (Fig. 5) were fabricated in accordance with ASTM E8 [15]. Strains were extracted using an extensometer with a gauge length of 100 mm. Both coupons were tested in uniaxial tension at a strain rate of 0.015 mm/mm/min.

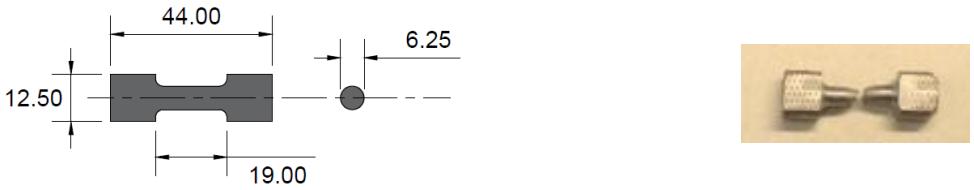

a) Geometry of stud coupon b) Failed coupon after testing

Fig. 4. Geometry of stud coupons for material testing

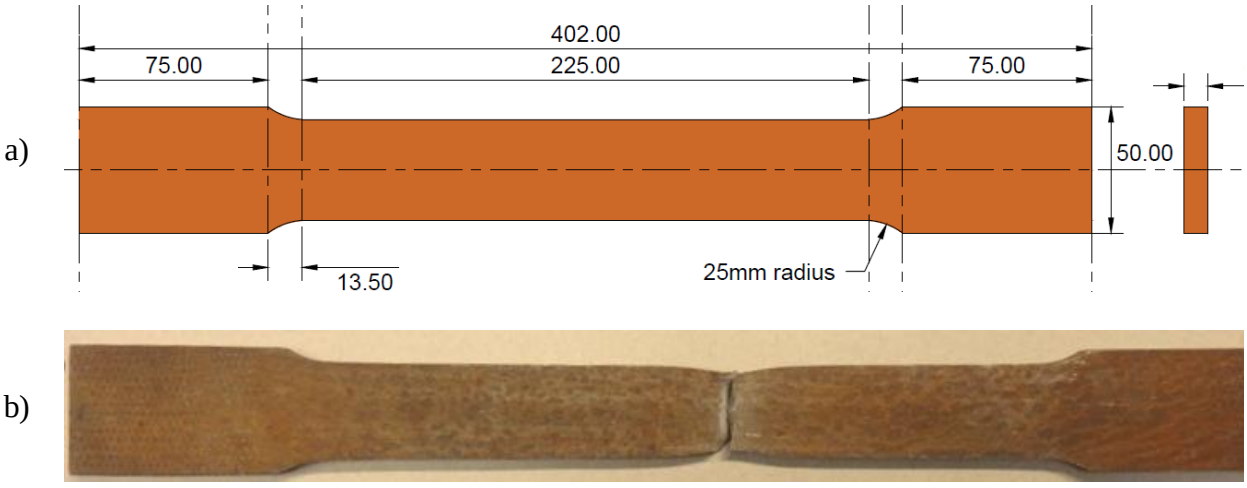

Fig. 5. Beam section coupons for material testing

Fig. 6 shows the experimental stress vs. strain response for both steel materials. The yield strength of the web plate is approximately 280 MPa, while the stud material yields at 405 MPa. This illustrates the variation in steel material which was used for structural steel from the 1950's. The ultimate strength of the beam and stud material is 452 MPa and 531 MPa, respectively. These results are consistent with the findings of Brockenbrough who reported that U.S. structural steel specifications called for A373-58T during that time [16]. This material is no longer used in modern construction. The undamaged response was generated using the traditional relationship between engineering stress (σ_i) and true stress ($\bar{\sigma}_i$), outlined in Equation 1. From these results, the true stress values were used so that damage models may be incorporated such that the experimental results could be replicated.

$$\bar{\sigma}_i = \sigma_i(1 + \varepsilon_i) \qquad (1)$$

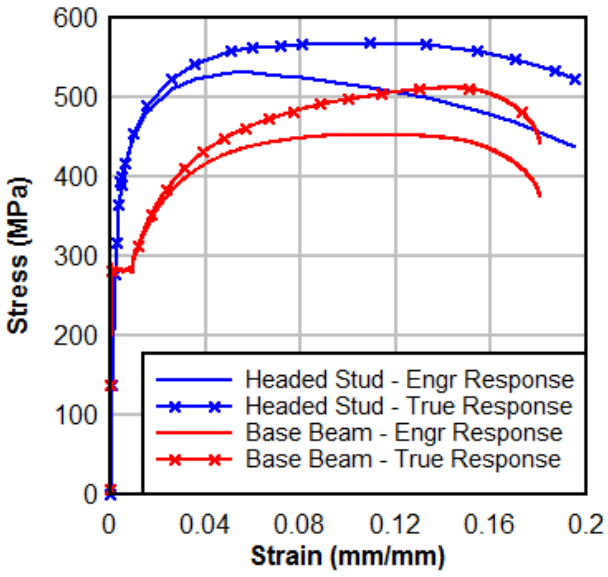

Fig. 6. Web Plate Stress vs. Strain results

The damage models were calibrated according to plasticity relationships and fracture laws developed by Rice and Tracey [17]. Damage parameters ensure that the model captures damage initiation, damage accumulation and softening of the stud and beam materials. Accurate estimation of the damage is critical to validating the experimental results because one of the objectives is to capture the damage to the web plate as well as to the studs. Since the headed studs are welded onto a thin web plate with reduced mechanical properties, capturing the damaged response of both materials and identifying the demands on each is crucial. Ductile damage with damage evolution laws were assigned to both steel materials according to their plasticity curves. Ductile damage parameters require the equivalent plastic strain as a function of stress triaxiality. This parameter describes the plastic strain experienced at the onset of necking of the steel coupon. When plastic strains were captured, the equivalent plastic strain according to stress triaxiality was entered according to the following relationship:

$$\varepsilon_{pl}(\theta) = \varepsilon_u\left[exp\left(-\beta\left(\theta - {}^{1}/_{3}\right)\right)\right] \qquad (2)$$

, where ε_{pl} is the equivalent plastic strain, ε_u is the strain at ultimate engineering stress, β is a material parameter typically assumed as 1.5, and θ is stress triaxiality. Stress triaxiality values were considered from -0.33 to 2.0. Damage evolution was assigned to describe the accumulation of damage (and thus reduction in stiffness) after the necking point. Damage evolution was assigned in tabular form using the damage relationship proposed by Lemaitre [18] as shown in Eq. 2. In the equation, α_D is a damage eccentricity factor introduced to account for the difference between observed and calculated damage values [19]. Damage was assigned as a function of plastic displacement after the onset of necking as outlined in Eq. 3. Here, u_i^{pl} is the plastic displacement after necking, u_f^{pl} is the ultimate displacement at failure, ε_i^{pl} is the plastic strain after necking, and

ε_f^{pl} is the ultimate strain at failure. The ductile damage and damage evolution relationships for both materials is shown in Fig. 7a and 7b, respectively. When these damage models were incorporated to the true stress response, good agreement was achieved between the simulated and physical test coupons (Fig. 8).

$$D_i = \alpha_D \left[1 - \frac{\overline{\sigma}_i}{\sigma_i}\right] \quad (3)$$

$$u_i^{pl} = u_f^{pl} \frac{(\varepsilon_i^{pl} - \varepsilon_u)}{(\varepsilon_f^{pl} - \varepsilon_u)} \quad (4)$$

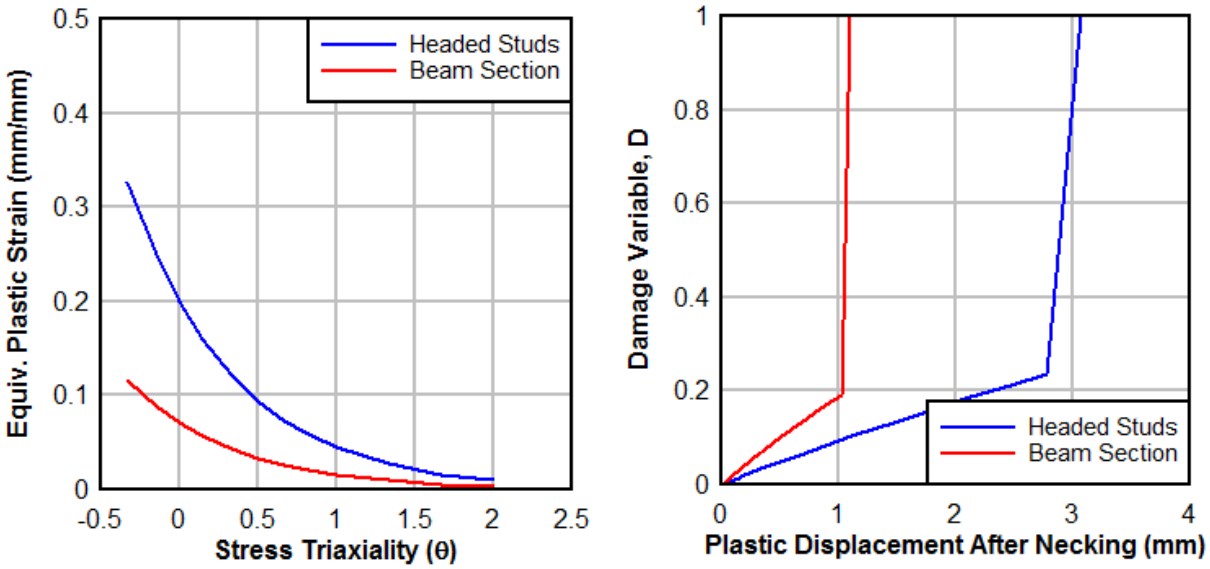

a) Ductile damage b) Damage evolution laws

Fig. 7. Damage initiation and accumulation laws

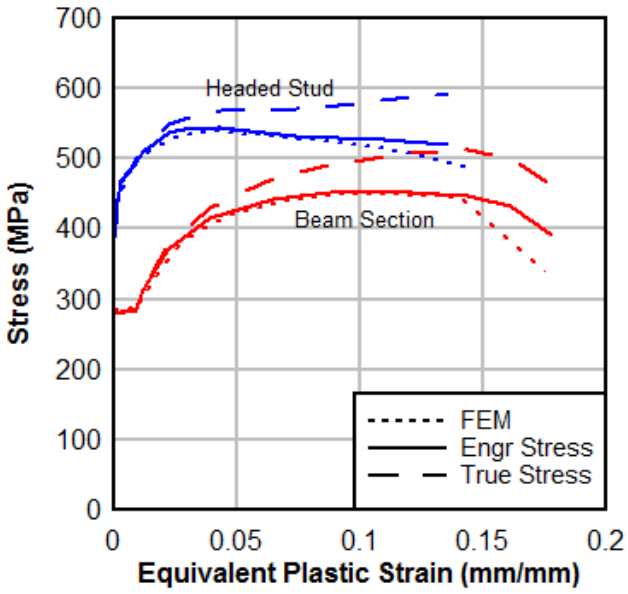

Fig. 8. Calibration of steel material properties

UHPC Material

For the UHPC material, Concrete Damaged Plasticity (CDP) was incorporated. This model was used because it allows for calibration of damage parameters to represent the degradation of stiffness and plastic deformations [20]. This model captures high confinement stresses of the UHPC which is important to capturing local damage at the base of the studs during flexure. Additionally, the characteristic failure mode of headed studs embedded in UHPC involves fracture of the stud shank which results in the weld collar sliding across the UHPC panel interface, leaving a sliver of UHPC remaining under the weld collar. This bearing action significantly contributes to the capacity of a headed stud, and thus must be modeled adequately from the material side. The CDP model allows for assigning compression and tension properties with varying yield strengths [21]. To assign compressive behavior, stress vs. strain properties were obtained experimentally. A UHPC cylinder with similar geometry (75 mm diameter and 150 mm height) was modeled in

ABAQUS (Fig. 9). The dilation angle and eccentricity factors were assigned as 17° and 0.1 [22]. The ratio of biaxial compressive strength to uniaxial compressive strength (f_{b0}/f_{c0}) was assigned as 1.16. The ratio of the second stress invariant on the tensile meridian to that on the compressive meridian (K) is 0.667. Finally, the viscosity parameter was set to 0. Since UHPC fails in a brittle manner with no clear softening curve, compression damage was assigned such that a damage variable of 1 was assigned almost immediately after the compressive strength is reached.

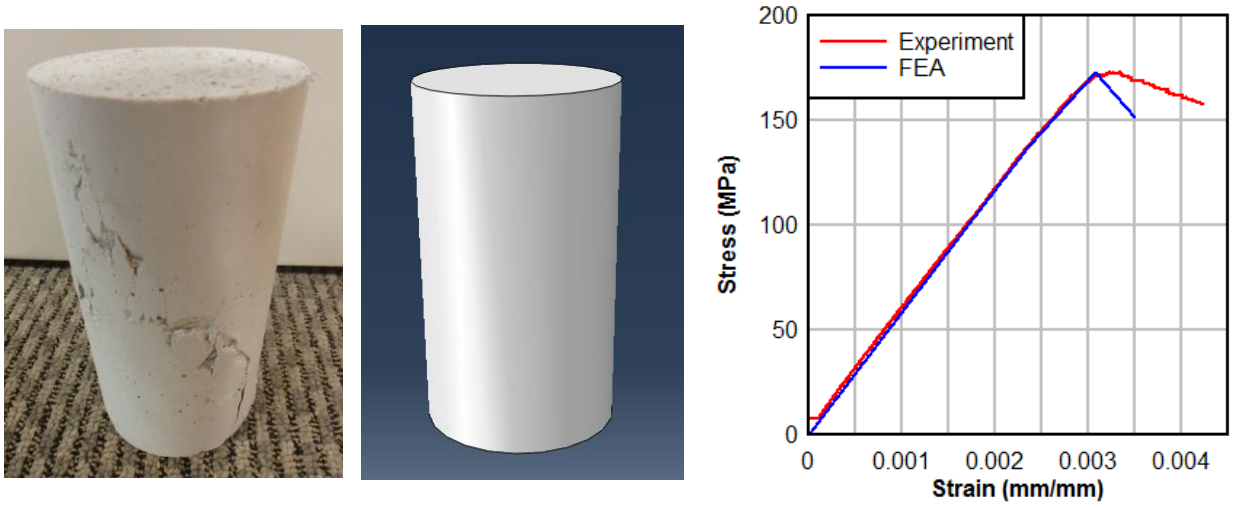

a) Physical UHPC cylinder

b) Modeled cylinder

c) Stress vs. strain comparison

Fig. 9. UHPC material calibration

Construction of Finite Element Model

A schematic of the geometry of the models used for experimental validation is shown in Fig. 10. For computational efficiency, quarter models were developed to validate the three stud diameters as two planes of symmetry were available. To validate the eccentrically loaded stud groups, half models were created since only one plane of symmetry was present.

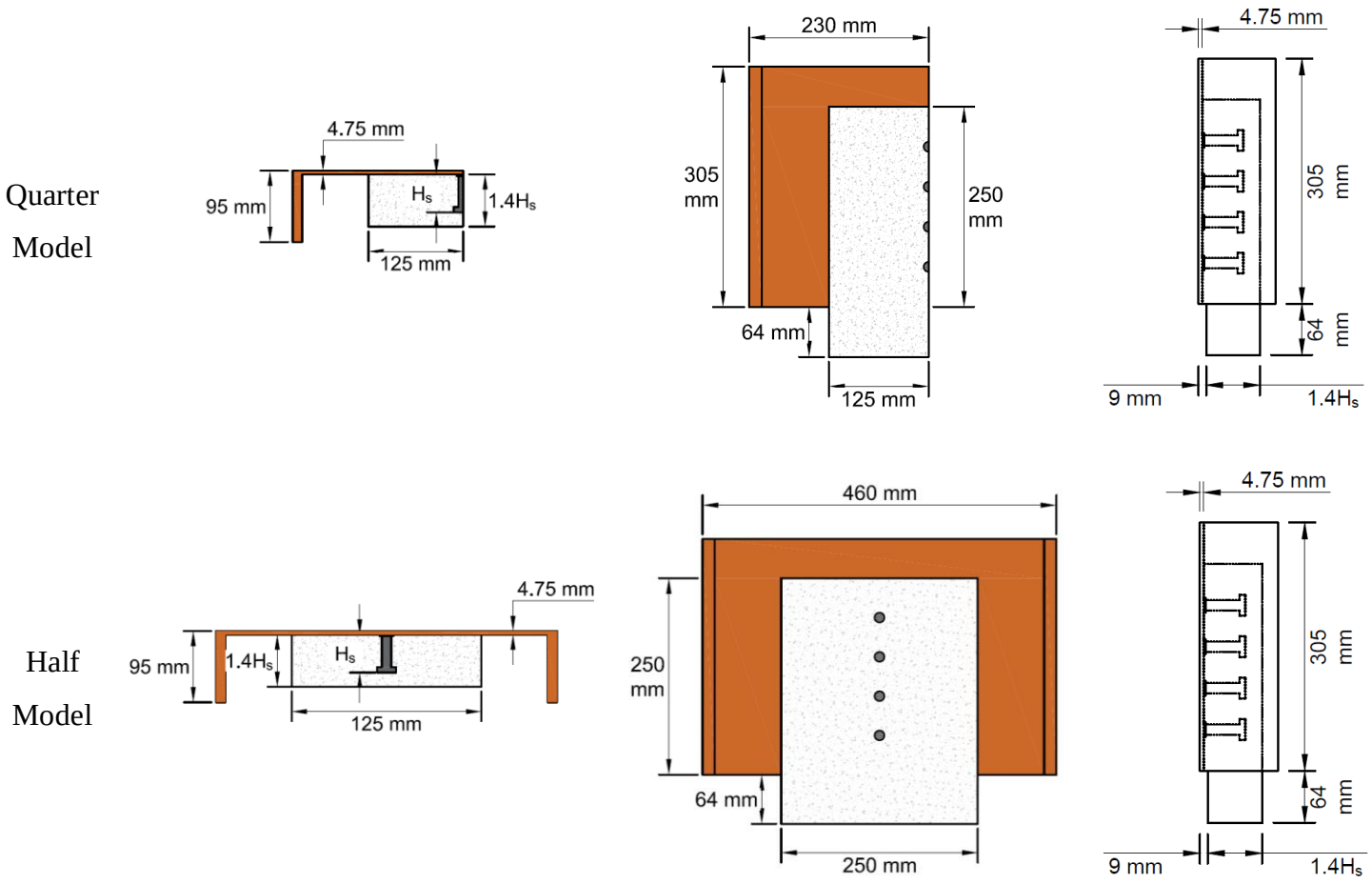

a) Plan view b) Elevation c) Cross Section

Fig. 10. Geometry of quarter and half models

Several boundary conditions were imposed. First, the normal vector of each plane of symmetry was restrained to satisfy the quarter model and half model conditions. For the quarter models, the base of the UHPC panel was tied to a reference point approximately 25 mm below the bottom of the panel. This was to replicate the spherical bearing which was used during the experimental portion of this work. Displacement was restrained in all directions except normal to the UHPC panel (i.e. slab splitting was allowed). Rotations were permitted to replicate the behavior of the spherical bearing. For the eccentric specimens, the spherical bearing was accurately modeled to replicate the friction contribution during rotation. The loading was applied by applying a

displacement of approximately 8 mm to the entire flange and a portion of the web plate, simulating the loading conditions of the physical scenario. The displacement was applied with a tabular amplitude to ensure a quasi-static loading. An accurate representation of the headed shear stud was modeled. Since it is known that the presence of a weld collar significantly contributes to its shear capacity of a stud in UHPC [5, 9, 22], over 150 measurements of weld collar dimensions were collected. The weld collars for various studs were modeled as flat cylinders with a diameter and height of 1.4db and 0.14db, respectively. The studs were generated using the geometry that was used in the experiments. The dimensions of each stud diameter are shown in Fig. 11.

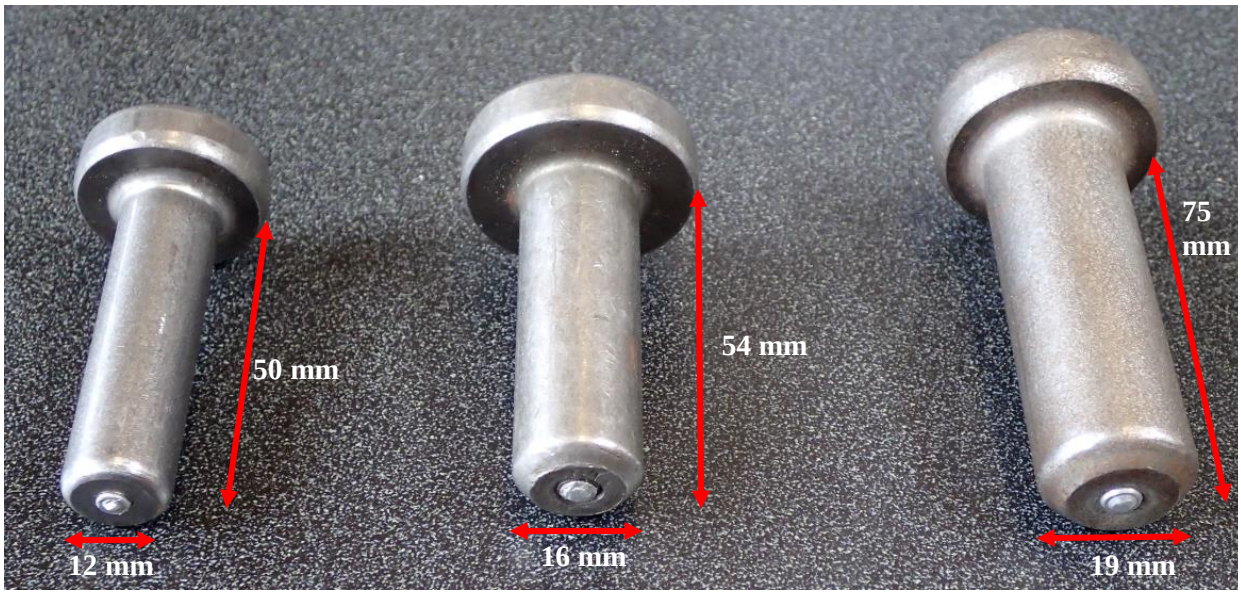

a) 12 mm stud b) 16 mm stud c) 19 mm stud

Fig. 11. Stud diameters used for validation

The mesh was assigned similarly in each quarter model to maximize computational efficiency and also capture local strains with accuracy. Eight node linear brick elements with reduced integration and hourglass control (C3D8R) were assigned to the model. A fine mesh was employed at the base of the stud just above the weld collar by introducing a single bias seeding

scheme. A total of 20 seeds were assigned along the stud shank with a bias ratio of 20. This is because the governing failure mode of the headed studs is concentrated at the stud shank just above the weld collar and thus a fine mesh was assigned at the anticipated failure plane. The weld collar was modeled with four longitudinal seeds to observe its bearing action onto the UHPC. The web plate was also meshed finely around the stud region using a custom-sketched mesh. Since the flange and far portions of the web plate were not as critical, a coarse mesh was introduced to speed up simulation times. Table 2 shows the geometry and mesh assignments for various components of the push-out model.

Table 2. Overview of Models for Stud Diameter Validation

	Stud Mesh	Beam and Studs	Complete Assembly
12 mm	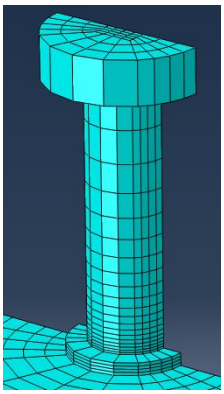	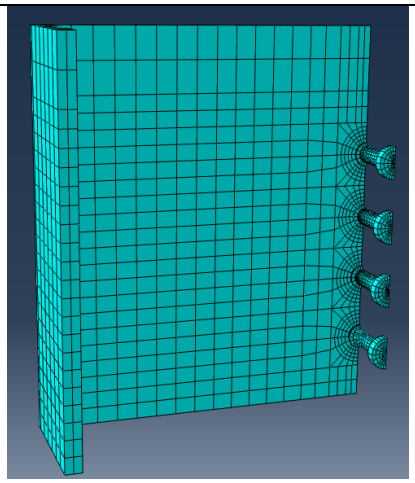	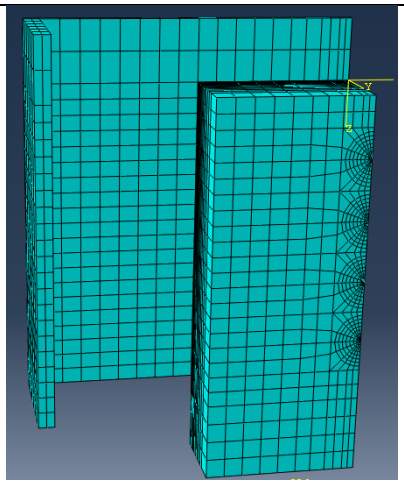
16 mm	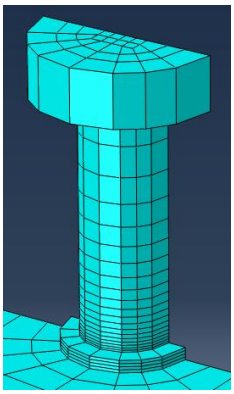	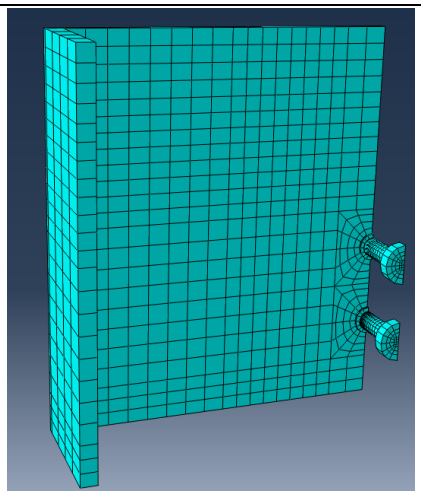	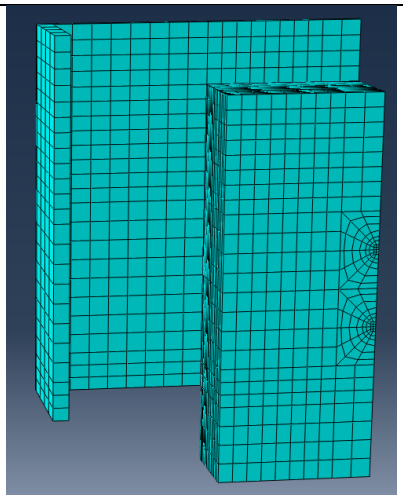
19 mm	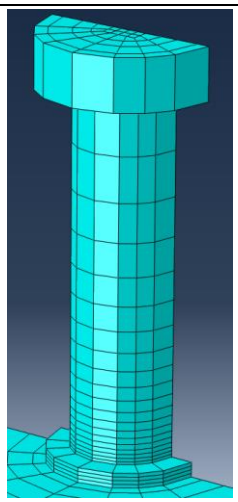	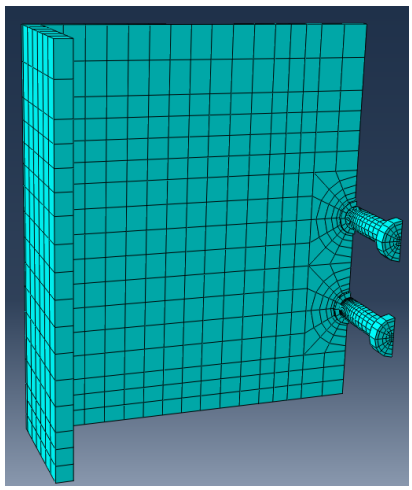	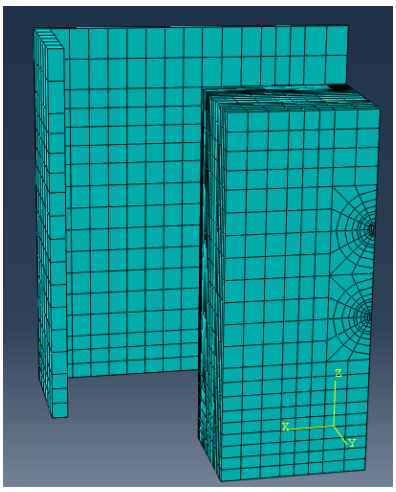

Two interaction properties were assigned to the model. The first interaction was assigned as a surface-to-surface contact between the UHPC panel and the web plate. Tangential behavior with a penalty friction formulation and friction coefficient of 0.3 was assigned to represent the friction bond between the web plate and the UHPC. The second interaction defined the contact between the headed studs (inclusive of the weld collar) and UHPC. Here, surface-to-surface contact was assigned with tangential contact, normal contact, and damping. Tangential behavior was defined with a penalty friction formulation and a friction coefficient of 0.3. Normal contact was defined to simulate the bearing effect of the studs onto the UHPC panel. A damping coefficient of 0.8 was applied to promote stability during damage initiation of the studs and UHPC.

Validation of Stud Diameters

To provide credibility to the finite element model so that further parametric analyses may be conducted, local and global behavior was captured and compared to experimental results. Fig. 12 shows the force vs. slip relationship for all three stud diameters. The figure shows good agreement between the finite element analysis (FEA) and experimental results. The finite element model is able to capture softening of the headed shear studs over a large slip range with reasonable agreement to the experimental results. The failure mechanism for the simulation involves shear rupture of the stud shank similarly to the physical scenario (Fig. 13). For clarity, the UHPC panels were removed from the viewport to observe the deformation in the headed studs. Fig. 13a shows the initial loading on the headed stud with a stress concentration at the base of the stud near the weld collar. The figure shows that the weld collar is engaged even during the elastic stage. Fig. 13b displays the yield point of the stud just prior to significant deformation. Additional stress accumulation has developed at the root of the stud. Once yielding occurs, large deformations are

experienced by the stud as shown in Fig. 13c. Here, because the beam is sliding against the UHPC surface, the weld collar becomes more engaged as indicated by the stress concentration just above the web plate. Finally, at a slip of approximately 5 mm, the studs rupture at the interface just above the weld collar as indicated by the stress release in Fig. 13d.

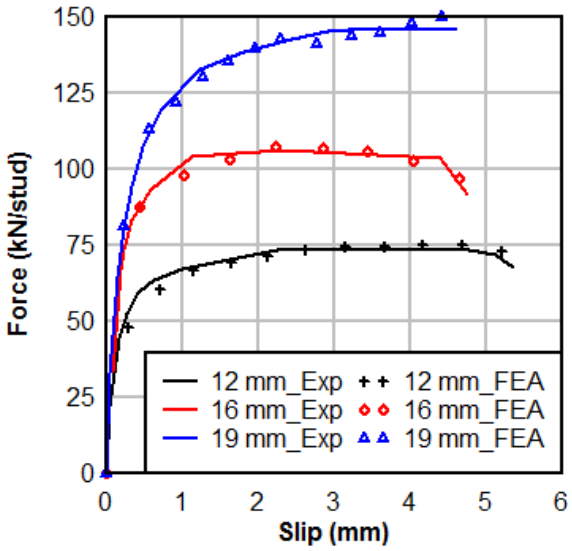

Fig. 12. Force vs. slip comparison between experimental and simulated results

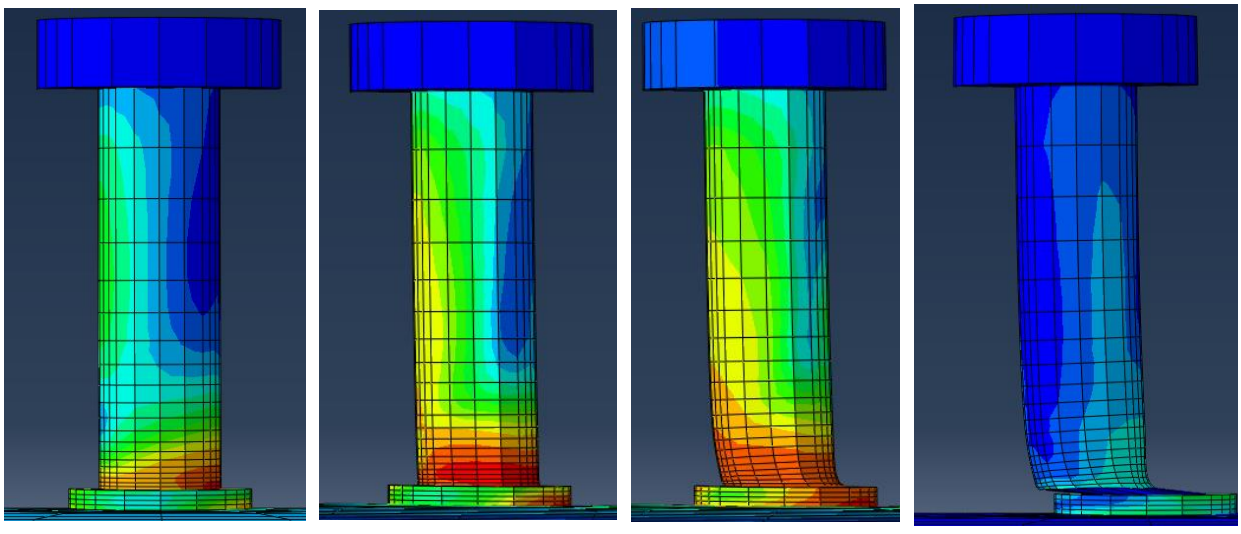

a) Initial loading b) Yield point c) Shear yielding d) Complete rupture

Fig. 13. Von-mises stress distribution on studs during loading sequence

Fig. 14 shows the force vs. web strain adjacent to the base of the studs. The experimental results were captured through strain gauges which were installed approximately 8 mm from the base of the headed stud on the compression side. The FEA results show the equivalent plastic strain at the same location. The graph shows some deviation of strain from the experimental results. Typically, the finite element model under predicted the web strain compared to the strain gauges in the physical scenario. This is likely because the large stress concentrations adjacent to the stud base create a scattered strain field which changes rapidly as a function of distance away from the stud base. Therefore, an exact match for web strains may be difficult to capture. However, the observed strains are within a reasonable range compared to the experimental results and are therefore deemed sufficient.

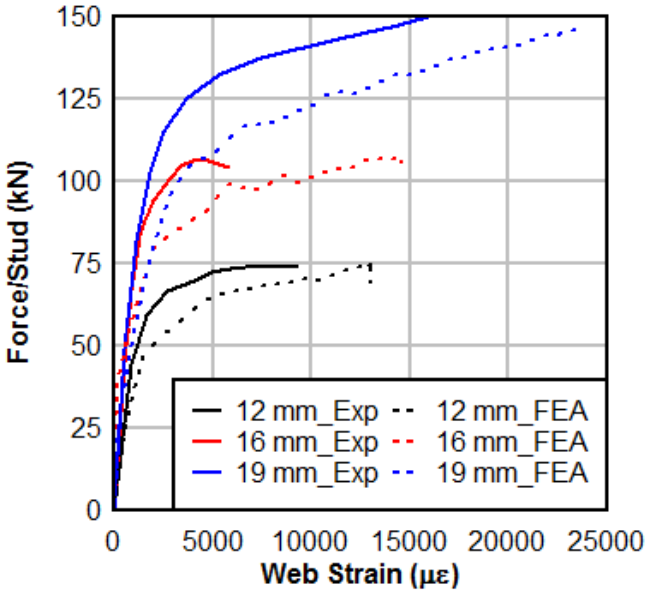

Fig. 14. Comparison of web strains adjacent to the stud base

Validation of Eccentrically Loaded Samples

Two experiments with 50 mm and 100 mm eccentricities are used to calibrate the finite element models for eccentricity. Since half models were used for these simulations, the back side of the web plate was restrained to satisfy the boundary conditions. To adequately model the rotational effect, the spherical bearing was modeled with realistic geometry. The spherical bearing was modeled with an elastic material model using an elastic modulus and Poisson's ratio of 300,000 and 0.3, respectively. To introduce the spherical bearing, two additional interactions were defined (in addition to the existing interaction parameters as outlined in 3.2. The third interaction was defined between the bottom of the UHPC panel and the top of the spherical bearing. Normal surface-to-surface "hard" contact was assigned with a tangential friction coefficient of 0.2 and a damping coefficient of 0.5. Next, an interaction between the bearing sphere and the nesting was modeled using normal surface-to-surface "hard" contact with a tangential friction coefficient of 0.05 to promote rotation of the bearing. The nodes at the bottom of the spherical bearing were constrained to a reference point such that the total reaction force could be extracted. Fig. 15 shows the rotated specimens at an overall displacement of approximately 2 mm. It is observed that the rotations between both samples are reasonable.

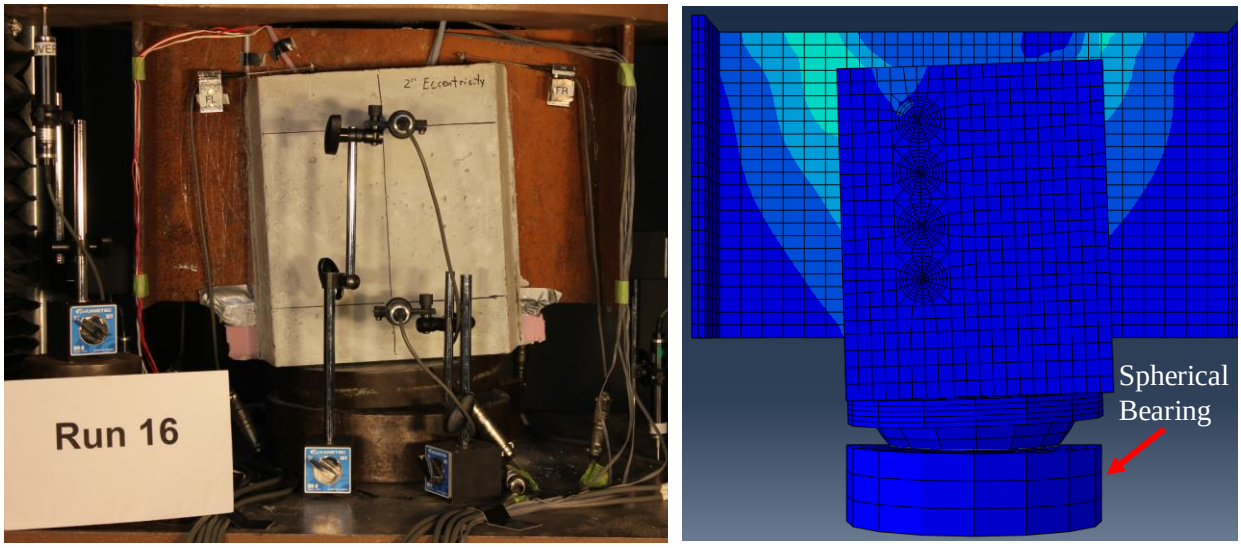

a) Physical specimen during testing b) Simulated test result

Fig. 15. Validation of experimental results

Fig. 16 shows the force vs. overall displacement of the two eccentric samples used for model validation. The finite element model predicted the total load bearing capacity well, but did not capture the ductility of the headed studs when a moment was applied. This may be due to the material model which was defined with damage models as described in section 3.1.1. In addition, there may be physical phenomena occurring in the experiment that is not captured by the finite element model such as shear friction between the UHPC panels and the web plate. However, for the purposes of this study, the results are sufficient to proceed with a force vs. eccentricity analysis.

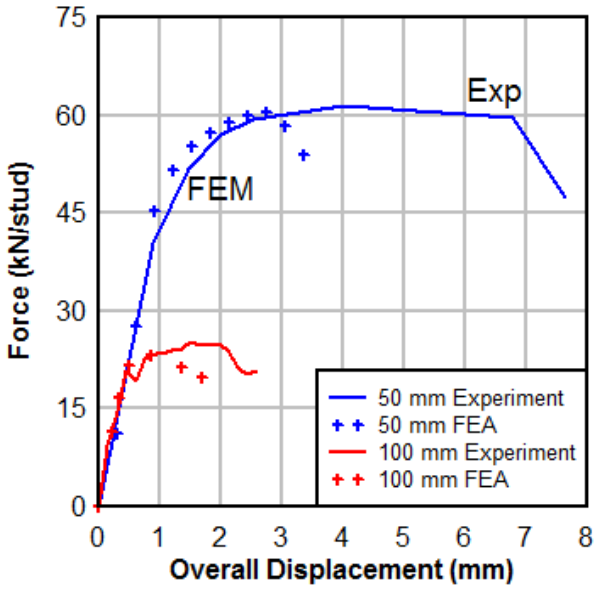

Fig. 16. Validation of experimental results

Evaluation of Design Parameters

To guide engineers through the design process, parametric studies relevant to the repair were conducted. First, the performance of a stud group under various eccentric loadings is considered. Eccentricity must be carefully understood when headed studs cannot be welded along the centerline of the loading axis. Similar to bolt groups, studs may experience a decrease in capacity when subjected to an eccentric loading. For the purpose of demonstration, a single column of four headed studs is analyzed under several eccentricities ranging from 0 mm to 100 mm. Secondly, the influence of web thickness vs. stud diameter is studied. A critical aspect of the proposed repair is to preserve the structural performance of the intact web plate while providing support to the corroded region. Through efficient simulations, various web thicknesses may be assigned for the three stud diameters considered in this study. By analyzing the failure mechanisms when the web thickness is reduced, an acceptable ratio of web thickness to stud diameter can be generated to satisfy the stud yielding limit state.

Eccentric Loading

Eccentricity is an important design parameter which must be carefully assessed prior to field installation. Based on the experimental results presented in 3.3, it is shown that a larger eccentricity decreases the overall capacity of the stud group due to a combination of in-plane torsion and shear. The 50-mm and 100-mm eccentric samples generated a capacity of 61.1 kN/stud and 23 kN/stud, respectively. These results are relevant to the bridge repair as an eccentrically loaded stud group may not perform as expected if this reduction is not accounted for. To gain a better understanding of the performance of headed studs under an eccentric loading, simulations were conducted with the benchmark stud arrangement (i.e. one column of four studs) welded to the web plate of the beam section at various offsets ranging from 0 mm to 100 mm (Fig. 17). The location of the stud group was shifted by 12 mm for each simulation for a total of 9 analyses. Table 3 shows the summary of all simulations conducted. Eccentricity is defined as the distance from the centerline of the specimen to the centerline of the studs. Critical side cover is defined as the distance between the outer edge of the stud shank to the edge of the UHPC panel on the side where the studs are offset.

Table 3. Summary of eccentricity specimens

Specimen ID	Number of Studs	Stud Diameter	Stud Spacing	Eccentricity (e)	Critical Side Cover
		mm	mm	mm	mm
D12_S4_ecc0	4	12	50	0	112
D12_S4_ecc12	4	12	50	12	100
D12_S4_ecc25	4	12	50	25	87
D12_S4_ecc37	4	12	50	37	75
D12_S4_ecc50	4	12	50	50	62
D12_S4_ecc62	4	12	50	62	50
D12_S4_ecc75	4	12	50	75	37
D12_S4_ecc87	4	12	50	87	25
D12_S4_ecc100	4	12	50	100	12

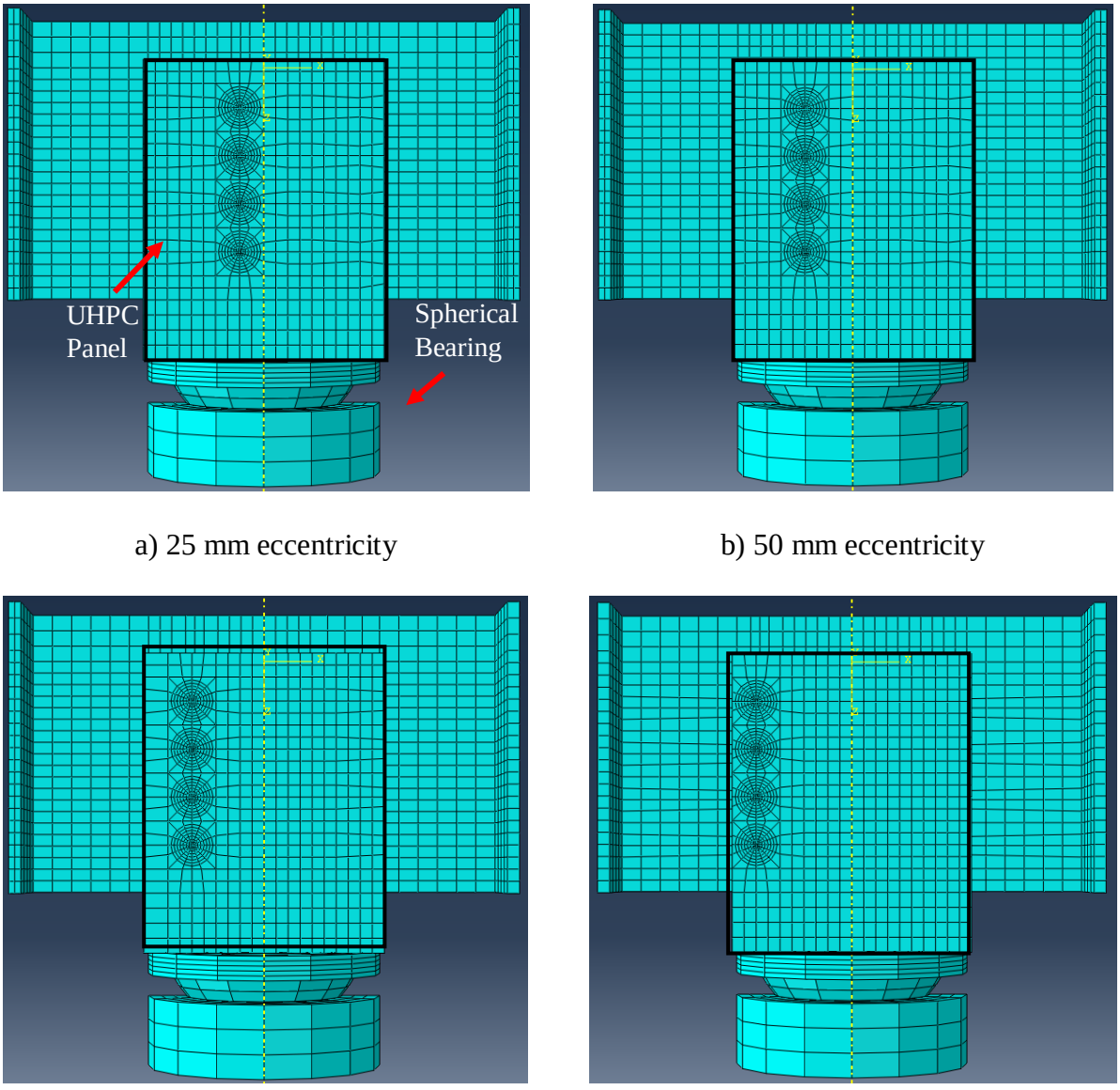

a) 25 mm eccentricity

b) 50 mm eccentricity

c) 75 mm eccentricity

d) 100 eccentricity

Fig. 17. Mesh assembly for eccentricity samples

Fig. 18 shows the normalized stud capacity as a function of eccentricity. The capacity of the stud group for each eccentric sample (P_o) was normalized by the capacity of the stud group with no eccentricity (P) and divided by the number of studs (N). At smaller eccentricities such as 12 mm and 25 mm, the stud capacity is not significantly hindered as the stud group generated 96%

and 92% of the original capacity respectively with no eccentricity. However, at larger eccentricities, the capacity reduces more significantly, as indicated by the change in slope of the scatter plot after approximately an e/h ratio of 0.25. At an eccentric loading of 100 mm, the stud capacity is just 33% of the stud group with no eccentricity.

To generate a formulation for the capacity of a single column stud group under an eccentric loading, the elastic rotation method was adopted which is traditionally used for bolts. This method assumes that the force in each stud is proportional to its distance from the center of gravity (CG). The capacity of a stud group comprised of a single column can be summarized by the following equation from the elastic method:

$$P = \frac{P_o}{N} + \frac{Ped_i}{\sum d_i^2} \quad (5)$$

, where P is the capacity the stud group with no eccentricity (kN), P_o is the capacity of the stud group under an eccentric loading (kN), N is the number of studs, e is the eccentricity (mm), and d_i is the distance from each stud to the CG. Equation (5) can be rearranged such that the normalized capacity of one single stud can be found under an eccentric loading, as follows:

$$\frac{P_o}{PN} = 1 - \frac{\alpha e}{\sum d_i} \quad (6)$$

, where α is a modification factor to for curve fitting. To fit the simulated results, it was found that a value of 1.3 for α fits the data well as shown in Fig. 18. However, the figure shows that the elastic method yields a conservative stud capacity at small eccentricities. This is because the use of principle superposition assumes that the translational and rotational actions are independent of each other, which is why the equation is comprised of two components. In reality, these actions are coupled together especially at lower eccentricities when the moment is less

prominent. When a larger eccentricity is introduced (i.e. at e/h ratios greater than 0.5), the rotational moment is so large that the translation action of the stud is almost independent of the rotation. Therefore, better agreement is achieved.

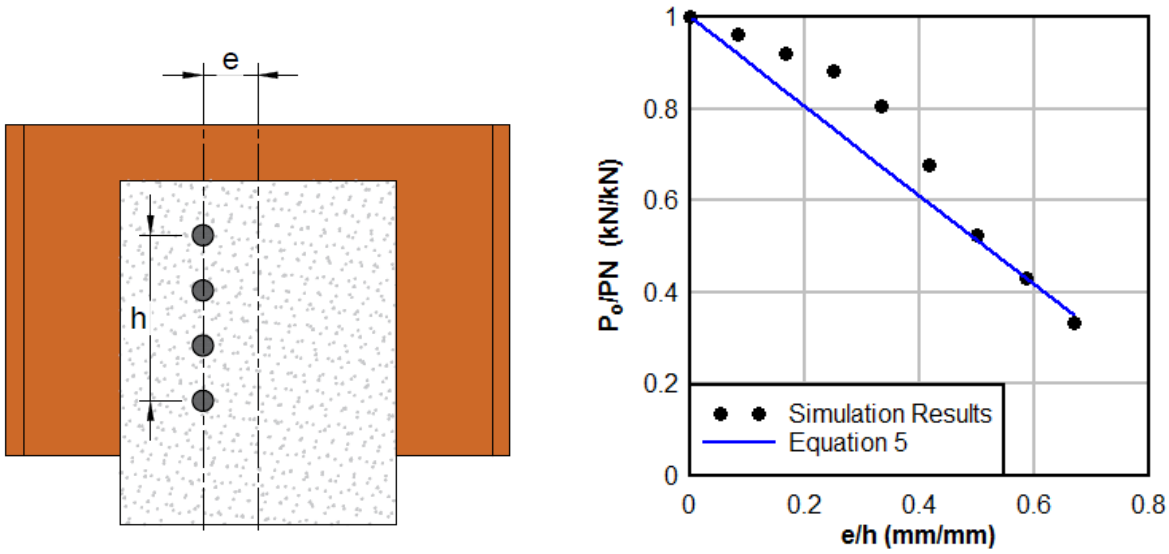

a) Schematic of eccentric samples b) Force vs. eccentricity relationship

Fig. 18. Relationship between eccentricity and force

Fig. 19 shows the rotated specimen under an eccentricity of 100 mm. Due to a large eccentricity, the rotational action of the studs around their instantaneous center of rotation (ICR) is more prominent (Fig. 19b). The studs deform in a counter clockwise manner with stress concentrations at the base of the studs until they rupture in a combination of shear and torsion.

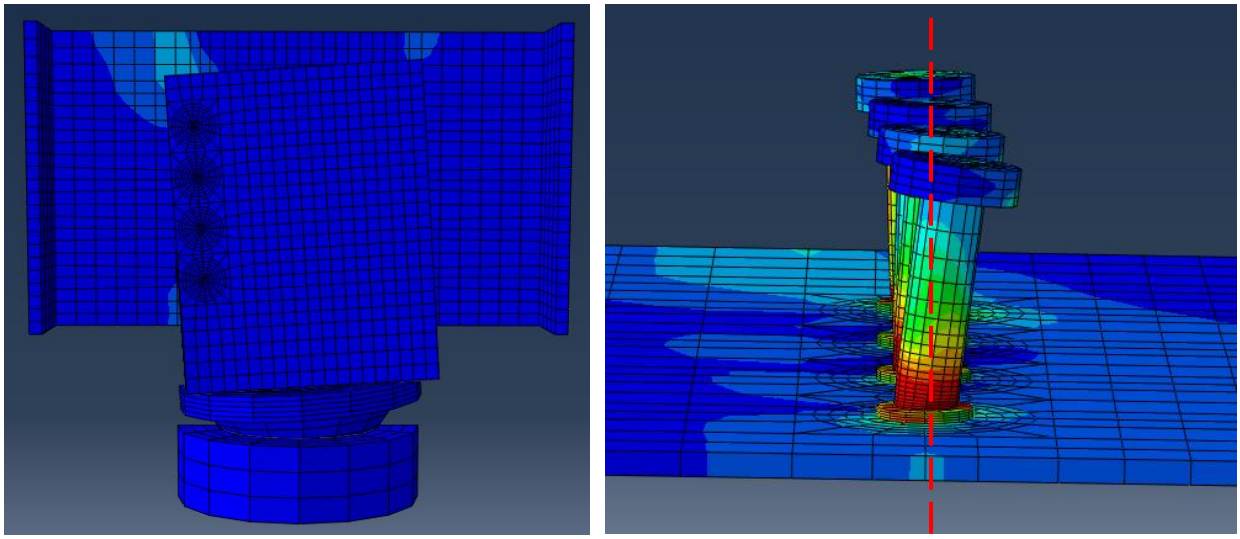

a) Rotated UHPC panel b) Stud deformation

Fig. 19. 100 mm eccentric specimen with large rotation

Web Thickness to Stud Diameter Ratio

For the purpose of field implementation and design guidelines, the web thicknesses considered in this analysis are a ratio of the stud diameter. All three stud diameters (12, 16 and 19 mm) were analyzed. To simplify the comparison, two studs of each diameter were modeled on the web plate. The experimental portion of this work was conducted with 9.5-mm thick web plates, corresponding to an initial web thickness to stud diameter ratio (t_w/d_b) of 0.75, 0.6, and 0.5 for 12 mm, 16 mm and 19 mm studs. These ratios were considered the upper limit because the headed studs were welded on a 9.5-mm thick web plate and thus the initial ratio was dependent on the stud diameter. Additionally, the aforementioned experimental results revealed that all three studs failed in shear rupture of the stud shank when welded on a 9.5 mm thick web plate. Therefore, only ratios smaller than the benchmark were considered as larger ratios were considered redundant. From the benchmark ratios, the web thickness was reduced by a t_w/d_b increment of 0.1 for each stud diameter

to observe the force vs. slip relationship, corresponding web strains adjacent to the studs, and failure mechanism. Fig. 20 shows a comparison of web thicknesses used for these simulations.

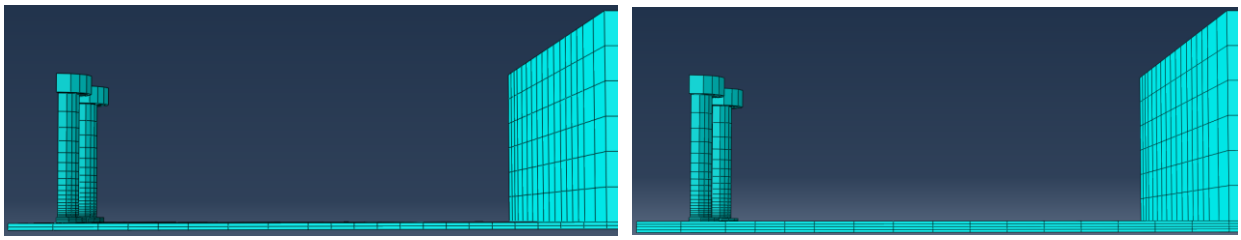

a) Reduced web thickness b) Benchmark web thickness (9.5 mm)

Fig. 20. Comparison of web thicknesses

Table 4 shows the results from these simulations. The table is arranged according to each stud diameter, as every ratio was evaluated for the three stud diameters considered in this study. It is important to note that these results are valid for the material properties assigned to this model as outlined in 3.1. The three failure mechanisms observed include stud yielding (SY), stud rupture (SR), web bearing (WB), and web shear (WS). Stud yielding is occurs when some deformation is experienced at the base of the stud but no rupture. Stud rupture is when the stud detaches from the weld collar with no capacity left. Web bearing is defined as conventional bearing failure of the web plate where the stud is welded. Finally, web shear occurs when the shear capacity of the web plate governs due to a higher capacity of the studs. Web shear typically occurs at the loading reading where a high shear force is present. A representation of these failure mechanisms is shown in Fig. 21.

Table 4. Results for web thickness simulations

Stud Diameter	t_w/d_b	Equivalent Web Thickness	Yield Force	Max. Force	Max. Web Strain at Stud Interface	Failure Mechanism*
mm	mm/mm	mm	kN	kN	με	---
12.7	0.75	9.5	56.4	77.9	13,400	SR
	0.6	7.6	56.2	77.4	46,900	SR
	0.5	6.4	55.4	76.6	63,100	SR
	0.4	5.1	50.8	74.1	143,000	SY/WB
	0.3	3.8	39.7	63.1	462,000	WB
16	0.6	9.6	83.2	107	17,600	SR
	0.5	8.0	79.8	107	23,800	SR
	0.4	6.4	70.2	106	59,100	SY/WB
	0.3	4.8	54.2	88.5	123,900	SY/WB/WS
19	0.5	9.5	92.3	149	23,400	SR
	0.4	7.6	58.4	91.9	26,200	WS
	0.3	5.7	48.1	72.1	24,800	WS

*SR: Stud Rupture; SY: Stud Yielding; WB: Web Bearing; WS: Web Shear

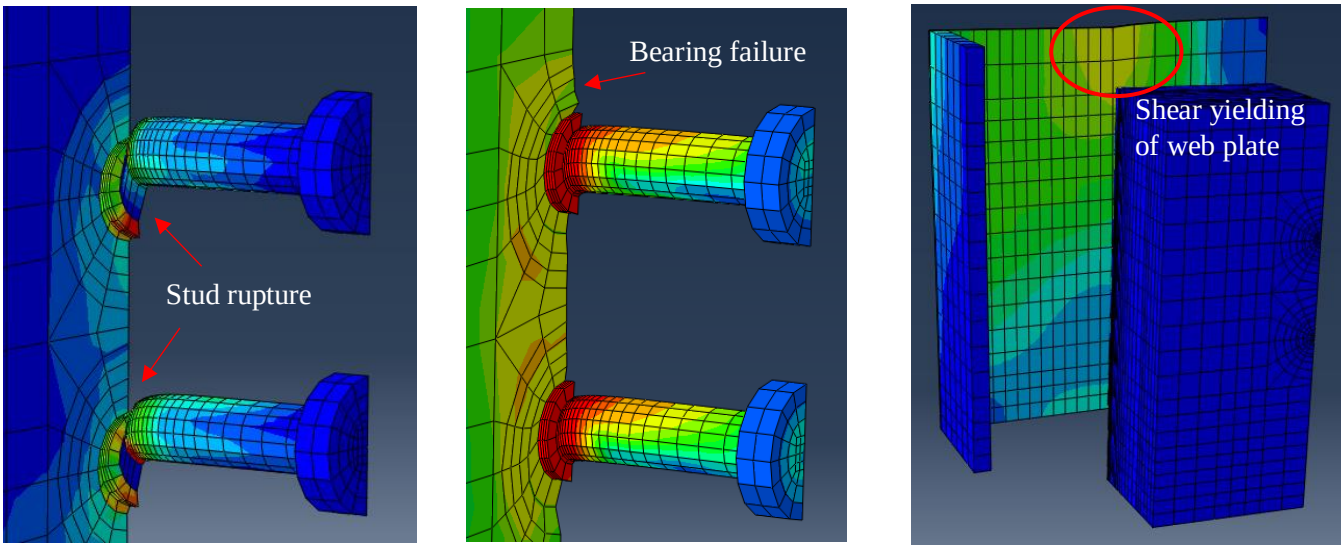

a) Stud yielding/rupture b) Web bearing c) Web shear

Fig. 21. Visualization of failure mechanisms for t_w/d_b assessment

From the table, it is observed that a ratio of 0.5 is the threshold for development of full plastic capacity of the headed shear studs. When a t_w/d_b ratio below 0.5 was implemented, the failure mechanism shifted away from stud rupture. For the 12 mm studs, a t_w/d_b ratio of 0.4 resulted in a combination of stud yielding and web bearing failure as characterized by the large web strains experienced adjacent to the headed stud. This is because the bearing strength of the reduced web plate was lower than the shear strength of the stud. However, at a ratio of 0.4, some stud yielding was still observed. When a ratio of 0.3 was analyzed, complete web bearing failure was achieved with little to no stud yielding, resulting in very large strain demands on the web plate (462,000 με). Similar results were obtained from simulations with 16 mm studs. At a t_w/d_b ratio of 0.4, a combination of stud yielding and web bearing was observed. At a ratio of 0.3, a combination of stud yielding, web bearing and global web shear was observed. Here, global web shear failure is defined as the web yielding at the location of the loading point. This is because the larger diameter studs generate a higher bearing capacity, so the failure mechanism shifts to the next weakest link which is global web shear. For the 19 mm studs, similar results are achieved. At a t_w/d_b ratio of 0.5, stud rupture is the controlling mechanism. At a ratio of 0.4 and 0.3, global web shear is observed because of the high bearing capacity generated by the larger studs. This is further confirmed through the lower web strains experienced at the stud interface (24,800 με and 26,200 με for 0.3 and 0.4, respectively). This indicates that the larger web strains resulting in significant yielding are experienced at the loading interface, causing the global web shear phenomenon.

Fig. 22 shows the force vs. slip relationships for all simulations conducted in this parametric study. Fig. 20a depicts the force vs. slip curves for 12 mm studs. For the experimental part of this work, an initial ratio of 0.75 was used, corresponding to a web thickness of 9.5 mm. From there, ratios of 0.5 and 0.6 generate at least 98% of the plastic capacity with a failure

mechanism of stud rupture as characterized by significant softening after a slip of 4 mm. When a ratio of 0.4 was incorporated, no such softening was observed due to a combination of stud yielding and local web yielding. At a ratio of 0.3, the connection was governed mostly by web bearing failure, as little demand was placed on the stud shank. For the 16 mm studs, the shape of the force vs. slip curves looks similar to the experimental benchmark sample when a ratio of 0.5 – 0.6 was used. When a ratio of 0.4 was considered, a combination of stud yielding and web bearing was the governing failure mechanism. At 0.3, a new mechanism was introduced as global web shear failure was observed. This is characterized by the sharper elbow at the yield point of the force vs. slip curve. Finally, the 19 mm studs only achieved full plastic capacity at a t_w/d_b ratio of 0.5. Below this ratio, the failure mode shifted to global web shear because of the higher bearing strength generated from a larger stud. The force vs. slip for the global web shear displays no ductility because slip is defined as the relative displacement between the UHPC panel and the web plate. However, global web shear occurs at the loading point away from the panel. Therefore, some elastic displacement is experienced by the system until the web begins to yield outside of the panel zone.

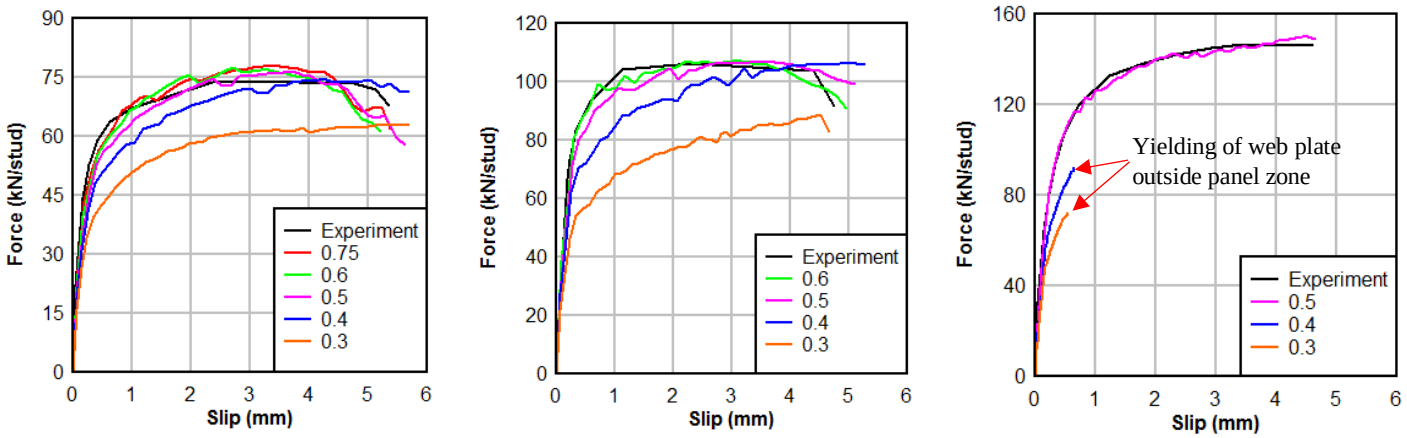

a) 12 mm studs b) 16 mm studs c) 19 mm studs

Fig. 22. Force vs. slip for various stud diameters according to t_w/d_b ratio

Conclusions

The validation of push-out experiments was conducted with headed studs welded on thin web plates of weathered girders and embedded in UHPC through finite element analysis using ABAQUS. Based on the physical material properties, material models were assigned with damage models developed through classical formulations. With good agreement achieved between the simulations and experimental results, two parametric analyses were conducted. One study focused on the effect of an eccentrically loaded stud group with various offsets. The second analysis captured the effect of web thickness to stud diameter assuming the defined material properties. The following conclusions are made from this study:

- Material models were calibrated for the base beam section, headed studs, and UHPC materials used in this study. Using classical formulations, damage models were incorporated into the true stress responses. Simulated coupon results showed good agreement to the physical coupon test results.
- The shear behavior of headed studs welded on a 9.5-mm thick web plate and embedded in UHPC was validated through finite element simulations. Five push-out samples were considered: three stud diameters (12 mm, 16 mm and 19 mm) and two specimens with an eccentricity of 50 mm and 100 mm. With proper boundary conditions and calibrated interaction parameters, good agreement was achieved.
- An eccentrically loaded stud group embedded in UHPC was studied under various eccentricities. It was observed that, as the eccentricity increased, the total load bearing capacity of the stud group decreased. The relationship between in-plane torsion and

longitudinal shear capacity was studied and a formulation for the load bearing capacity of an eccentrically loaded single-column stud group was proposed.

- A parametric study was conducted to determine the influence of web thickness to stud diameter ratio with the given material properties. It was found that a minimum t_w/d_b ratio of 0.5 should be maintained to generate full plastic capacity of the studs without significant yielding of the web plate.
- When a t_w/d_b ratio below 0.5 was introduced, the failure mechanism shifted away from stud failure. For 16 mm studs, bearing of the web plate was the controlling mechanism. When larger studs diameters (i.e. 19 mm) were incorporated into the model, a larger bearing capacity of the web plate was generated. This shifted the failure mode to global shear failure of the web plate under the defined loading conditions.

References

1. Zaghi, A.E., Wille, K., Zmetra, K., and McMullen, K. (2015). "Repair of Steel Beam/Girder Ends with Ultra High Strength Concrete (Phase I)." Connecticut Department of Transportation. University of Connecticut. SPR-2282 (Report #CT-2282-F-15-2).
2. Zmetra, K. (2015). “Repair of Corrosion Damaged Steel Bridge Girder Ends by Encasement in Ultra-High Performance Concrete.” Ph.D. Dissertation, University of Connecticut, Storrs, CT.
3. Zmetra, K., McMullen, K., Zaghi, A.E., Wille, K. (2017). “Experimental Study of UHPC Repair for Corrosion-Damaged Steel Girder Ends.” Journal of Bridge Engineering, 22(8).
4. McMullen, K., Kruszewski, D., Zaghi, A.E., Wille, K. (2017). “A Novel Repair Method for Steel Girders with Corrosion Damage Utilizing UHPC.” Proc. of the International Bridge Conference 17-106, National Harbor, Maryland, USA.
5. Kruszewski, D., Wille, K., Zaghi, A.E. (2018) “Push-Out Behavior of Headed Shear Studs Welded on Thin Plates and Embedded in UHPC.” Engineering Structures 173(1). pp 429 – 441.
6. Xu, C., Su, Q., Sugiura, K. (2017). “Mechanism study on the low cycle fatigue behavior of group studs shear connectors in steel-concrete composite bridges.” Journal of Constructional Steel Research 138. pp 196 – 207.
7. Rocha, J.D.B., Arrizabalaga, E.M., Quevedo, R.L., Morfa, C.A.R. (2012). “Behavior and strength of welded stud shear connectors in composite beam.” Rev. Fac. Ing. University of Antioquia 63.

8. Kim, J.S., Kwark, J., Joh, C., Yoo, S.W., Lee, K.C. (2015) “Headed stud shear connector for thin ultrahigh-performance concrete bridge deck.” Journal of Constructional Steel Research, 108(1), 23-30.
9. Hegger, J., Sedlacek, G., Döinghaus, P., Trumpf, H., and Eligehausen, R. (2006) "Studies on the ductility of shear connectors when using high-strength steel and high-strength concrete." *Proc., International Symposium on Connections between Steel and Concrete*, University of Stuttgart, 1025-1045.
10. Luo, Y., Hoki, K., Hayashi, K., Nakashima, M. (2016). “Behavior and Strength of Headed Stud-SFRCC Shear Connection. II: Strength Evaluation” Journal of Structural Engineering 142(2), ASCE.
11. Bouchair, A., Bujnak, J., Duratna, P., Lachal, A. (2012). “Modeling of the steel-concrete push-out test.” Procedia Engineering 40, Steel Structures and Bridges. pp 102 – 107.
12. AASHTO (2012). *AASHTO LRFD Bridge Design Specifications,* American Association of State Highway and Transportation Officials, Washington, DC 20001.
13. Pavlovic, M., Markovic, Z., Veljkovic, M., Budevac, D. (2013). “Bolted shear connectors vs. headed studs behavior in push-out tests” Journal of Constructional Steel Research 88(1). pp 134 – 149.
14. ABAQUS Use Manual. Version 6.9. Providence, RI, USA: DS SIMULIA Corp. 2009.
15. ASTM E8 (2016). “Standard Test Methods for Tension Testing of Metallic Materials”. ASTM International, West Conshohocken, PA, 2016. www.astm.org
16. Brockenbrough (2002). “AISC Rehabilitation and Retrofit Guide – A Reference for Historic Shapes and Specifications”. American Institute of Steel Construction (AISC), Pittsburgh, PA.

17. Rice, J.R., Tracey, D.M. (1969). "On the ductile enlargement of voids in triaxial stress fields." Journal of Mechanical Phys. Solids 17(201).
18. Lemaitre, J. (1985). "A continuous damage mechanics model for ductile fracture." Journal of Engineering Material Technology 107(1). pp 83-90.
19. Bonora, N., Ruggiero, A., Esposito, L, Gentile, D. (2006). "CDM modeling of ductile failure in ferritic steels: assessment of the geometry transferability of model parameters." International Journal of Plastics. 22(11).
20. Lee, J., Fenves, G.L. (1998). "Plastic-damage model for cyclic loading of concrete structures." Journal of Engineering Mechanics, Vol. 124, No. 8. pp 892 – 900.
21. Lubliner, J., Oliver, J., Oller, S., Onate, E. (1989). "A plastic-damage model for concrete." International Journal for Solid and Structures, 25(3). pp 299 – 326.
22. Li, J. (2011). "Evaluation of Elastic-Plastic and Damage Models for Ultra High Performance Concrete (UHPC)." University of Connecticut Master's Thesis.

Chapter 4

Durability Study of Headed Shear Studs Embedded in Ultra High Performance Concrete via Electrochemical Corrosion

Introduction

According to the Federal Highway Administration, U.S. federal and state government agencies spend billions of dollars each year on bridge rehabilitation and maintenance as a direct result of damage due to corrosion (NACE International 2018). Particularly in regions where deicing chemicals are used, corrosion at the girder ends of bridges may result in significant section loss, posing a threat to the users of the structure. Corrosion has been cited as a contributing factor in several bridge failures of varying severity, ranging from failed load ratings to complete collapses (FHWA Report HIF-16-002, 2015). Several studies have examined the influence of realistic levels of section loss on the load-bearing capacity of bridge girders. When corrosion damage is present over more than 10% of the height of the web plate and its thickness is reduced by more than 50%, the ultimate bearing strength of the girder end decreases significantly (Tohidi et al., 2015). Experiments performed with girders containing approximately 70% section loss in the web plate showed that the bearing capacity was reduced by approximately 76% (Zmetra et al., 2015). Thus, particular attention should be paid to the repair of damaged girder ends to restore the strength.

An efficient and easy-to-implement repair strategy has been developed to quickly restore the strength of girder ends suffering from section loss (Fig. 1). In this repair, headed shear studs are welded to the web plate just above the reduced area and encased in ultra-high performance concrete (UHPC) to support the weakened web and bearing stiffeners. Extensive experimental and numerical studies have been conducted to prove the structural effectiveness of this repair through a multi-year research project funded by the Connecticut Department of Transportation. First, large-scale experiments were conducted to evaluate the strength of one-third scale rolled girders with simulated corrosion damage (Zaghi et al., 2015; Zmetra et al., 2017). The results showed that the implementation of the repair lessens strains on the reduced section of the web plate, and instead transfers the demands to the studs and UHPC panels. Additionally, a comprehensive series of push-out experiments was conducted to evaluate the capacity of headed studs when welded onto thin, weathered web plates and embedded in UHPC (Kruszewski et al., 2018a, b). The results revealed that when 12-, 16-, and 19-mm headed studs are welded to a 9.5-mm thick web plate and loaded

in shear, stud shank failure governs with little to no damage to the UHPC panels or web plate. Finally, several large-scale tests were conducted with 140-cm deep plate girders with 75% section loss in the web plate and approximately 50% section loss in the bearing stiffeners (McMullen et al., 2018). After implementing the UHPC repair on the weakened girders, the results showed that the bearing capacity was approximately 450% stronger than that of the unrepaired girder. The repaired girder even surpassed the design shear capacity of an original, as-built girder by over 30%.

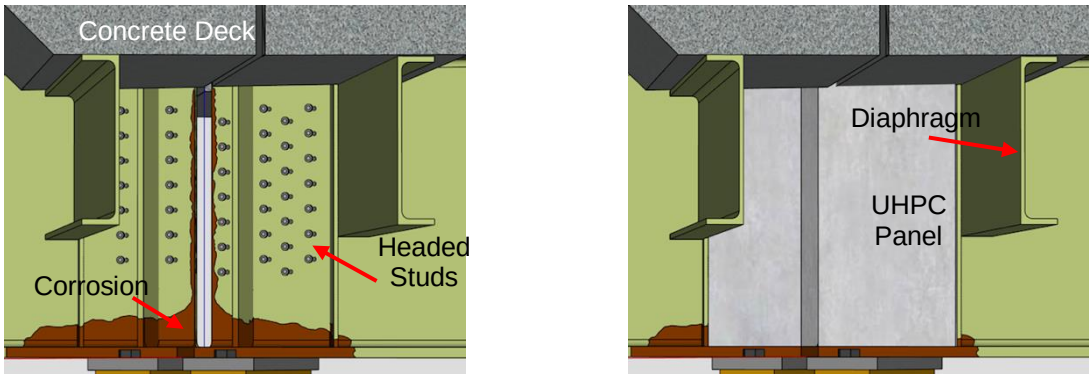

a) Studs welded to intact web plate b) UHPC panels cast

Fig. 1. Schematic of UHPC repair method

Others have made similar efforts to restore the strength of corroded steel bridge girders. One repair method involves the encasement of newly welded stiffeners with high-strength grout (Wu et al., 2018). The composite connection is created with threaded rods which are welded to the new stiffeners and embedded in high-strength grout to support the weakened web. It was found that the implementation of this procedure strengthened the girder capacity by 230% compared to that of the damaged specimen.

While significant progress has been made to prove the effectiveness of this new repair method, the durability of the repair after implementation remains a parameter of critical interest. Confirmation of the long-term durability of the repair is important to the bridge designers and owners because it provides confidence that the repair is effective in preventing further deterioration, while effectively sustaining or improving the original capacity. Significant efforts have been taken by other researchers to understand the

cause and effect of corrosion in composite connections involving headed studs embedded in concrete. When subjected to accelerated electrochemical corrosion, the ultimate strength of headed studs embedded in regular strength concrete (RSC) decreased by 50% as the corrosion rate increased to approximately 23% (Chen et al., 2016). Similar results were obtained for various stud diameters (Xue et al., 2017). However, these studies are limited to RSC and thus more information is needed to be applicable to the proposed repair, as the embedment material is UHPC. Another aspect of interest may be the influence of corrosion as a function of repeated loadings, a scenario which will occur due to service loads after field implementation. When stud connectors are subjected to corrosion and fatigue, it was found that their maximum slip at each fatigue cycle increased with an increasing corrosion rate (Chen et al., 2016). When evaluating the coupled impact of corrosion and load, it was found that long-term forces in a steel-concrete composite connection strongly influence the development of strain in the concrete, while corrosion strongly affects the stiffness and capacity of the connectors (Cao et al., 2018). However, these results again pertain to studs embedded in RSC, and the available literature regarding the performance of studs when embedded in UHPC is scarce.

Since the headed studs in the repair method are embedded in UHPC, their mechanical performance may differ from the performance exhibited when they are embedded in conventional concrete. This is because UHPC is known to have superior durability properties compared to RSC due to its dense microstructure (Fehling et al., 2014). Further, the headed studs in this repair will always be welded to an old and weathered web plate of a bridge which was likely constructed decades ago. Corrosion may have a more significant impact on older base material with a different chemical composition than modern steel (Brockenbrough 2012). In addition, the protective nature of UHPC must be assessed when it is cast against a web plate with a thickness of 9.5 mm to determine if further section loss should be anticipated. This may lead to a different failure mechanism, as the 9.5-mm web plate is already thin compared to the flanges onto which studs are traditionally welded.

This paper presents the experimental results from six push-out tests to develop a better understanding of the influence of corrosion on headed studs embedded in UHPC. Each specimen was

carefully designed to evaluate a parameter of interest relevant to the repair method. The factors studied include a) the influence of chlorides initially present on web plate, b) the deterioration of the bond between the UHPC and web plate through cyclic service loads, and c) the performance of high-strength concrete as the embedment material. To induce accelerated deterioration, electrochemical corrosion was used according to Faraday's theory. Experimental results such as force-slip relationships and failure mechanisms were studied. The UHPC panels were visually examined for corrosion penetration. The results of this study are used to close the knowledge gap related to the effect of corrosion on headed studs embedded in UHPC or HSC.

Experimental Methodology

The objective of this study is to assess the behavior of headed shear studs embedded in UHPC when subject to corrosion. This section discusses the methodology used to evaluate various conditions of corrosion induced onto the headed studs. First, details are presented regarding the fabrication process for the push-out samples. Stress-strain characteristics of the base beam section, headed studs, UHPC and HSC materials are presented. Next, the concept of electrochemical corrosion is introduced to describe the method used to corrode the push-out specimens. The various specimens used for experimental evaluation are presented in detail to address the parameters of interest.

Details of Push-Out Specimens

To duplicate the materials expected during field implementation, a beam was salvaged from a demolished bridge which was originally erected in 1958. The rolled beam is approximately 535 mm deep and contains a 9.5-mm thick web plate. First, remnants of loose material and lead paint were removed through sandblasting to reveal the steel surface. Next, 305-mm sections were cut such that individual push-out specimens could be created. Using typical construction practice, a stud gun was used to weld headed shear studs to the web plate. A total of eight headed studs (one column of four studs on each side) were welded with a vertical spacing of four times the diameter of the stud shank, i.e. $4d_b$. This stud arrangement

was kept consistent for all samples. The 12-mm diameter studs used in these experiments are approximately 50 mm long, corresponding to a stud height-to-diameter ratio of 4. The studs were embedded in concrete panels with a clear cover of 20 mm. The concrete was cast such that the steel section was elevated 70 mm above the bottom surface of the panels. The panels were separated under the web plate using a 12-mm piece of foam such that two individual concrete panels were created. This allowed for the steel section to be pushed down during testing, thus activating the headed studs in shear. The 12-mm gap also prevented bearing of the steel onto the concrete panels such that only the headed stud provided shear resistance. A schematic of the fabrication process is shown in Fig. 2.

a) Salvaged Beam | b) Stud Shooting | c) Studs Welded on Beam | d) Push-Out Specimen

Fig. 2. Push-Out Specimen Prepared for Submersion

Two concrete materials are used in this study. The fraction composition of each mix by weight is shown in Table 1. The UHPC mix design is the commercially available Ductal JS1212 which is produced by LaFarge Holcim (Ductal JS1212, LaFarge Holcim). This mix is comprised of a premix powder, water, two high-range water reducers, an accelerator, and high-strength steel fibers. The high-range water reducers and accelerator additives are included to maintain a low water-cement ratio and to promote high early-age strength. When cured at a temperature of 53 °C, this mix is specified to achieve 83 MPa in 12 hours. The HSC mix contains a mixture of cement, water, fine aggregate, and a high-range water reducer. This mix was designed for an ultimate strength of approximately 55 MPa.

Table 1. Concrete Material Designs

Mix Designs (% by weight)			
Component	UHPC	Component	HSC
Premix	86.6	Cement	40.7
Water	5.1	Water	16.9
HRWR 1	0.7	Fine Aggregate	42.2
HRWR 2	0.5	HRWR 1	0.03
Accelerator	0.9		
Steel Fibers	6.2		

Fig. 3 shows the geometry of a typical push-out specimen. To compare the efficiency of the setup, the geometry and dimensions of the concrete panels were kept consistent for each sample. As shown in Fig. 2, no reinforcement was used for the specimens with UHPC, as the high-strength steel fibers in the mix are sufficient to prevent tensile splitting from the studs during testing. However, for the push-out sample with HSC panels, a reinforcement cage was implemented to account for the weak tensile strength of the concrete. To create the reinforcement cage, several #3 bars with 90° hooks on each end were spliced together with sufficient development length (ACI 2012). These small reinforcement bars were selected due to the tight geometry of the concrete panel. The reinforcement was placed with a 32-mm offset from the web such that the cage was resting 6 mm below the stud head (Fig. 3b).

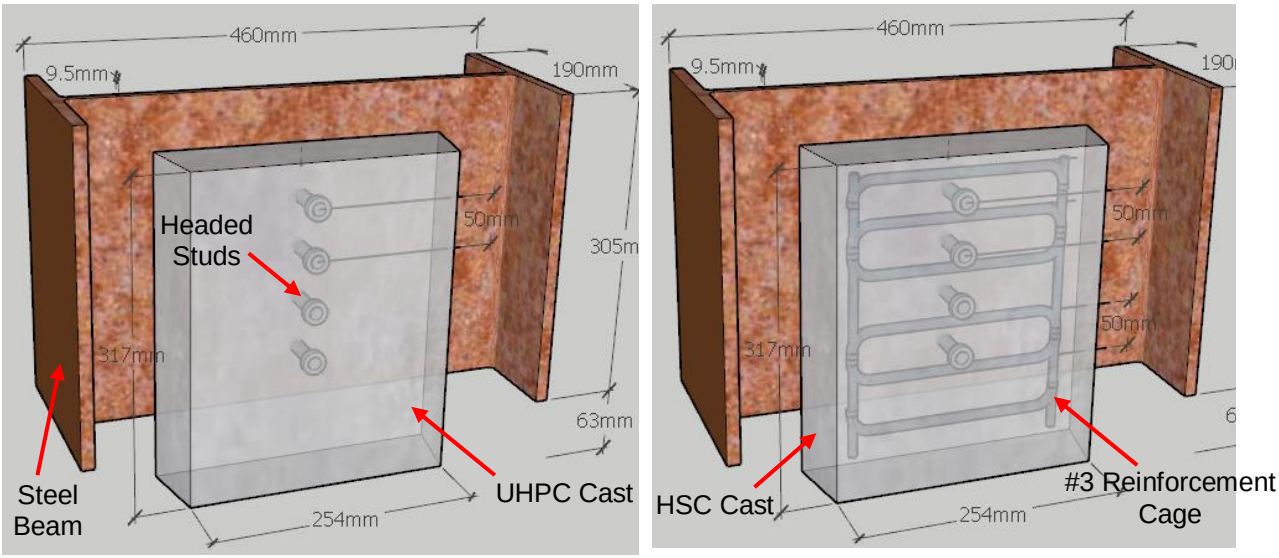

a) UHPC Panels b) HSC Panels with Reinforcement

Fig. 3. Overview of Push-Out Specimen Geometry

Material testing was conducted to extract the stress-strain relationships for the UHPC, HSC materials, base beam section, and headed studs. For the concrete materials, typical cylinders measuring 76 mm x 152 mm were cast for each specimen for quality control. The cylinders were tested in uniaxial compression to generate the stress-strain properties of the UHPC material (ASTM C39). For the steel materials, dog-bone shaped coupons were fabricated. Since the studs are small, a custom-shaped coupon with a reduced throat area was created so that triaxiality effects would be mitigated during testing. Strain was extracted through a high-elongation strain gauge. For the base beam material, coupons were fabricated in accordance with ASTM E8 (ASTM E8). Since the beam coupons were larger than the stud coupons, a 100 mm extensometer was used to monitor the strain in the throat region. All coupons were tested in uniaxial tension at a strain rate of 0.015 mm/mm/min until rupture. The experimental stress-strain results are shown in Fig. 4.

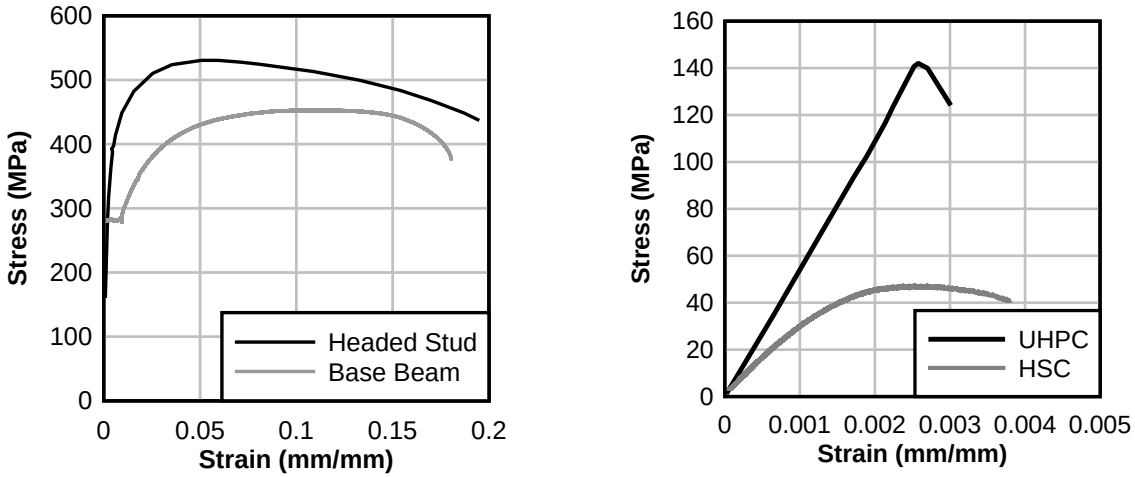

a) Steel Material b) Concrete Material

Fig. 4. Stress-Strain Properties

Accelerated Electrochemical Corrosion

The general phenomenon of corrosion can be summarized as an electrochemical process which requires the simultaneous presence of oxygen and an electrolytic solution (Revie and Uhlig, 2008). An electrolytic solution is one that contains electrolytes which conduct electricity because of the ions present in it. For example, when dissolved in a fluid, salt breaks apart into its component ions (positive ion of sodium and negative ion of chloride) to create an electrolytic solution. A chemical reaction occurs when electrons from the atoms of a metal are transferred to a suitable depolarizer by traveling through the electrolyte (Stansbury and Buchanan, 2000). In this reaction, the metal with the lower reduction potential, i.e. the anode, gets oxidized. Therefore, the cathode undergoes reduction, resulting in section loss. The chemical reaction for this process is shown in Equations 1 and 2, where *Fe* represents Iron which is the dominant chemical present in steel, *e* symbolizes electrons, and *M* stands for a metal of a higher electric charge, corresponding to the anode. For corrosion in steel bridge girders, this phenomenon occurs at the anodic regions on the surface of the steel. When exposed to an electrolyte (such as water or a mixture of salt and water), the ferrous ions present in the steel go into the solution. In this process, electrons transfer

to the structural steel and settle to form hydroxyl ions, which eventually react with the ferrous ions to produce rust. Over time, this process leads to significant section loss of the web plate and flanges.

$$Fe_{(s)} \rightarrow Fe^{2+}_{(aq)} + 2e^{-} \quad (1)$$

$$M^{2+} + 2e^{-} \rightarrow M_{(s)} \quad (2)$$

To simulate this process, electrochemical corrosion was used to corrode the push-out specimens in an accelerated manner. A schematic of this assembly is shown in Fig. 5a. In this setup, the sample was first submerged into an electrolytic solution comprised of 5% sodium chloride (NaCl). Next, a current was impressed onto the specimen through the positive end of a DC power supply. The negative end of the power supply was attached to the anode to complete the circuit. The anode used in this setup was a stainless steel coupon which is known to have a lower reduction potential than the beam section in the push-out specimen. To preserve the portions of the steel beam which are necessary for testing, a two-part epoxy-based paint with cathodic protective properties was applied. The entire surface area of the beam was painted except for the web plate, which was covered by the concrete panels. Additionally, a corner of the flange measuring 75 mm x 75 mm was left unpainted to allow monitoring of the section loss on the beam over time. The painted sample is shown in Fig. 5b.

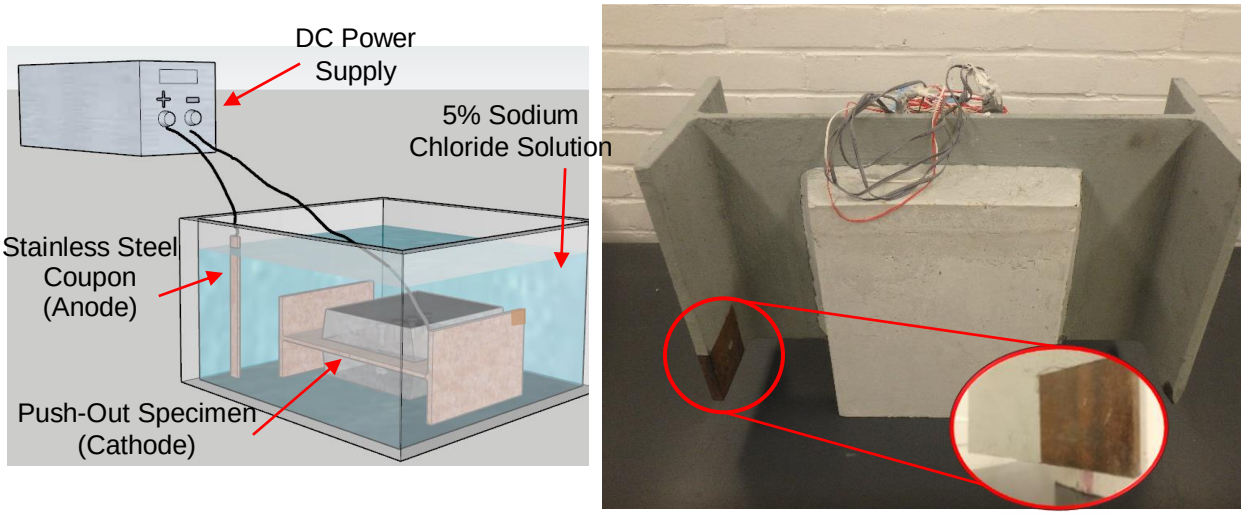

a) Schematic of Corrosion Setup b) Push-Out Specimen with Exposed Flange Section

Fig. 5. Setup for Corrosion

To estimate the equivalent section loss as a result of the electrochemical corrosion, Faraday's theory was incorporated. This allowed for a comparison of the observed and expected corrosion rate. According to Faraday's law (Equation 3), there is a linear relationship between the current applied to the metal and its associated mass loss, as follows:

$$\frac{dm}{dt} = \frac{I_{corr} K (EW)}{\rho A} \qquad (3)$$

, where I_{corr} is the corrosion current (amperes), K is the corrosion rate constant (8.964 mm/day), EW is the equivalent weight (g/equivalent), ρ is the material density (g/mm^3), and A is the exposed area of the sample (mm^2). Using this relationship, the loss of thickness of the exposed flange can be computed if the surface area is known.

A current of 2 Amperes was induced onto the section, corresponding to an expected corrosion rate (CR) of approximately 0.47 mm/day at the exposed corner of the flange. The area of the web plate encased by concrete was not included in the calculation because it was assumed the panels provided corrosion protection. The section loss was regularly measured at the exposed corner and compared to the expected

CR. Fig. 6 shows the corrosion process over time. First, the sample was submerged into the corrosion tank using straps which were suspended from a frame. The positive end of the power supply was attached to the corner of the flange which was not needed for testing. The negative end was attached to a stainless steel coupon which served as the anode. The corrosion was induced until the exposed portion of the flange was reduced by 4 mm, corresponding to an equivalent reduction of approximately 40% of the web thickness. The exposed flange thickness was measured at five locations such that a representative average could be generated. If any section loss of the web plate occurred, it was measured after testing.

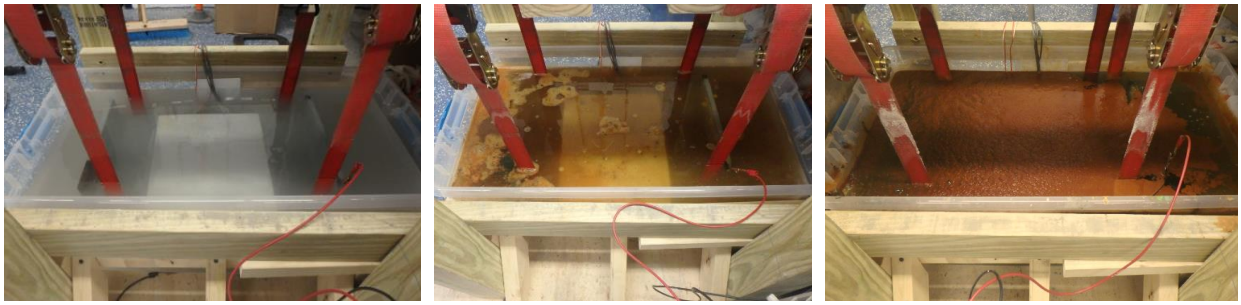

a) Initial Setup b) Start of Corrosion c) Completion of Corrosion

Fig. 6. Overview of Corrosion Process

Experimental Setup

Once the corrosion procedure was complete, the push-out specimens were tested in a 1,700 kN compressive testing machine. The sample was installed so that the concrete panels rested on a spherical bearing, which was used to accommodate for imperfections or misalignment during testing. To prevent excessive axial strain or local buckling of the web plate, the loading was applied through the flanges, which transferred the force to the studs embedded in the UHPC panel. The upward reaction from the spherical bearing ensured that the studs were loaded in shear. Prior to testing, the contact surfaces of the steel beam were smoothened to ensure an even loading plane. The experimental setup is shown in Fig. 7.

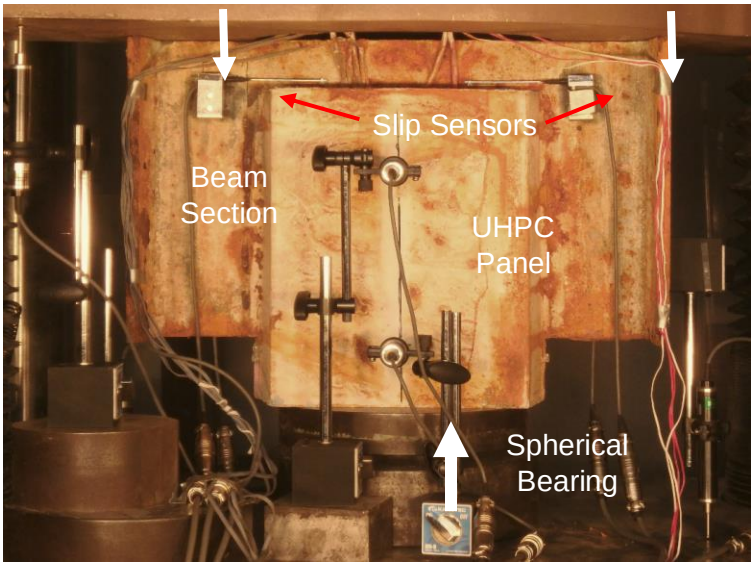

Fig. 7. Experimental Setup for Corroded Samples

Overview of Push-Out Specimens

A total of six push-out samples are considered in this study. Two "benchmark samples" were tested; one contained UHPC panels and the other contained reinforced HSC panels. To reflect the typical behavior of studs embedded in each respective concrete material, these samples were not subject to corrosion. Two similar samples were subjected to electrochemical corrosion to assess their performance after a section loss of 4 mm was achieved on the exposed flange. These samples were designed to investigate whether this process resulted in any penetration of the UHPC panels, thickness reduction of the encased web plate, or deterioration in the headed studs.

The remaining two samples were designed to evaluate a particular aspect of corrosion which may be relevant to field conditions. First, the initial presence of chlorides on the web plate from existing corrosion is of interest. This scenario is important because the candidate bridge girders in need of this repair likely contain some surface rust above the heavily deteriorated portion of the web plate. It may be hypothesized that the initial presence of chlorides could provide an avenue to allow corrosion to further penetrate the web plate, even after the UHPC panels are cast. To investigate this theory, a push-out sample was subjected to corrosion using the accelerated electrochemical process. Following the typical procedure,

the portions of the beam which were necessary for testing were protected with cathodic protective paint. In addition, the studs were wrapped in corrosion-resistant tape so that they were not exposed to the electrolytic solution, thus preventing deterioration. This procedure replicated the scenario in which new headed studs are welded to a web plate with some surface rust present. The initial corrosion was induced for approximately 60 hours, corresponding to 0.2 mm of section loss on the web plate. After 60 hours, the sample was removed from the corrosion tank and the essential portions of the beam were repainted. Next, the UHPC panels were cast onto the corroded web plate and allowed to cure for 7 days. Finally, the sample was re-submerged into the corrosion bath and further corroded until the target section loss of 4 mm was achieved on the exposed flange section. A schematic of the procedure is shown in Fig. 8.

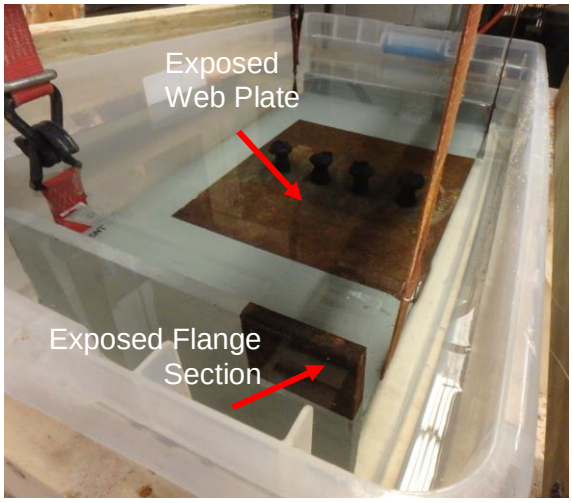

a) Initial corrosion of web plate

b) Condition of beam after initial corrosion

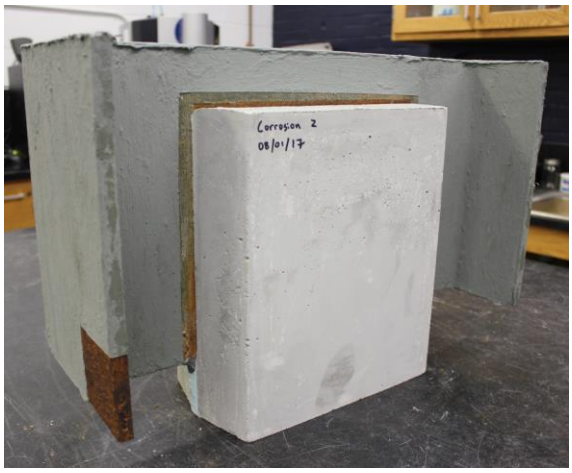

c) UHPC cast over corroded web plate

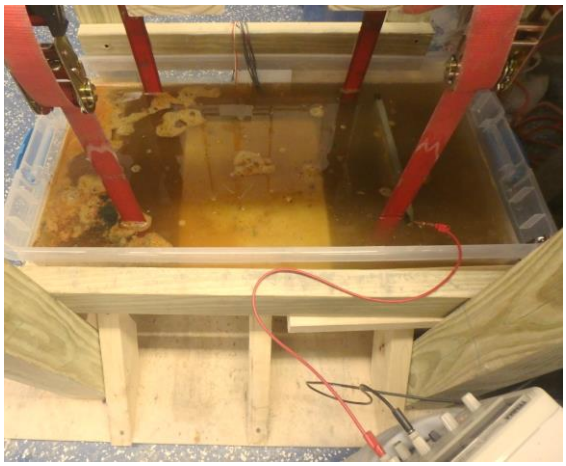

d) Further corrosion

Fig. 8. Procedure for evaluation of initial chloride presence

The second parameter of interest in this study involved breaking the bond between the UHPC cast and the web plate. Engineers may wonder if service loads over the bridge eventually diminish the bond between these two components. If so, this may permit water and additional chlorides to enter the interface and result in further corrosion of the web plate. To address this concern, an experiment was designed consisting of a typical push-out specimen exposed to repeated loading cycles, followed by typical exposure to electrochemical corrosion. First, a sample was cast and painted using standard procedure. Next, the

specimen was mounted into the testing machine. Then, a total of 25 cycles to 40% of the expected yield force, i.e. 17.8 kN/stud, were applied. Next, 25 more cycles up to 80% of the expected yield force, i.e. 35.6 kN/stud, were applied. After each cycle, the specimen was unloaded to a force of approximately 4.5 kN (Fig. 9). These rigorous loading cycles were applied to replicate the demands which may be encountered in the field. When the cycles were complete, the specimen was submerged into the corrosion tank. The current was induced onto the sample such that it corroded until the target section loss of 4 mm on the exposed flange was achieved.

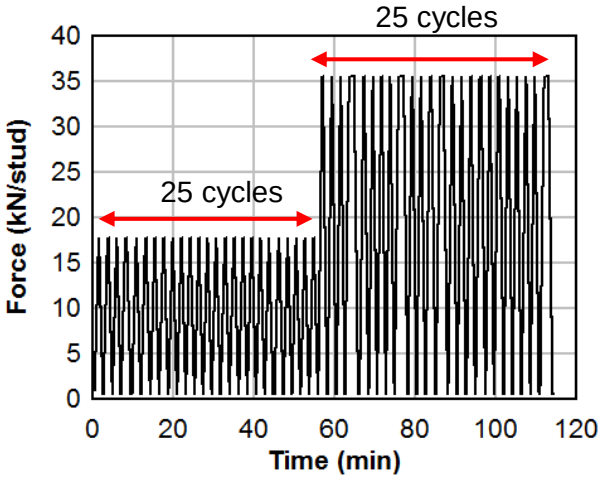

Fig. 9. Cyclic loadings applied prior to corrosion

Table 2 shows a summary of the specimens which were evaluated in this study. The specimen identification format is as follows: [Concrete Material]_[presence of corrosion on web plate][1, 0][cyclic loadings][1, 0]_[electrochemical corrosion]. The concrete materials varied between UHPC and HSC. The binary system of [1, 0] was used to indicate the presence of each parameter, where 1 indicates the presence of the parameter and 0 indicates its absence. For example, the specimen labeled as "UHPC_w0c1_corr1" indicates a push-out sample that contains UHPC panels, does not contain initial chloride presence on the web plate, undergoes cyclic loadings prior to corrosion, and receives accelerated electrochemical corrosion treatment.

Table 2. Summary of Push-Out Experiments

Specimen ID	Concrete Mix	Corrosion	Corroded Web Plate	Cycles
UHPC_w0c0_corr0	UHPC			
UHPC_w0c0_corr1	UHPC	x		
UHPC_w1c0_corr1	UHPC	x	x	
UHPC_w0c1_corr1	UHPC	x		x
HSC_w0c0_corr0	HSC			
HSC_w0c0_corr1	HSC	x		

Results and Discussion

Fig. 10a shows the section loss of each sample as a function of time. The specimen with UHPC panels and a corroded web plate, UHPC_w1c0_corr1, achieved the target section loss in 190 hours, a time period approximately 110 hours less than that of the regular corroded sample (UHPC_w0c0_corr1). The specimen which experienced cyclic loadings prior to corrosion, i.e. UHPC_w0c1_corr1, achieved the target section loss in about 248 hours, a time period approximately 53 hours less than that of the sample with typical corrosion. Fig. 10b shows a representative corroded specimen after achieving the target section loss on the exposed flange region.

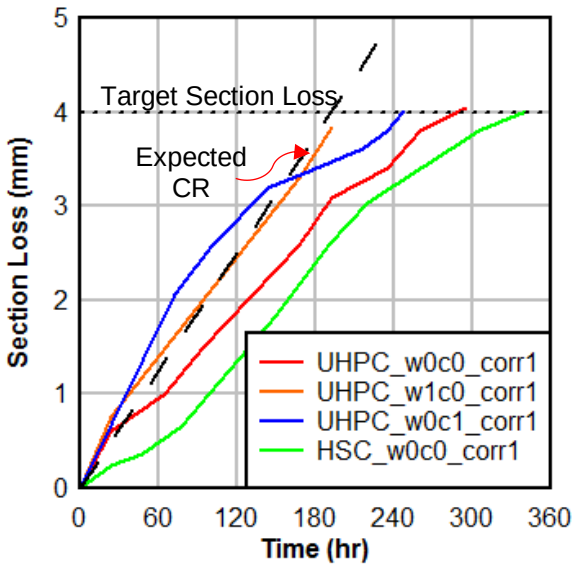

a) Section Loss Over Time

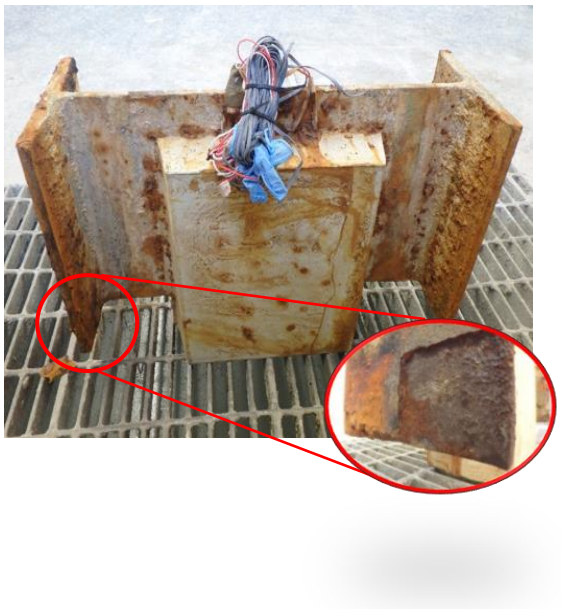

b) Reduced Flange Section

Fig. 10. Results of the Corrosion Process

Table 3 shows a summary of the experimental results. In the following summary, elastic stiffness is defined as the slope of the force-slip curve up to one-third of the overall capacity in the elastic region (JSSC 2002). The yield slip and yield force for each curve was calculated using a method adopted for 12-mm diameter headed shear studs embedded in UHPC, by extending a yield line with a slope of 220 kN/mm with an offset of 0.1 mm (Kruszewski et al., 2018). Ultimate slip is defined as the maximum slip experienced prior to rupture of the studs, including brief softening at the end of the loading before failure. Ultimate force is considered to be the maximum force sustained by the specimen divided by the number of studs.

The table shows that all specimens with UHPC panels generated a stud capacity of 74 – 79 kN with a corresponding ductility of 4.63 – 5.08 mm. The sample with the lowest total capacity was the one subject to cyclic loading prior to corrosion. This result is expected, as some residual stresses may have accrued during the cycles. The push-out samples with HSC generated a stud capacity of 48 – 50 kN. Ultimate slip was not reported for the specimens with HSC because the softening phase of the samples was characterized by significant displacement due to local crushing of the concrete. This failure mechanism did not allow for identification of a particular "slip at failure". However, it is observed that the induction of corrosion had no significant effect on the capacity of the studs. This observation extends to the specimens with initial web corrosion and also the sample which was subject to cyclic loadings prior to corrosion. Fig. 11 shows the force-slip results for all specimens tested. The elastic stiffness is comparable among all samples with UHPC panels. A slight deviation in elastic stiffness is observed for the specimens containing HSC panels, which may be attributed, in part, to the corrosion present behind the panels.

Table 3. Experimental Results

Specimen ID	Concrete f'c	CR	Elastic Stiffness	Yield Slip	Yield Force	Ultimate Slip	Ultimate Force	Failure Mechanism
Unit	MPa	mm/day	kN/mm	mm	kN/stud	mm	kN/stud	---
UHPC_w0c0_corr0	165	---	238	0.51	62.1	4.94	77.7	Stud Rupture
UHPC_w0c0_corr1	164	0.33	230	0.54	67.2	5.08	79.4	Stud Rupture
UHPC_w1c0_corr1	145	0.50	232	0.47	53.7	4.84	78.9	Stud Rupture
UHPC_w0c1_corr1	155	0.39	218	0.52	64.1	4.63	74.3	Stud Rupture
HSC_w0c0_corr0	55	---	39.5	1.76	42.7	---	50.5	Concrete Crushing
HSC_w0c0_corr1	54	0.28	26.9	1.19	27.64	---	48.4	Concrete Crushing

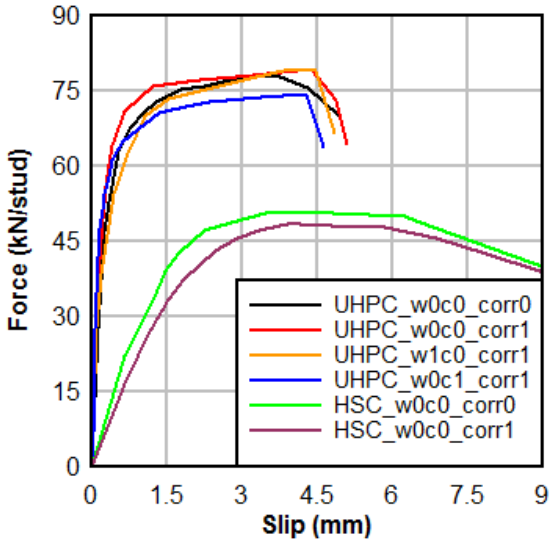

Fig. 11. Results of corrosion process

Two failure modes were observed in these experiments. All UHPC samples failed via stud rupture, which is characterized by shear failure of the stud shank just above the weld collar near the surface of the UHPC (Fig. 12a). For these samples, the weld collar remained welded on the beam section. This failure mechanism indicates that the studs utilized their full plastic shear capacity. From the figure, it may be observed that there is little to no presence of surface rust around the location of the studs. This indicates that the bond between the UHPC panels did not allow the solution to enter the interface, thus preventing corrosion of the web plate adjacent to the studs. On the other hand, Fig. 12b shows the specimens which

contained HSC panels. The governing failure mode (for both samples with HSC) was local crushing and separation of concrete due to a lack of cover and crowding of the reinforcement (Kruszewski et al., 2018). The premature crushing of the concrete did not allow for the full engagement of the studs, resulting in a softer response. Upon further displacement, the studs started to drive through the crushed concrete which resulted in a long softening phase. Some flexural yielding in the studs was observed; however, this was not the governing failure mode.

a) Samples with UHPC panels b) Samples with HSC panels

Fig. 12. Push-out specimens after testing

Since UHPC is the main candidate embedment material in the proposed repair method, one parameter of interest is the condition of the studs inside the panels after the corrosion process. To allow visual observation of their condition, the UHPC panel was cut down the centerline of the studs. Fig. 13a shows the condition of the studs for the corroded sample. It is observed that no visible rust is present around the perimeter of the studs. Additionally, no rust of the fibers was noticed. The condition of the studs was compared to the uncorroded benchmark sample (Fig. 13b). The visual observations indicate that the studs are in comparable condition. This assessment ensures that UHPC exhibits protective behavior for headed studs. This result is expected, as shear connectors for bridge decks typically exhibit little to no corrosion throughout the lifespan of a bridge. However, this analysis provides reassurance regarding the superior durability of the proposed repair.

a) Corroded Specimen b) Benchmark Specimen

Fig. 13. UHPC Panels Cut Down Centerline

Conclusions

This paper presents the experimental evaluation of headed shear studs embedded in UHPC and HSC and subject to accelerated electrochemical corrosion. Push-out samples were fabricated and corroded in a 5% NaCl solution. Faraday's theory was used to calculate the expected corrosion rate for the samples. After significant section loss on a representative portion of the steel beam, the specimens were tested to identify any deterioration in their mechanical behavior. The following conclusions are made from this study:

- Faraday's theory generated reasonable agreement between the expected and observed corrosion rate. The rates were not perfectly matched; the variables of interest may have introduced additional surface areas which were exposed to the electrolytic solution, thus deviating the observed corrosion rate from the expected one.
- The results show that push-out specimens with UHPC achieved a stud capacity of 74 – 80 kN with a corresponding ductility of 4.63 – 5.08 mm. The failure mode was stud shank rupture. These results were consistent for the benchmark corrosion sample, as well as for samples with initial chlorides present on the web plate, and for those with cyclic loadings prior to corrosion.

- Push-out specimens with HSC panels generated a stud capacity of 48.4 – 50.5 kN/stud. The failure mode was concrete crushing due to overcrowding of the reinforcement in the tight geometry of the panels. No ultimate slip was identified due to a lengthy softening phase.
- The accelerated electrochemical corrosion induced on the samples did not hinder the mechanical performance of studs embedded in UHPC or HSC. This may be because both types of concrete panels (UHPC and HSC) prevented the electrolytic solution from penetrating through to the web plate, thus protecting the headed studs.

References

ACI – 239 Committee in Ultra-High Performance Concrete (2012). *Minutes of Committee Meeting October 2012*, ACI Annual Conference 2012, Toronto, ON, Canada.

ASTM C39 (2018). *Standard Test Method for Compressive Strength of Cylindrical Concrete Specimens,* ASTM International, West Conshohocken, PA, 2016. www.astm.org

ASTM E8 (2016). *Standard Test Methods for Tension Testing of Metallic Materials,* ASTM International, West Conshohocken, PA, 2016. www.astm.org

Brockenbrough, R.L. (2002). *AISC Rehabilitation and Retrofit Guide – A Reference for Historic Shapes and Specifications,* American Institute of Steel Construction (AISC), Pittsburgh, Pennsylvania, U.S.A.

Cao, G., Yang, L., Zhang, W., Peng, X., Dai, Y. (2018). *Long-Term Mechanical Properties of Steel-Concrete Connectors Subjected to Corrosion and Load Coupling,* Journal of Materials in Civil Engineering, ASCE 30(5).

Chen, J., Jiang, W., Jin, W. (2016). *Behaviour of Corroded Stud Shear Connectors under Fatigue Loading,* Proceedings of the 5th International Conference on Durability of Concrete Structures, Shenzhen University, Shenzhen, Guangdong Province, P.R. China.

Chen, J., Zhao, Y., Wu, L., Jin, W. (2016). *Experimental investigation and design of corroded shear stud connectors,* Advances in Structural Engineering 19(2), pp. 218 – 226.

Ductal JS1212 (2016). *JS1212 Rapid Strength Product Data Sheet*, Ductal, LaFarge Holcim, New Haven, Connecticut, U.S.A. https://www.lafargeholcim.com/

Fehling, E., Schmidt, M., Walraven, J., Leutbecher, T., Frohlich, S. (2014). *Ultra-High Performance Concrete, UHPC. Fundamentals, Design, Examples*, Wilhelm Ernst & Sohn, Berlin, Germany.

FHWA Report No. HIF-16-002 (2015). *Steel Bridge Design Handbook: Corrosion Protection of Steel Bridges*, Federal Highway Administration, McLean, Virginia, U.S.A.

JSSC (Japan Society of Civil Engineers). (2002). *Guidelines for performance-based design of steel-concrete hybrid structures*, Tokyo, Japan.

Kruszewski, D., Wille, K., Zaghi, A.E. (2018). *Design Considerations for Headed Shear Studs Embedded in Ultra-High Performance Concrete as Part of a Novel Bridge Repair Method*, Journal of Constructional Steel Research 149(1). pp 180 – 194.

Kruszewski, D., Wille, K., Zaghi, A.E. (2018). *Push-Out Behavior of Headed Shear Studs Welded on Thin Plates and Embedded in UHPC*, Engineering Structures 173(1). pp 429 – 441.

LaFarge Holcim. (2018). *Building materials, cement, aggregates and concrete*, LaFarge Holcim, New Haven, Connecticut, U.S.A. https://www.lafargeholcim.com/

McMullen, K., Zaghi, A. E., Culmo, M. (2018). *Repair of Corroded Steel Plate Girders with Ultra-High Performance Concrete*, 9th International Conference on Bridge Maintenance, Safety, and Management, IABMAS. July 9-13, 2018, Melbourne, Australia.

NACE International: Highways and Bridges (2018). *Corrosion Resources for Highways and Bridges*, NACE International. https://www.nace.org/Corrosion-Central/Industries/Highways-and-Bridges/

Revie, R.W., Uhlig, H.H. (2008). *Corrosion and Corrosion Control*, John Wiley & Sons, Inc., Hoboken, New Jersey, U.S.A.

Stansbury, E.E., Buchanan, R.A. (2000) *Fundamentals of Electrochemical Corrosion*, ASM International, Materials Park, Ohio, U.S.A.

Tohidi, S., Sharifi, Y. (2016). *Load-carrying capacity of locally corroded steel plate girder ends using artificial neural network."* Thin-Walled Structures (100). pp 48 – 61.

Wu, B., Cao, J., Kang, L. (2018). *End patch loading behavior and strengthening of locally corroded steel I-beams,* Journal of Constructional Steel Research 148. pp 371 – 382.

Xue, W., Chen, J., Zhu, J. (2017). *Behaviour of Corroded Single Stud Shear Connectors,* MDPI Materials 10. pp 1 – 12.

Zaghi, A.E., Wille, K., Zmetra, K., and McMullen, K. (2015). *Repair of Steel Beam/Girder Ends with Ultra High Strength Concrete (Phase I),* Connecticut Department of Transportation. University of Connecticut. SPR-2282 (Report #CT-2282-F-15-2).

Zmetra, K. (2015). *Repair of Corrosion Damaged Steel Bridge Girder Ends by Encasement in Ultra-High Performance Concrete*, Ph.D. Dissertation, University of Connecticut, Storrs, CT.

Zmetra, K., McMullen, K., Zaghi, A.E., Wille, K. (2017). *Experimental Study of UHPC Repair for Corrosion-Damaged Steel Girder Ends,* Journal of Bridge Engineering, 22(8).

Chapter 5

Experimental Evaluation of Shear Connectors Embedded in Ultra-High Performance Concrete

Introduction

Civil infrastructure applications are drastically evolving with new and innovative concepts to push the limits of structural design practice. The main benefits that push engineers to use novel design concepts include producing structural components that are lighter, stronger, and more durable than their outdated counterparts. A major avenue of innovation is developing alternative shear connectors with new, high-performance materials to promote more efficient composite connections. While shear connectors such as headed studs are typically installed on relatively thick plates such as top flanges for bridge deck connections (Ollgaard et al., 1971), there is a need to push this limitation so that they may be applied to broader applications. This paper focuses on the experimental evaluation of several simple shear connectors installed on relatively thin plates and embedded in Ultra-High Performance Concrete (UHPC). The results of this study are expected to inform designers about the mechanical characteristics of these novel connectors and to encourage their use in design practice.

There is a plethora of literature regarding novel shear connectors embedded in high-strength concrete (HSC) or UHPC which is already driving novel composite connections forward. To inform the reader, a few examples are presented here. Innovative shear connectors such as a combined fixing strips, t-profiled connectors, sleeved stud connectors, and bolted connections were experimentally evaluated when embedded in high-strength concrete (HSC) (Hegger et al., 2001). It was found that the t-bulb fixing strip exhibited excellent shear capacity and ductility compared to headed stud connectors. To enhance their ductility, the implementation of a larger weld collar or sleeve shaft was recommended for headed studs. Another study by the same author evaluated the puzzle strip and saw tooth shear connectors embedded in UHPC (Hegger et al., 2009). It was found that the puzzle strip shear connector carries high shear loads with satisfactory ductility according to the Eurocode (Eurocode-4, 2004). The saw tooth connector generated a high shear capacity and ductility but only when loaded in its optimal direction. The fatigue performance of puzzle-shaped composite dowels was assessed when embedded in UHPC (Classen et al., 2016). He concluded that UHPC breakout governs the connection when a load range of 55% up to 80% of the static

pull-out capacity is applied. 24 push-out experiments were conducted with perfobond strip connectors, concluding that a UHPC dowel surrounding a transverse reinforcement bar increases the resistance of the standard connection by 46% (He et al., 2017). Wang et al. observed the influence of aspect ratio for demountable headed stud connectors in UHPC, concluding that a minimum aspect ratio of 1.5 must be maintained to generate stud failure (Wang et al., 2018).

Although many shear connectors have been designed to improve upon the mechanical performance of those currently used in practice, many of these connectors are intended to be used in composite connections for bridge decks (Suwaed et al., 2017). In this application, the connectors are often installed on the top flange of the superstructure which is usually thicker than 12 mm. However, several novel applications require shear connectors to be installed on thinner plates. For example, a novel bridge repair method for corroded steel girder ends has been developed involving the use of headed shear studs welded on the web plate of the affected girder and embedded in UHPC (Zmetra et al., 2015; Zaghi et al., 2015; Zmetra et al., 2017; McMullen et al., 2017). In this repair, the weakened web plate is strengthened through the composite action of the studs bearing onto the UHPC panels. However, in many cases, web plates of girders can be as thin as 9.5 mm. When shear connectors are installed on such a thin plate, a different failure mechanism may govern and thus the design may not perform as intended. Another similar concept involves strengthening deteriorated girder ends by welding new stiffeners to the affected region (Wu et al., 2018). This method utilizes threaded rods which are welded to the new stiffeners and embedded in high-strength grout, creating a composite connection to support the weak web plate. However, there is a need to understand the behavior of threaded rods when installed on a relatively thin plate to avoid unintended damage to the stiffener. The implementation of plate-reinforced composite coupling beams is another novel design concept involving shear connectors on thin plates (Lam et al., 2013). This concept involves an alternative design for conventional reinforced concrete coupling beams to improve the strength, ductility and dissipation. In this design, a vertical steel plate with welded shear studs is embedded as a coupling

mechanism to enhance the ductility of the connection. However, the critical shear transfer mechanism must be carefully studied, as the vertical plate may be as thin as 12 mm.

While an extensive study has been conducted to understand the performance of headed studs when welded on such thin plates (Kruszewski et al., 2018a, b). However, there is still a need to evaluate other shear connectors in a similar manner. This paper presents the experiments results of six push-out tests which were designed to address the mechanical uncertainties associated with installing shear connectors on thin plates. Three simple shear connections are considered in this study: 1) headed shear studs, 2) demountable threaded bars, and 3) UHPC dowels with no transverse reinforcement. Failure mechanisms, force-slip relationships, and strain demands on the plate are presented to provide an in-depth understanding of the behavior of these connectors when installed on thin plates.

Experimental Program

To evaluate the performance of the alternate shear connectors when installed on thin plates, push-out experiments were designed such that the mechanical behavior of each connector could be observed. Three types of shear connectors are proposed in the study: a) headed shear studs, b) demountable threaded bar, and c) UHPC dowel. These connectors were selected because the materials are readily available, the shear connection mechanism is straight forward, and their installation is simple. This section discusses the fabrication process of the push-out specimens, the material properties of each connector, the experimental setup, and the experimental setup and loading protocol.

Push-Out Specimens

Table 1 presents the six specimens that were designed and fabricated for experimental evaluation. The benchmark headed stud sample (Fig. 1a) contained a column of four 12-mm headed studs arranged in one column and spaced at 4 times the diameter of the stud (d_b) per AASHTO specifications (AASHTO 2012). The headed studs are welded back-to-back on each side of the plate. The threaded bar specimens

(Fig. 1b) contain a similar layout to the sample with headed studs. The threaded bars are passed through a 13 mm hole and secured using high-strength nuts. The nuts were hand-tightened with a wrench to a torque of 135 N-m. The height of the threaded bar on each side of the web plate is approximately 55 mm. The clear cover for each threaded bar is 15 mm. Although the threaded bars did not contain a head (as the shear studs do), the coarse threads were relied upon for lateral engagement to the UHPC. The UHPC dowel specimens (Fig. 1c) contained four holes in the web plate of the girder through which fiber reinforced UHPC flowed through. No additional reinforcement was passed through the holes. Two diameters were considered for the UHPC dowels: 38 mm and 50 mm. Two fiber contents (2% and 4%) were also considered. However, after evaluating the 38 mm sample with a 4% fiber content, it was deemed that the UHPC was not flowable enough to be considered as part of this repair, and thus the sample with 50 mm dowels was not evaluated with a 4% fiber content.

Table 1. Summary of specimens

Specimen ID	Shear Mechanism	UHPC f'_c	Fiber Content	Connector Diameter	Connector F_y	Connector F_u	Connector Spacing
		MPa	%	mm	MPa	MPa	mm
Stud_D12	Headed Stud	131	2	12	388	530	50
TR_D12_A	Threaded Rod A	158	2	12	597	814	50
TR_D12_B	Threaded Rod B	157	2	12	944	1004	50
Dowel_D38_2%	UHPC Dowel	149	2	38	---	---	127
Dowel_D38_4%	UHPC Dowel	148	4	38	---	---	127
Dowel_D50_2%	UHPC Dowel	144	2	50	---	---	127

(a)

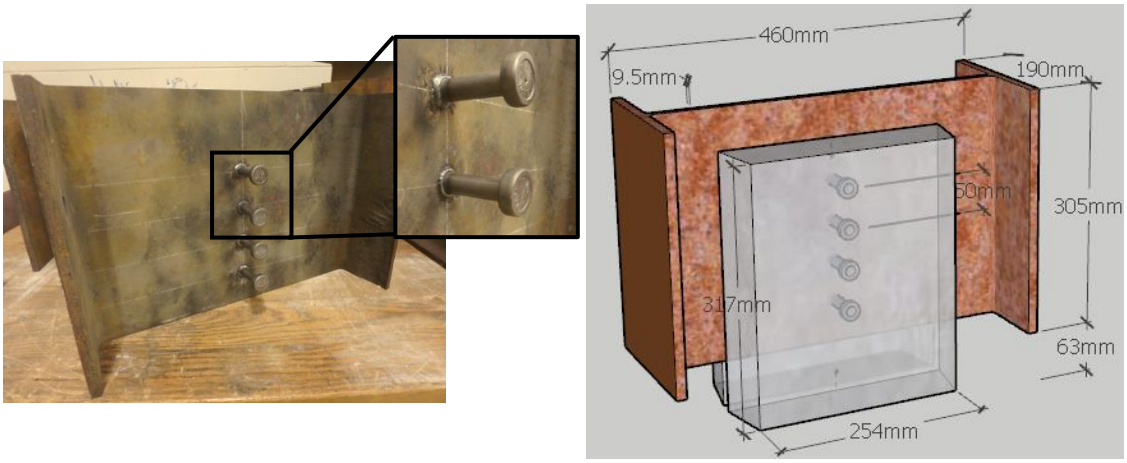

(b)

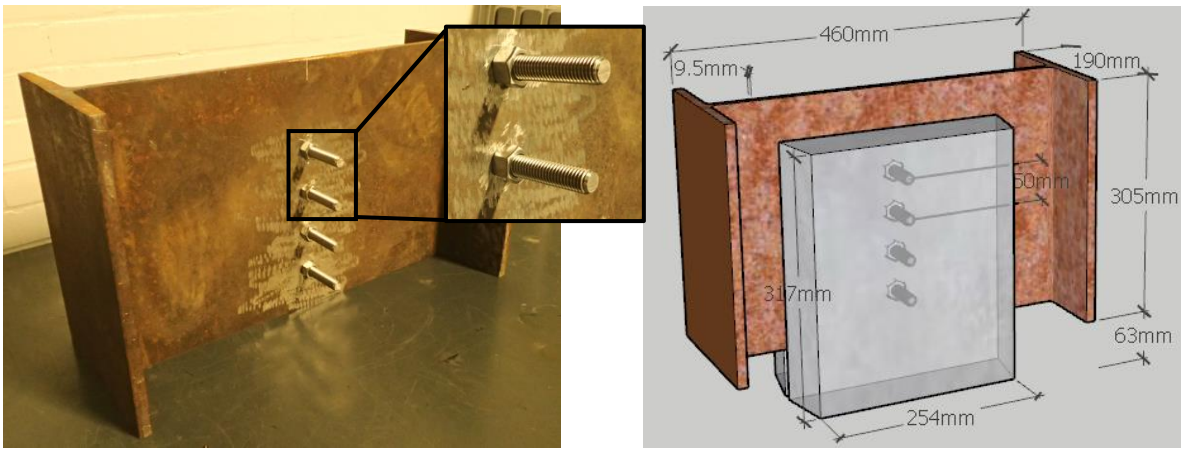

(c)

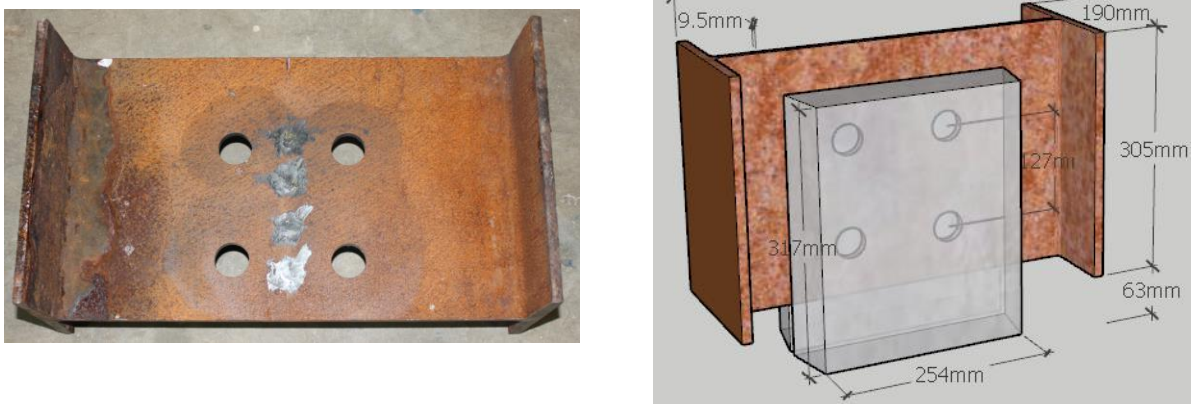

Fig. 1. Push-out specimens with a) headed studs, b) threaded bars and c) UHPC dowel

Material Properties

Steel Properties

The steel materials used in this series included the base beam section, headed shear studs, and two types of threaded rods. The headed studs are typical Type B headed shear studs specified for a minimum tensile strength of 450 MPa (Nelson Stud Welding 2017). Threaded Rod A is comprised of B8 material which is specified for an ultimate strength of690 MPa. Threaded Rod B is comprised of Grade 8 material, corresponding to a specified ultimate strength of 1000 MPa. To confirm the mechanical characteristics, all steel materials were tested in uniaxial tension (ASTM E8). Fig. 2 shows the stress-strain responses for the base beam section, headed studs, and both threaded bars. The base beam section is the weakest steel material in this assembly with a yield strength and ultimate strength of 280 MPa and 452 MPa, respectively. The headed studs are comprised of a stronger material with an ultimate strength of 530 MPa. Both threaded rod materials are comprised of stronger steel than the headed studs. The yield strength for Threaded Rod material A and B is 597 and 944 MPa, respectively. The corresponding ultimate strengths are 814 and 1004 MPa. These material strengths were chosen to evaluate a wide array of connector material strengths.

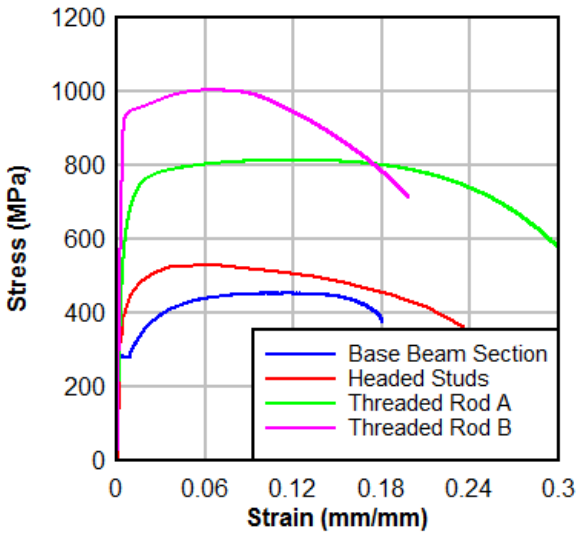

Fig. 2. Stress vs. strain properties for steel materials

UHPC Properties

Table 1 shows the mix composition for the UHPC material used in this study. The UHPC mix selected is Ductal JS1212, developed by LaFarge Holcim (LaFarge Holcim, 2018; Ductal JS1212, 2016). This particular mix contains two high-range water reducers (HRWR) and an accelerator to promote high early strength development. The fiber content was modified for the UHPC dowel specimen with a 4% fiber content by volume. Fig 3 shows the UHPC mixing sequence. First, the premix was dry-mixed for approximately 5 minutes to remove any large clumps. Next, the water and HRWR's were added slowly to prevent significant clumping. The accelerator was added immediately after the HRWR's. The material mixed for approximately 20 minutes after adding the liquids until it turned over. Once turn-over was complete, the fibers were added slowly until they were uniformly incorporated into the mix.

Table 2. Composition of the UHPC Mixes

Component	% by weight	
	UHPC – 2% Fibers	UHPC – 4% Fibers
Premix	86.6	81.7
Water	5.1	4.8
HRWR 1	0.7	0.7
HRWR 2	0.5	0.4
Accelerator	0.9	0.9
Steel Fibers	6.2	11.5

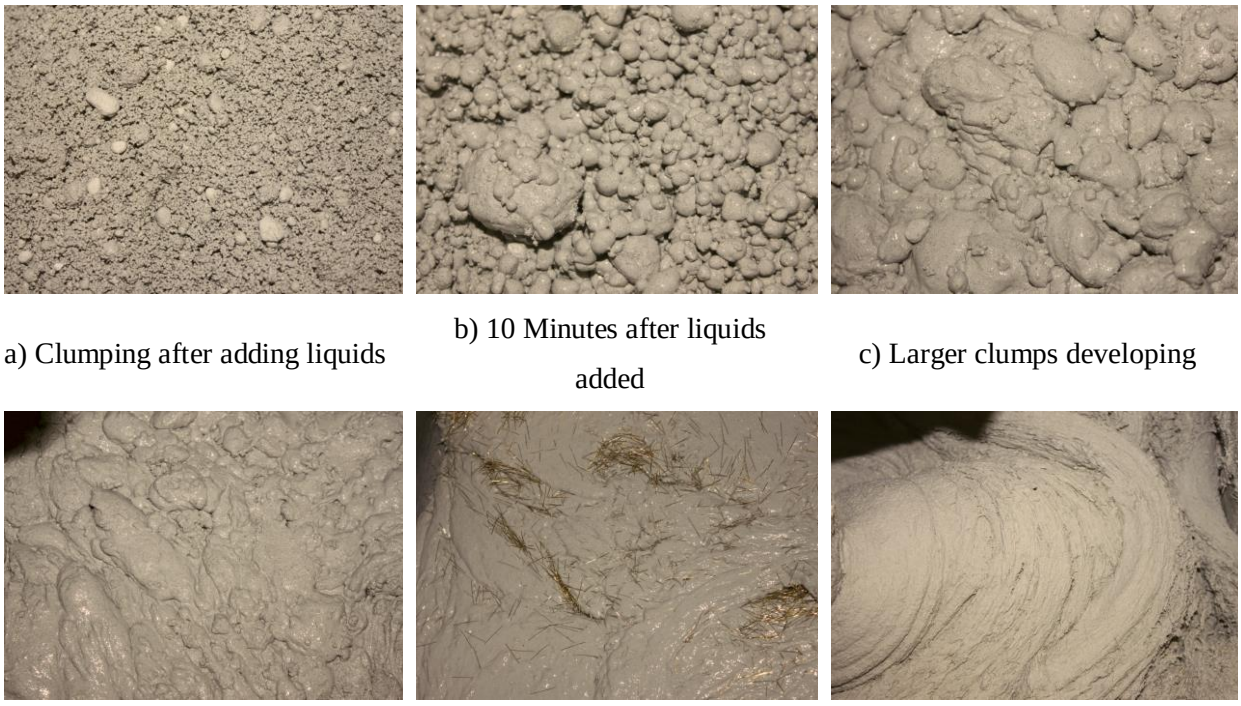

a) Clumping after adding liquids

b) 10 Minutes after liquids added

c) Larger clumps developing

d) Final Clumping Stage

e) Addition of fibers

f) Final consistency

Fig. 3. Mixing sequence of UHPC

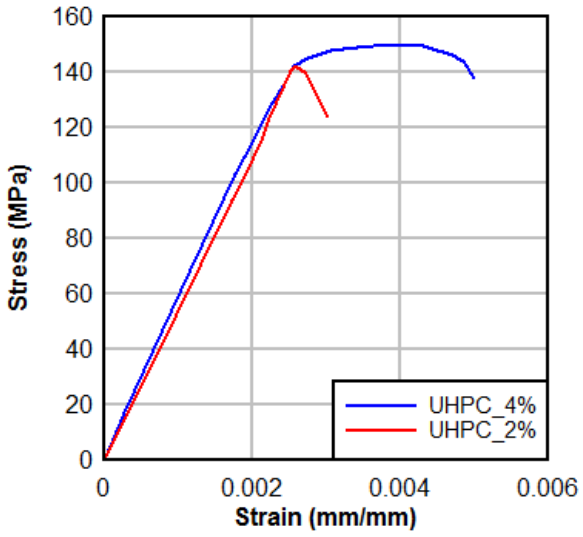

Fig. 4. Typical stress vs. strain properties for UHPC material

Experimental Setup and Loading Protocol

The push-out tests were conducted on using a 1,800 kN hydraulic actuator using an MTS Flextest controller (MTS Systems Corporation 2014). A unique experimental setup was employed due to the thin 9.5-mm web plate of the base beam section. The force was applied to the flanges and a small portion of the web plate and transferred through the shear connectors which were embedded in the UHPC panels. The panels rested on a spherical bearing which accommodated for slight rotations or imperfections during testing. A series of cyclic loadings were incorporated to observe the change in stiffness or detect the onset of damage. Displacement increments of approximately 3 mm were applied at 0.03 mm/s to load the push-out specimen. This was followed by an unloading phase to 4 kN at a similar rate to complete each cycle. A schematic of the loading time-history is shown in Fig. 3.

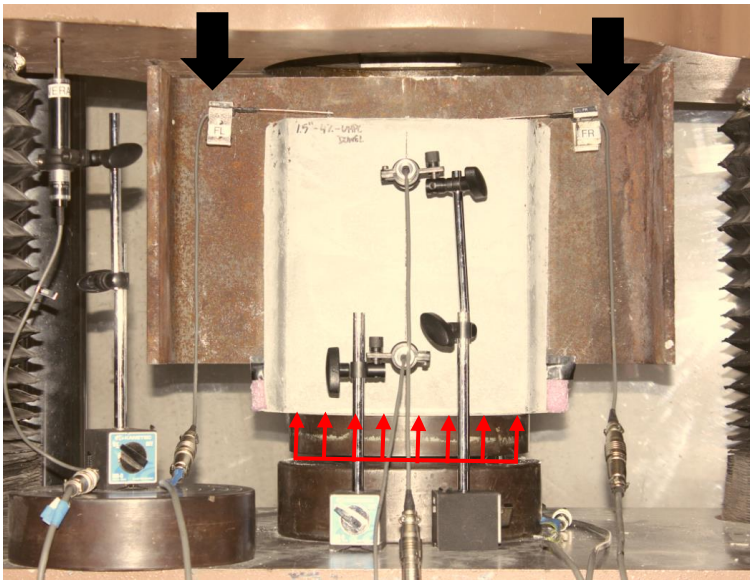

Fig. 5. Experimental setup for push-out specimens

Results and Discussion

This section discusses the critical engineering parameters for all three shear connectors. First, the failure mechanism for each sample is presented. Next, the force-slip behavior and mechanical properties

are discussed. Finally, the demand on the thin plate is shown to discuss the such as failure mechanism, capacity and stiffness, and strain demand on the plate.

Failure Mechanisms

The headed shear stud sample failed via shear rupture of the stud shank just above the weld collar at the interface of the UHPC panel (Fig. 5). This failure mechanism is typical for headed shear studs embedded in UHPC (Kim et al., 2015; Kruszewski et al., 2018). As shown in Fig. 5a, the weld collars remained on the plate after failure. Once the studs ruptured, the weld collars slid along the UHPC surface and sheared off a small sliver of the material (Fig. 5b). To check for any other damage to the UHPC, a wet-saw was used to cut down the center line of the studs. Fig. 5c shows that no additional crushing or damage was sustained to the UHPC. The studs remained fully embedded in the panel with little to no indications of flexural deformation in the studs throughout their length. This indicates that the connection is solely governed by material strength of the headed studs. The rupture always occurs at the interface between the weld collar and the UHPC panel because this is where the highest shear forces are sustained.

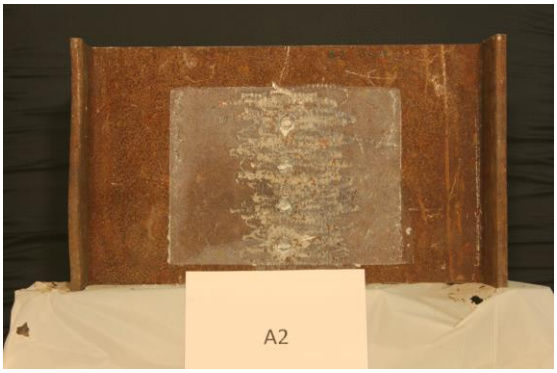

a) Web plate

b) UHPC Panel

c) Sliced UHPC panel down centerline of studs

Fig. 6. Push-out specimen after testing

The failure mode of the threaded rod connector was similar to the headed studs, involving shear rupture of the threaded rod material at the interface between the web plate and the UHPC panel. However, for this connection, However, the plate sustained a significantly higher demand based on visual observations. First, significant deformation was observed at each hole, indicating that the plate may have exceeded its bearing strength (Fig. 6a). In addition, it was observed that the threaded rods penetrated the inside of the drilled hole, as damage markings of the thread pattern were observed after removing the thin piece which remained inside the hole. Additionally, the plate sustained further damage from the "pinching" effect of the high-strength nuts. This occurs when the threaded rods begin to deform in flexure, and thus the high-strength nuts rotate to compress the plate on the top side of the nuts (Pavlovic et al., 2013). While the plate sustained significant damage, no local crushing or other damage was observed in the UHPC. As

opposed to the weld collars of the studs, the high-strength nut was not monolithically attached to the plate. Thus, the nuts remained completely embedded in the UHPC.

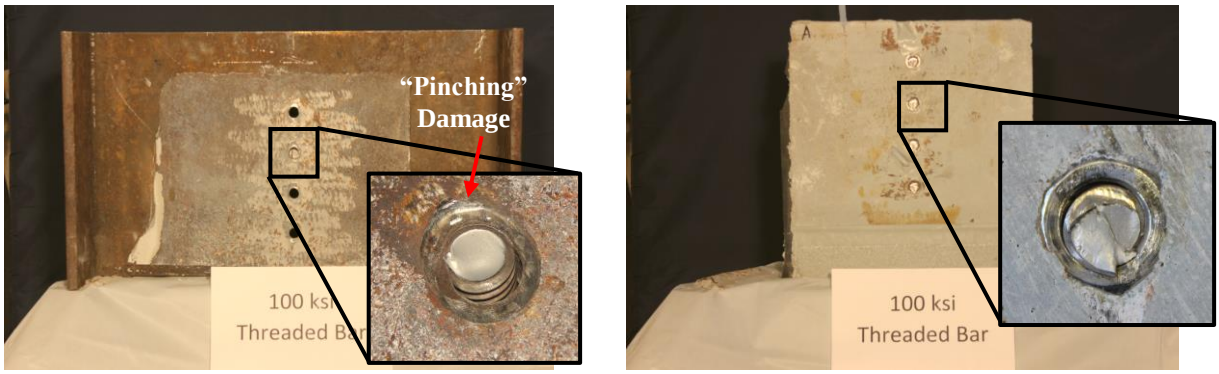

a) Web plate b) UHPC Panel

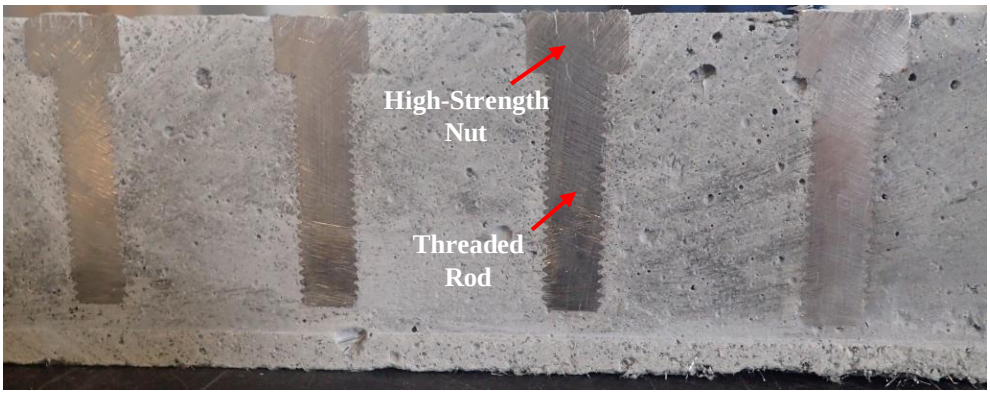

c) Sliced UHPC panel down centerline of threaded bars

Fig. 7. Push-out specimen after testing

All UHPC dowel specimens failed in a similar manner: shear failure of the UHPC material at the interface between the web plate and the panel. A plug of UHPC remained inside of the hole which was drilled in the steel plate (Fig. 7a). The plug contained fibers which were angled upwards (i.e. in the direction of the reaction). This is because after the sudden failure of the UHPC material, the fibers activated to sustain a significant loading. Upon further displacements, the fibers slowly pulled out from the UHPC matrix until the connection eventually diminished (Fig. 7b).The fibers which remained embedded in the UHPC cast were angled downwards, as they were pulled away from the beam and thus travelling upwards. Other than the shear failure at the interface of the hole, no other damage was observed. This was further confirmed

after the panel was cut down the center line of two of the dowels (Fig. 7c). This mechanism was consistent for both diameters (38 mm and 50 mm) and both fibers contents (2% and 4%).

a) Web plate b) UHPC Panel

c) Sliced UHPC panel down centerline of plug

Fig. 8. Push-out specimen after testing

Capacity and Stiffness

Table 2 shows a summary of the experimental results for all specimens. Elastic shear stiffness is computed as the slope of the force vs. slip curve up to one-third of the maximum shear capacity (JSSC 2002). For the headed studs and threaded rods, the yield slip and yield force were identified by extending a line with a 0.1 mm offset at a slope of 220 kN/mm (Kruszewski et al., 2018). For the threaded rods, the yield slip and yield force were identified by extending a line with a 0.1 mm offset at a slope of 700 kN/mm. The ultimate force is assumed as the maximum load bearing force which was sustained by the connector

prior to rupture. Ultimate slip is defined as the slip at ultimate force. To compare against the UHPC dowels, softening was ignored while computing ultimate slip.

Table 2. Experimental results

Specimen ID	UHPC f'c	Elastic Stiffness	Yield Slip	Yield Force	Ultimate Slip	Ultimate Force
	MPa	kN/mm	mm	kN	mm	kN
Stud_D12_550MPa	131	249	0.48	57.2	3.46	74.0
Bar_D12_800MPa (A)	158	158	0.29	28.1	4.37	68.6
Bar_D12_1000MPa (B)	157	124	0.32	33.6	3.55	80.58
Dowel_D38_2%	149	676	0.059	88.6	0.19	123
Dowel_D38_4%	148	722	0.098	88.8	0.33	128
Dowel_D50_2%	144	892	0.123	113	3.13	201

The force vs. slip curves for the stud and threaded bar connectors is shown in Fig. 3. The headed studs generated an ultimate load bearing capacity of 74 kN/stud with a corresponding ultimate slip of 3.46 mm (excluding softening). The governing failure mechanism was comprised of shear rupture of the headed studs just above the weld collar. Other than a small shear plane from sliding of the weld collar, no damage was sustained to the UHPC panels. The threaded rods exhibited a much softer elastic stiffness as indicated by the smaller yield forces and yield slips. Two sources may contribute to this yielding: 1) some slippage may have occurred between the nuts and the web plate as they were not tightened to a slip critical state, and b) the sharp threads of the bar may have penetrated into the hole of the web plate. Threaded Bar A generated a load bearing capacity of 68.6 kN/stud with an ultimate slip of 4.37. This was followed by a significant softening phase after the ultimate force was achieved. Approximately 2 mm of additional slip during the softening phase was experienced prior to failure. Threaded Bar B experienced similar mechanical behavior with a higher stiffness, generating an ultimate force of 80.58 kN/stud and an ultimate slip of 3.55 mm. It is observed that a higher strength steel generated a higher capacity but less ductility which is characteristic behavior of steel material. However, stud rupture occurred much more abruptly for Threaded Bar B. The failure mechanism for both threaded bar samples was consistent: rupture of the threaded bar shank at the

interface between the nut and the web plate. However, significant yielding of the web plate was observed at each hole location. Fig. 5 shows the failed specimens after testing.

The ultimate capacity of the UHPC dowel was approximately 107 kN per hole. While the capacity was much larger, the connection was governed by brittle shear failure of the UHPC dowel at an ultimate slip of 0.32 mm. After the UHPC dowel sheared off, the steel fibers activated at a force of 38 kN per hole. After further cyclic loadings, the bond between the fibers and the UHPC matrix eventually degraded as characterized by the softening behavior at higher slip ranges.

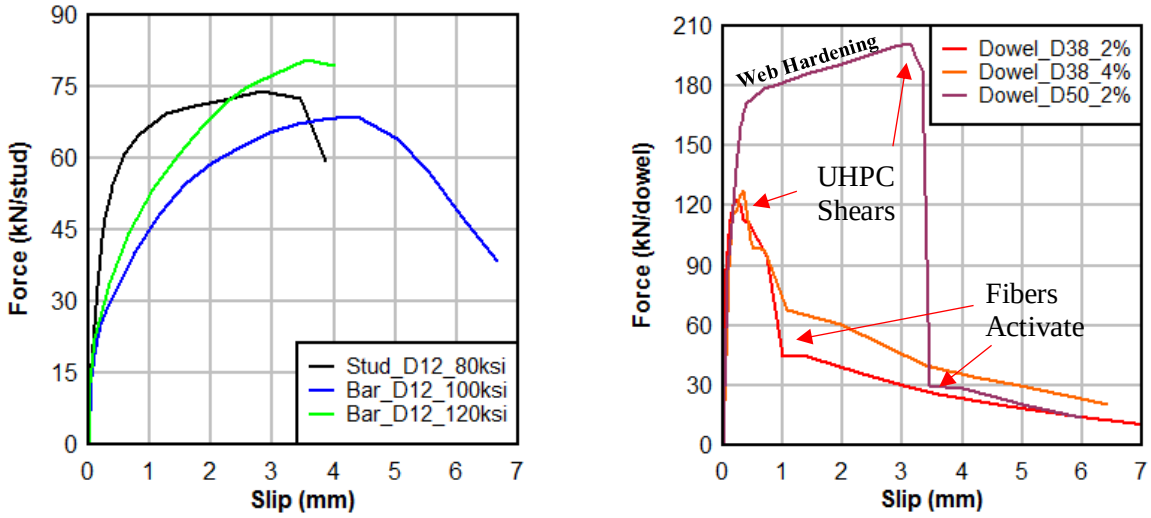

a) Stud and threaded bar connectors b) UHPC dowels

Fig. 9. Force vs. slip summary

Fig. 9 shows a graph of the stiffness comparison of each connector. The threaded bars exhibited the smallest stiffness. Interestingly, the threaded rod comprised of a stronger material (1000 MPa) exhibited a lesser composite stiffness than the one with an ultimate strength of 800 MPa. The authors speculate that this is due to the threaded rods penetrating the inner surface of the hole in the plate.

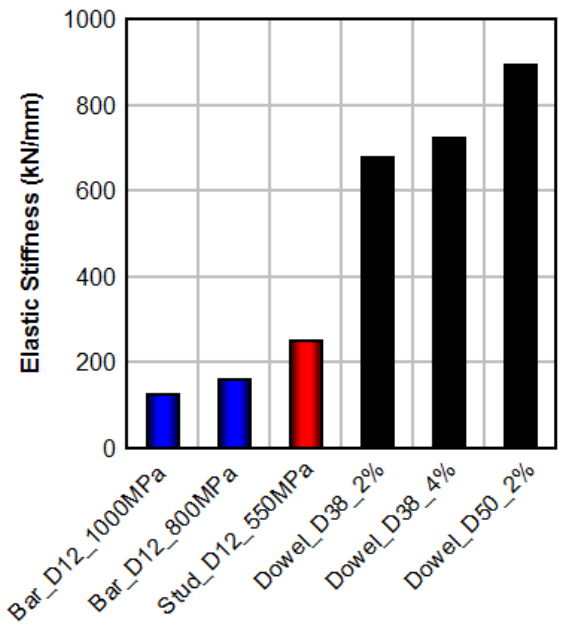

Fig. 10. Stiffness summary

Strain Demand on Plate

A particular parameter of interest in this study is the demand on the thin plate when the connectors are loaded in shear. When using a base plate thickness of 9.5 mm, it is important to preserve its condition to utilize the full plastic capacity of the connector and to ensure an adequate design. To capture the demands on the plate, strain gauges were installed directly adjacent to each connector which large strains are anticipated. For the headed studs and threaded bars, the strain gauges were mounted on the plate adjacent to the base of the connector. Each sensor was mounted on the compression side of the connector. In other words, the strain gauges were installed at the location where the highest demands are anticipated due to high confinement from the UHPC panels or bearing forces due to the reaction from the applied loading. Fig. 11 shows the location of all sensors used to capture the demands on the thin plates.

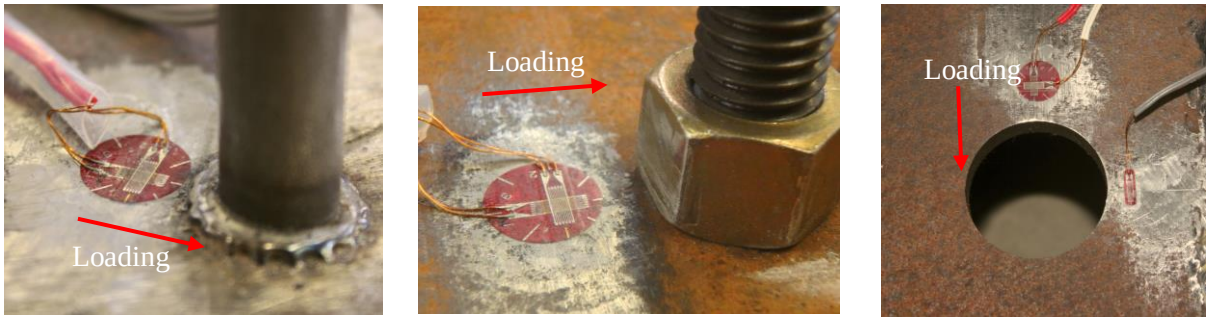

a) Headed Studs b) Threaded Rods c) Dowels

Fig. 11. Locations of Strain Gauges

Von-Mises strains were computed from the biaxial strain gauges. In-plane shear strain (ε_{12}) was ignored. Fig. 11 shows the force-strain relationship for the headed studs and threaded rods. In Fig. 11a, the plate experiences a significant strain demand as the headed studs resists more force. At a force of approximately 89 kN, the plate yields as indicated by the significant strain accumulation. At a force of approximately 127 kN, the studs reach their yield point. Once the studs yield, no additional strain accumulation is experienced by the plate as characterized by the overlapping cyclic loadings in Fig. 11a.

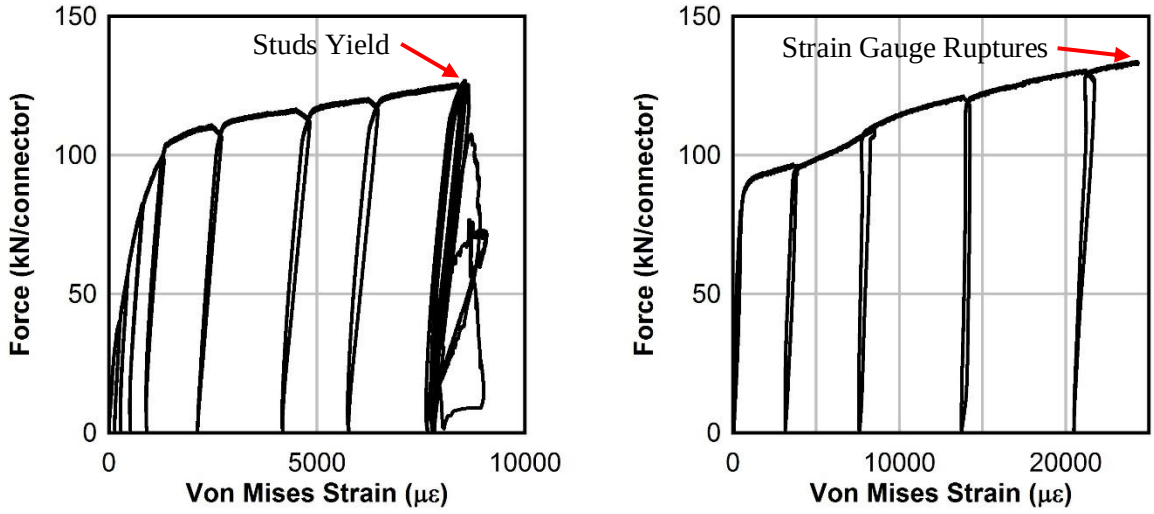

a) Headed Studs b) Threaded Rods

Fig. 11. Von-Mises Strain Demand on Plate

Fig. 12 shows the Von-Mises strain demands on the plate generated by the UHPC dowel connection. The strains on the plate when a 38-mm dowel is installed are relatively low. The figure shows that the plate remains elastic throughout the loading sequence. During the initial loadings, the stiffness of the connection deteriorates due to cracking of the UHPC at the shear interface. When the UHPC reaches its shear strength at a force of 123 kN, the resistance drastically drops until the fibers activate at approximately 16 kN. Upon further displacements, the plate experiences cyclic web strains but remains elastic. However, when a 50-mm dowel is implemented, the demands on the plate as drastically different (Fig. 12b).

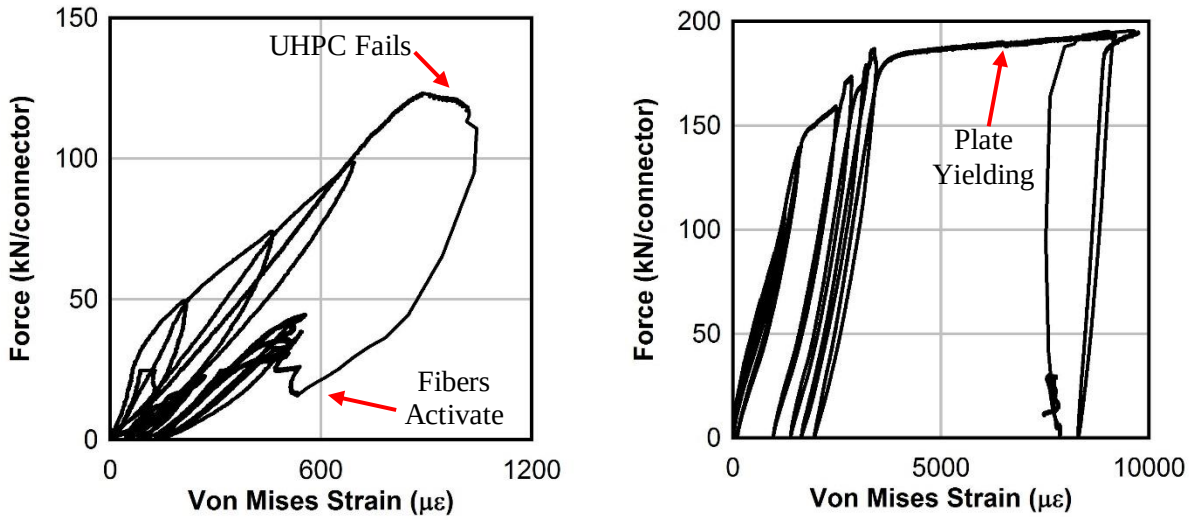

a) 38-mm Dowel

a) 50-mm Dowel

Fig. 12. Von-Mises Strain Demand on Plate

CONCLUSIONS

- Full plastic capacity was achieved using a demountable threaded bar with no damage to the UHPC panel. Yielding of the web was observed, indicating that the threads of the rods penetrated into the plate causing local damage.
- A UHPC dowel with 2% fiber content may be used to develop a significant load bearing shear connection. One 63 mm hole generates a shear capacity of 103 kN. This connection is characterized by a brittle failure mechanism, as the UHPC dowel failed in sudden shear. The fiber fraction did not have an influence on the load bearing capacity.
- Strain demands were captured on the plate. For welded headed studs, the plate experiences no additional strain accumulation after they reach their yield point. Significant strain demands accumulate when threaded rods are used.
- 38-mm UHPC dowels ensured that the plate remained elastic throughout the loading sequence. When 50-mm UHPC dowels were used, the plate experienced significant yielding as indicated by the high strain demands above the drilled hole.

References

Ollgaard, J.G., Slutter, R.G., Fisher, J.W. (1971). *Shear strength of stud connectors in lightweight and normal weight concrete*, AISC Engineering Journal, April 1871 (71-10).

Hegger, J., Sedlacek, G., Doinghaus, P., Trumpf, H. (2001). *Studies on the ductility of shear connectors when using high-strength steel and high-strength concrete*, Connections between steel and concrete, 2001. pp 1025 – 1045.

Hegger, J., Gallwoszus, J., Rauscher, S. (2009). *Load-Carrying Behaviour of Connectors under Shear, Tension and Compression in Ultra High Performance Concrete*, Nordic Steel Construction Conference Proceedings.

Eurocode-4 (2004). *Design of Composite Steel and Concrete Structures*, European Committee for Standardization. Brussels, Belgium.

Classen, M., Gallwoszus, J., Stark, A. (2016). *Anchorage of composite dowels in UHPC under fatigue loading*, Structural Concrete 17(2). pp 183 – 193.

He, S., Fang, Z., Mosallam, A. (2017). *Push-out tests for perfobond strip connectors with UHPC grout in the joints of steel-concrete hybrid bridge girders*, Engineering Structures 135. pp 177 – 190.

Wang, J.Y., Guo, J., Jia, L., Chen, S., Dong, Y. (2017) *Push-out tests of demountable headed stud shear connectors in steel-UHPC composite structures*, Composite Structures, accepted manuscript.

Suwaed, A.S.H, Karavasilis, T.L. (2017). *Novel Demountable Shear Connector for Accelerated Disassembly, Repair, or Replacement of Precast Steel-Concrete Composite Bridges,* ASCE Journal of Bridge Engineering 22(9).

Zmetra, K. (2015). *Repair of Corrosion Damaged Steel Bridge Girder Ends by Encasement in Ultra-High Performance Concrete,* Ph.D. Dissertation, University of Connecticut, Storrs, CT.

Zaghi, A.E., Wille, K., Zmetra, K., and McMullen, K. (2015). *Repair of Steel Beam/Girder Ends with Ultra High Strength Concrete (Phase I),* Connecticut Department of Transportation. University of Connecticut. SPR-2282 (Report #CT-2282-F-15-2).

Zmetra, K., McMullen, K., Zaghi, A.E., Wille, K. (2017). *Experimental Study of UHPC Repair for Corrosion-Damaged Steel Girder Ends,* Journal of Bridge Engineering, 22(8).

McMullen, K., Kruszewski, D., Zaghi, A.E., Wille, K. (2017). *A Novel Repair Method for Steel Girders with Corrosion Damage Utilizing UHPC,* Proceedings of the International Bridge Conference 17-106, National Harbor, Maryland, USA.

Wu, B., Cao, J.L, Kang, L. (2018). *End patch loading behavior and strengthening of locally corroded steel I-beams,* Journal of Constructional Steel Research (148). pp 371 – 382.

Lam, W.Y., Li, L., Su, R.K.L., Pam, H.J. (2013). *Behaviour of Plate Anchorage in Plate-Reinforced Composite Coupling Beams,* The Scientific World Journal (2013).

Kruszewski, D., Wille, K., Zaghi, A.E. (2018) "Push-Out Behavior of Headed Shear Studs Welded on Thin Plates and Embedded in UHPC." Engineering Structures 173(1). pp 429 – 441.

AASHTO (2012). "AASHTO LRFD Bridge Design Specifications." American Association of State Highway and Transportation Officials, Washington, DC 20001.

Nelson Stud Welding (2017). "Stud, Ferrule and Accessory Catalog." Product Catalog, Nelson Fastener Systems Company. 7900 W. Ridge Rd, Elyria, Ohio, USA.

ASTM E8 (2016). "Standard Test Methods for Tension Testing of Metallic Materials". ASTM International, West Conshohocken, PA, 2016. www.astm.org

LaFarge Holcim (2018). "Building materials, cement, aggregates and concrete." LaFarge Holcim, 2018. https://www.lafargeholcim.com/

Ductal JS1212 (2016). " JS1212 Rapid Strength Product Data Sheet", Ductal, LaFarge Holcim.

MTS Systems Corporation (2014). "MTS FlexTest Controller Family." 100-183-824b Datasheet, MTS Systems, Eden Prairie, MN, USA.

Kruszewski, D., Wille, K., Zaghi, A.E. (2018). *Design considerations for headed shear studs embedded in ultra-high performance concrete as part of a novel bridge repair method.* Journal of Constructional Steel Research 149(1). pp 180 – 194.

Kim, J.S., Kwark, J., Joh, C., Yoo, S.W., Lee, K.C. (2015). *Headed stud shear connector for thin ultrahigh-performance concrete bridge deck,* Journal of Constructional Steel Research, 108(1), 23-30.

Pavlovic, M., Markovic, Z., Veljkovic, M., Budevac, D. (2013). *Bolted shear connectors vs. headed studs behavior in push-out tests,* Journal of Constructional Steel Research 88(1). pp 134 – 149.

JSSC (Japan Society of Civil Engineers). (2002). *Guidelines for performance-based design of steel-concrete hybrid structures,* Tokyo, Japan.

Chapter 6

Design of Various Shear Connectors for Repair of Corroded Steel Girders with UHPC

Introduction

An overwhelming number of bridges in the United States are in need of repair or replacement. According to the U.S. Department of Transportation, the annual investment by the federal government is less than 66% of what is required to repair the current state of the infrastructure (1). Approximately $125 billion is needed to catch up on the backlog of projects in need of repair or replacement (2). Corrosion is one of the primary causes of the reduction of the design life of bridges. Specifically, in simple-span bridges, water and deicing salts leak through expansion joints and result in significant local damage at the bearing region (Figure 1). Over time, the section loss of the web and bearing stiffener plates impairs the load-bearing capacity. In many cases, the reduced bearing capacity lowers the load rating of the entire bridge structure. Several experimental studies have been conducted to evaluate the bearing capacity of steel girders with section loss due to corrosion near the bearing region (3, 4). These studies suggested that a 70% section loss in the web and flange area may decrease the bearing capacity of the girder by 76%. Due to the severity of the consequences that may stem from corrosion, there is a pressing need for novel and efficient repair methods for deteriorated bridge girders.

Fig. 1. Typical girder end corrosion at the bearing.

In an attempt to address this pressing issue, an extensive experimental and analytical research study was supported by the Connecticut Department of Transportation. This led to the development of a novel bridge repair method that provides a structurally efficient and easy-to-implement repair option for steel bridge girders with corroded ends (6 – 8). To restore the bearing capacity of the girder, small-diameter headed shear studs are welded to the intact portion of the web plate, i.e. the region with no section loss, above the bearing. The studs are encased in a thin panel of Ultra-High Performance Concrete (UHPC), which is cast to the bottom flange. A schematic of the proposed repair method is shown in Figure 2. The transfer of shear forces from the web to the studs and then to the UHPC panels creates an alternate load path to alleviate the weakened girder. The proposed repair eliminates the need for jacking of the superstructure, thus avoiding a sensitive and expensive procedure (9). This significantly reduces the cost of the repair and prevents closure of the bridge. Since most of the work is done under the bridge deck, only minimal lane closures are needed. Welding the studs is an efficient process, as they are quickly

"shot" using a stud gun. Because of the high compressive strength of the material, a small volume of UHPC is required for each panel. No rebar reinforcement is needed since the UHPC contains high-strength steel fibers that provide sufficient tensile ductility.

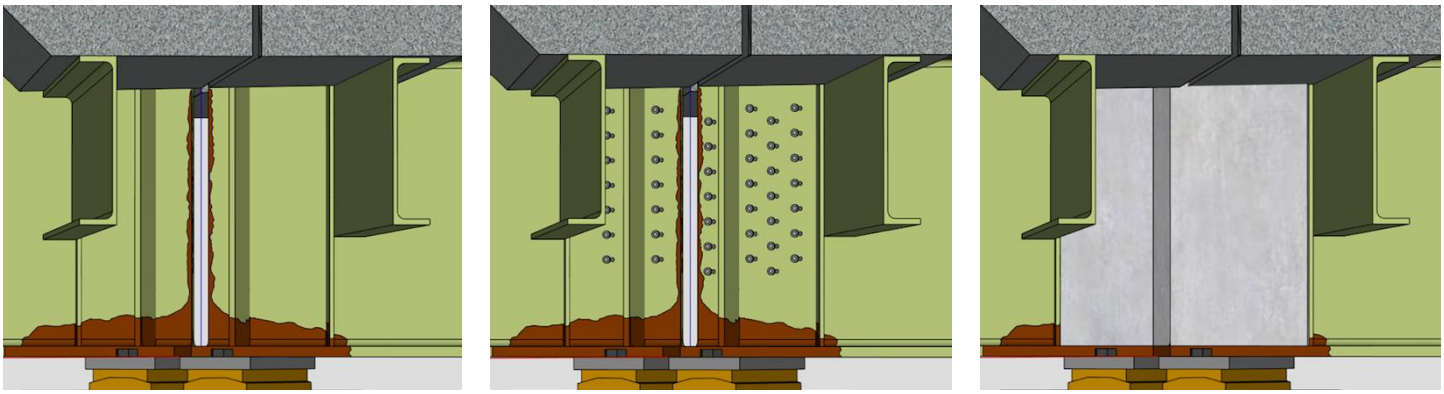

a) Typical corroded girder end b) Headed studs on the web plate c) UHPC casts in completed repair

Fig. 2. Schematic of the proposed repair method

While the extensive experimental data has established the efficiency of headed studs as a reliable shear-transfer mechanism, alternative shear connectors were investigated as part of this study to provide a wide range of design options for bridge engineers. The objective of this paper is to demonstrate how different types of shear connectors may be integrated in the repair design and how designers may approach the design checks for certain performance objectives. To achieve this goal, a brief overview of the mechanical performance of several simple shear connectors, including headed studs, threaded bars, and UHPC dowels embedded in UHPC, is discussed. A realistic repair design is presented to restore the capacity of a bridge suffering from section loss due to corrosion. Several design scenarios are addressed with various shear connector options. The repairs are presented graphically for clear presentation of the various options. Finally, the

fatigue performance of headed studs is discussed to ensure the longevity of the repair. Some limitations of and design considerations for this novel repair method are addressed.

Performance of Shear Connectors in UHPC

Figure 3 shows the three shear connectors considered in this study: headed shear studs with diameters of 0.5 in., 0.625 in. and 0.75 in., threaded bar connectors with a 0.5-in. diameter, and a 1.5-in. diameter UHPC dowel. These connectors were selected because of their simplicity of installation and effective shear transfer mechanism. The headed studs are typical Type B studs specified for 65,000 psi and minimum 20% elongation in a 2-in. gauge length (10). The threaded bar considered in this study is comprised of Grade 8 material, specified for 120,000-psi ultimate strength (11). Although the threaded bars do not have a "head" such as the headed studs do, the threads provide sufficient engagement to the UHPC. The UHPC dowel concept involves UHPC flowing through a perforated plate such that the connection is developed through direct shear of the UHPC material. This design concept has been investigated by He et. al (12). Dowels are not a traditional shear transfer mechanism for achieving composite action between steel and concrete; however, the excellent shear strength of UHPC enables transfer of large forces between the elements.

UHPC was chosen for this repair because of its flowability, proven durability, high-tensile strength, and fatigue resistance (13). The UHPC mix design used in this study is Ductal JS1212, developed by LaFarge Holcim (14, 15). This mix is specified for minimum design values of 20,000 psi, 4,300 psi and 1,160 psi for compression, flexure, and direct tension, respectively. The constituents include a premix powder, chemical admixtures, water, and high-strength steel fibers. The premix powder is comprised of cement, silica fume, silica powder and fine-graded sand. The mix design contains two high-range water reducers and an accelerator which promotes high early-

age strength. When heat treated at 120°F, a compressive strength of 12,000 psi may be achieved within 12 hours. This feature is particularly favorable as it enables fast and efficient field implementation. High-strength steel fibers are included (2% by volume) to minimize the tensile crack opening and enhance ductility. This replaces the need for conventional steel reinforcement in the UHPC panels, omitting the laborious procedure of placing reinforcement prior to casting.

a) Headed shear studs b) Threaded bars c) UHPC dowel

Fig. 3. Shear connectors considered for UHPC bridge repair

A large set of push-out experiments was conducted to evaluate the shear capacity of the three connector details proposed in this study (16). A schematic of each push-out specimen is shown in Figure 4. To produce results relevant to the proposed repair, an old beam section was salvaged from a demolished bridge, originally erected in 1958. The yield strength and ultimate strength of the base beam section is 41,000 psi and 67,000 psi, respectively, corresponding to the A373-58T specification for structural steel during the time of erection (17). The beam was cut into 12-in. sections so that the connectors could be installed on the web plate to create the specimens for testing. The headed studs were “shot” onto the web plate using a stud gun to adhere to typical construction practice. A conventional ferrule was used to develop the weld collar at the base of the

stud. The threaded bars were installed onto the web plate by passing them through a hole which was just large enough to fit the threaded bar. The hole was not oversized, to prevent slippage during the initial loading. The threaded bar was secured to the web plate with high-strength nuts tightened to a torque of 100 lb-ft. The headed studs and threaded rods were spaced at 4 times the diameter of each connector ($4d_b$). The connectors were embedded in UHPC panels such that a push-out specimen was created. Finally, the UHPC dowel specimen was fabricated by machining 1.5-in. holes into the web plate and allowing the UHPC to flow through the hole. The hole diameter of three times the steel fiber length of 0.5 in. was chosen to allow the free flow of UHPC from one side to another. The specimen was cast from one location to allow the fibers to develop in tension through the hole. Each push-out specimen was tested using a 400-kip hydraulic machine. The force was applied onto the flange of the beam section such that the connectors resisted the loading through bearing action on the UHPC panels, which were mounted on a spherical bearing.

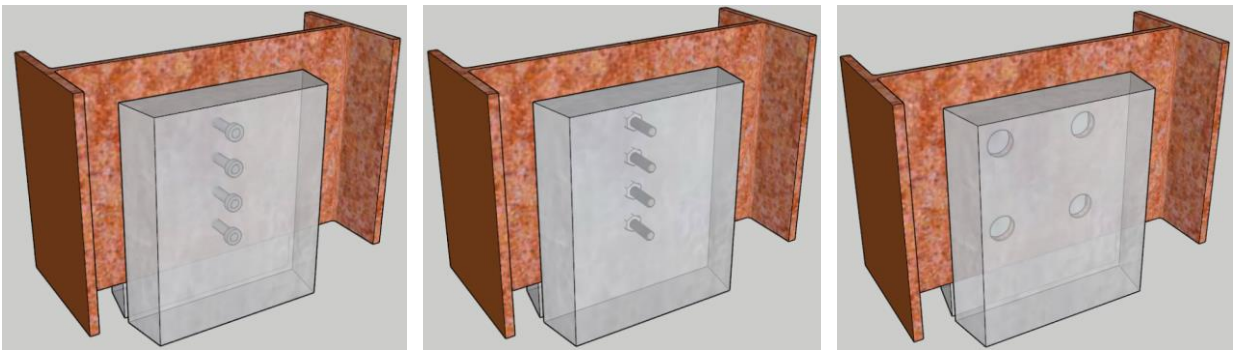

a) Headed shear studs b) Threaded bars c) UHPC dowel

Fig. 4. Push-out specimens with different shear connectors

Figure 5 shows the force-slip results obtained from the push-out tests. Slip is defined as the relative displacement between the steel web and the UHPC panels. This parameter shows the stiffness of the shear connection itself. The figure shows that the 0.5-in., 0.625-in. and 0.75-in. studs generate a capacity of 16.8 kip/stud, 24 kip/stud, and 32.8 kip/stud, respectively. The studs displayed a ductile failure mode, i.e. shear rupture of the stud shank, with no damage to the UHPC panels other than a sliver sheared off at the base of the weld collar (Figure 6a). The threaded bar specimen exhibited a similar failure mechanism (Figure 6b) with a total load bearing capacity of 15.4 kip/bar. The 1.5-in. UHPC dowel generated a load bearing capacity of 26.9 kip/hole. The UHPC dowels had the largest stiffness within the shear connector types. Shear failure of the UHPC was the governing failure mechanism at the interface between the web plate surface and the inside surface of the UHPC panel (Figure 6c). A plug of UHPC remained inside the 1.5-in. hole of the web plate. After the shear failure of the UHPC, the fibers activated and sustained the load at approximately 10 kip. By increasing in displacements, the fibers exhibited pull-out from the UHPC matrix, as characterized by the softening curve after a slip of 0.05 in.

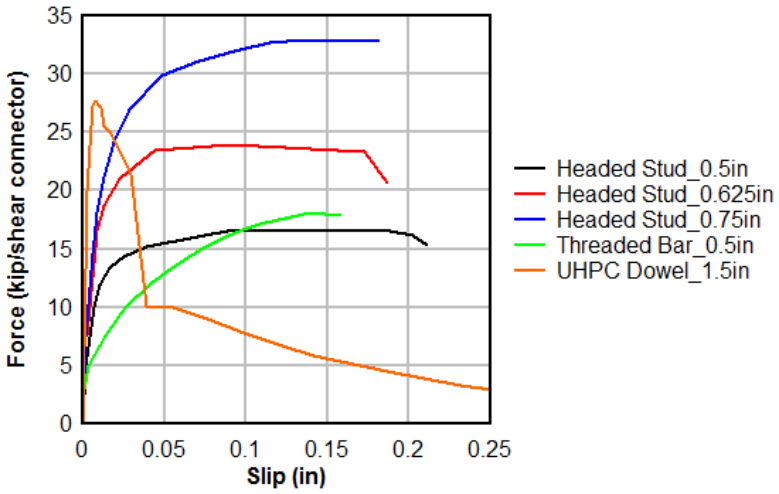

Fig. 5. Experimental force-slip relationship of shear connectors

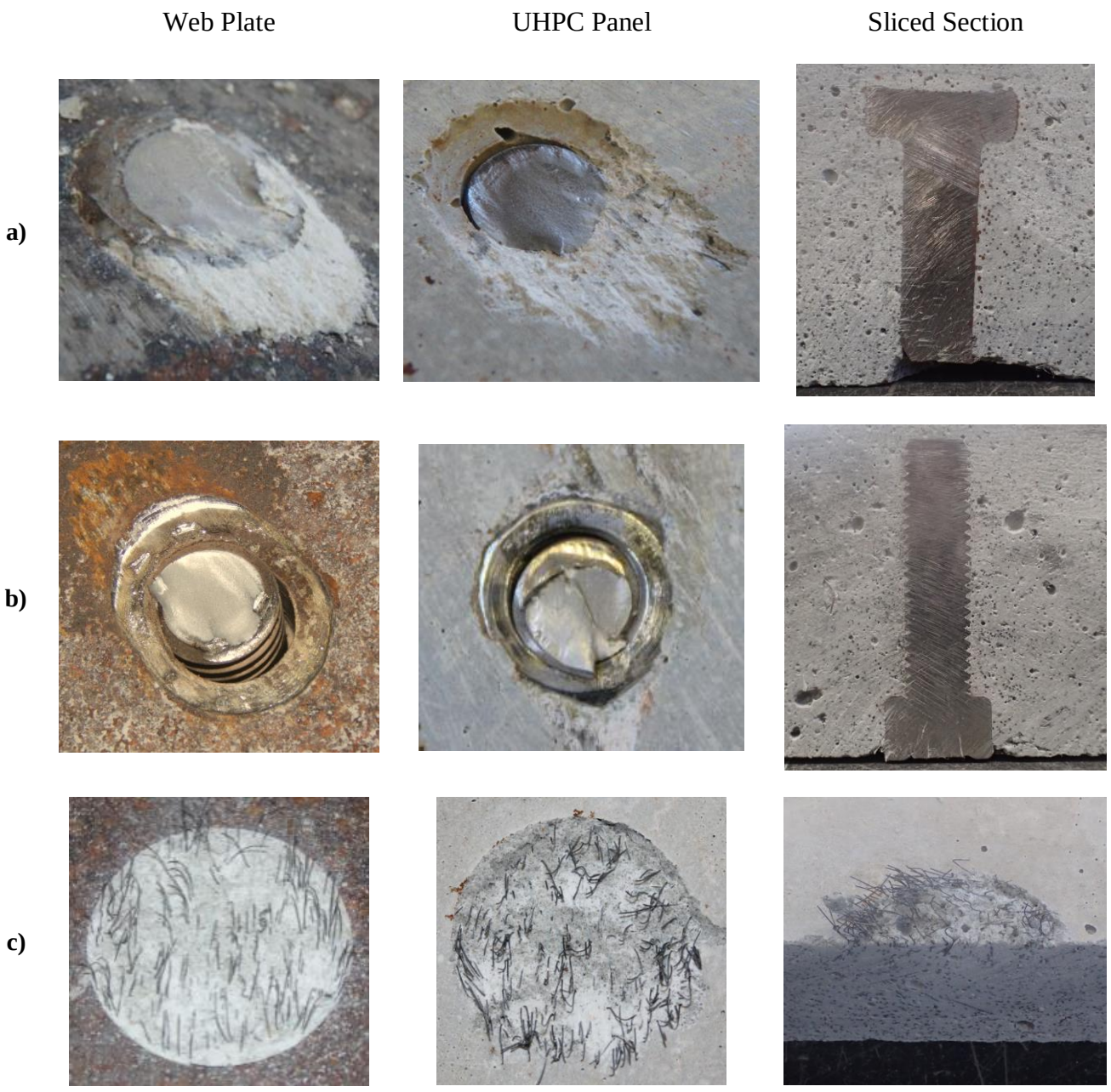

Fig. 6. Shear connectors after testing: a) headed studs, b) threaded bar, c) UHPC dowel

The capacities of the headed studs from these experimental results are validated through a formulation developed by Hegger et al. (18), who developed a formulation for the shear capacity of headed studs embedded in high-strength concrete (Equation 1). This formulation states that the

stud capacity is the sum of the material strength of the stud shank, $A_{sc}F_u$, and the bearing contribution of the weld collar onto the concrete, $\eta f_{cu} d_{wc} l_{wc}$. In this equation, A_{sc} is the area of the stud shank, F_u is the ultimate tensile capacity of the stud, f'_c is the compressive strength of the concrete, d_{wc} is the diameter of the weld collar, l_{wc} is the height of the weld collar, and η is an empirical factor typically taken as 2.5 for UHPC. However, experimental results by Kruszewski et al. (16) found that assuming a constant value for η is not accurate because the contribution of the weld collar is dependent on the compressive strength of UHPC. To incorporate the variation of η, Equation 1 was refined to remove the dimensions of the weld collar which may be difficult to obtain without a physical sample. Instead, the weld collar dimensions were normalized by the diameter of the stud shank to simplify the equation for the capacity of headed studs in UHPC (Equation 2). In the equation, the value of η is a function of UHPC compressive strength, f'_c, as outlined by Equation 3, where β is a unitless factor taken as 0.0119 MPa or 0.0822 ksi, depending on the unit systems being used. Using Equation 2, the capacities of the headed studs obtained from the experiments were confirmed for this study. Equation 2 predicts the capacity of 0.5-, 0.625-, and 0.75-in. diameters as 15.8 kip/stud, 24.0 kip/stud, and 34.1 kip/stud respectively, which are close to the failure loads shown in Figure 5.

$$P_u = A_{sc}F_u + \eta f'_c d_{wc} l_{wc} \quad (1)$$

$$P_u = A_{sc}F_u + 0.16\eta f'_c \, {d_b}^2 \quad (2)$$

$$\eta = \beta f'_c - 0.983 \quad (3)$$

Design of UHPC Repair

This section presents the results from a sample repair design of a real bridge with severe corrosion at the girder ends using the three types of shear connectors described in this study. The bridge used in this example is an in-service, four simple-span steel substructure with a reinforced concrete deck. The beams are rolled shapes, with the heights ranging between 33 in. and 36 in. The bridge is located in the Northeast region of the United States and services a major highway route with an average daily traffic (ADT) of 67,000 vehicles/day in one direction. Because of severe section loss due to corrosion, a 2016 Field Inspection Report rated the superstructure of the bridge as "in poor condition," with a rating of 4. The UHPC repair method is a viable repair option for this bridge because of a) the complex geometry of the superstructure due to different skew angles, b) obstacles such as connection and stiffener plates, and c) the need to minimize lane closures to avoid delays on the highway. The bridge was originally erected in the 1960's, a period during which structural steel may have been specified for a minimum yield strength as low as 33,000 psi (14). The span lengths range between 51 ft. and 92 ft., with skew angles between 24° and 37°.

The first step in the design process is to identify the force demands so that the required number of shear connectors can be calculated. For this design example, three design scenarios are considered: Live Load, Strength I, and Capacity Design. The calculations for these limit states are based on the AASHTO Bridge Design specifications (19). The Live Load scenario is defined as the shear demand generated from an HL-93 loading with the dynamic allowance factor of 1.75 based on Table 3.4.1-1 of AASHTO. This scenario assumes that the existing condition of the girder is sufficient to carry the permanent loads of the structure, while the live load is carried by the UHPC panels. The Strength I scenario assumes that the UHPC panels are able to carry the

loads obtained based on the shear or bearing demand including distribution factors. Capacity Design is the most conservative repair approach as it aims to restore the original shear or bearing capacity of the girder. In this example, both shear and bearing capacities were calculated so that the design was based on the governing capacity. To determine the bearing and shear strength of the girder, AASHTO 6.10 may be referenced. The shear strength of the girder is found using the effective area of the web plate and end panel (AASHTO 6.10.10.4.3). The bearing strength is assumed as the cross-sectional area of the web plate and bearing stiffeners (AASHTO 6.10.11.2.3). This design approach is very conservative because the shear or bearing capacity of the girder typically does not control the design. However, all three scenarios are presented in this design example to demonstrate the layout arrangements and flexibility of the UHPC repair.

Table 1 shows the number of headed studs, threaded bars or UHPC dowels required to generate the load bearing capacity based on the load demand of the three design scenarios considered. The number of shear connectors was calculated using a capacity reduction factor of 0.85 for each connector to introduce a source of conservatism. For Capacity Design, a range of shear connectors is shown due to the presence of various plate girder sections on the bridge; thus, a larger number of studs may be needed to restore the shear capacity of a larger girder. Between the different connectors and design cases, there is a wide variety of required shear connectors that may be installed. This variety offers flexibility to the designer. For example, only four 0.75-in. headed studs are required to accommodate the live load condition. However, as many as 42 0.5-in. headed studs are needed to satisfy the conservative capacity design scenario. If headed studs cannot be shot onto the web plate due to geometric constraints, 20 threaded bars may be installed through small holes to satisfy the Strength I demand. If the designer opts to omit the use of any

type of steel connector and simply use UHPC for the shear connection, as few as five UHPC dowels may be drilled to accommodate the Live Load scenario.

Table 1. Connector options for various designs

Shear Connector Type	Connector Diameter (in)	Live Load (HL-93)	Strength I	Capacity Design
Headed Stud	0.5	9	22	32 - 42
	0.625	6	15	20 - 28
	0.75	4	11	15 - 21
Threaded Bar	0.5	8	20	28 - 37
UHPC Dowel	1.5	5	13	18 - 25

Figure 7 shows the schematic to strengthen a deteriorated bridge girder on the candidate bridge according to the Capacity Design scenario. Here, 28 studs with a 0.625-in. diameter are shot onto the web plate using a typical stud gun. The studs are welded just above the corroded region, where no section loss is present. Since 28 studs are needed, four columns of seven studs are welded with a horizontal and vertical stagger to avoid welding the studs back-to-back. This reduces the strains on the web plate by ensuring that its bearing capacity is larger than the shear capacity of the studs. Since there is a large surface area present for welding, the studs are spaced at 3 in. center-to-center (C-C), vertically. However, if needed, the studs may be spaced as close as 3 times the diameter of the stud shank (i.e. 3db) and still achieve full capacity. Because less available surface area is present on the left side of the bearing stiffener, the horizontal stagger between the two columns of studs is 1 in. C-C. The right side of the bearing stiffener offers more surface area, and therefore the stud line is staggered 2 in. horizontally. The vertical stagger between

each stud on opposite sides of the web plate is approximately 1.5 in. The load bearing capacity of this stud arrangement is approximately 570 kip, with a reduction factor of 0.85 incorporated.

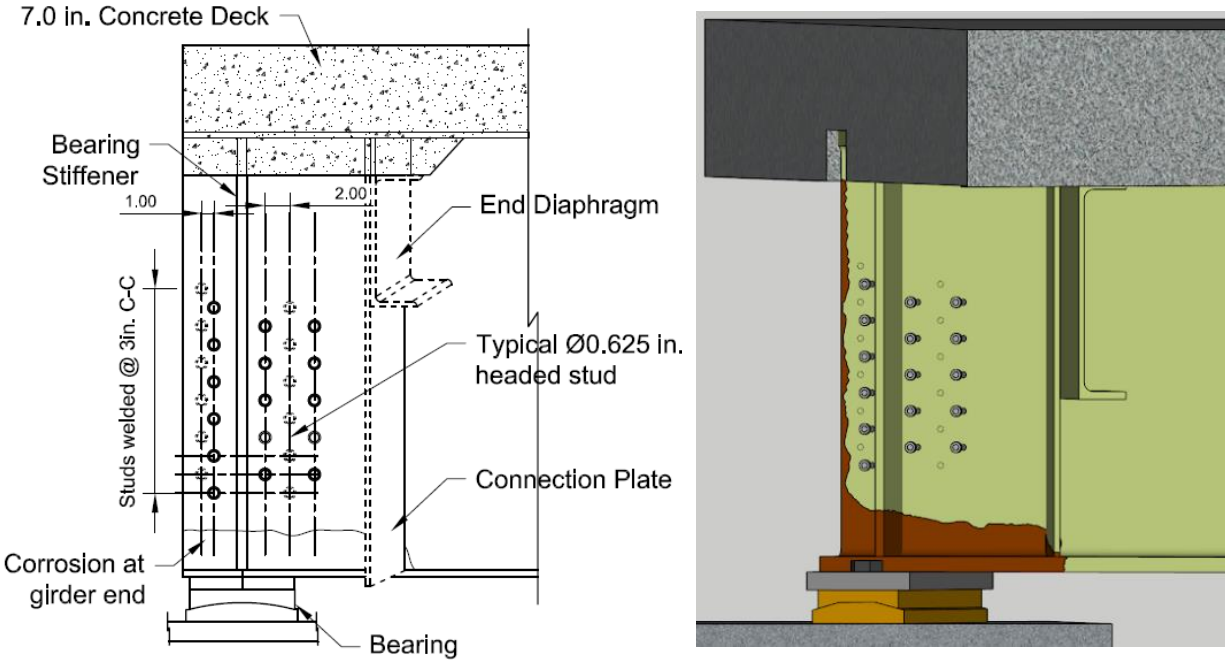

a) Side View b) 3-D Schematic

Fig. 7. Sample connector arrangement for 0.625-in. headed shear studs

Figure 8 shows the layout for 38 0.5-in. diameter threaded rods which are secured to the web plate using high-strength nuts (Grade 8). Here, 19 2.5 in. long threaded rods are passed through the web plate to create 38 individual connectors. Since the capacity of a 0.5-in. threaded bar is less than a 0.625-in. headed stud, a larger number of connectors is needed to meet the Capacity Design scenario. Each threaded rod extends approximately 2 in. from the surface of the web plate. Since one single threaded rod is extended through a tight hole in the web plate, staggering of the individual shear connectors on each side of the girder is not possible. However, each connector may be staggered independently of another connector, as is demonstrated in the figure. The rods were installed with a 3-in. vertical spacing. Similar to the headed studs, a 1-in.

horizontal stagger was introduced to the left of the stiffener, while a 2-in. horizontal stagger was applied to the rods to the right of the stiffener. The total capacity generated from this arrangement is approximately 586 kip, with a reduction factor of 0.85. The use of threaded rods instead of headed studs may be justifiable only if stud welding equipment cannot be mobilized on site. It is critical to note that headed studs and threaded rods shall not be used together because of the significantly different initial stiffness of the two types of connectors as shown in Figure 5. In general, the authors do not encourage the use of this type of shear connector because of the uncertainties involved in installation and pre-tensioning of the rods.

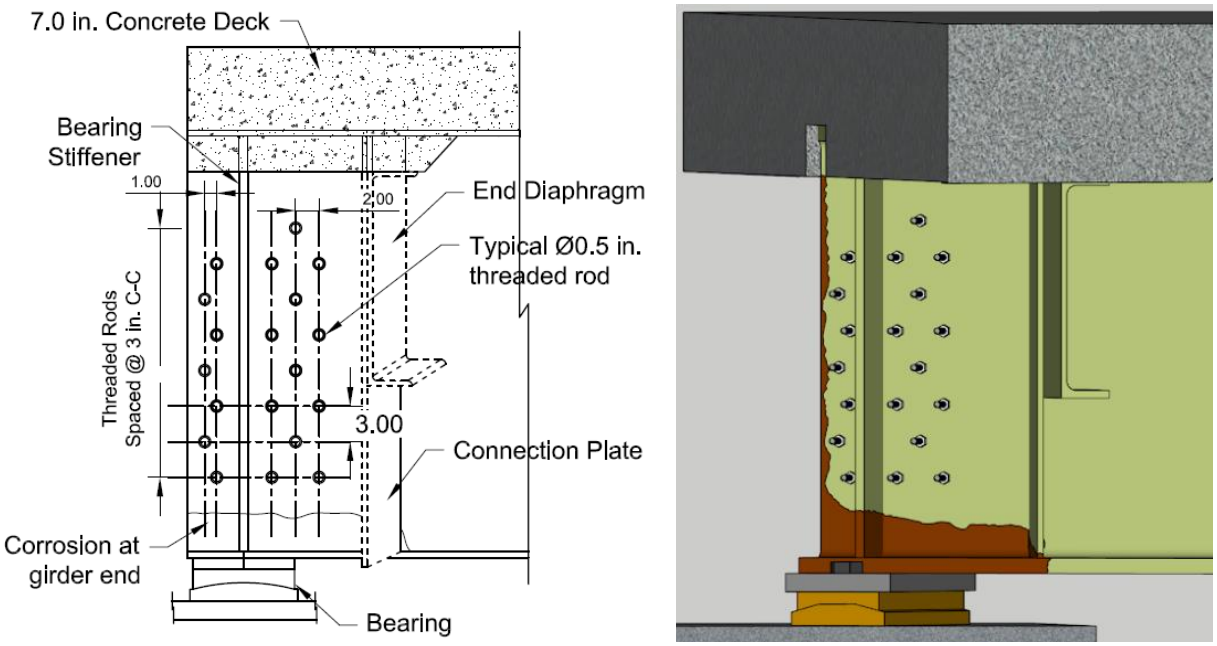

a) Side View b) 3-D Schematic

Fig. 8. Sample connector arrangement with 0.5-in. threaded rods

A sample arrangement for the UHPC dowel connection is shown in Figure 9. A total of 25 holes with a 1.5-in. diameter are drilled to the left of the stiffener. Five 1.5-in. holes with a

vertical spacing of 5 in. center-to-center are drilled to the left of the stiffener. To the right of the stiffener, four columns of five such holes are drilled with a horizontal spacing of 2.5 in. between columns. The columns are also offset vertically with a spacing of 2.5 in. to minimize the lost area in each plane. For this repair strategy, the UHPC may be poured into the formwork from one side of the web plate. This allows the UHPC to flow through the drilled holes, ensuring that the fibers are developed through the shear plane at the edge of the web plate. The total capacity generated by this dowel layout is approximately 573 kip, with a reduction factor of 0.85. This repair is applicable to geometries that allow the utilization of large drilling equipment such as an electromagnetic drill. The number of the holes may be reduced by using larger diameter dowels. However, because the experiment performed in this study was limited to 1.5-in. diameter dowels, the authors based the design on the capacity obtained from the experiment. In the absence of further experimental results, one may assume that the shear capacity of dowels is proportional to the area considering the shear failure mechanism. Thus, 2-in. diameter dowels are expected to have a capacity approximately 1.78 times larger than that of 1.5-in. diameter ones. For the same reasons mentioned earlier, the use of dowels with the other connector types is not recommended.

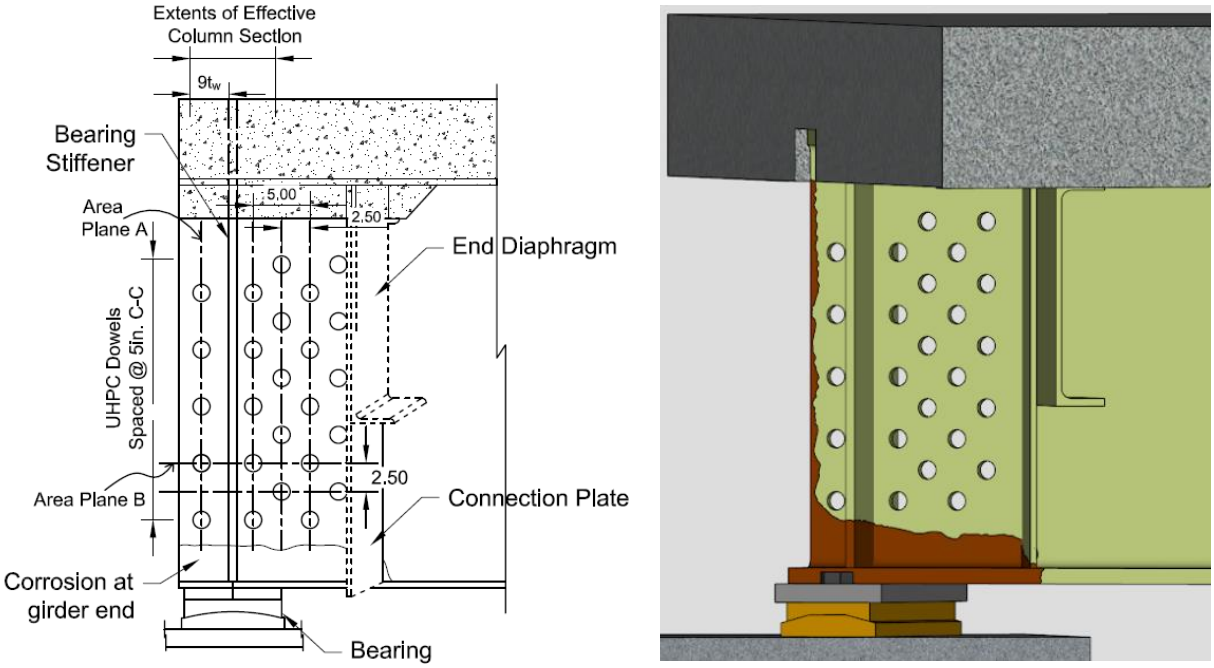

a) Side View b) 3-D Schematic

Fig. 9. Sample connector arrangement with 1.5-in. UHPC dowels

Designers may have concerns about the reduction of the girder capacity because of the presence of the holes. The authors acknowledge that this repair design results in a large number of holes in the web plate. To implement this connection type, a design check must be conducted to prevent shear failure of the web plate on a vertical section of the web due to the removed material. First, based on the inspection reports for this bridge, it is known that the girder contains approximately 90% section loss. Thus, it is assumed that the remaining 30% of the web plate is sufficient to carry the loading exerted on the bridge. This assumption is unique to this scenario; this threshold should be based on inspection reports which are unique to each bridge containing detailed accounts of the section loss present on each girder. However, this assumption allows for dowel holes to be drilled such that no more than 70% of the area of the web plate is removed from any other plane in the girder. In other words, the plastic shear capacity of the girder, V_p, as outlined

by AASHTO equation 6.10.9.2-2 should not be hindered by removal of material in excess of what is already missing due to corrosion. This is especially critical in the extents of the effective column section, which extends 9 times the thickness of the web plate ($9t_w$) away from each edge of the bearing stiffener (AASHTO 6.10.11.2.4b).

The plastic shear capacity, V_p, of a plate girder is presented in Equation 4, where 0.58 is a coefficient based on plasticity mechanics under the Von Mises yield criterion, F_{yw} is the yield strength of the web plate, and A_w is the area of the web plate. For the UHPC dowel design, the fraction of section loss, α, must be assessed through inspection reports. Next, the number and size of the dowels is calculated such that the plastic shear capacity of the repaired girder, V_P', is not reduced beyond the level produced by the existing corrosion. Using the inequality shown in Equation 5, the modified area of the web plate after drilling the holes, A_w', must be less than the already reduced section of the web plate (αA_w) to prevent shear yielding of the girder.

$$V_P = 0.58F_{yw}A_w \tag{4}$$

$$V_P' = 0.58F_{yw}A_w', \quad A_w' > (1-\alpha)A_w \tag{5}$$

In this design, the two planes that must be controlled are labeled in Figure 9 as "Area Plane A" and "Area Plane B." The vertical plane, i.e. Area Plane A, contains five dowel holes drilled vertically, just above the bearing. The original area of the web plate, which contributes to the shear capacity, A_w, is 13.1 in^2. After the holes are drilled, this area reduces to 10.3 in^2, corresponding to a 21.5% reduction in area. Since this reduction is less than the 70% already experienced due to corrosion, the plastic shear capacity is at least the same as it was prior to drilling the holes and

therefore the design is accepted. Similar results are obtained from "Area Plane B," as the holes result in a 40% reduction of area within the effective column section of $9t_w$ away from each edge of the bearing stiffener. It is important to note that this check may not have been satisfied if there was less section loss present due to corrosion. In this situation, the number of required dowels will be smaller. For example, in a beam with 60% section loss, the demand is 40% of the total force obtained based on the capacity design concept.

Fatigue Design Consideration

Due to live load traffic over the bridge, the shear connectors in the UHPC repair will experience a large number of loading cycles, which may lead to fatigue failure. The fatigue performance of thread bar and dowel shear connectors have not yet been studied. Thus, this section will only present a fatigue analysis for the headed shear studs used in the design example.

If long-term serviceability of the repair is a concern, a fatigue check may be conducted through provisions outlined in AASHTO 6.10.10 (20). To calculate the fatigue demand on the headed studs, the shear force generated from a design truck is calculated for the smallest span of 51 ft. The truck was placed on the girder such that the heaviest exterior axle, i.e. the 32 kip axle, was placed directly over the bearing at the corroded girder end. The second 32-kip axle extended towards the middle of the span, 14 ft. away from the bearing. The third 8-kip axle was placed 28 ft. away from the girder end to satisfy the dimensions of the design truck. From this loading, a reaction force of 58.8 kip was calculated at the bearing. This force is magnified using a dynamic allowance factor of 0.15 and load combination factor of 1.50, corresponding to the Fatigue I limit state per AASHTO Table 3.4.1-1. The total design fatigue load was multiplied by 0.7, as it is

assumed that 30% of the force is carried by the remaining portion of the corroded web plate. This force is divided by the number of studs and again divided by the area of a single 0.625-in. stud to generate a fatigue stress range of 8.3 ksi.

To generate the capacity stress range for headed studs in UHPC, an S-N curve must be used because the capacity is a function of daily truck traffic. An S-N curve describes the stress range that a stud can accommodate according to the expected cycles during its lifespan. First, the daily truck traffic in one direction (ADTT) is calculated using AASHTO equation 3.6.1.4.2-1 and presented here as Equation 1. In this equation, p is the fraction of truck traffic in a single lane and f_{truck} is a coefficient used to estimate the fraction of trucks out of the total traffic volume. Since there are 4 lanes on this highway, a p factor of 0.8 was used. The highway is classified as an "Urban Interstate," corresponding to a truck volume fraction of 0.15. For this particular bridge, based on an ADT of 67,000 vehicles per day in one direction, the $ADTT_{SL}$ is approximately 2,640 trucks/day. AASHTO equation 6.6.1.2.5-3 was used to calculate the expected number of cycles that the studs will experience (Equation 7). In the equation, Y corresponds to the lifespan of the repair and n is the number of stress range cycles per truck passage.

$$ADTT_{SL} = p \cdot f_{truck} \cdot ADT \quad (6)$$

$$N = 365(Y)n(ADTT_{SL}) \quad (7)$$

For this bridge, N is approximately 24 million cycles assuming a 25-year design life. From here, an S-N curve developed by Cao et al. (21) for the expected fatigue life of headed studs embedded in UHPC is used to calculate the capacity stress range. The S-N curve is presented by

Equation 2, where $\Delta\tau$ is the stress range (MPa), and N is the number of cycles anticipated during the lifespan of the connection.

$$8 \log \Delta\tau + \log N = 22.1131 \quad (8)$$

Using the equation, the stress range for the studs embedded in UHPC is 69 MPa or 10 ksi. Therefore, this analysis shows that the demand stress range exerted on the studs is less than the predicted fatigue capacity of the headed studs, deeming the proposed design as sufficient. It is important to note that the fatigue demand on the headed studs increases when fewer studs are used. For example, if the number of studs were selected based on the Strength I or Live Load demands as presented in Table 1, the fatigue control requirement would not have been satisfied. This indicates that a less conservative design approach may result in a fatigue-controlled design. However, several sources of conservatism are present in this analysis. First, the smallest span was considered for fatigue, which generated the largest girder end reaction, and thus the largest fatigue demand on the studs. Second, the bridge in this example is a very heavily traveled route with an ADT of 67,000 vehicles/day. Third, a 70% section reduction was incorporated to demonstrate the severity of the corrosion, magnifying the effectiveness of the proposed repair.

Conclusions

This paper presents the experimental results of three shear connections (headed studs, threaded bars, and UHPC dowel) which may be used as part of the presented bridge repair method. As an example for field implementation, a severely corroded bridge was selected for repair using this method. Based on three design scenarios, the number of shear connectors was computed as presented visually with realistic geometry and spacing. A fatigue assessment was conducted for the headed studs. The following conclusions can be made from this study:

- Three shear connectors have been identified as suitable candidates for the proposed repair method. Headed studs with a diameter of 0.5 in., 0.625 in., and 0.75 in. generate full plastic capacity when welded onto a 9.5-mm web plate, as characterized by the stud shank rupture. Similar results are obtained for 0.5-in. threaded bars. The UHPC dowel, while exhibiting a more brittle failure mechanism, also generates a significant load-bearing capacity with no damage to the web plate.
- An in-service bridge is selected for a repair design using the three shear connectors. Based on the Live Load, Strength I and Capacity Design scenarios, the required number of each connector is generated with a reduction factor of 0.85. The repair offers a wide variety of connector arrangements to restore the capacity of the bridge girder with significant section loss according to various limit states.
- The shear connectors were presented visually, with schematics drawn to scale. The spacing and arrangements of the shear connectors were reasonable and easy to implement. The spacing of the headed studs and threaded rods was much larger than the minimum spacing required by AASHTO.

- A fatigue assessment was conducted for the scenario with headed shear studs. It was found that the proposed schematic provides sufficient fatigue resistance for a heavily occupied bridge with severe section loss. More research is needed to conduct a fatigue check for threaded bars and UHPC dowels.

REFERENCES

1. NACE International. *Highways and Bridges.* NACE International, Houston, Texas. https://www.nace.org/Corrosion-Central/Industries/Highways-and-Bridges/ Accessed July 16, 2018.
2. ASCE (2017). "2017 Report Card for America's Infrastructure." American Society of Civil Engineers, Reston, Virginia. www.asce.org Accessed July 16, 2018.
3. Zmetra, K., McMullen, K., Zaghi, A.E., Wille, K. (2017). "Experimental Study of UHPC Repair for Corrosion-Damaged Steel Girder Ends." Journal of Bridge Engineering, 22(8).
4. McMullen, K., Kruszewski, D., Zaghi, A.E., Wille, K. (2017). "A Novel Repair Method for Steel Girders with Corrosion Damage Utilizing UHPC." Proc. of the International Bridge Conference 17-106, National Harbor, Maryland, USA.
5. Ahn, J.-H., Kainuma, S., and Kim, I.-T. (2013). "Shear Failure Behaviors of a Web Panel with Local Corrosion Depending on Web Boundary Conditions." *Thin-Walled Structures*, 73, 302-317.'
6. Zaghi, A.E., Wille, K., Zmetra, K., and McMullen, K. (2015). "Repair of Steel Beam/Girder Ends with Ultra High Strength Concrete (Phase I)." Connecticut Department of Transportation. University of Connecticut. SPR-2282 (Report #CT-2282-F-15-2).
7. Zaghi, A.E., Wille, K., Zmetra, K., McMullen, K., Kruszewski, D., Hain, A. (2017). "Repair of Steel Beam/Girder Ends with Ultra High-Strength Concrete (Phase II)." Connecticut Department of Transportation. University of Connecticut. SPR-2295 (Report #CT-2295-1-17-2).
8. Zmetra, K. (2015). "Repair of Corrosion Damaged Steel Bridge Girder Ends by Encasement in Ultra-High Performance Concrete." Ph.D. Dissertation, University of Connecticut, Storrs, CT.

9. FLDOT (2011). "Bridge maintenance and repair handbook." Steel Beam & Girder Repair, Florida Department of Transportation (4.6). pp 78-83.
10. ASTM A108 (2016). "Standard Specification for Steel Bar, Carbon and Alloy, Cold Finished". ASTM International, West Conshohocken, PA, 2013. www.astm.org
11. ASTM A193 (2016). "Standard Specification for Alloy-Steel and Stainless Steel Bolting for High Temperature or High Pressure Service and Other Special Purpose Applications". ASTM International, West Conshohocken, PA, 2017. www.astm.org
12. He, S., Fang, Z., Mosallam, A.S. (2017). "Push-out tests for perfobond strip connectors with UHPC grout in the joints of steel-concrete hybrid bridge girders" Engineering Structures 135(1). pp 177 – 190.
13. Graybeal, B., "Material Property Characterization of Ultra-High Performance Concrete," FHWA, U.S. Department of Transportation, Report No. FHWA-HRT-06-103, McLean, VA, 2006.
14. LaFarge Holcim, "Building materials, cement, aggregates and concrete." LaFarge Holcim, 2018. https://www.lafargeholcim.com/
15. Ductal JS1212 (2016). " JS1212 Rapid Strength Product Data Sheet", Ductal, LaFarge Holcim.
16. Kruszewski, D., Wille, K., Zaghi, A.E. (2018) "Push-Out Behavior of Headed Shear Studs Welded on Thin Plates and Embedded in UHPC." Engineering Structures 173(1). pp 429 – 441.
17. Brockenbrough (2002). "AISC Rehabilitation and Retrofit Guide – A Reference for Historic Shapes and Specifications". American Institute of Steel Construction (AISC), Pittsburgh, PA.

18. Hegger, J., Sedlacek, G., Döinghaus, P., Trumpf, H., and Eligehausen, R. (2006) "Studies on the ductility of shear connectors when using high-strength steel and high-strength concrete." *Proc., International Symposium on Connections between Steel and Concrete*, University of Stuttgart, 1025-1045.
19. AASHTO (2012). *AASHTO LRFD Bridge Design Specifications,* American Association of State Highway and Transportation Officials, Washington, DC 20001.
20. Lee, K.C., Abbas, H.H., and Ramey, G.E. (2010). "Review of Current AASHTO Fatigue Design Specifications for Stud Shear Connectors." *Structures Congress 2010,* American Society of Civil Engineers. pp 310 – 321.
21. Cao, J., Shao, X., Deng, L., Gan, Y. (2017) "Static and Fatigue Behavior of Short-Headed Studs Embedded in a Thin Ultrahigh-Performance Concrete Layer". Journal of Bridge Engineering, 22(5).

Appendix A: Raw Experimental Data

Test 2 – Benchmark #1 – Strains

Stud Strains

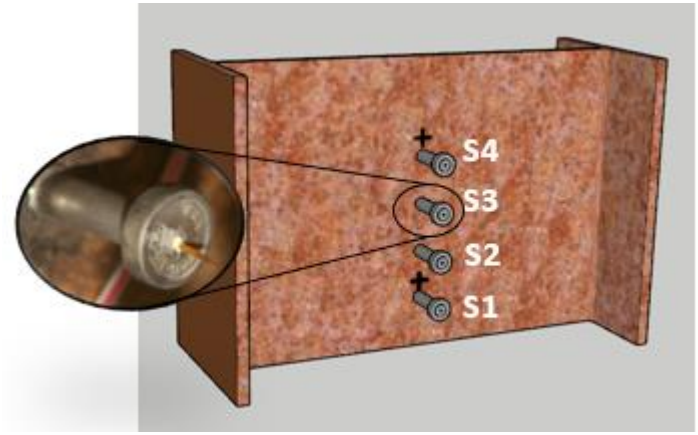

Web Strains

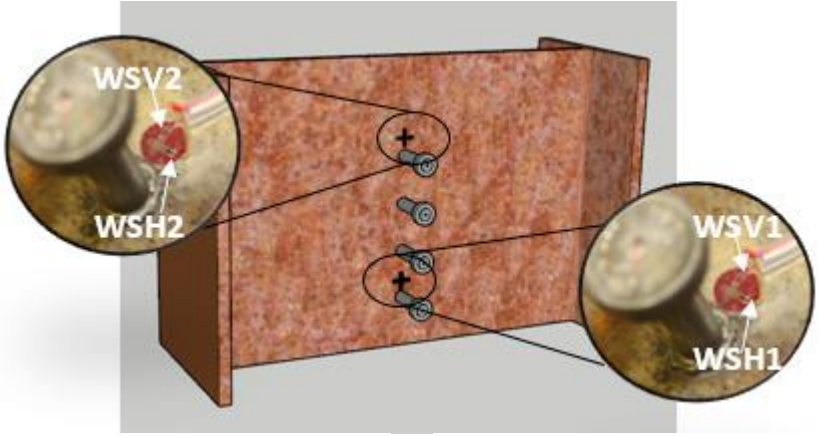

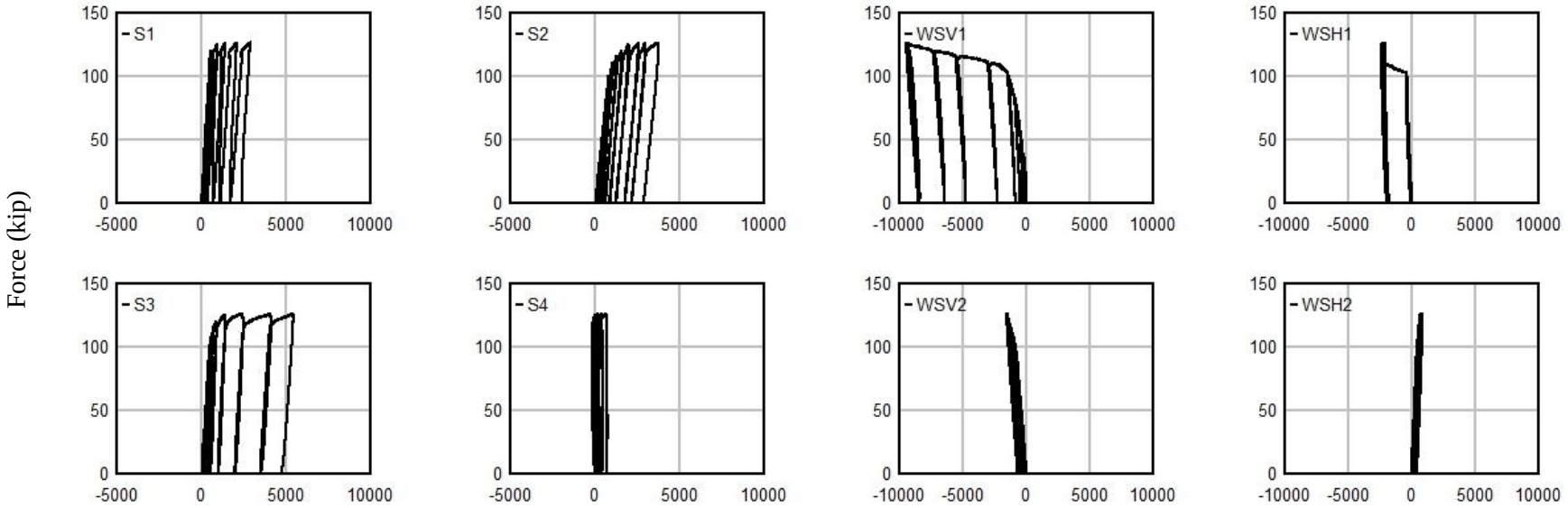

Test 2 – 3db Spacing – Displacements

Panel Slip

Out-Of-Plane Displacement

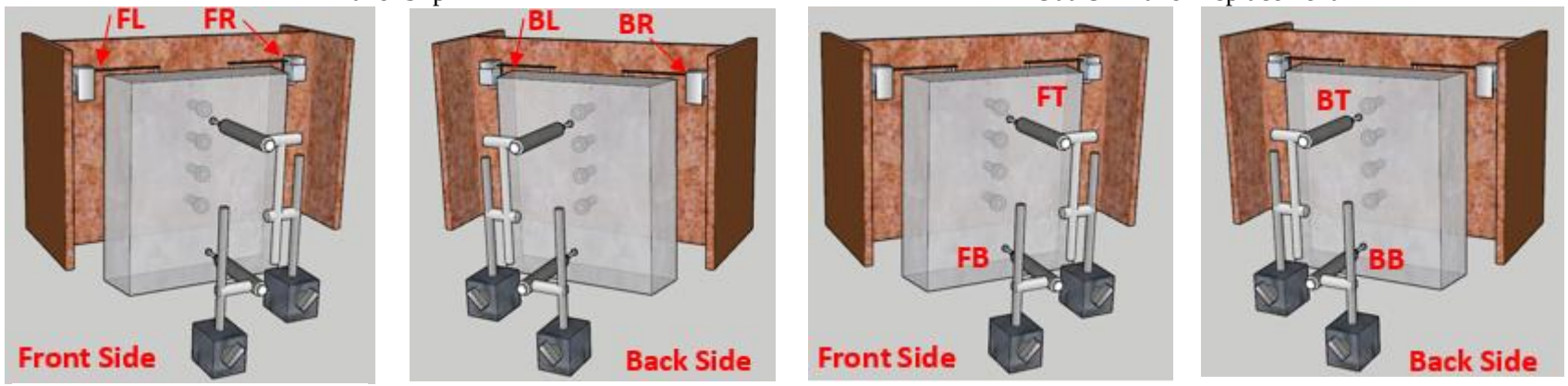

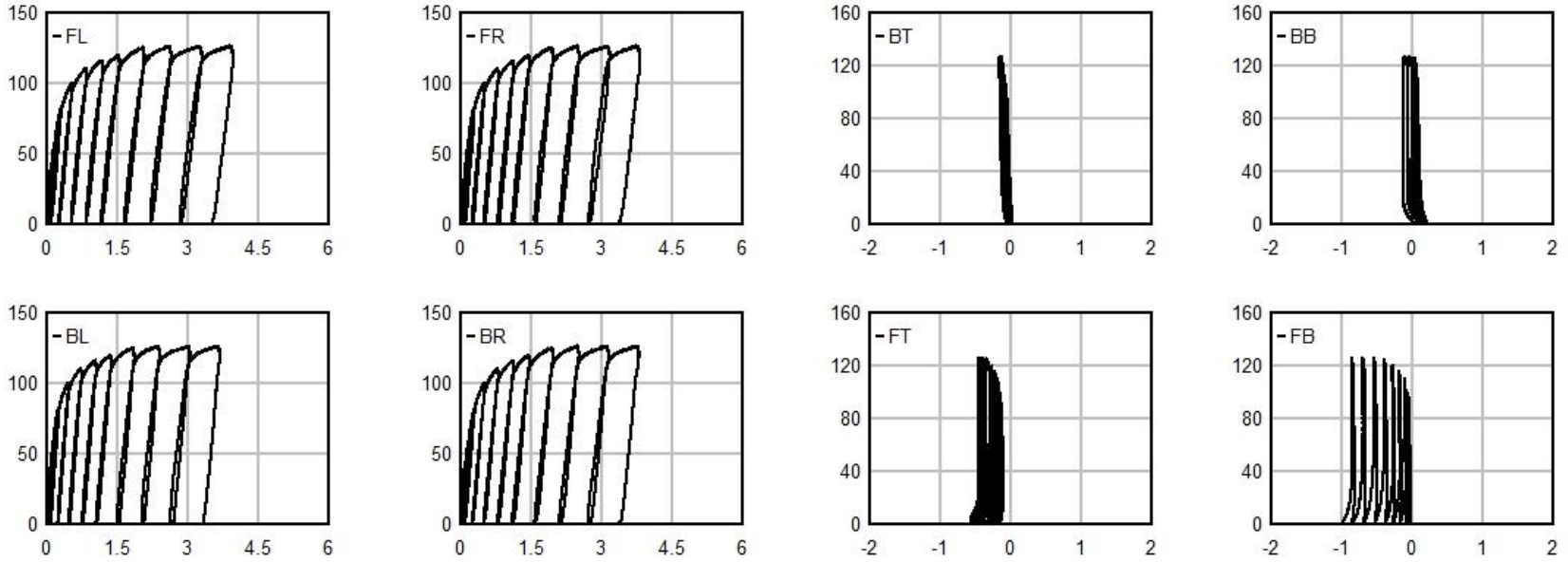

Test 3 – 5/8” Diameter Studs – Strains

Stud Strains

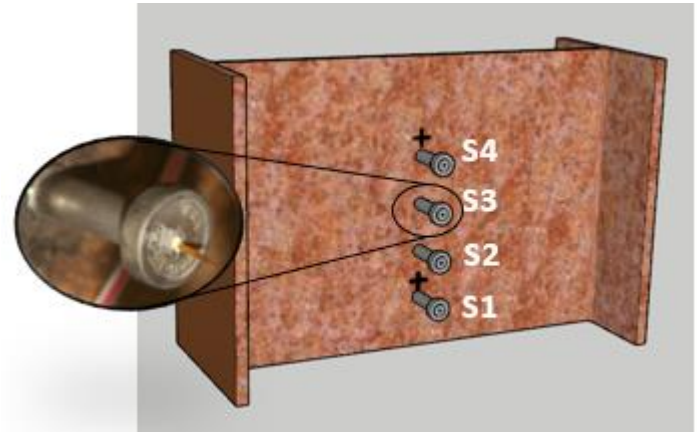

Web Strains

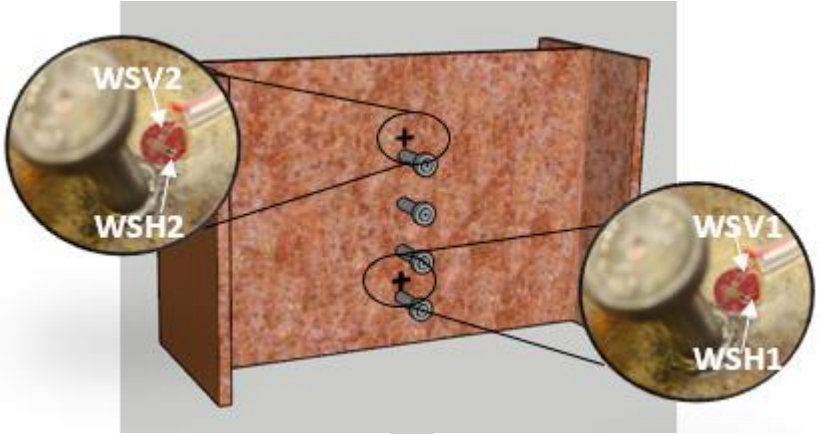

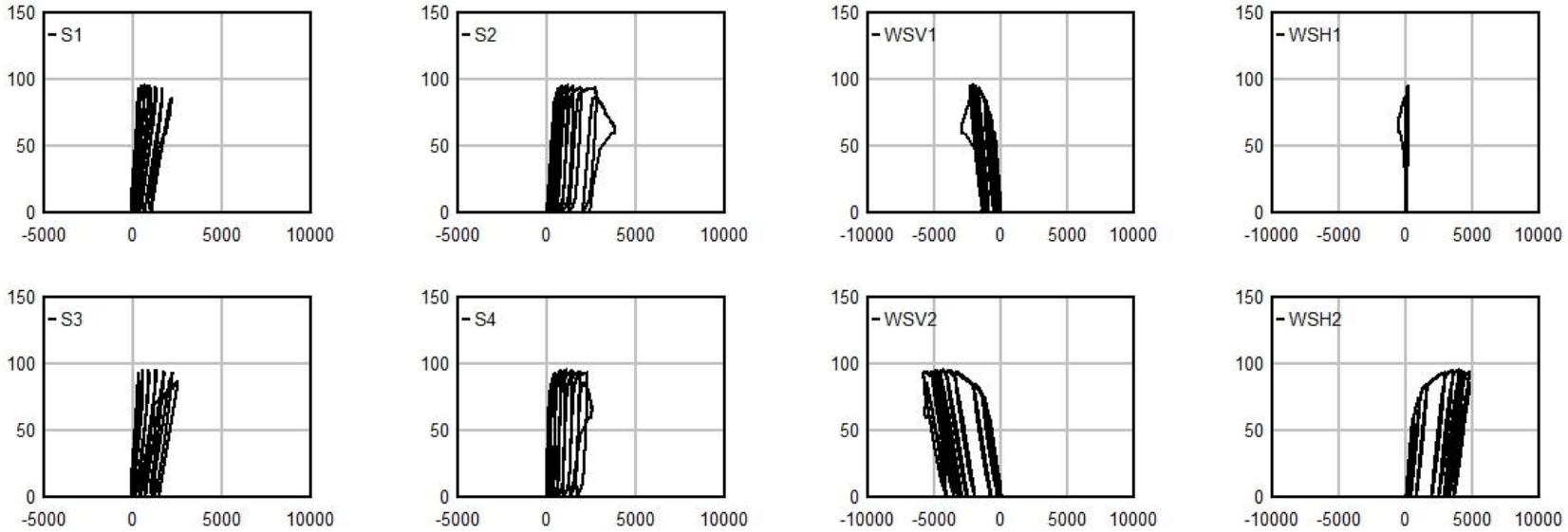

Test 3 – 5/8” Diameter Studs – Displacements

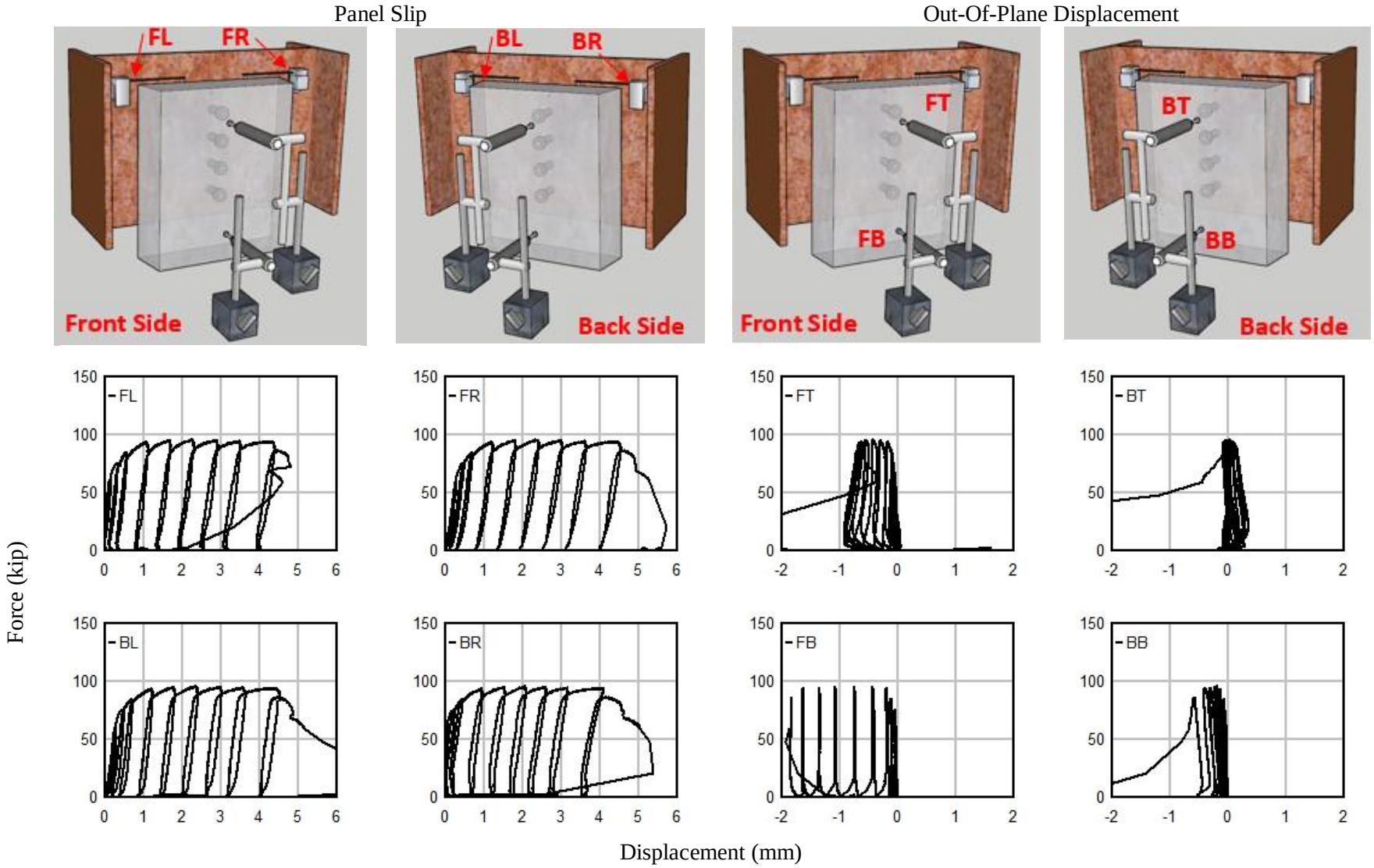

Test 5 – Vertical Stagger – Strains

Stud Strains

Web Strains

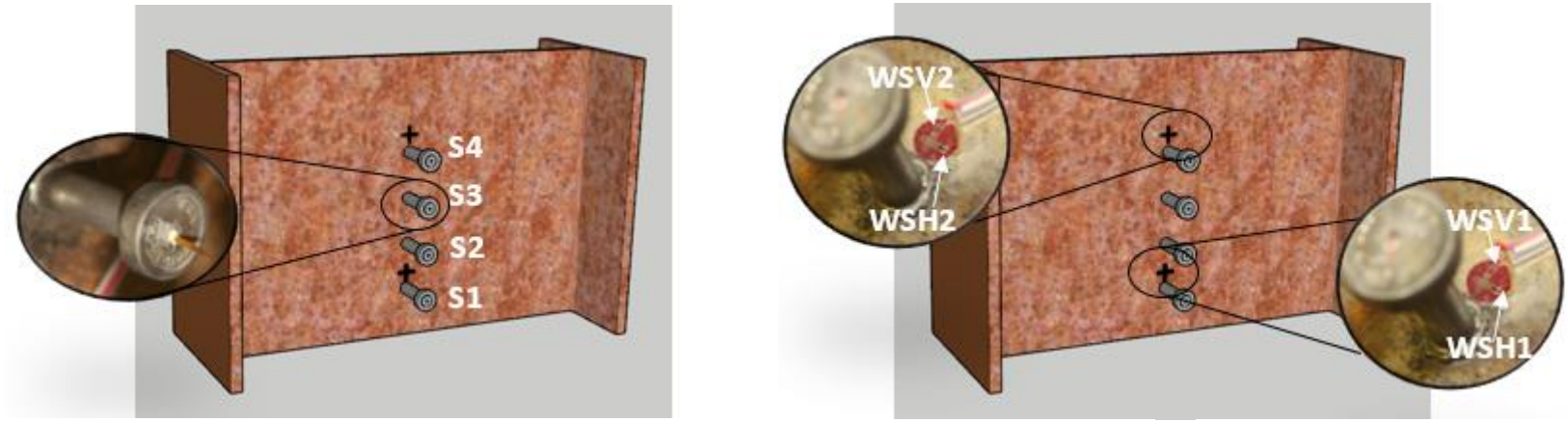

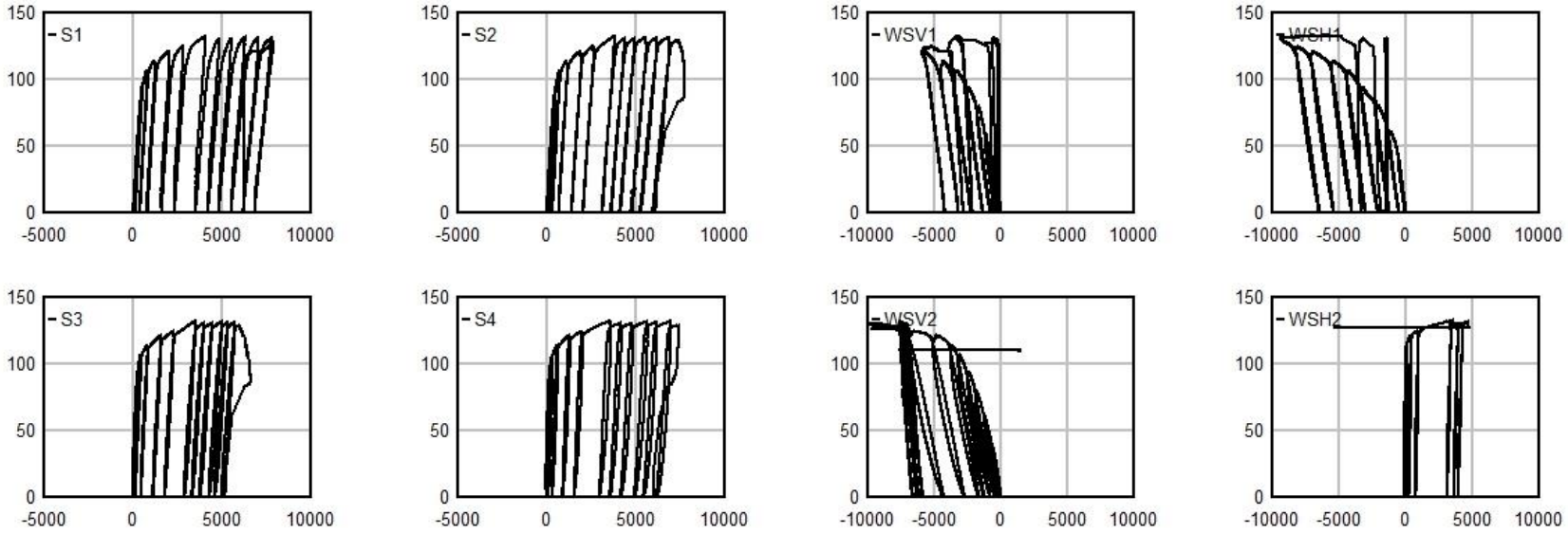

Force (kip)

Strain (με)

Test 5 – Vertical Stagger – Displacements

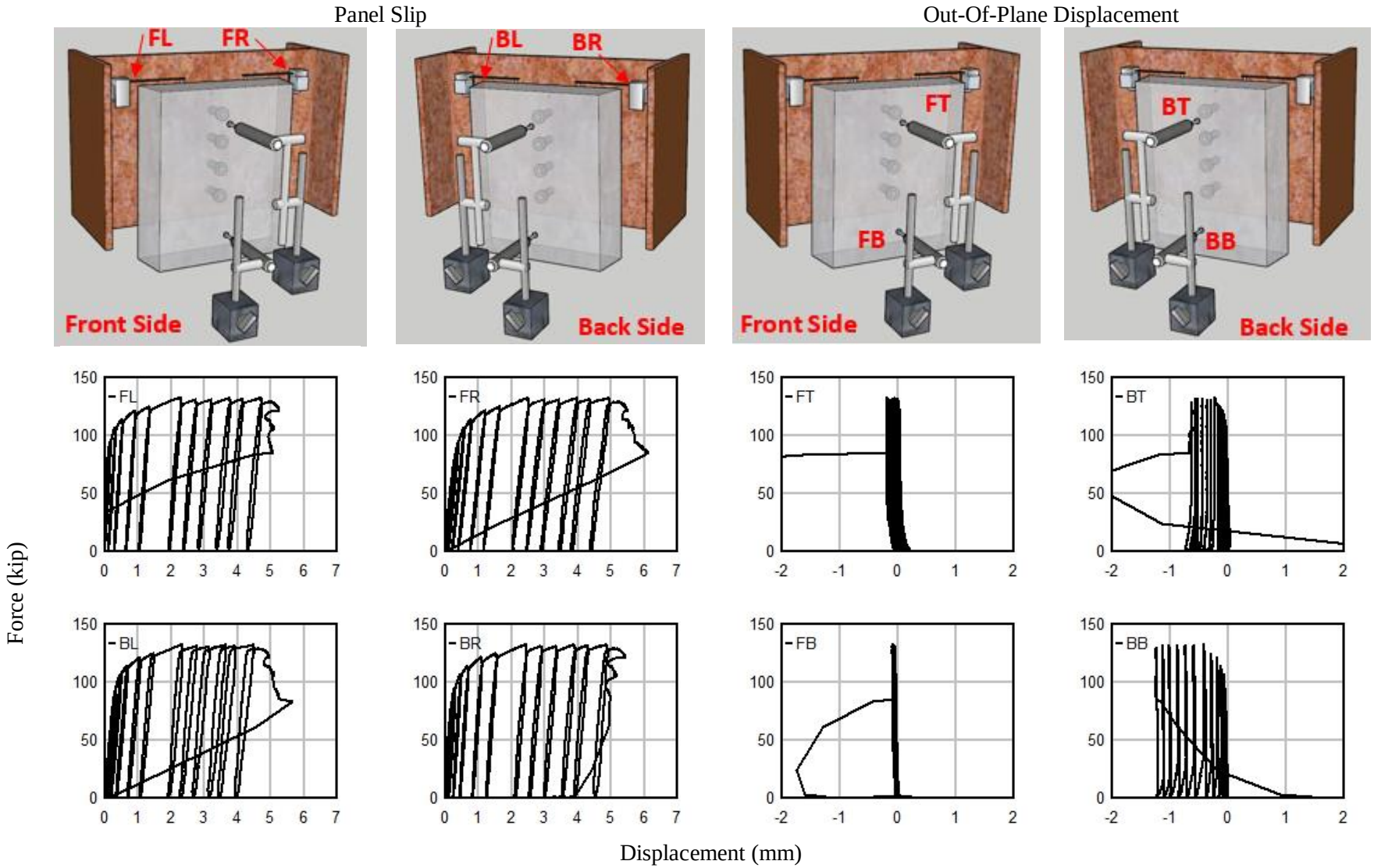

Test 6 – Vertical + Horizontal Stagger – Strains

Stud Strains

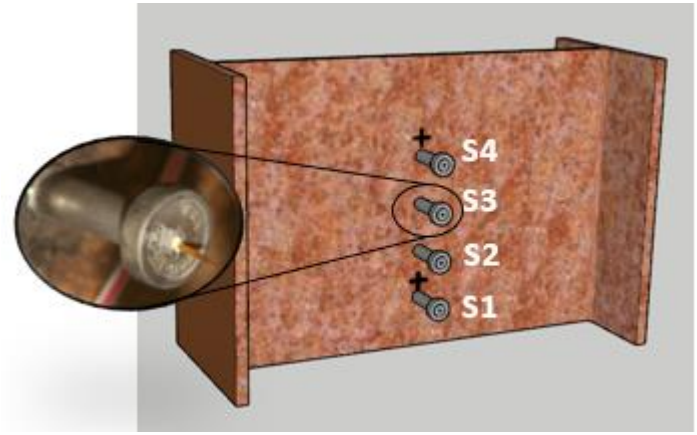

Web Strains

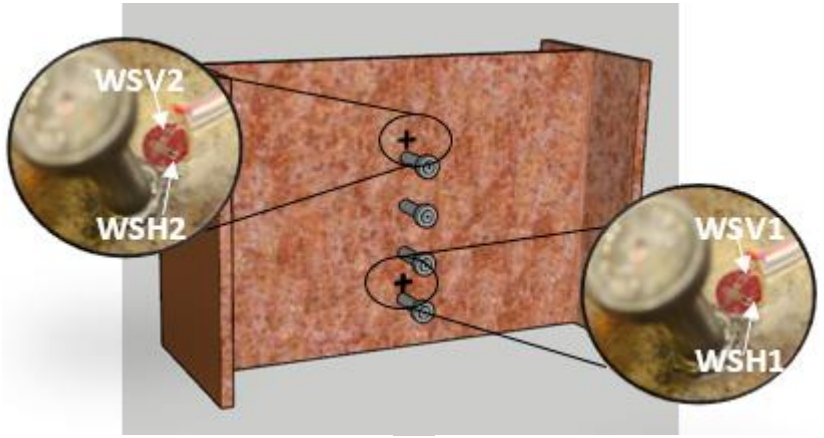

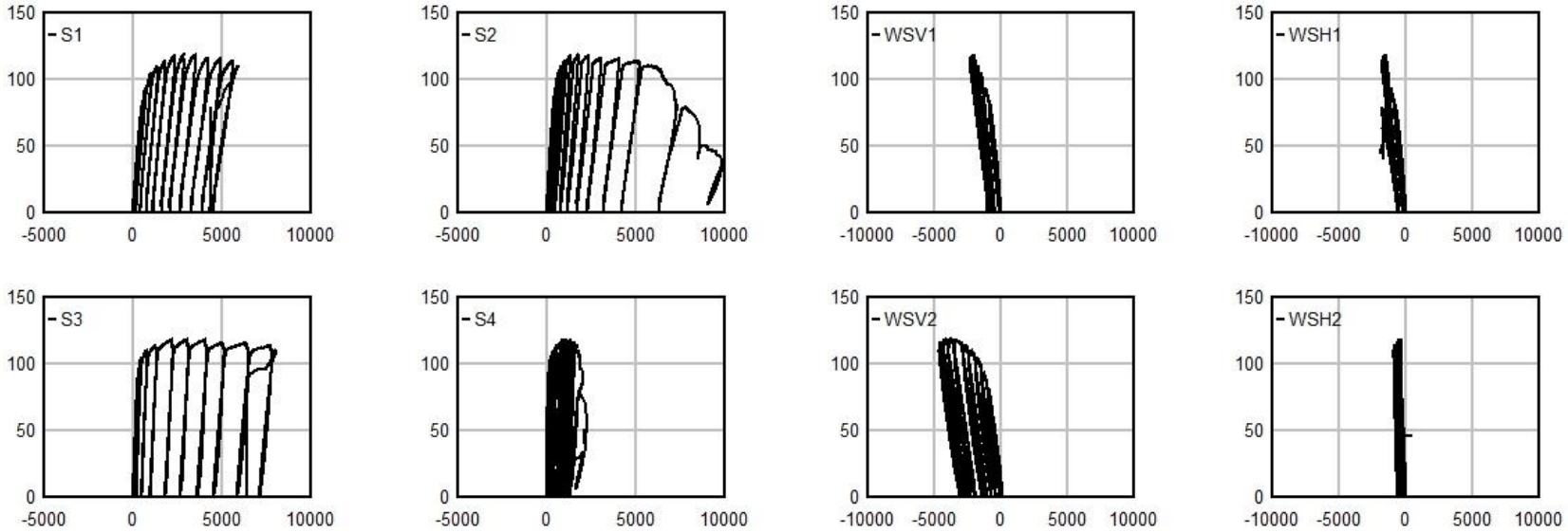

Force (kip)

Strain (με)

Test 6 – Vertical + Horizontal Stagger – Displacements

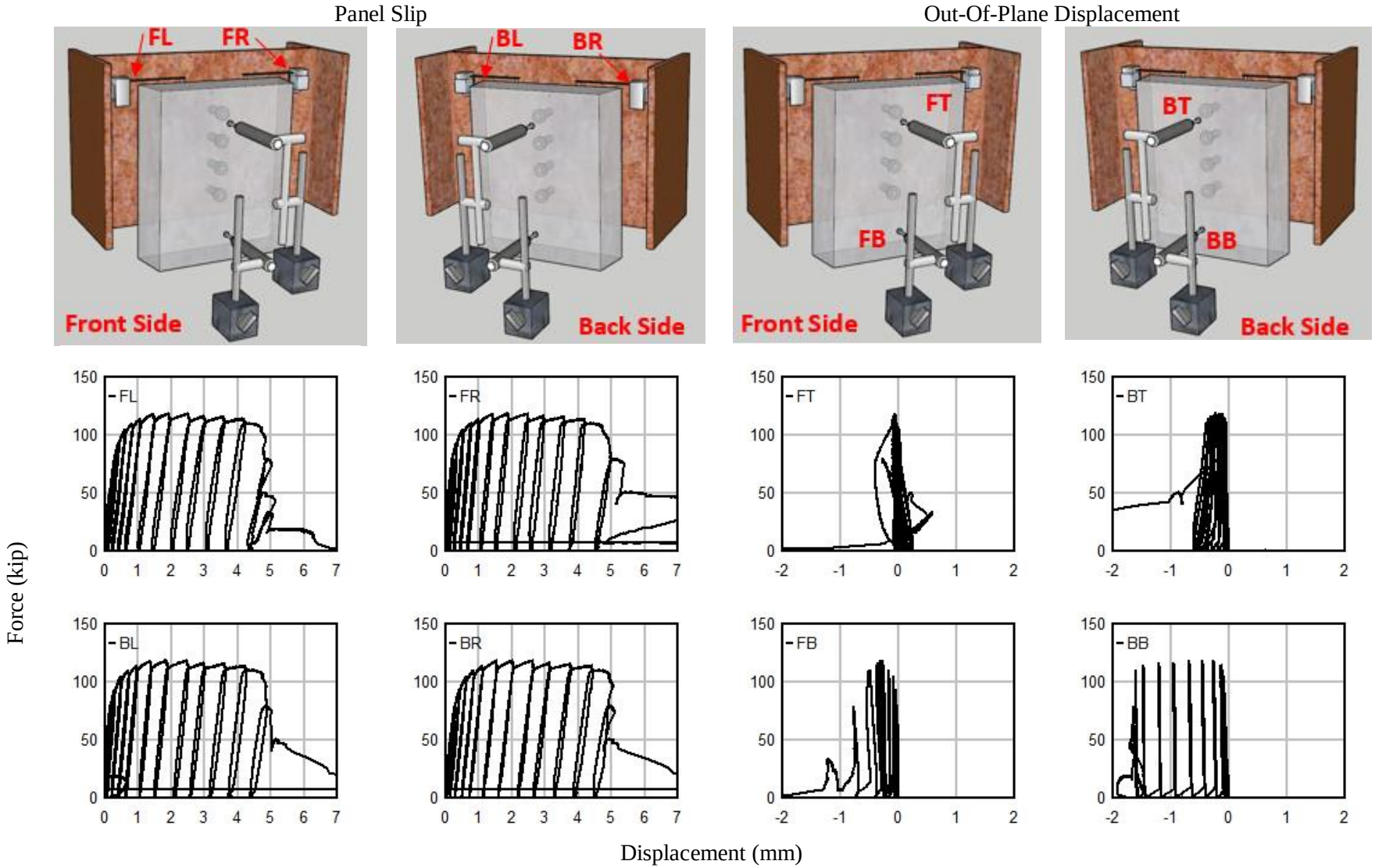

Test 7 – High-Strength Concrete – Strains

Stud Strains

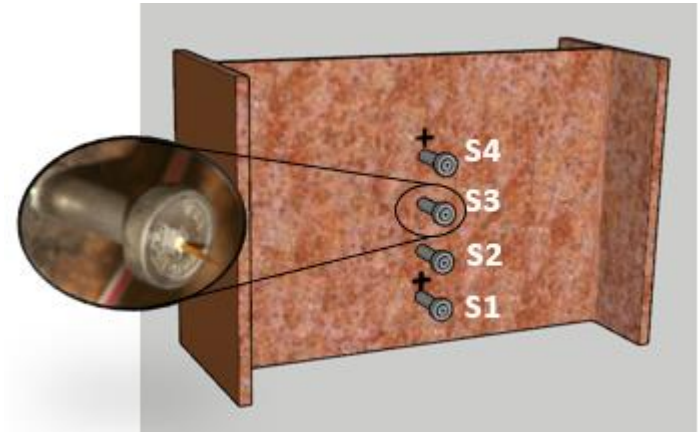

Web Strains

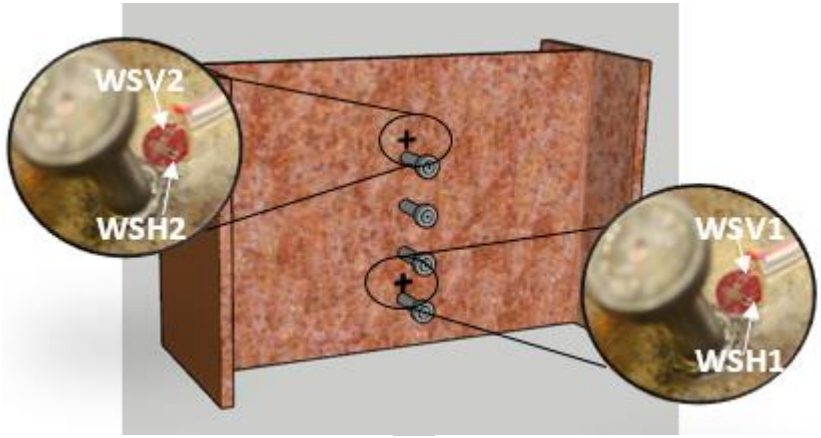

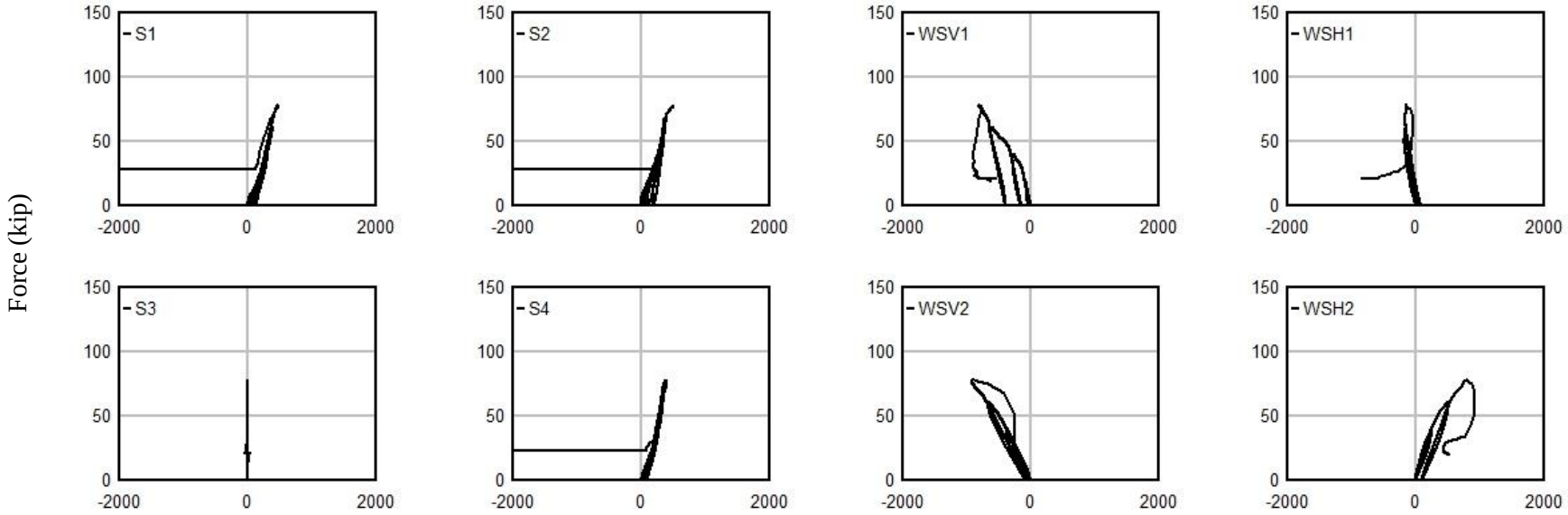

Test 7 – High-Strength Concrete – Displacements

Panel Slip

Out-Of-Plane Displacement

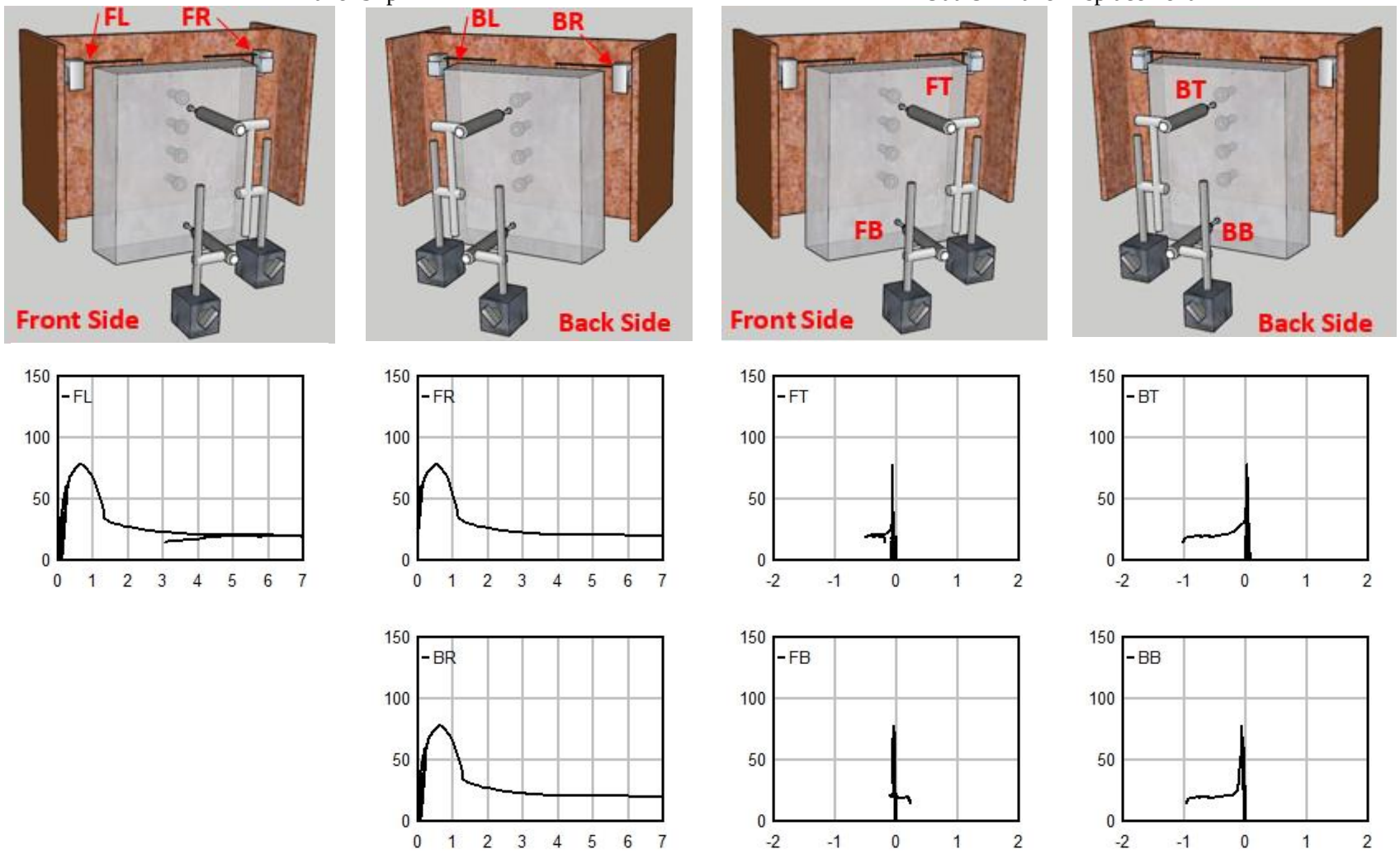

Test 8 – ¼" Clear Cover – Strains

Stud Strains

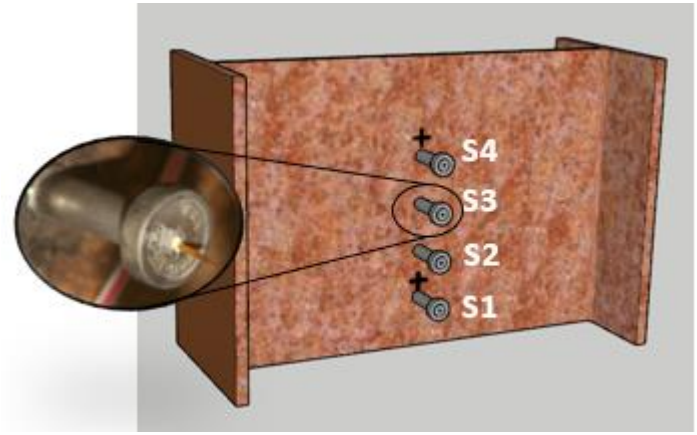

Web Strains

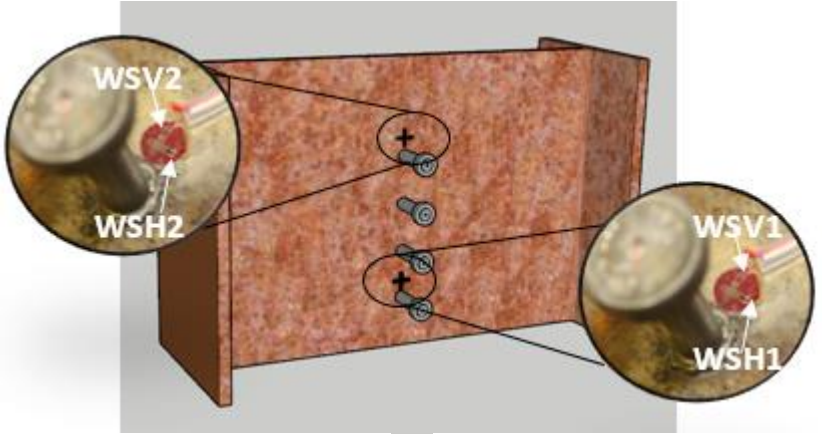

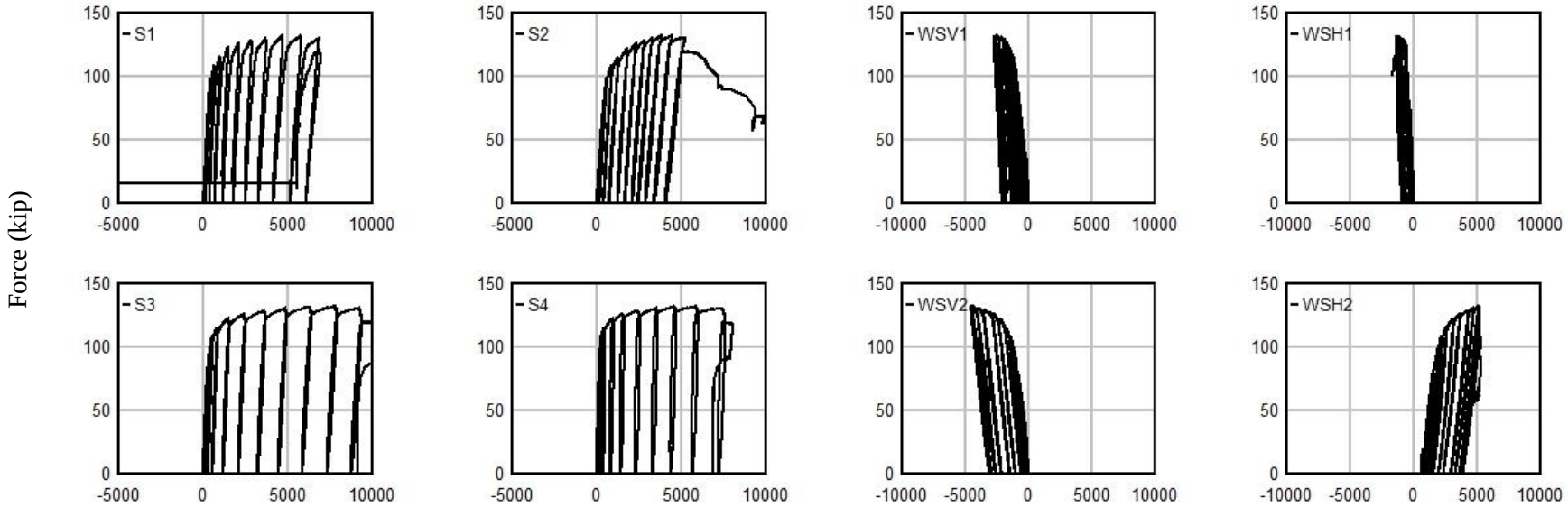

Test 8 – ¼" Clear Cover – Displacements

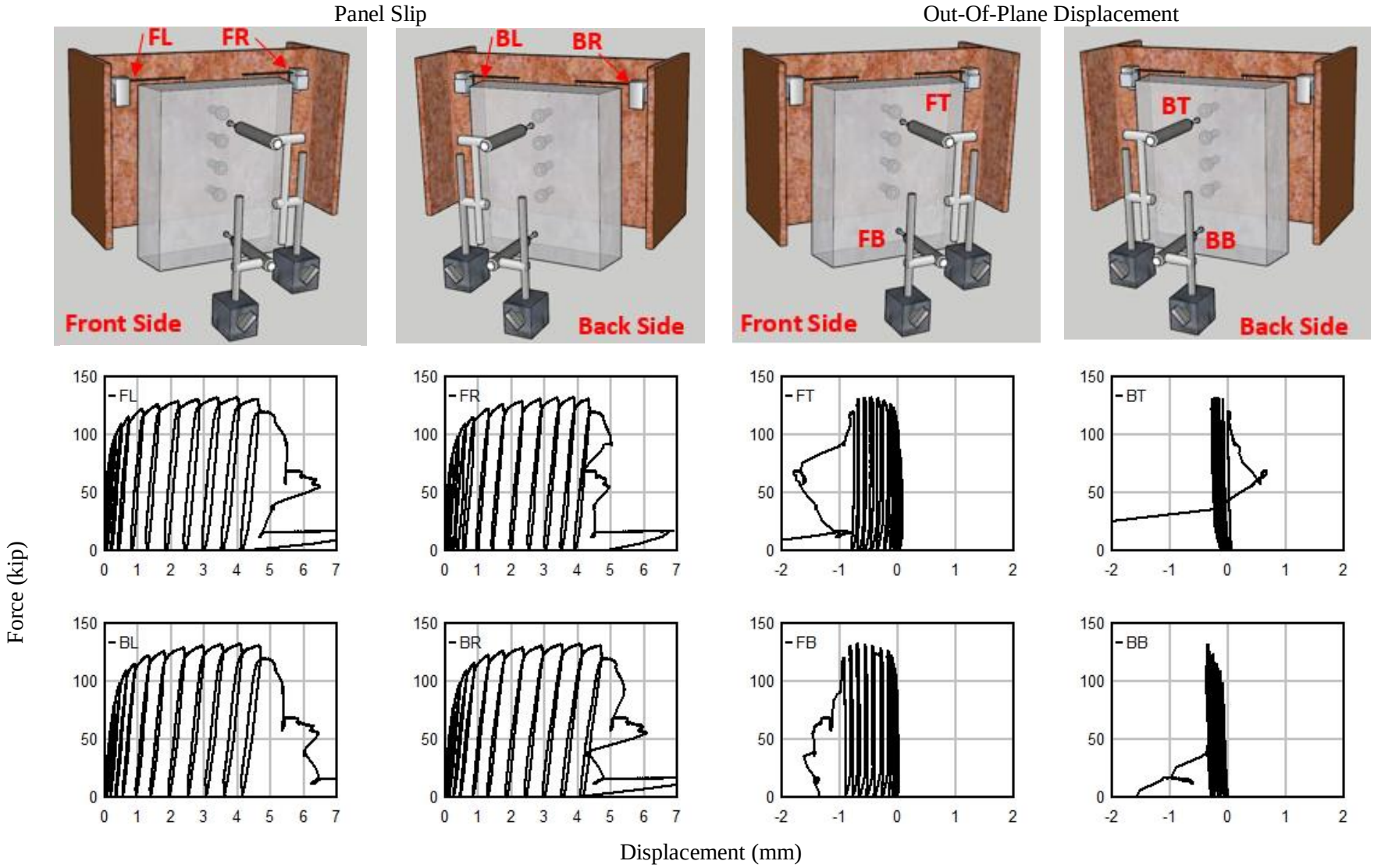

Test 9 – 28 ksi – Strains

Stud Strains

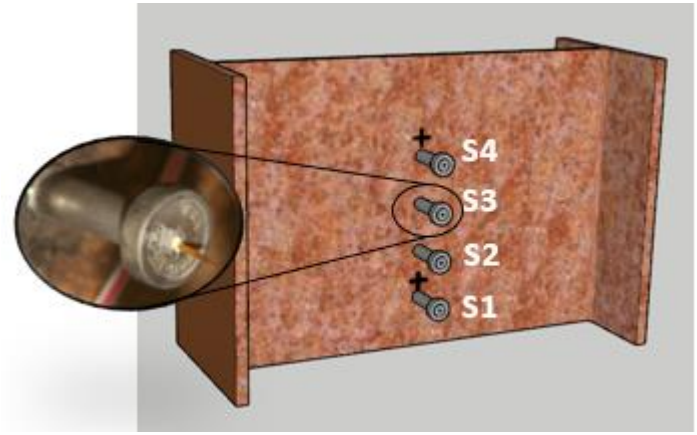

Web Strains

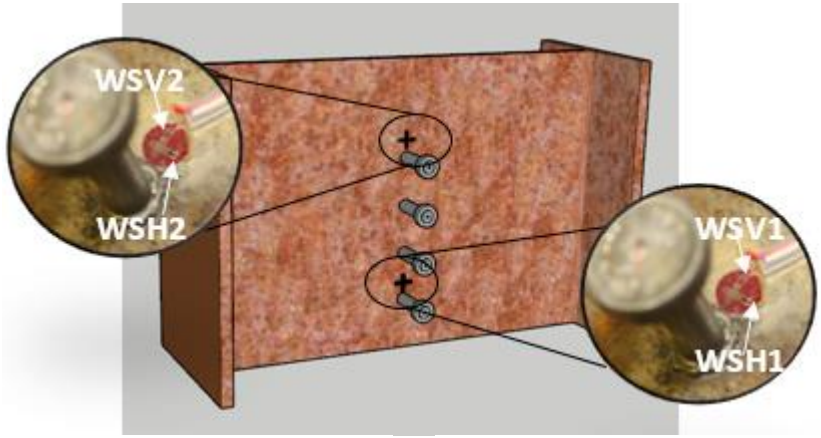

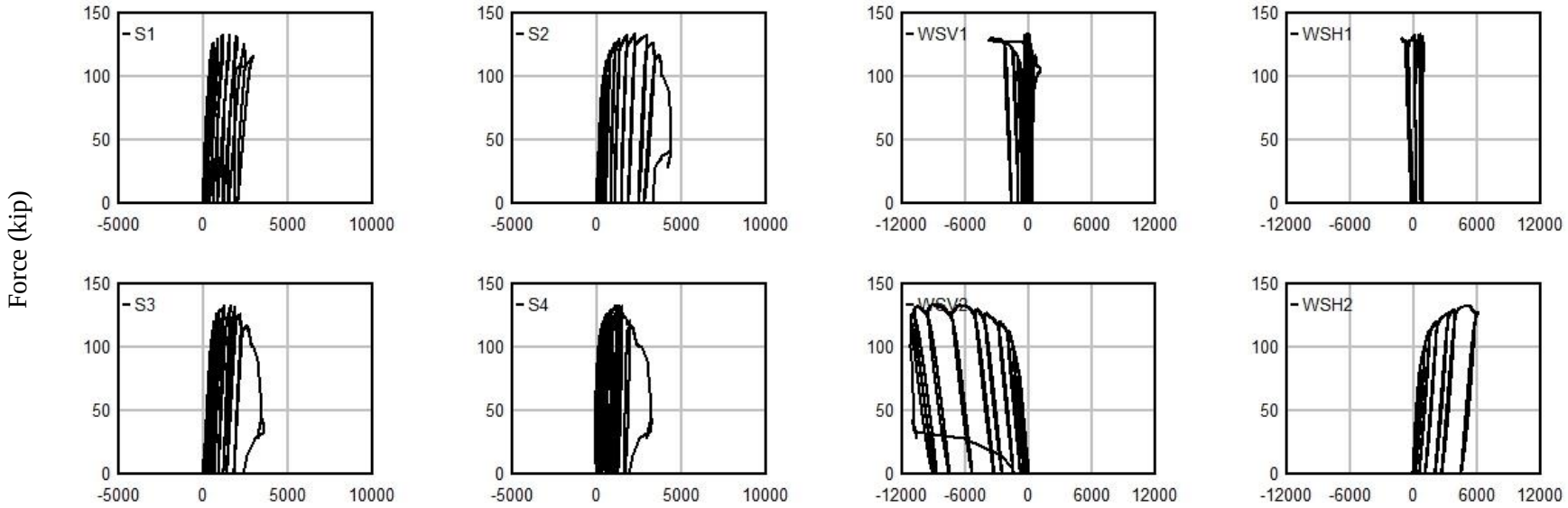

Test 9 – 28 ksi – Displacements

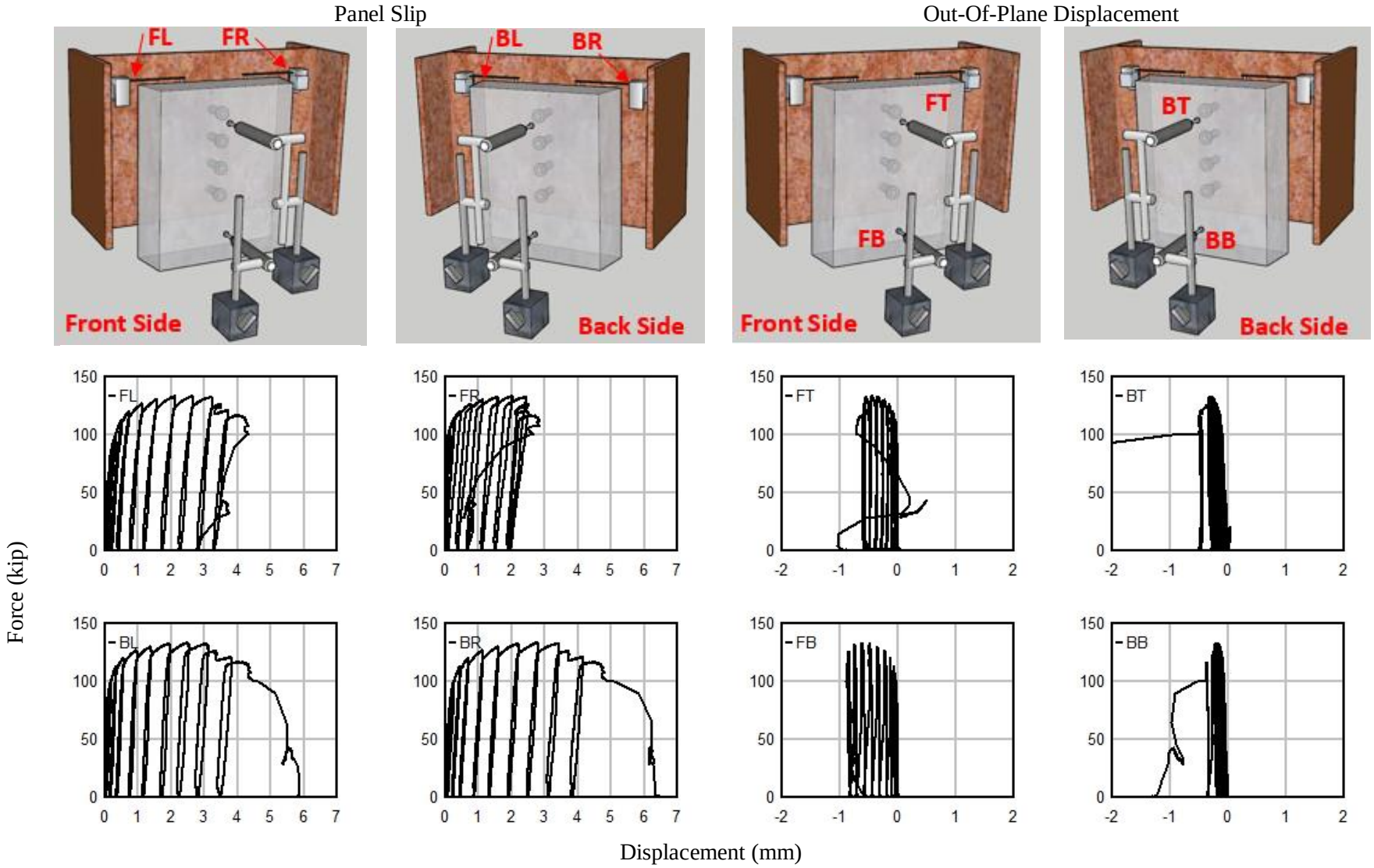

Test 10 – No Fibers – Strains

Stud Strains

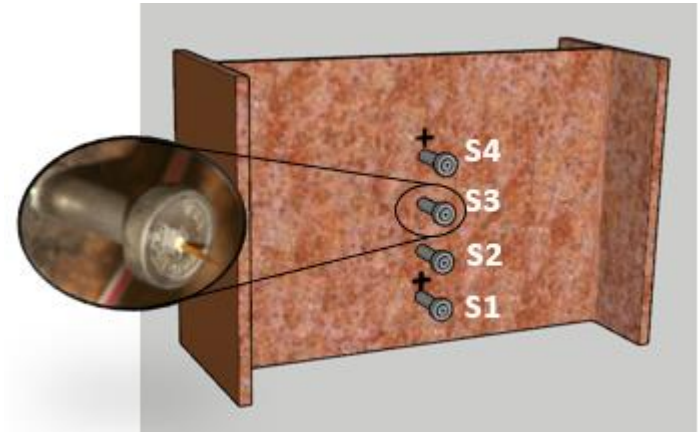

Web Strains

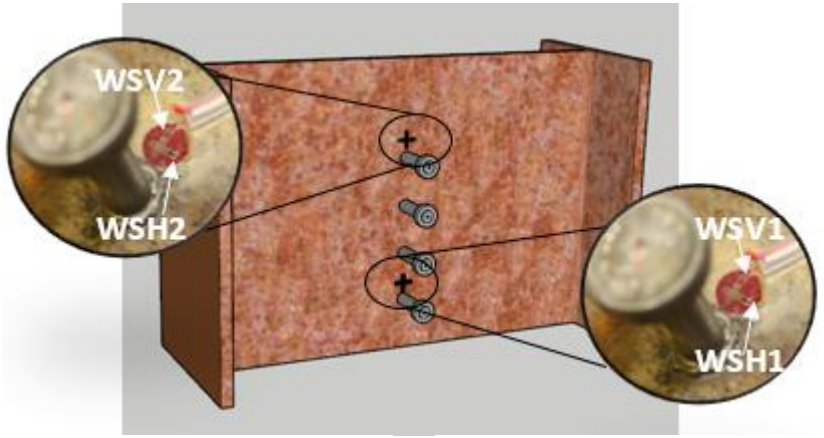

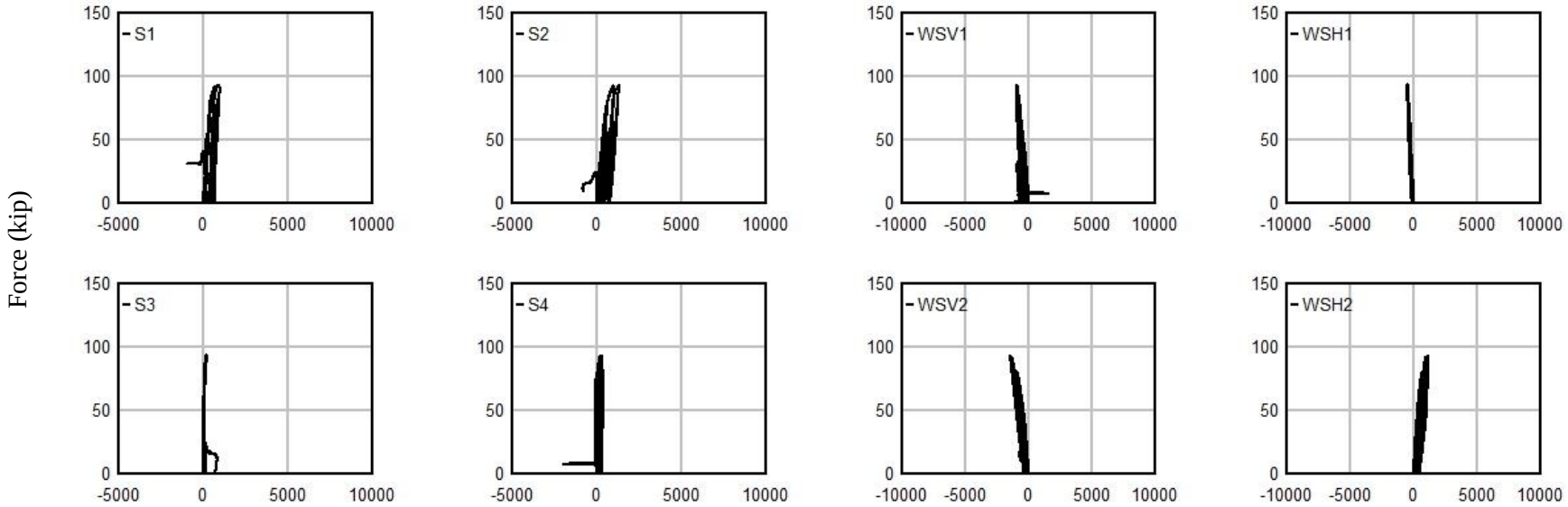

Test 10 – No Fibers – Displacements

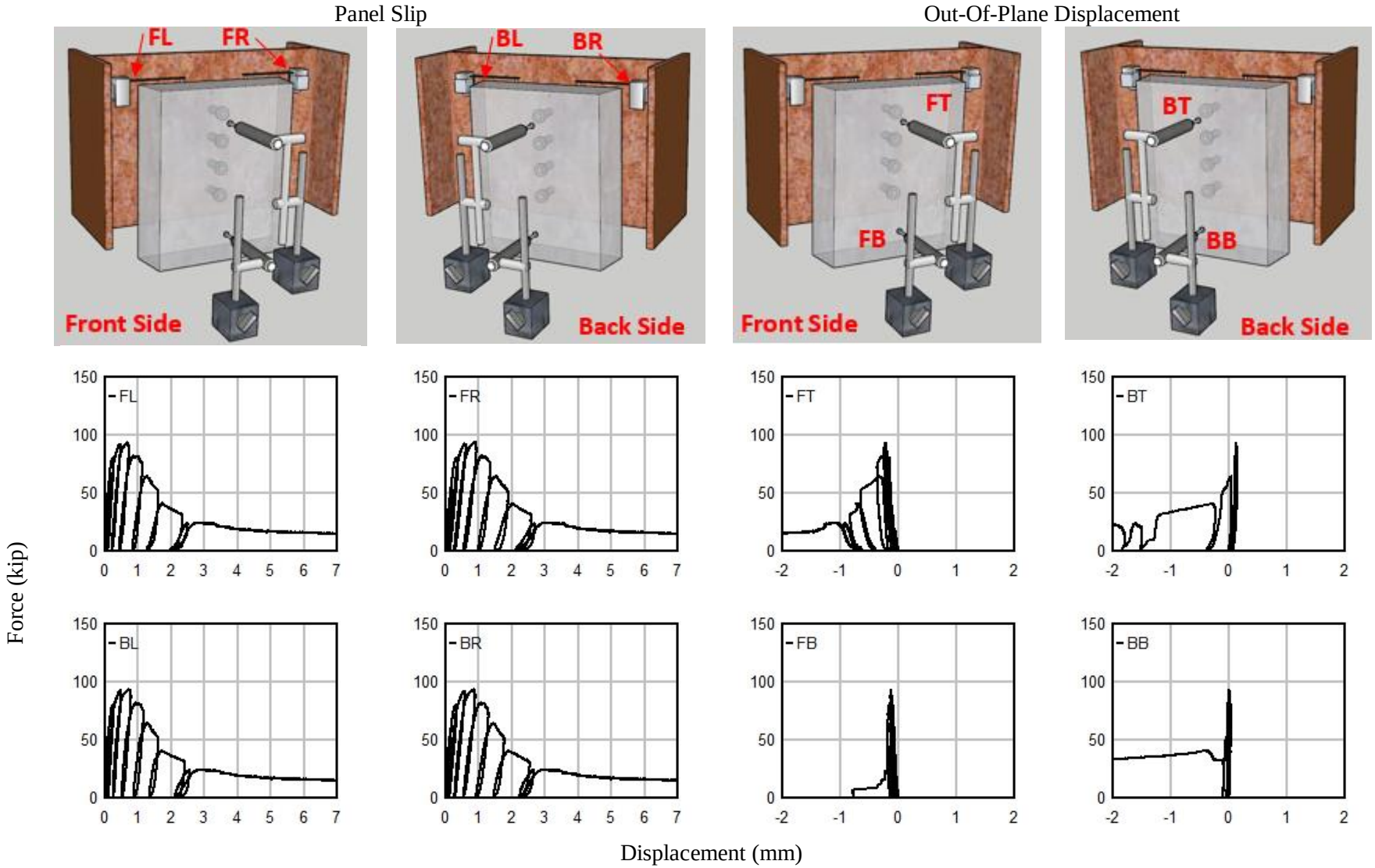

Test 11 – 4” Eccentricity – Strains

Stud Strains

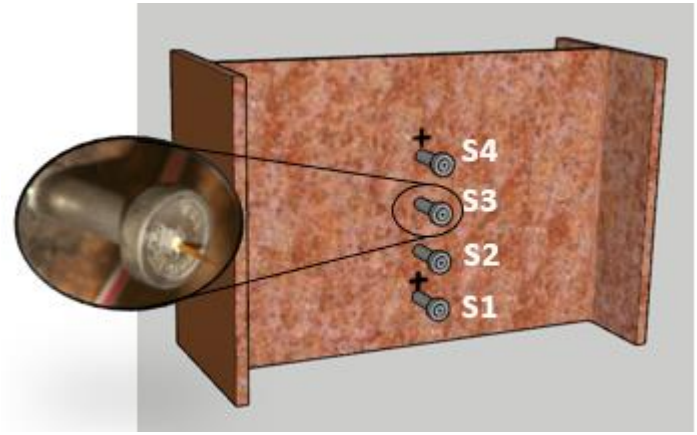

Web Strains

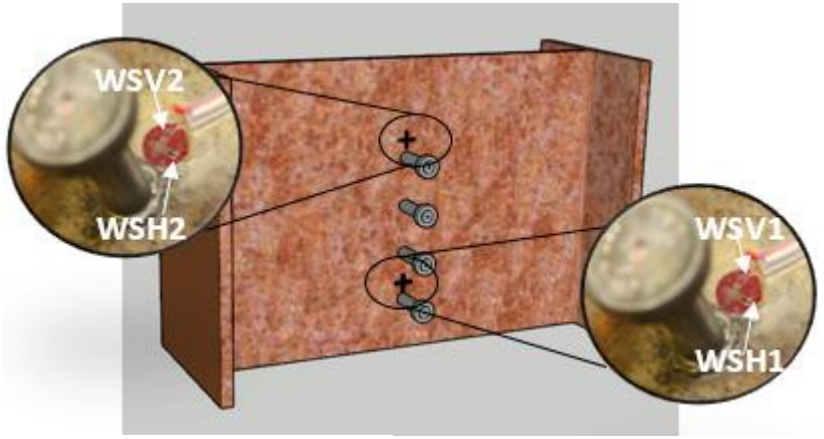

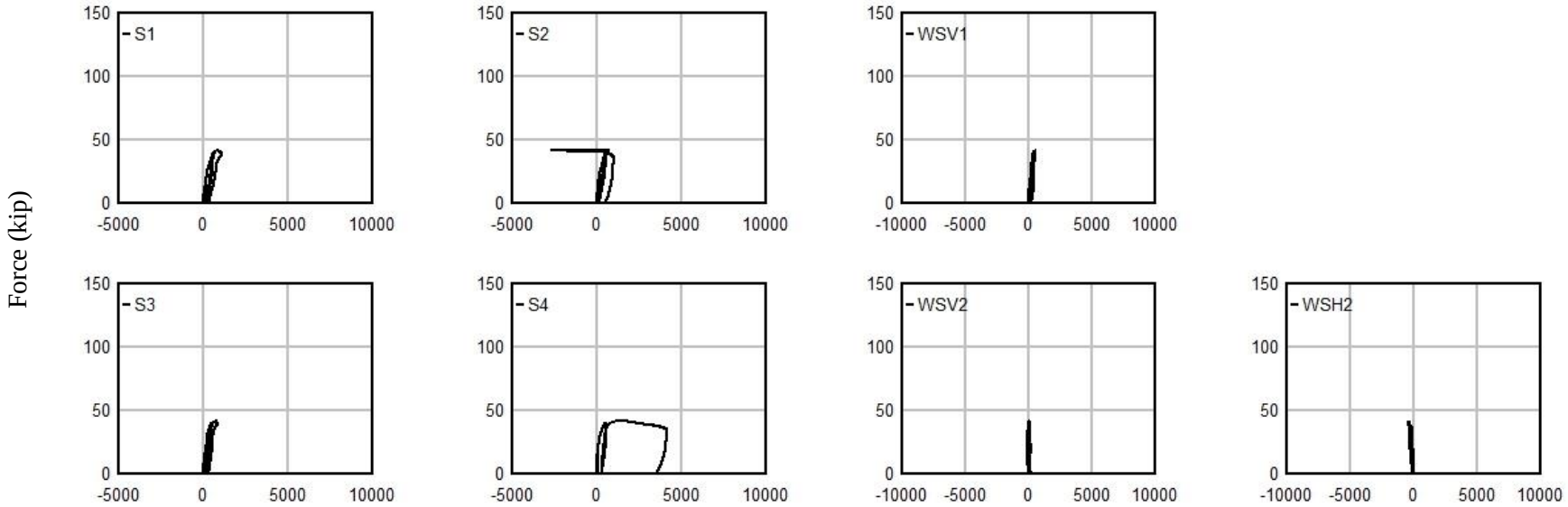

Test 11 – 4” Eccentricity – Displacements

Panel Slip

Out-Of-Plane Displacement

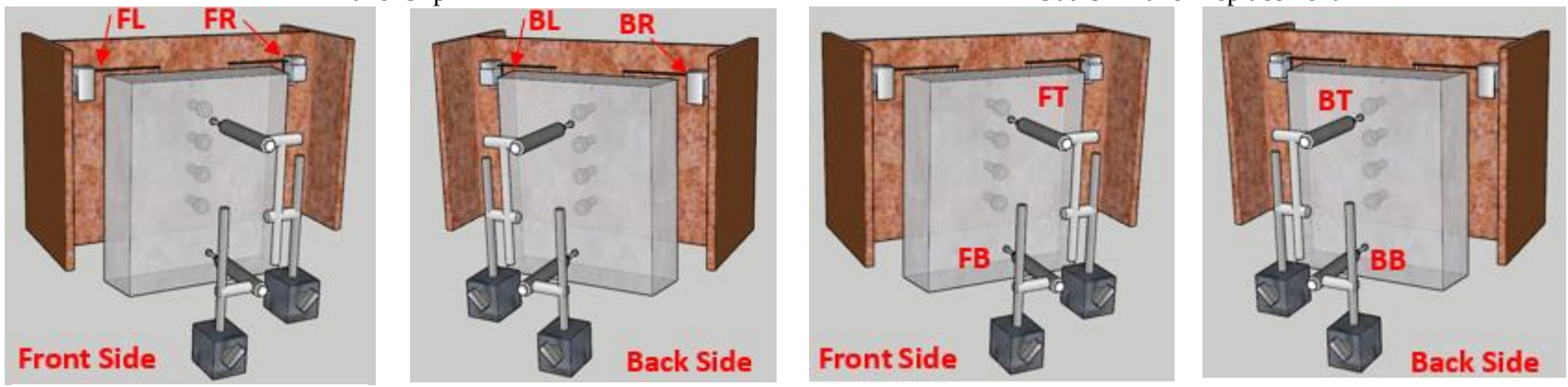

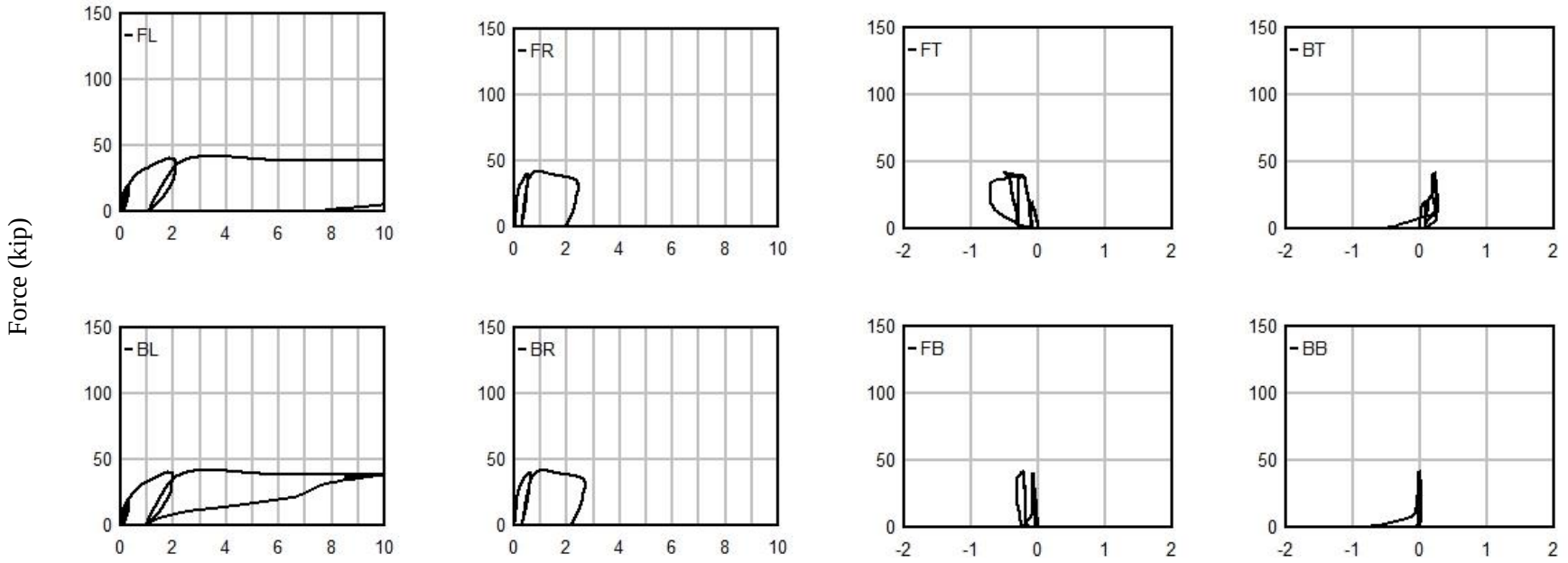

Force (kip)

Displacement (mm)

Test 12 – One-Sided Repair – Strains

Stud Strains

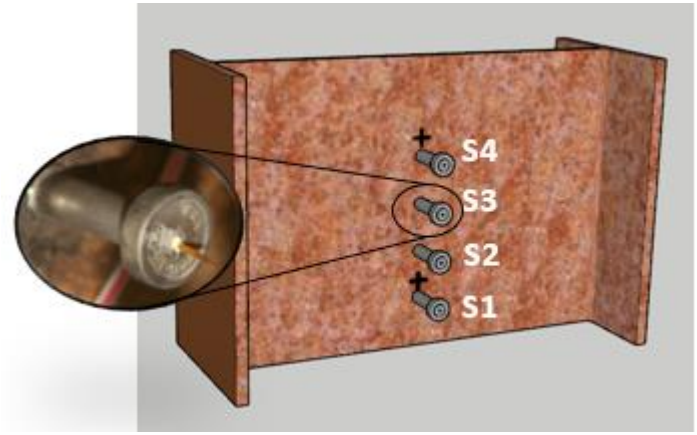

Web Strains

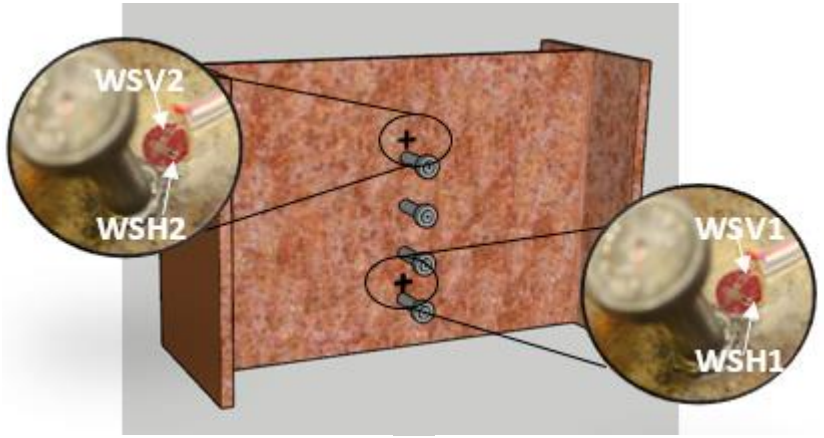

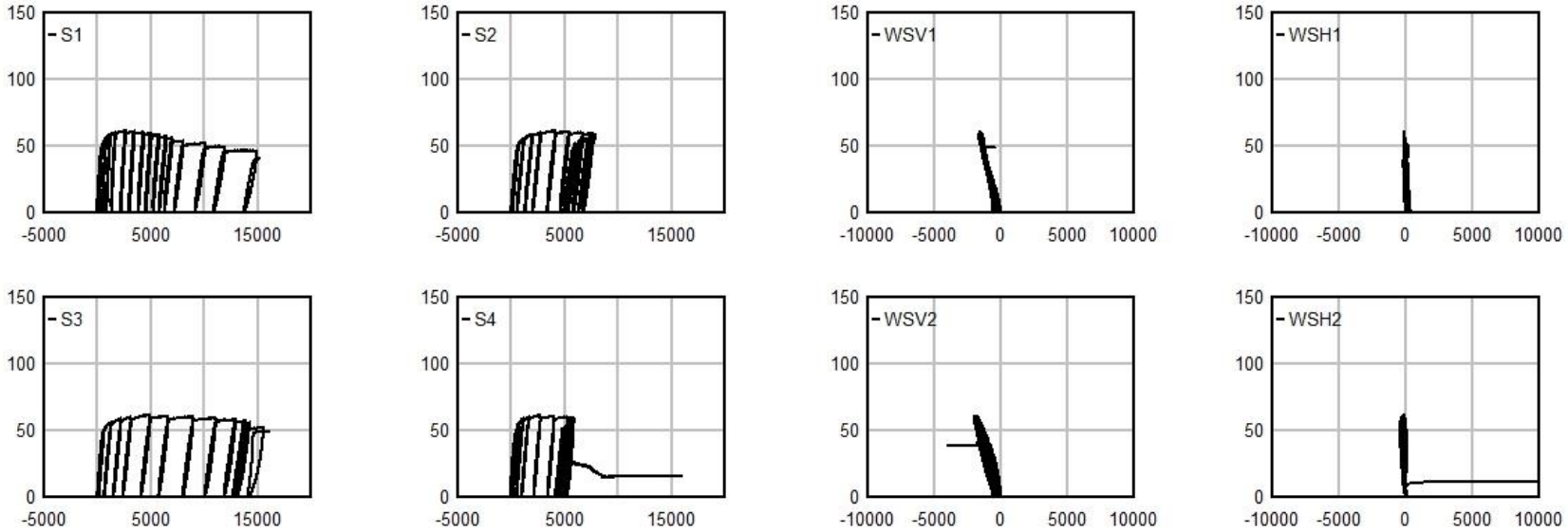

Test 12 – One-Sided Repair – Displacements

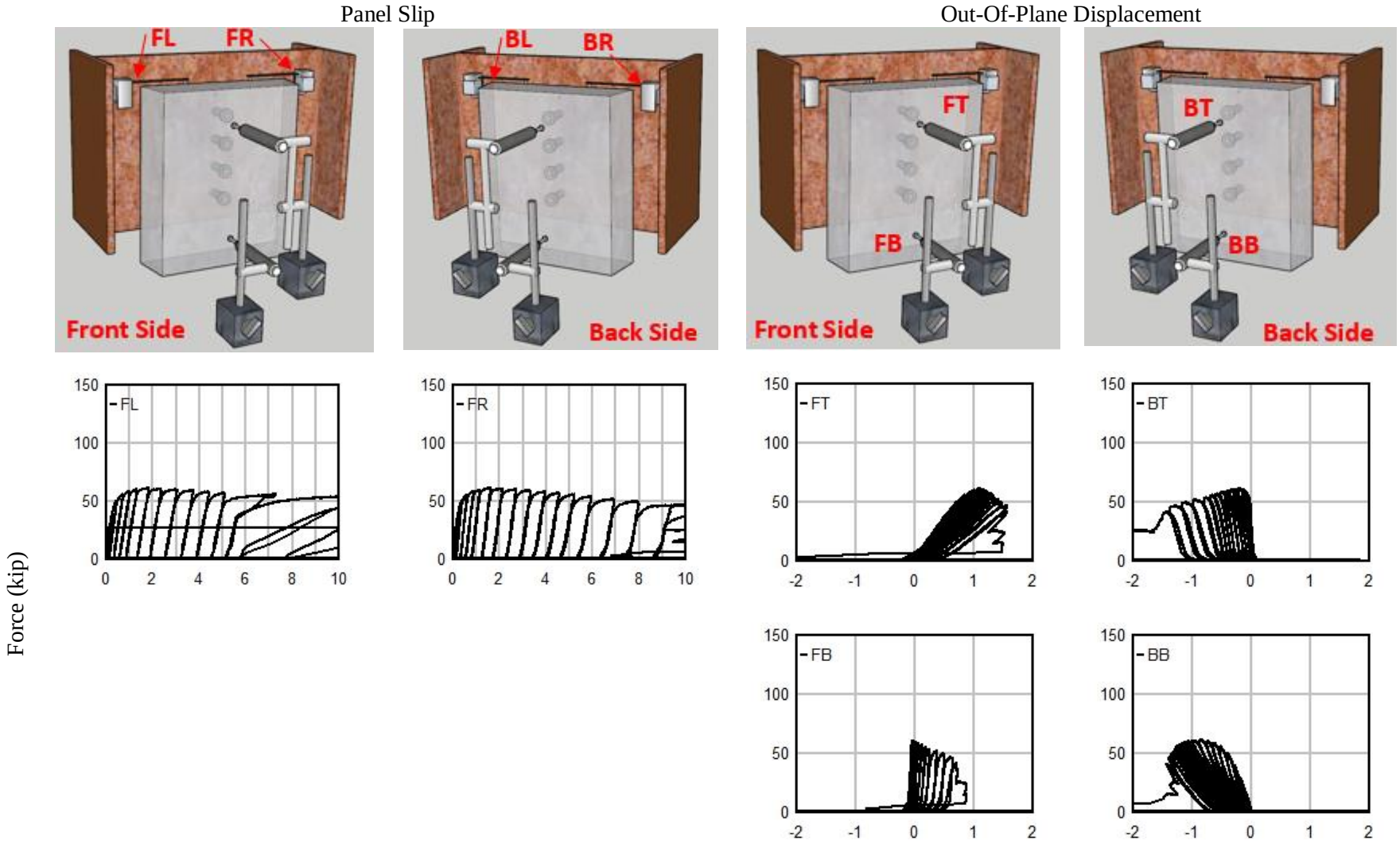

Test 13 – ¾" Stud Diameter - Short – Strains

Stud Strains

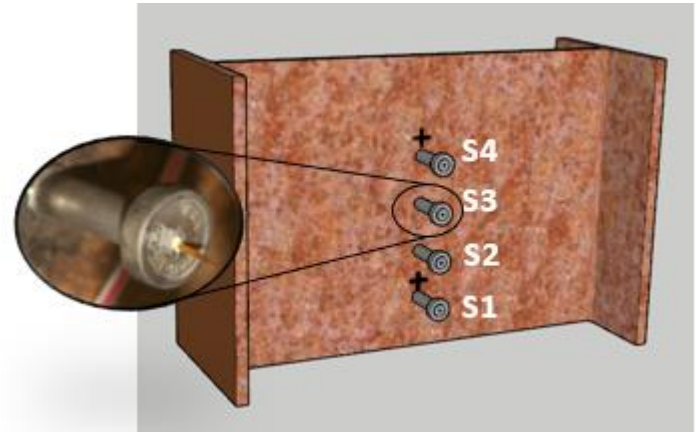

Web Strains

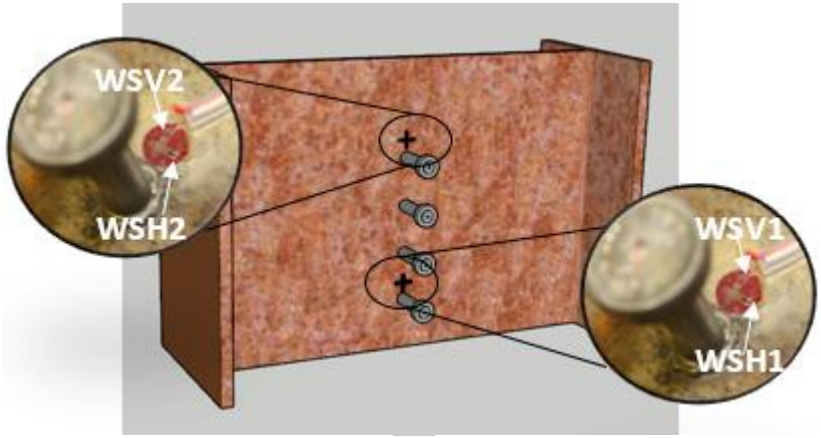

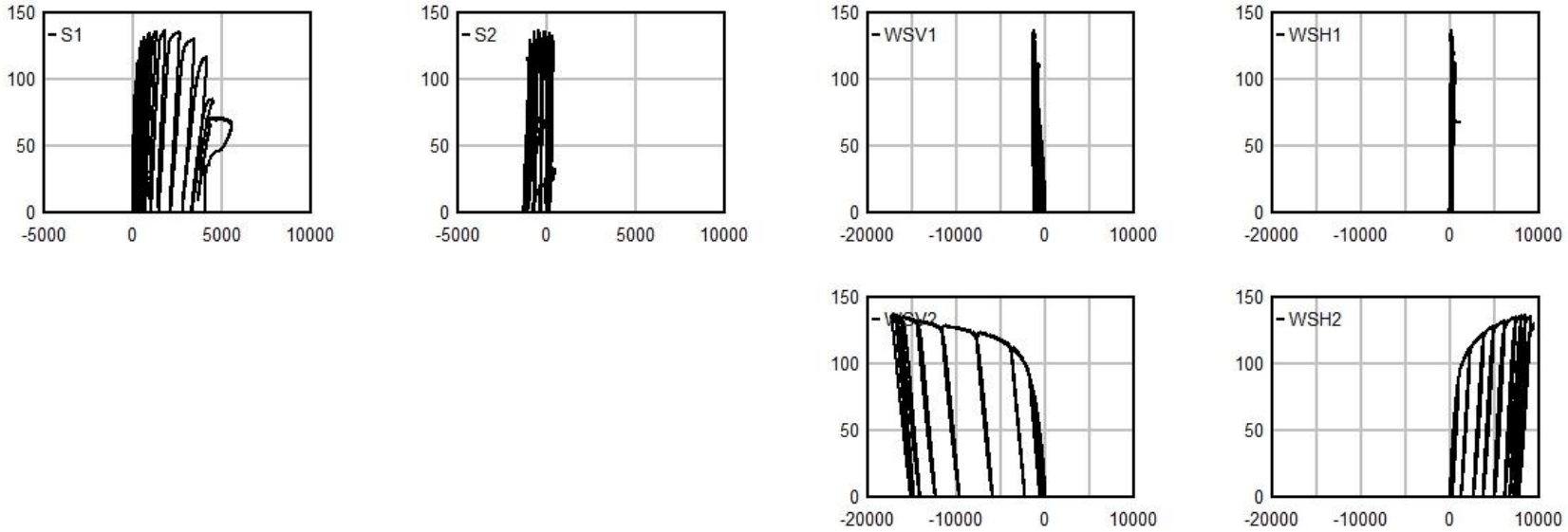

Force (kip)

Strain (με)

Test 13 – ¾" Stud Diameter - Short – Displacements

Panel Slip

Out-Of-Plane Displacement

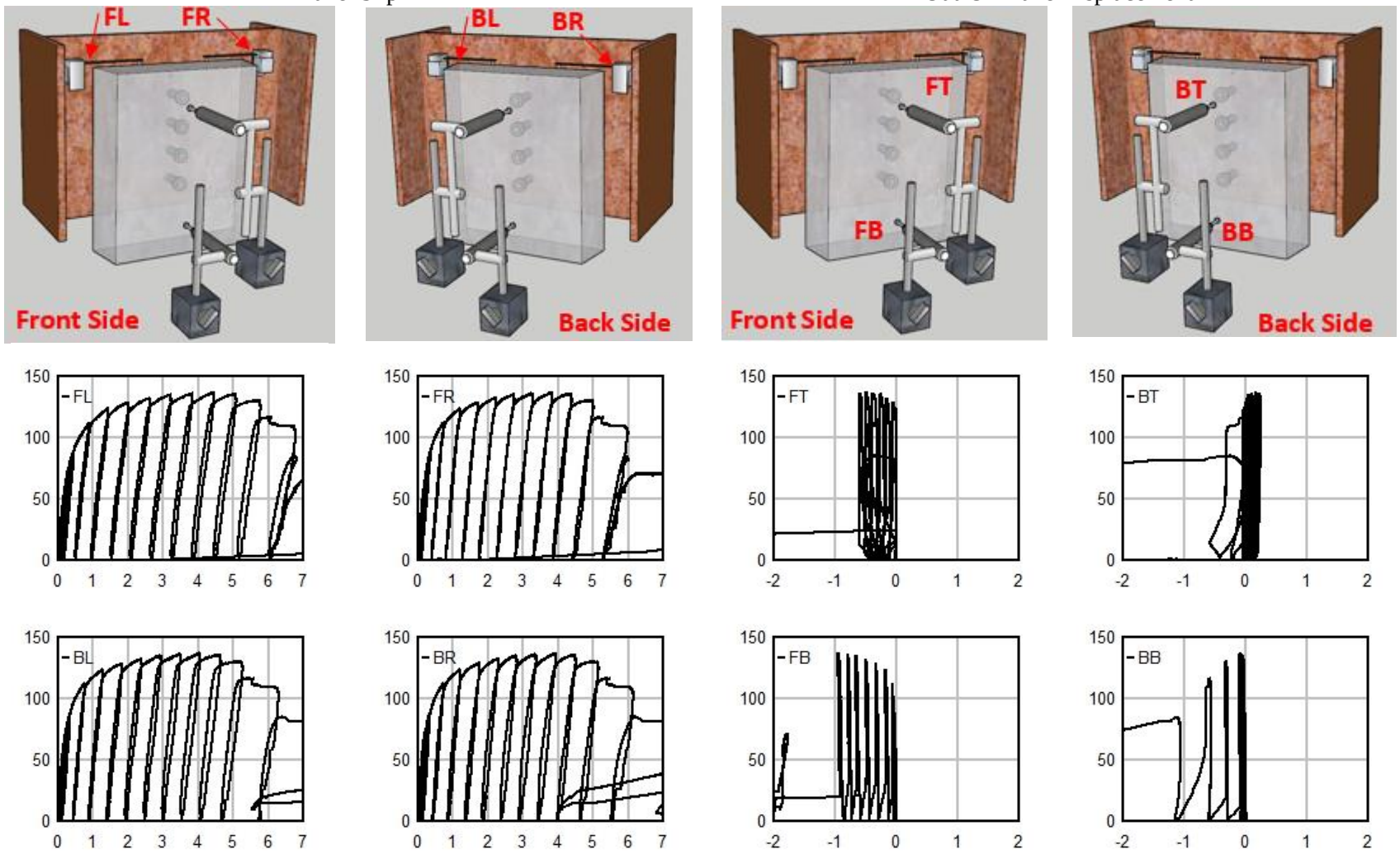

Test 14 – ¾" Stud Diameter - Long – Strains

Stud Strains

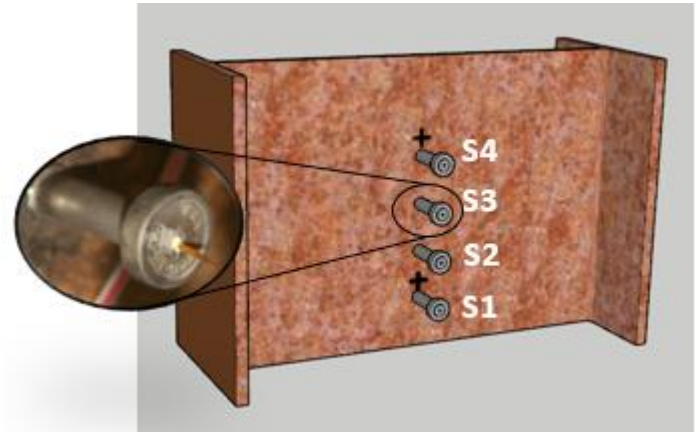

Web Strains

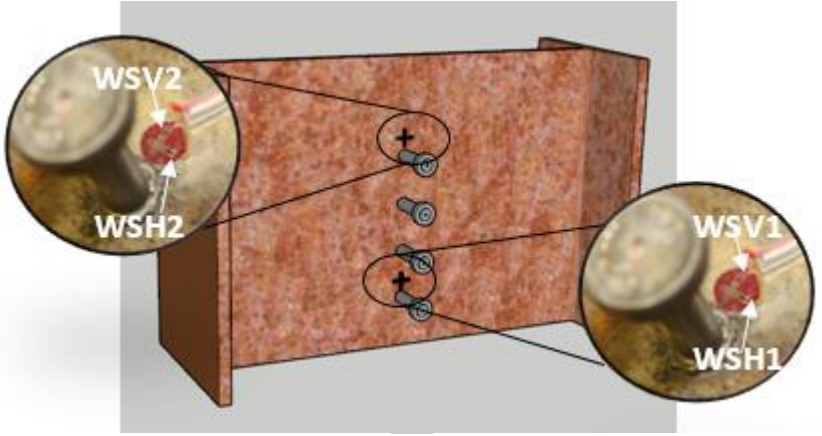

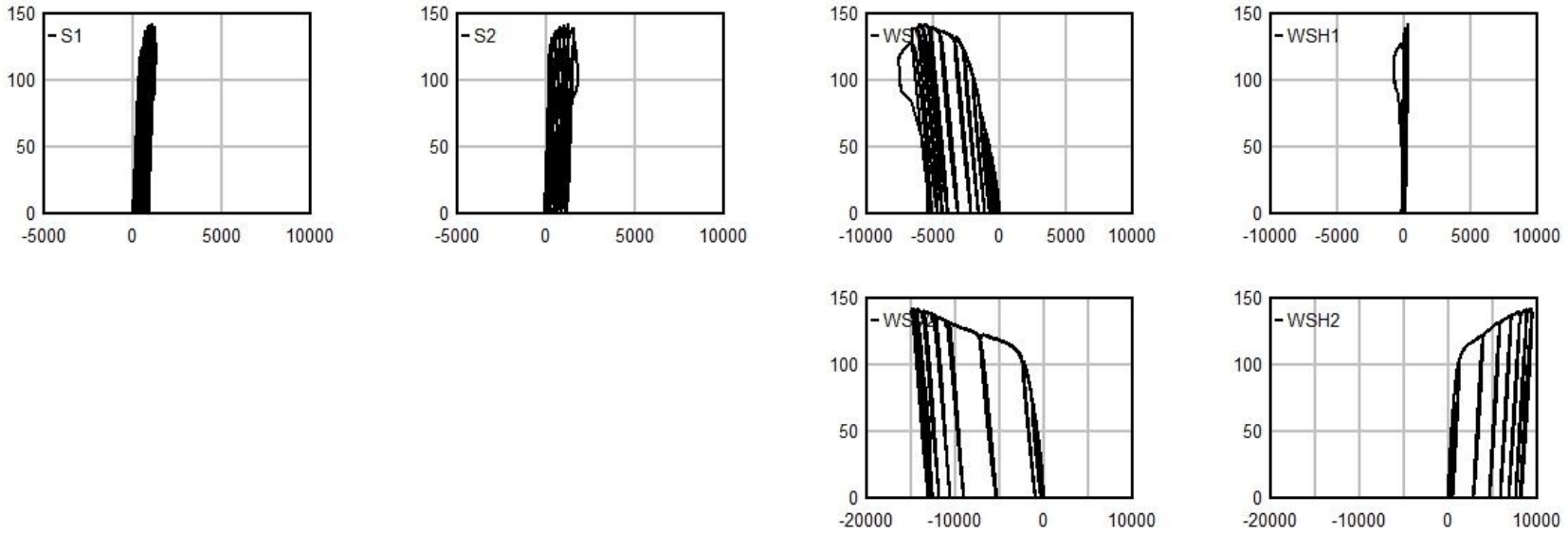

Force (kip)

Strain (με)

Test 14 – ¾" Stud Diameter - Long – Displacements

Panel Slip

Out-Of-Plane Displacement

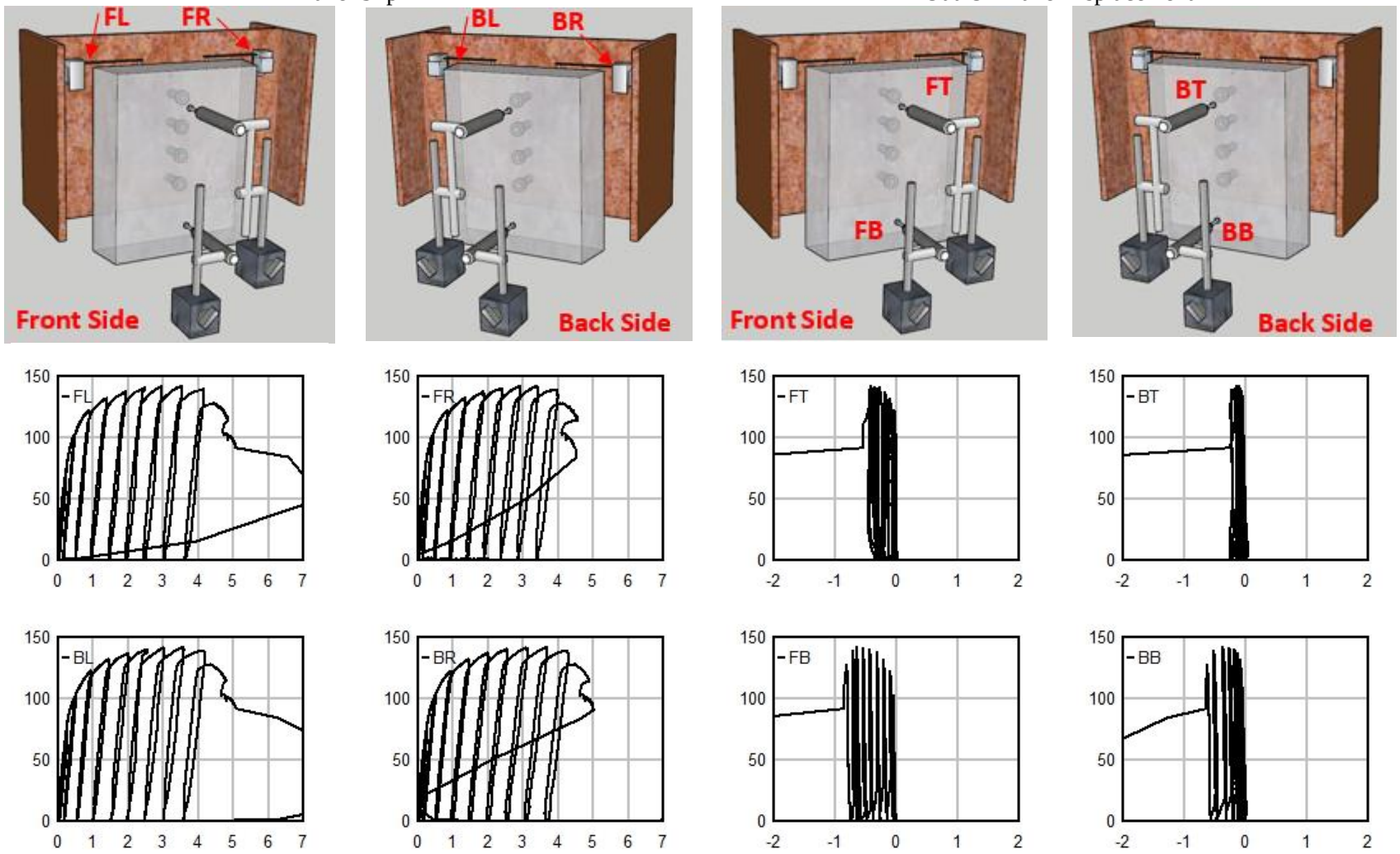

Test 15 – 2x2 UHPC – Strains

Stud Strains

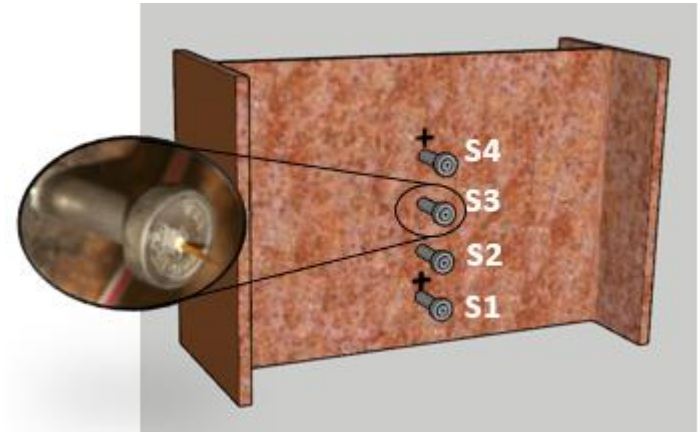

Web Strains

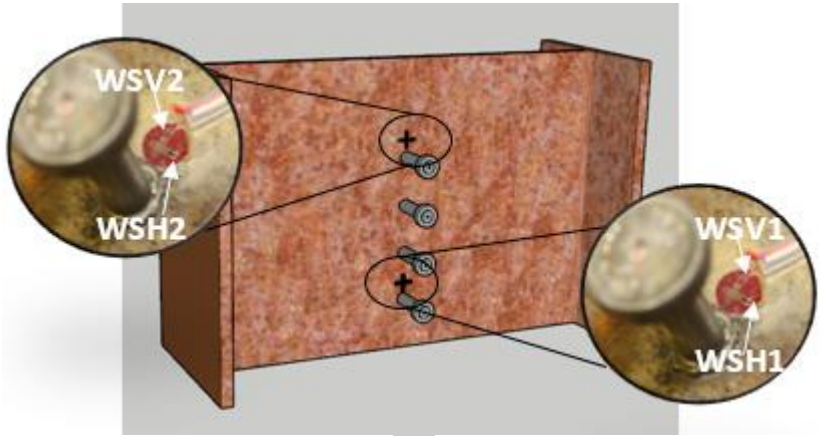

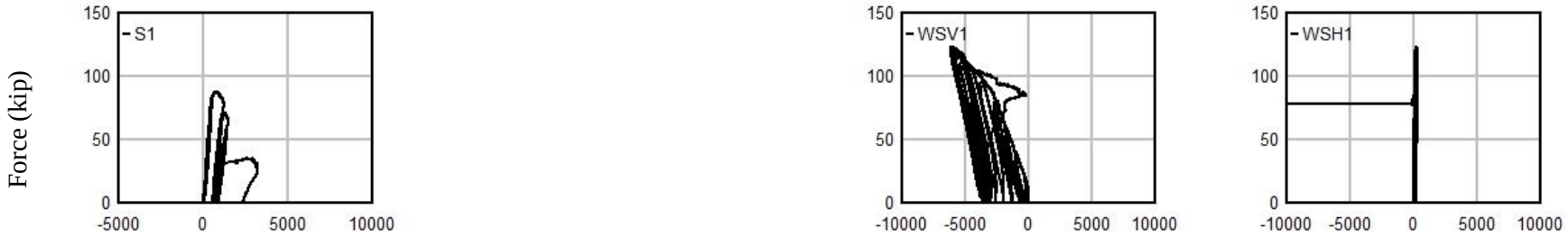

Strain (με)

Test 15 – 2x2 UHPC– Displacements

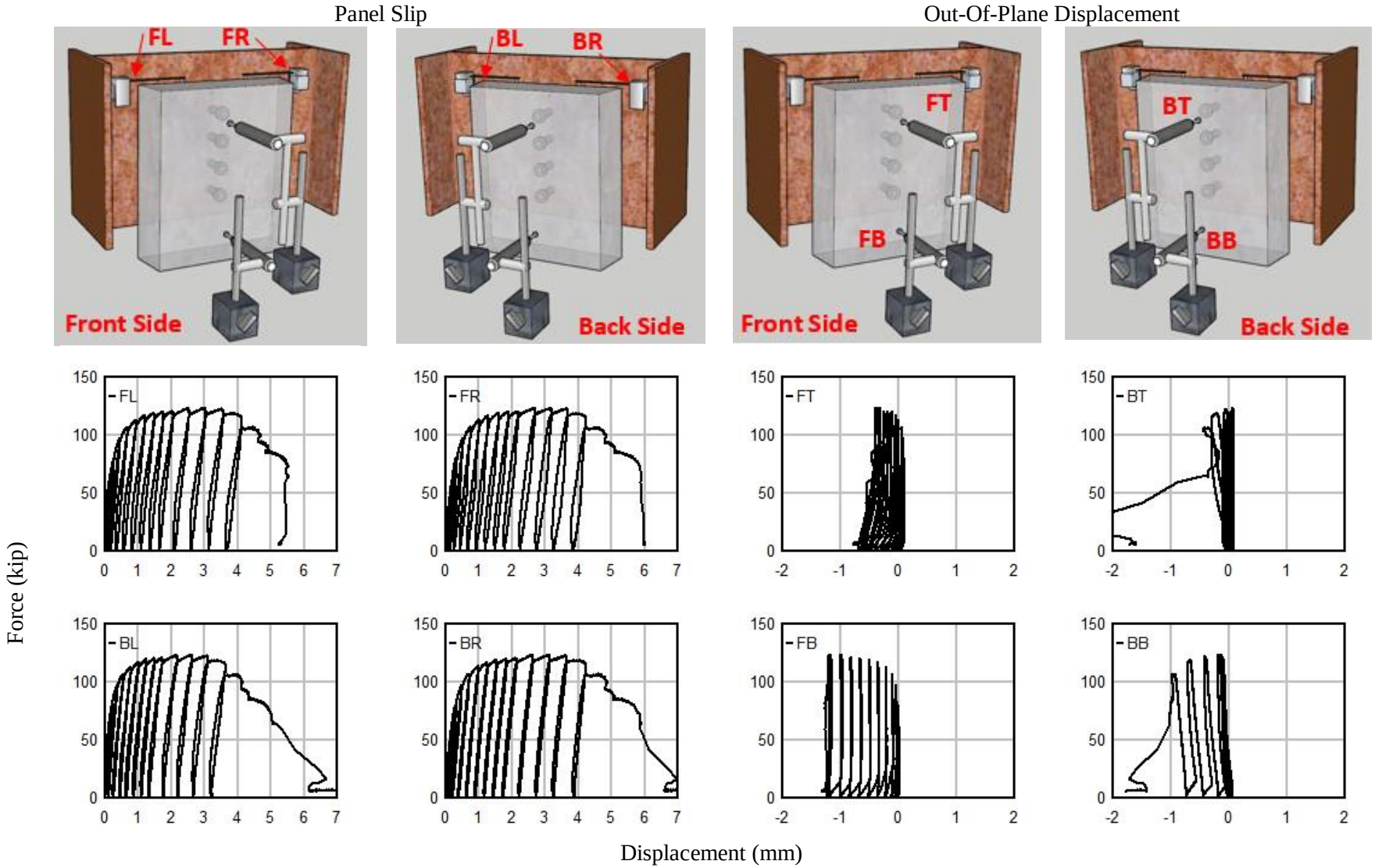

Test 16 – Precast Panel (2x2in) – Strains

Stud Strains

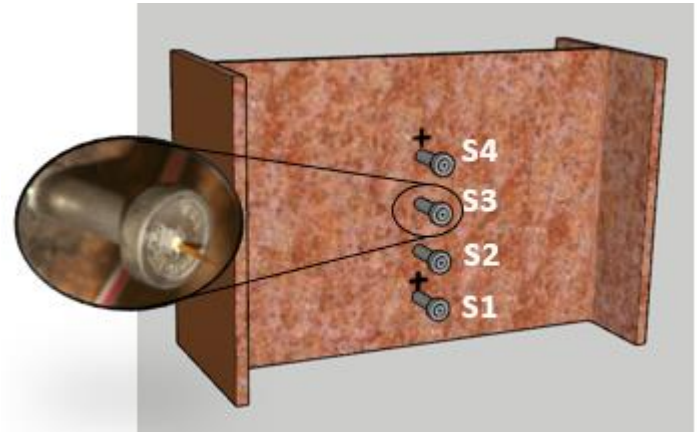

Web Strains

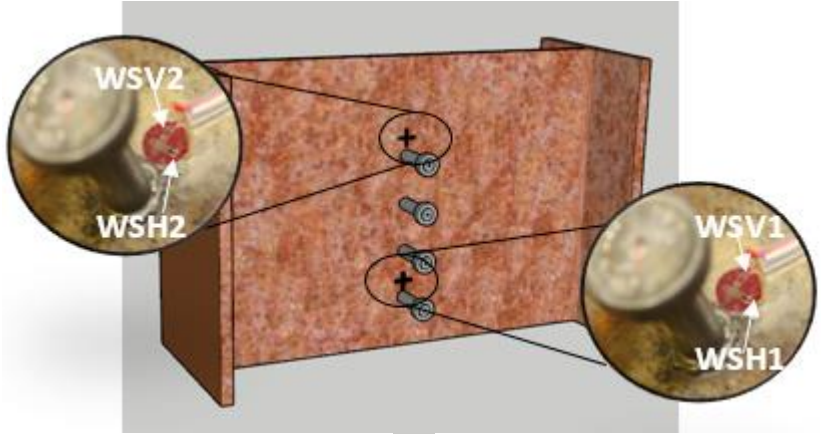

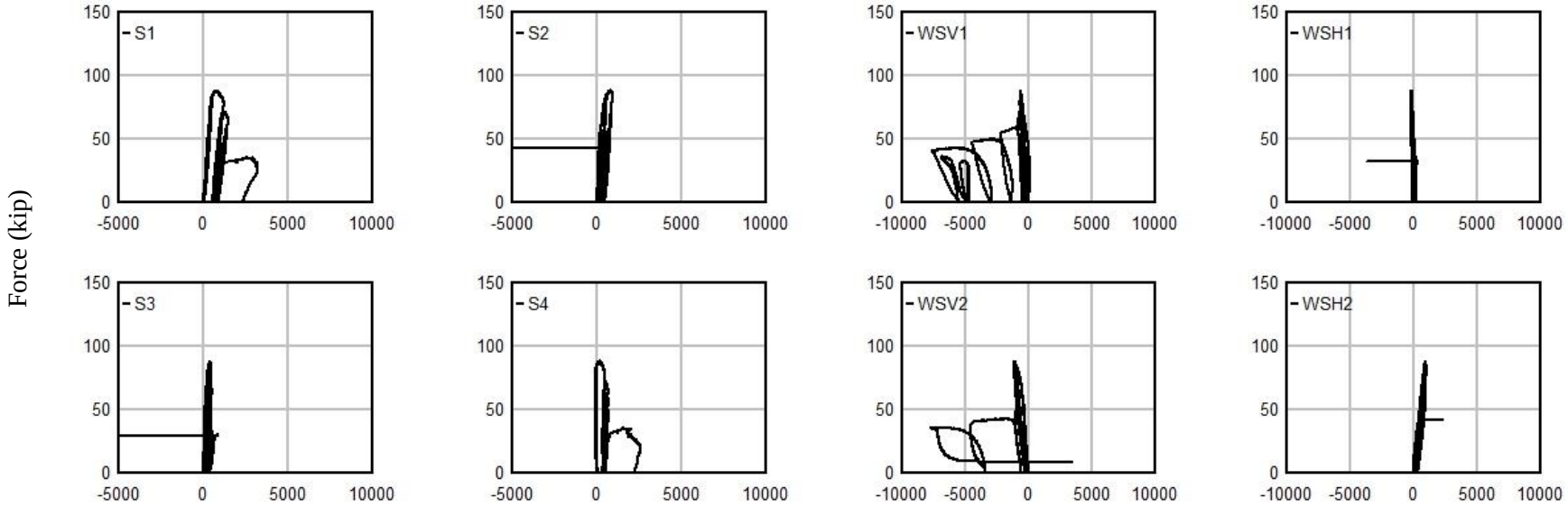

Test 16 – Precast Panel (2x2in) – Displacements

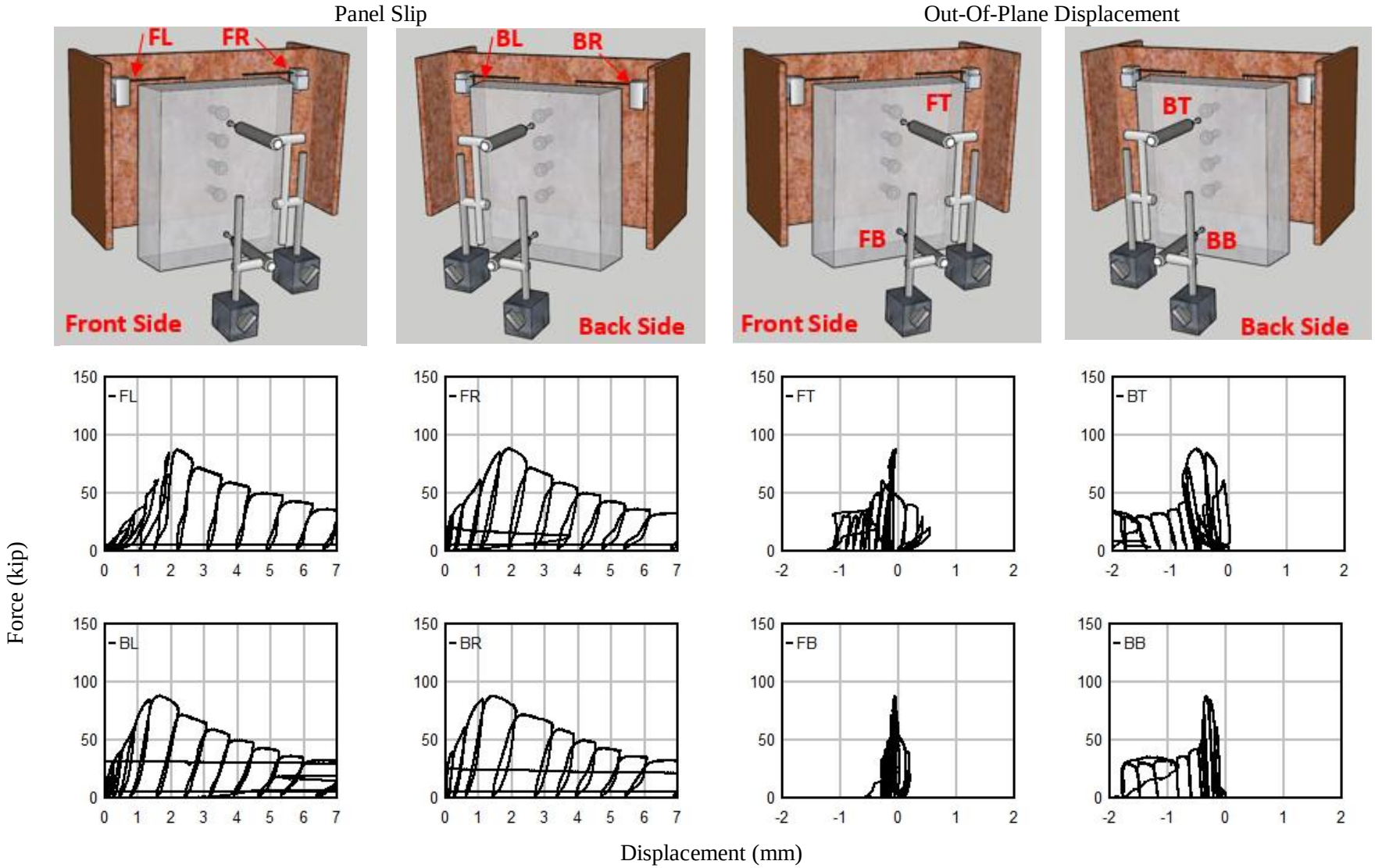

Test 17 – Corrosion 1– Strains

Stud Strains

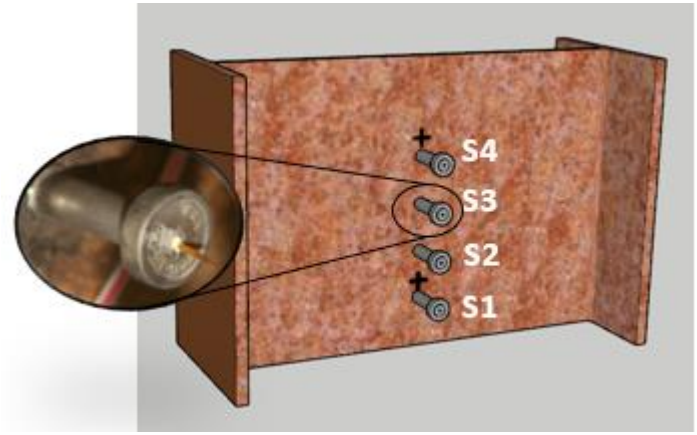

Web Strains

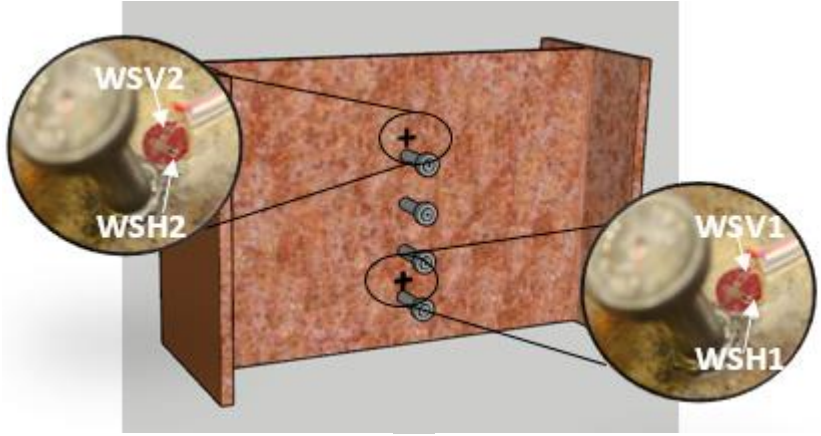

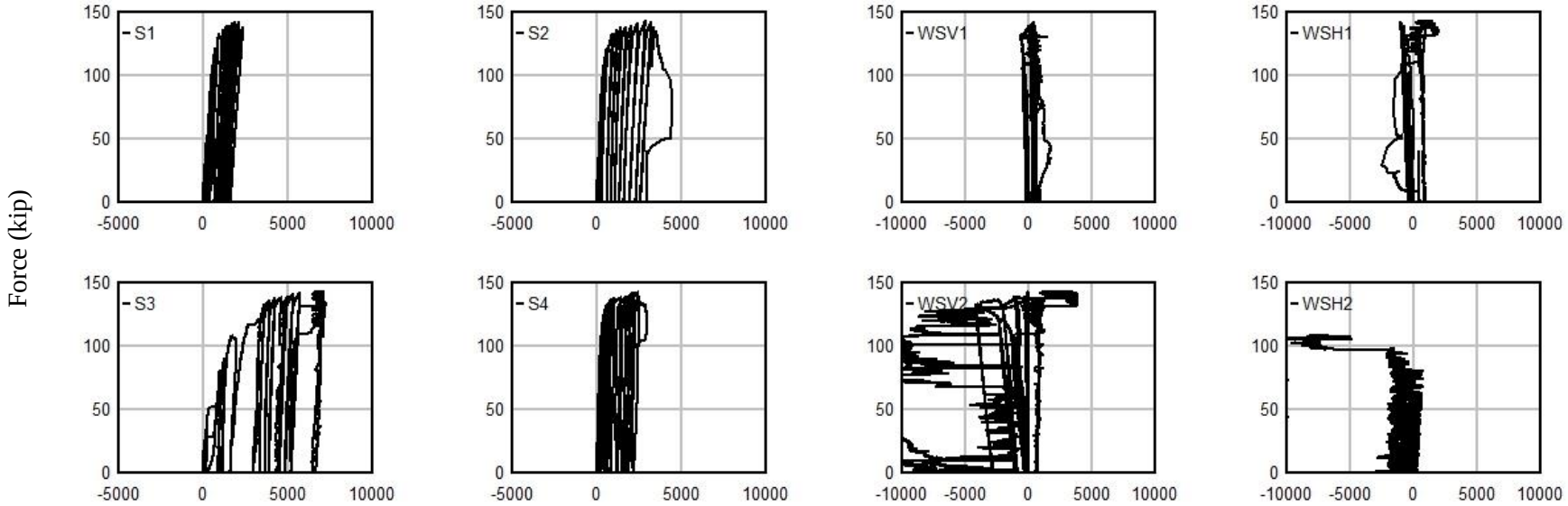

Test 17 – Corrosion 1 – Displacements

Panel Slip

Out-Of-Plane Displacement

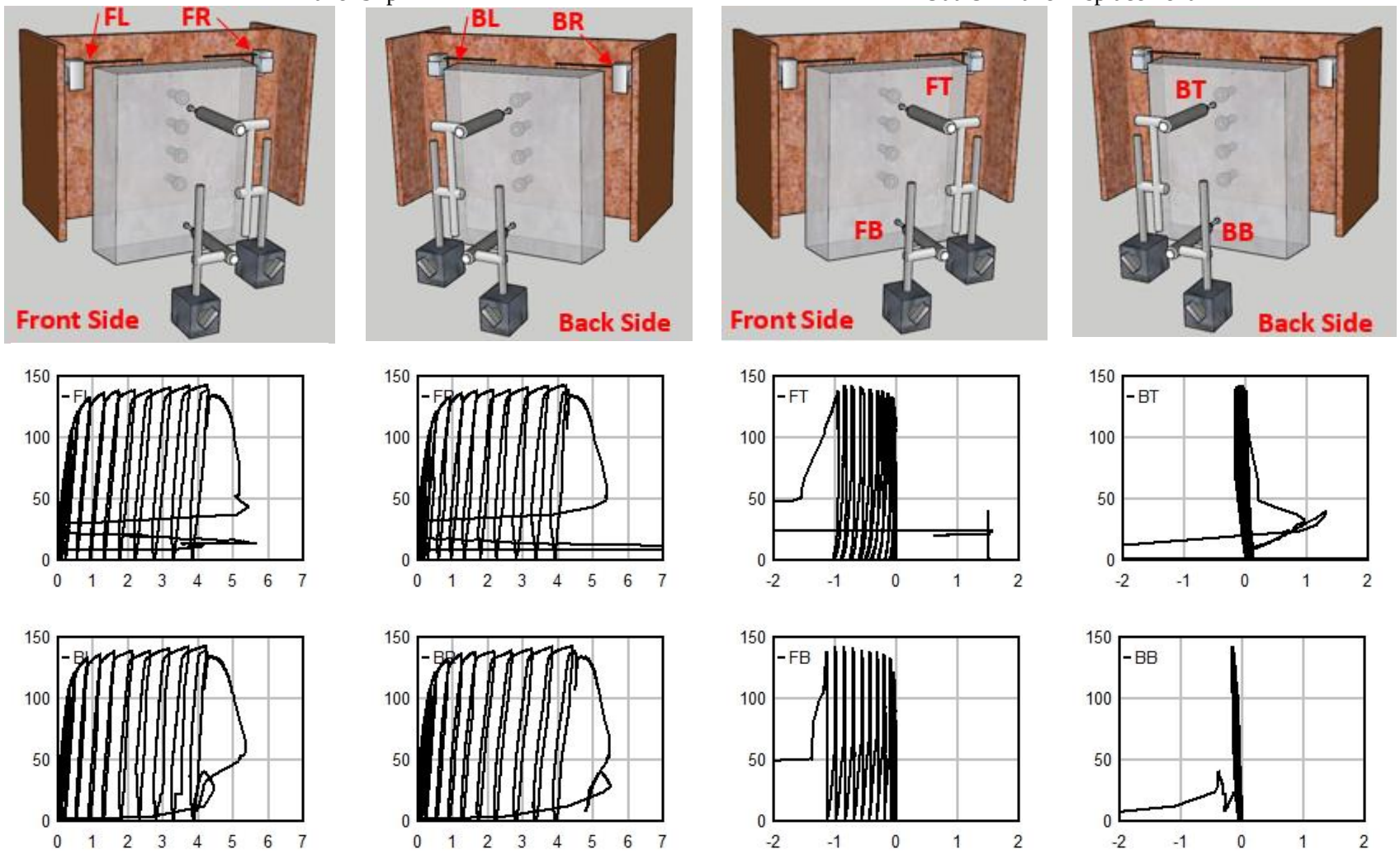

Test 18 – 12 Hour Heat Cure – Strains

Stud Strains

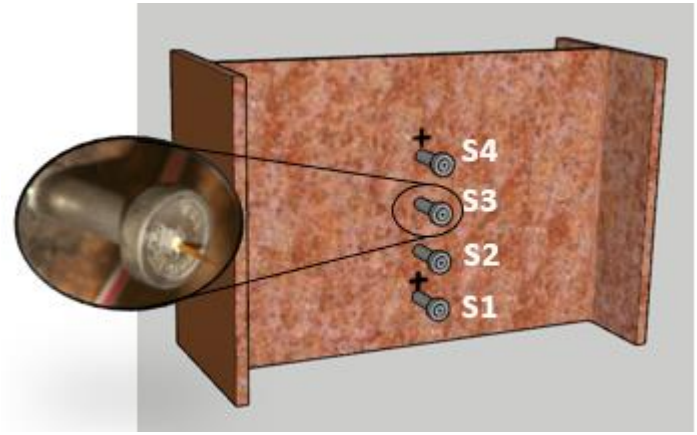

Web Strains

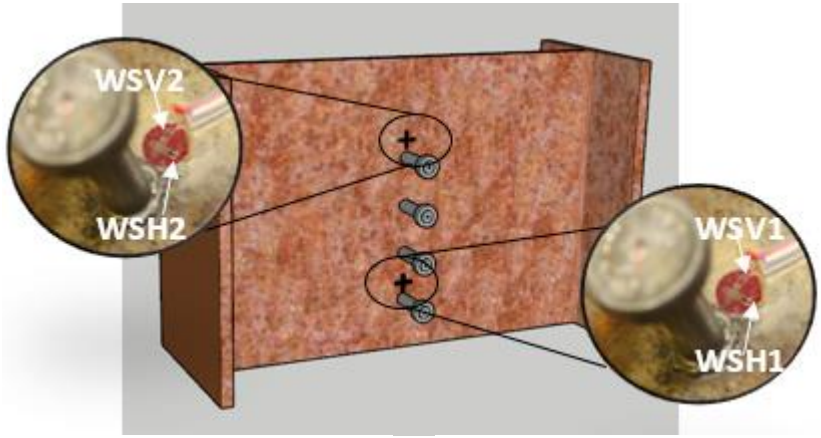

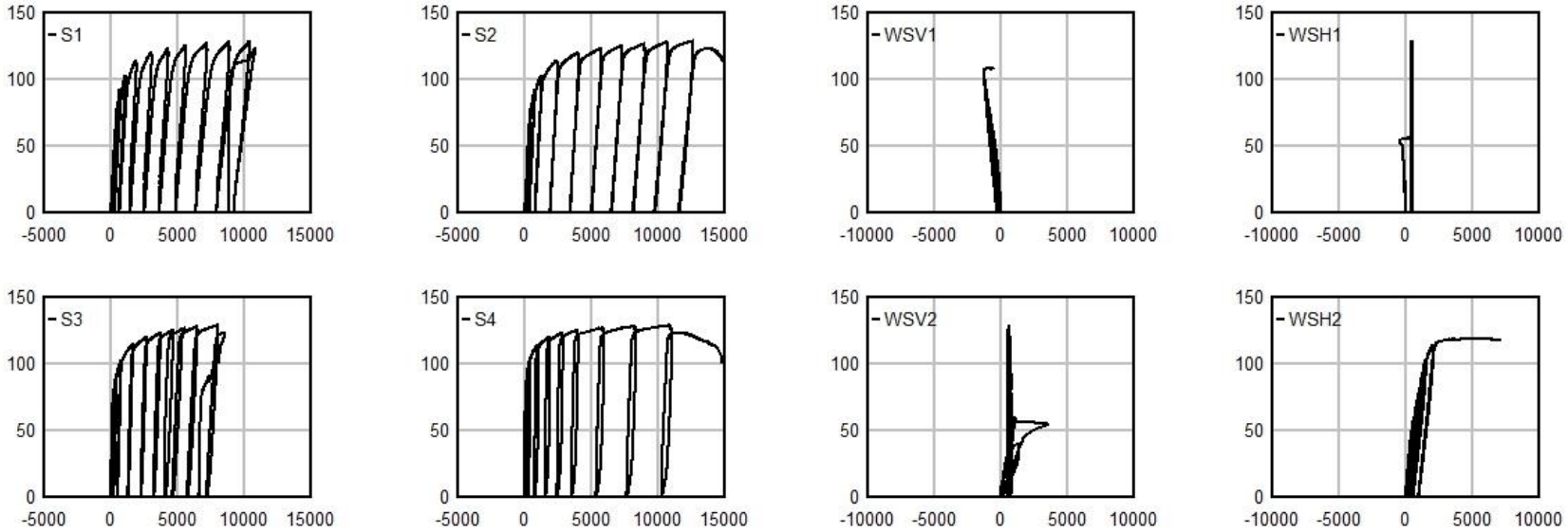

Test 18 – 12 Hour Heat Cure – Displacements

Panel Slip

Out-Of-Plane Displacement

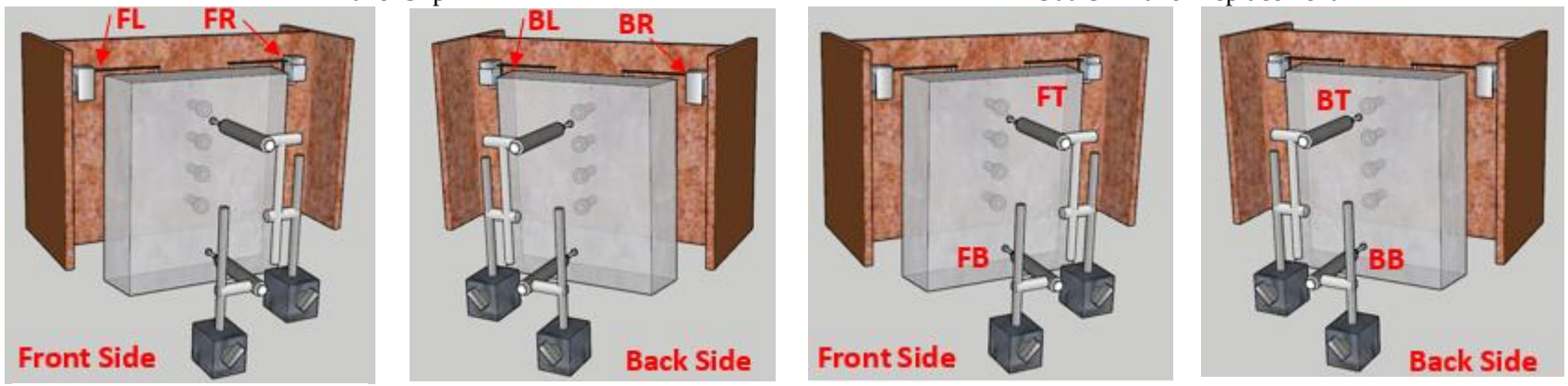

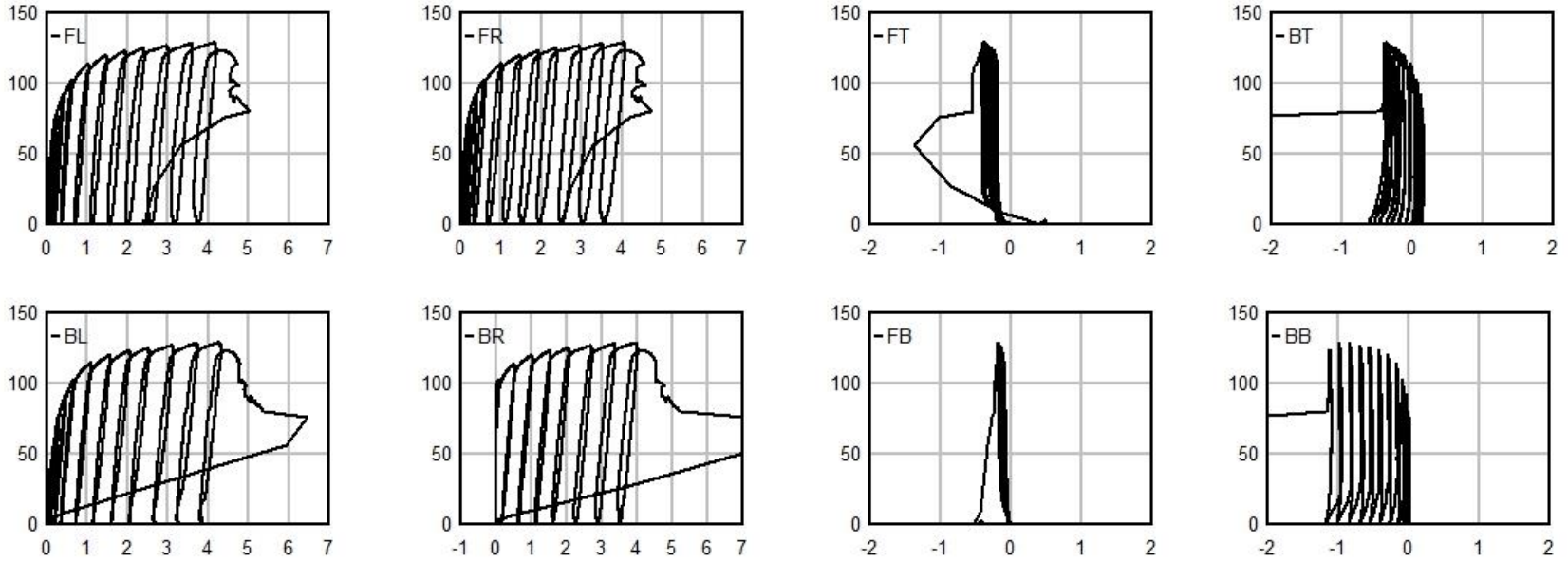

Test 19 – Precast Panel (2x4in) – Strains

Stud Strains

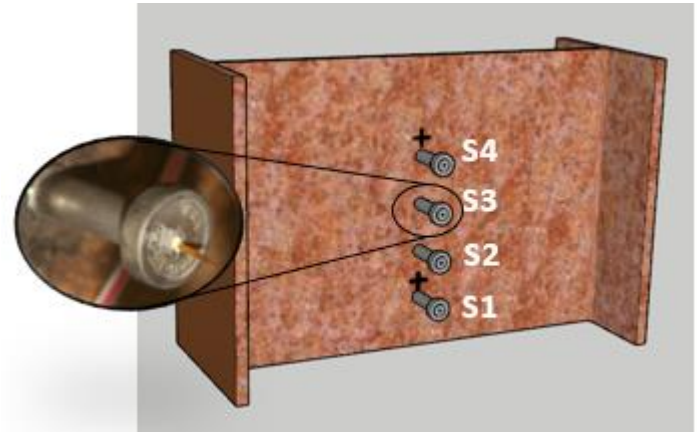

Web Strains

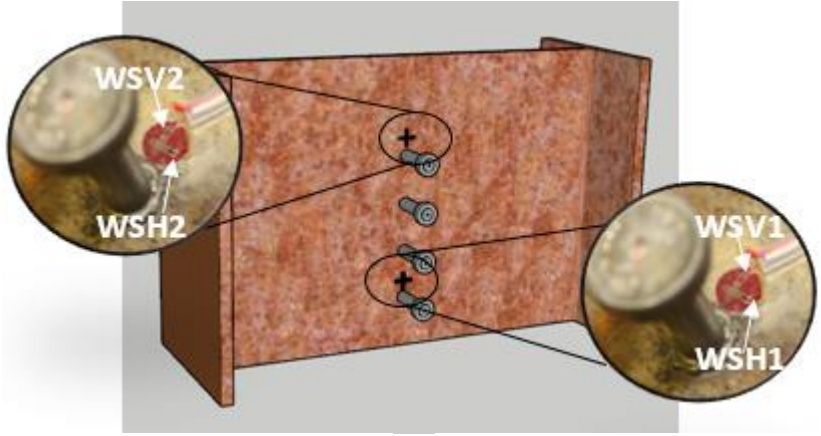

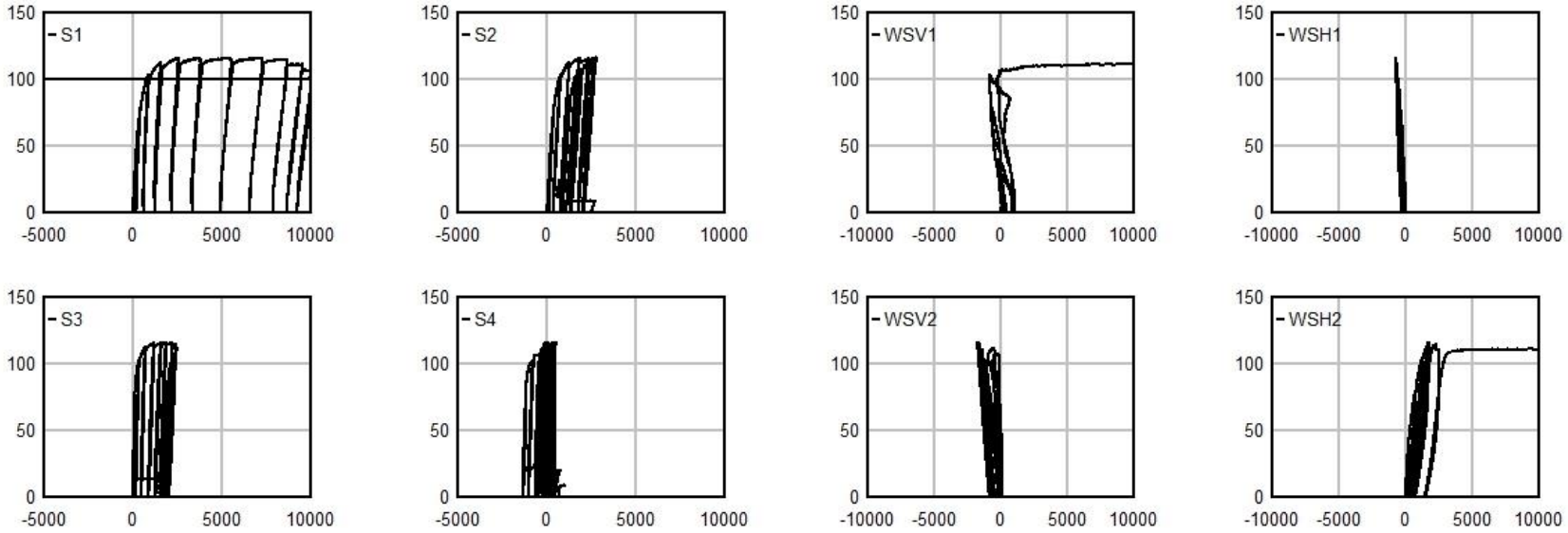

Test 19 – Precast Panel (2x4in) – Displacements

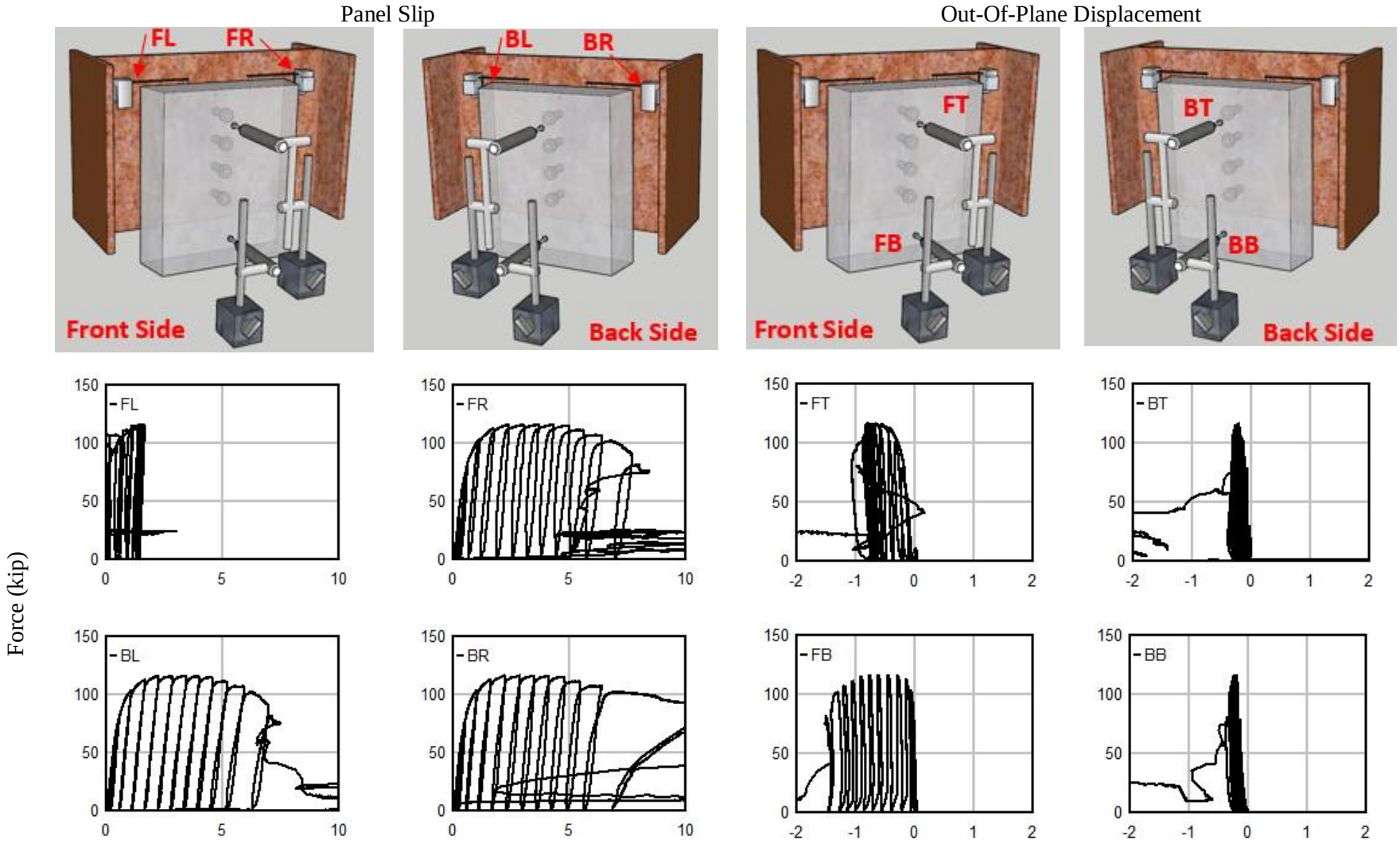

Test 20 – Benchmark #2 – Strains

Stud Strains

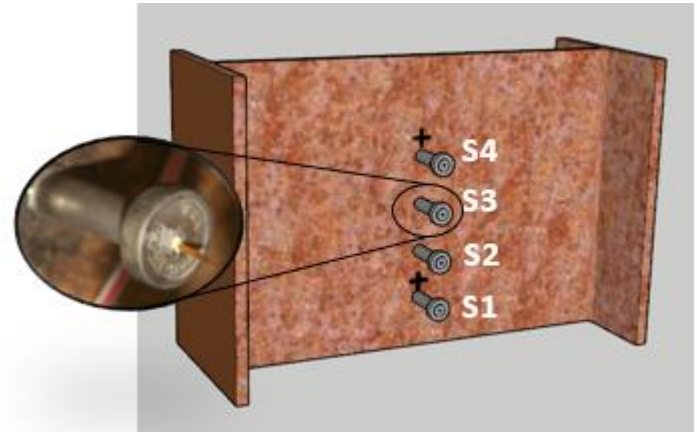

Web Strains

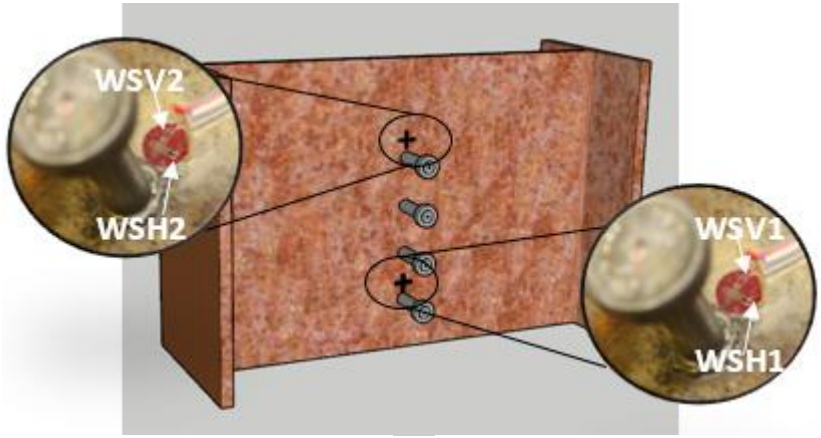

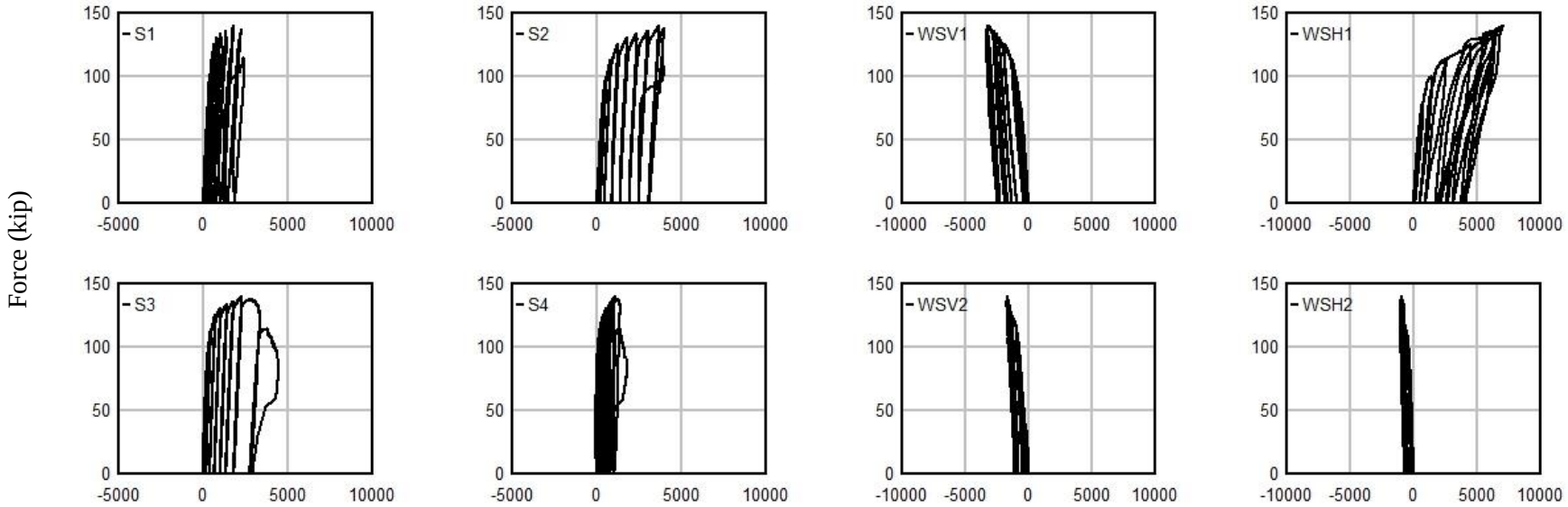

Test 20 – Benchmark #2 – Displacements

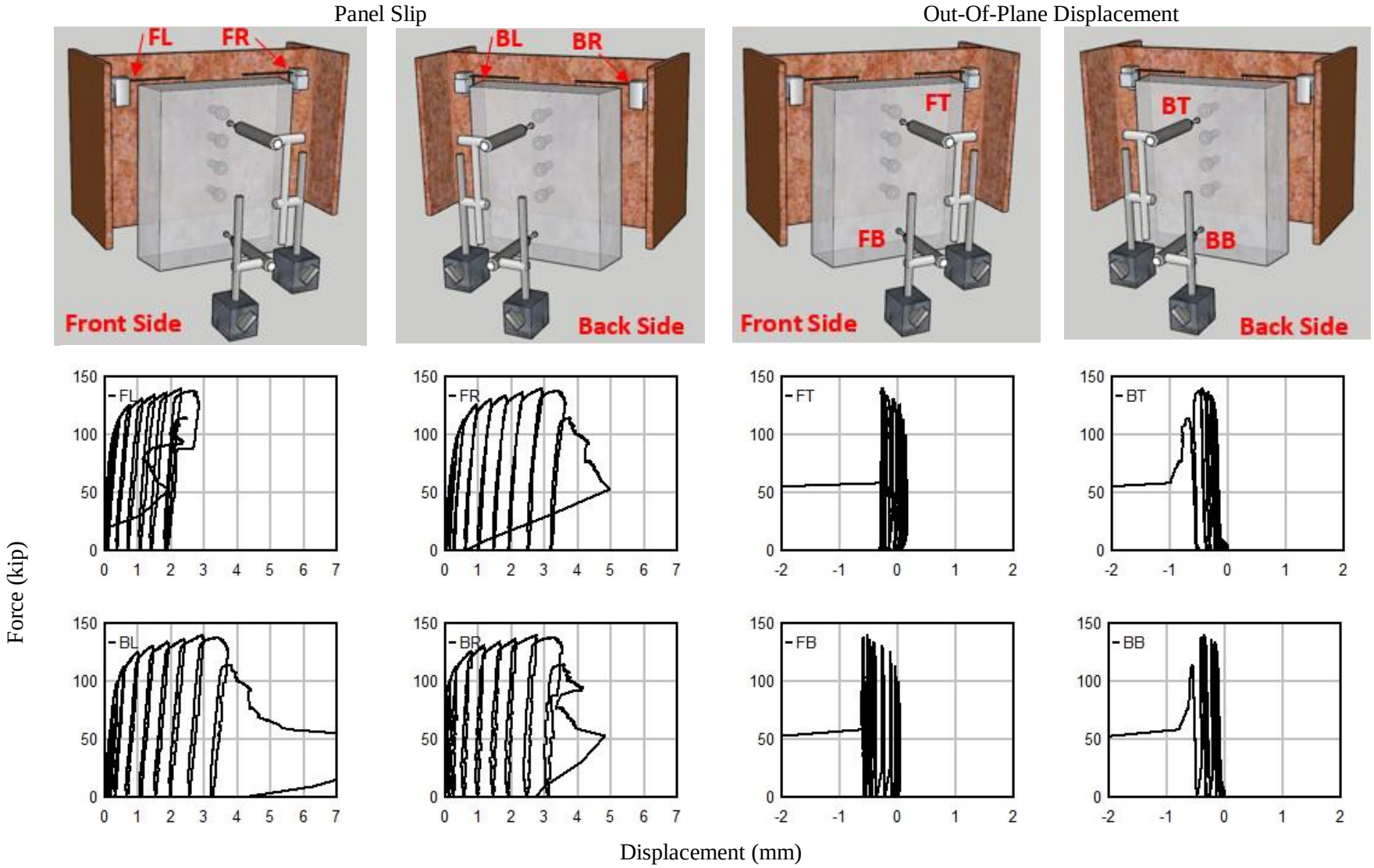

Test 21 – Benchmark #3 – Strains

Stud Strains

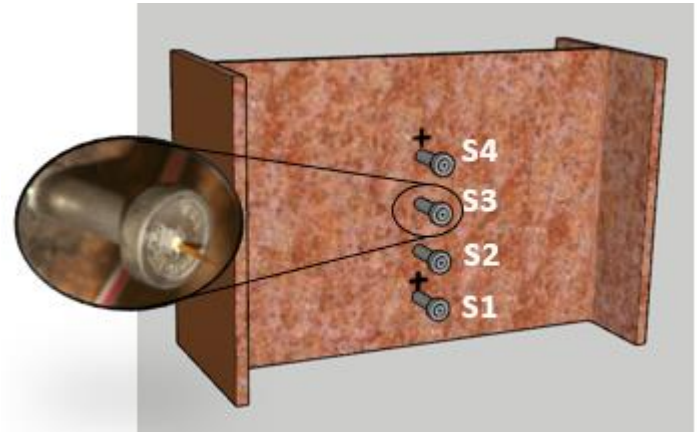

Web Strains

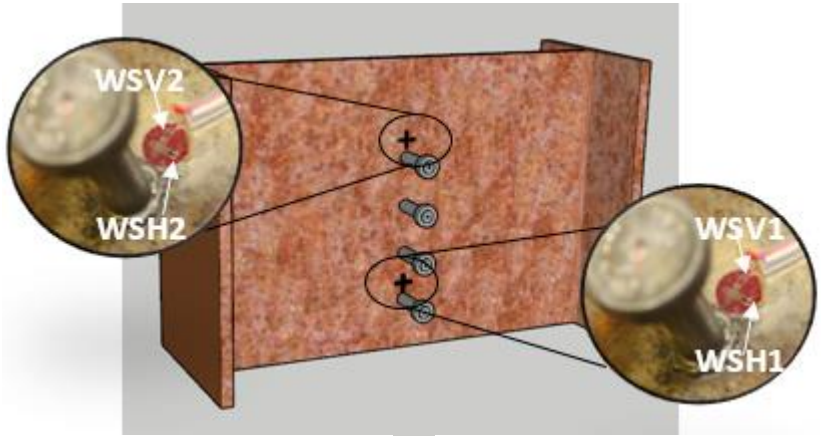

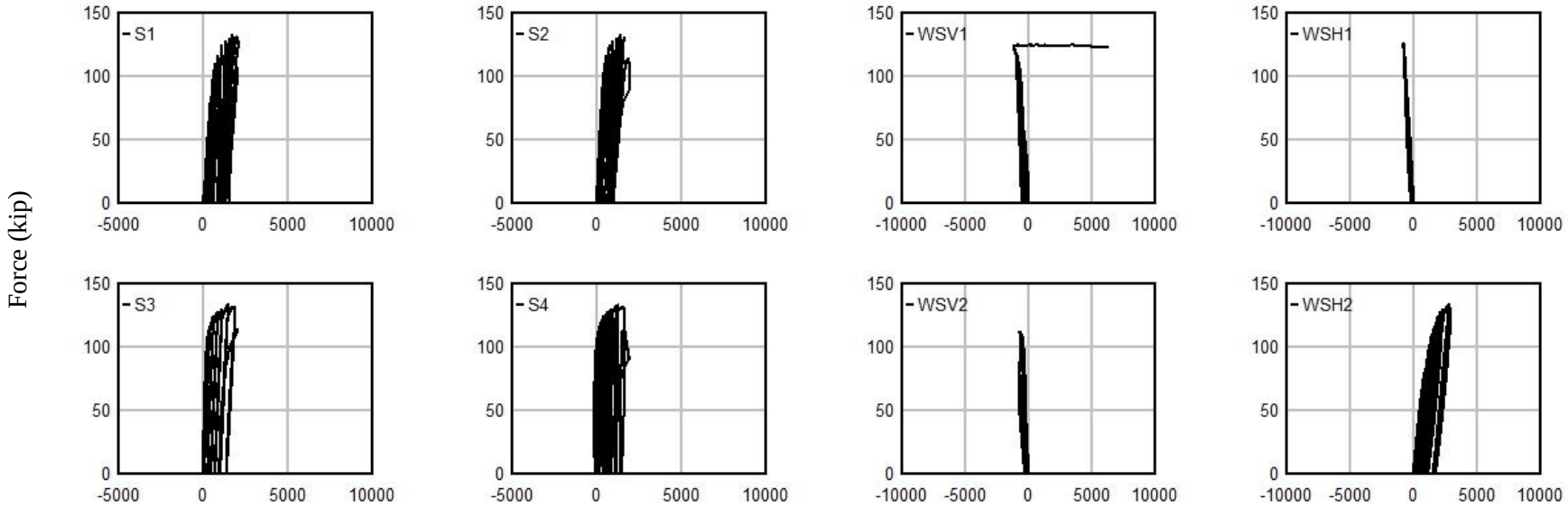

Test 21 – Benchmark #3 – Displacements

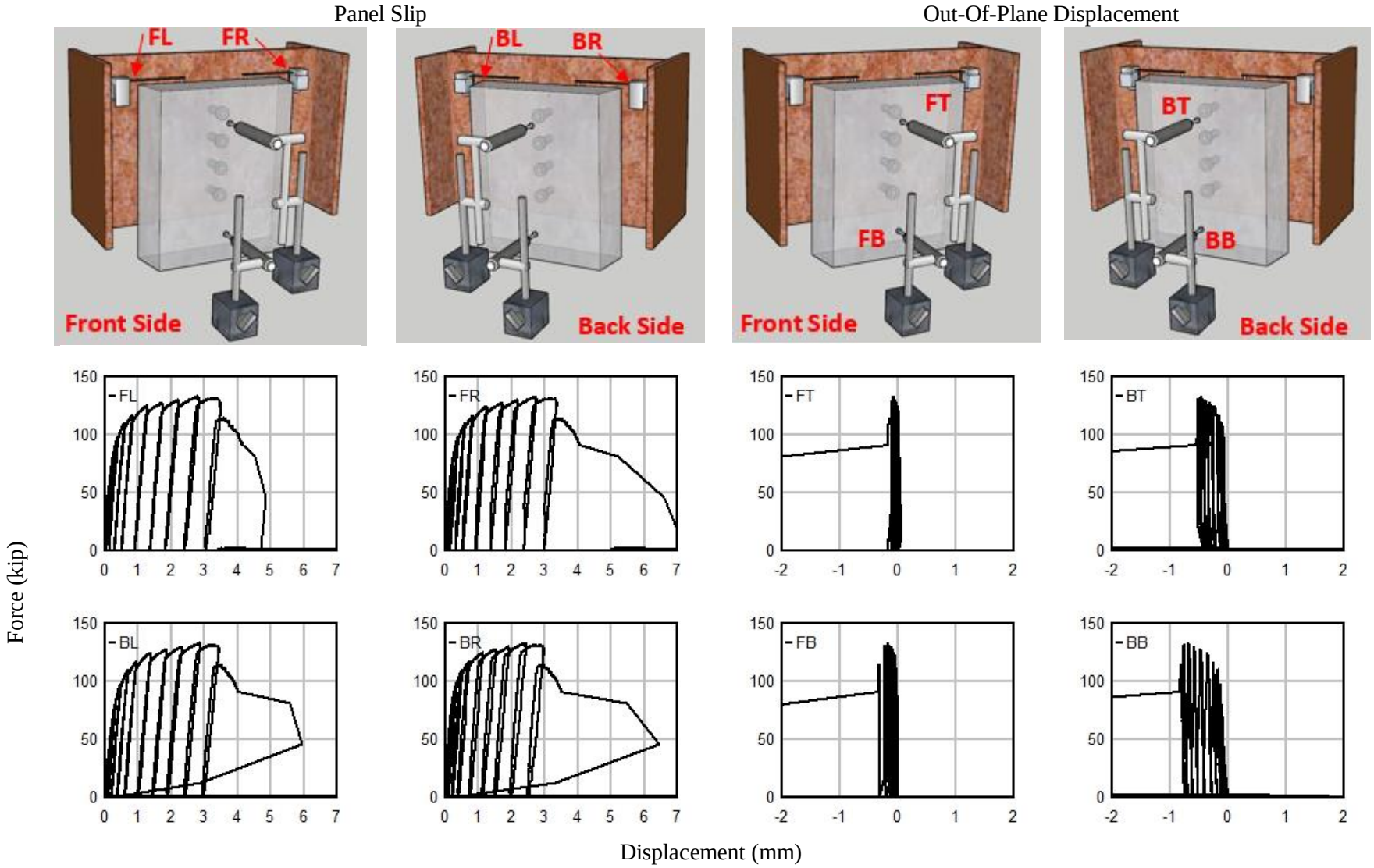

Test 22 – Corrosion 2 – Displacements

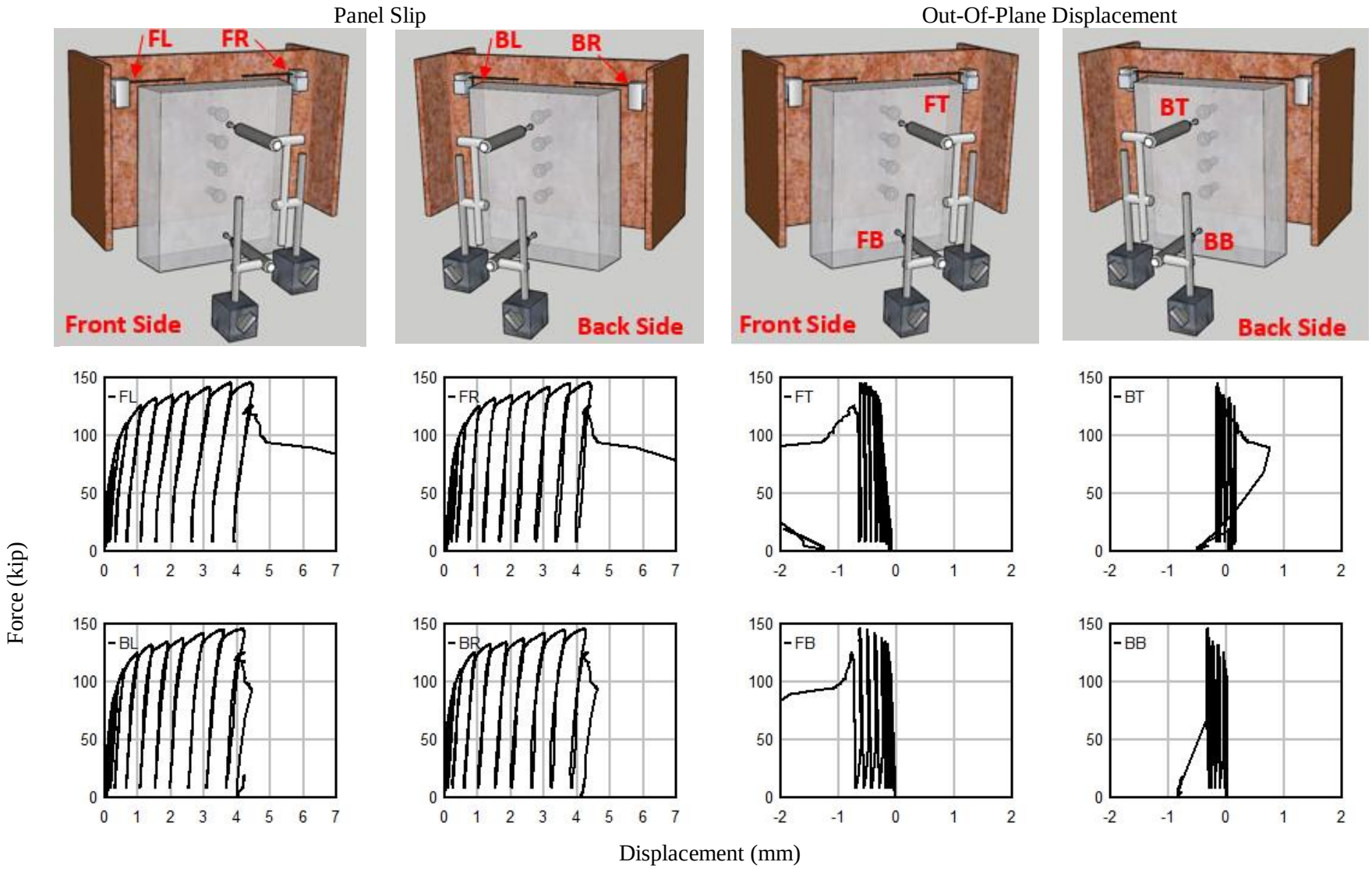

Test 23 – Painted Surface – Displacements

Panel Slip

Out-Of-Plane Displacement

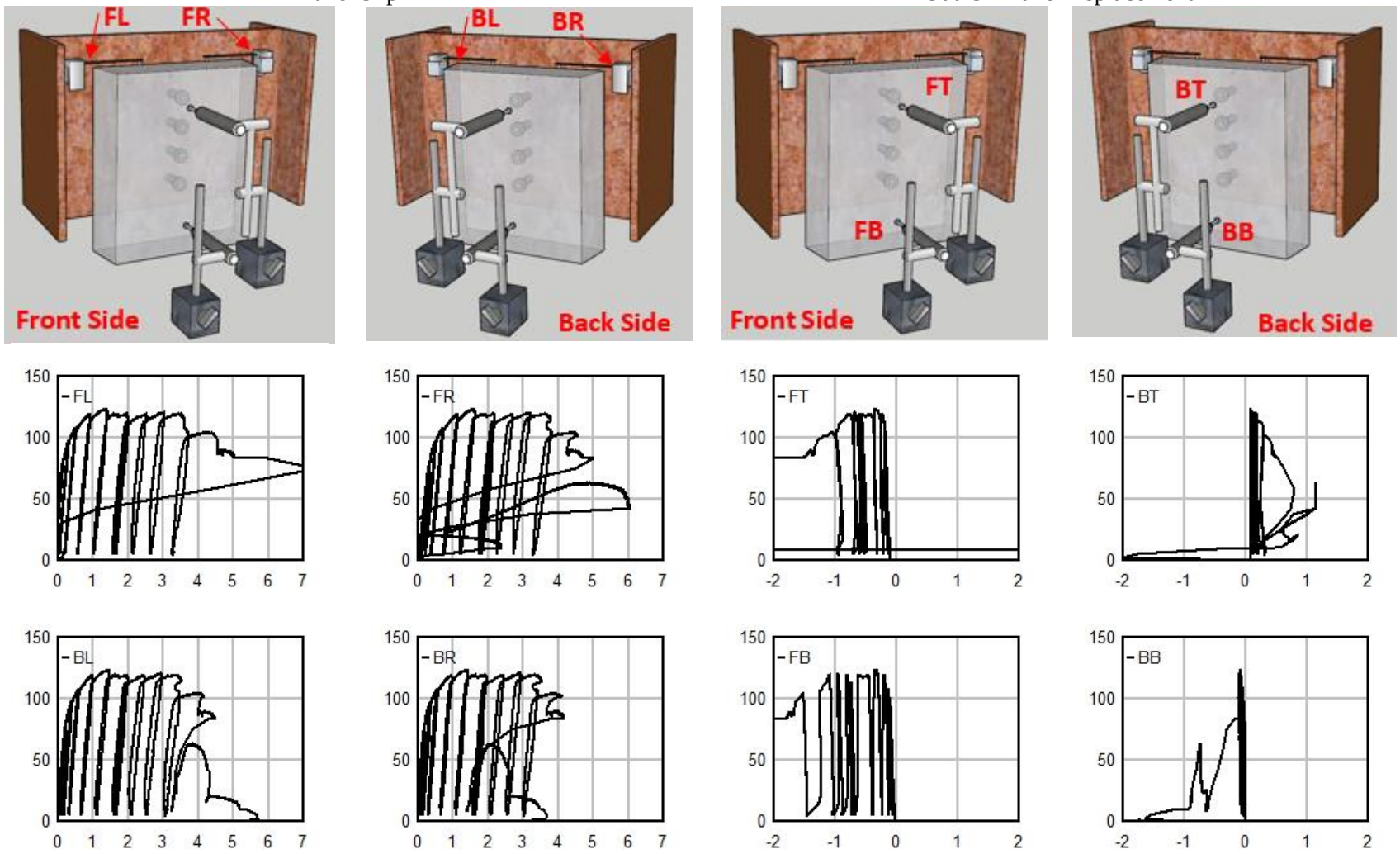

Test 24 – Vertical Ferrule – Displacements

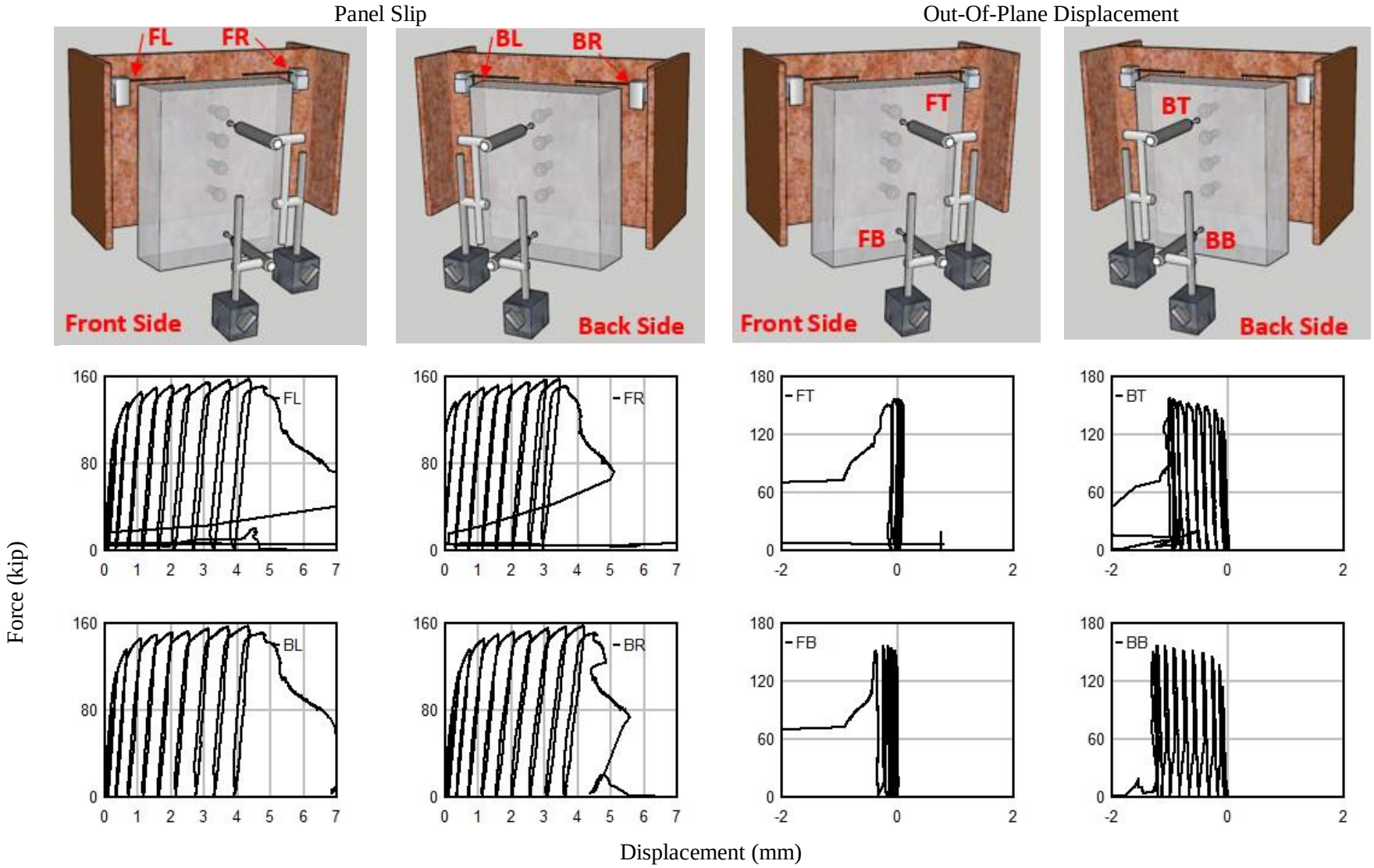

Test 25 – 2” Eccentricity – Strains

Stud Strains

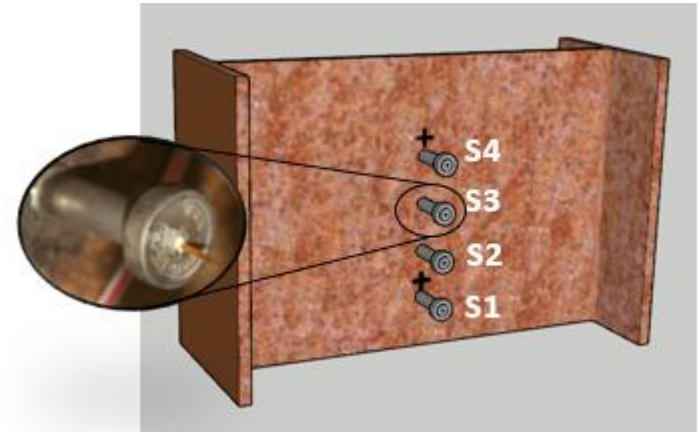

Web Strains

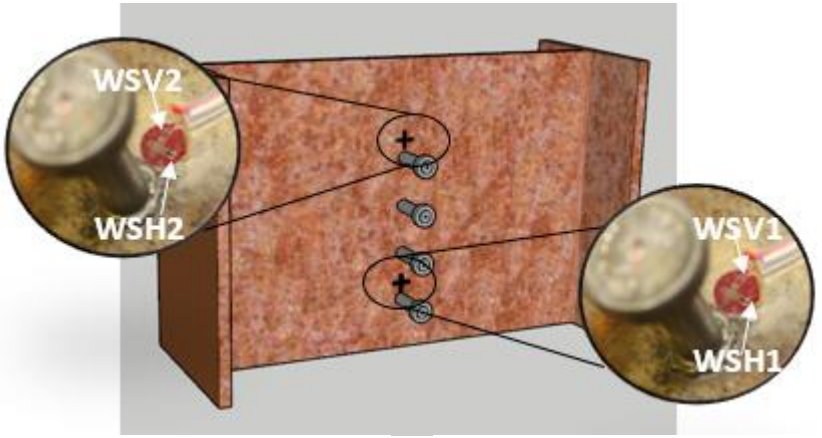

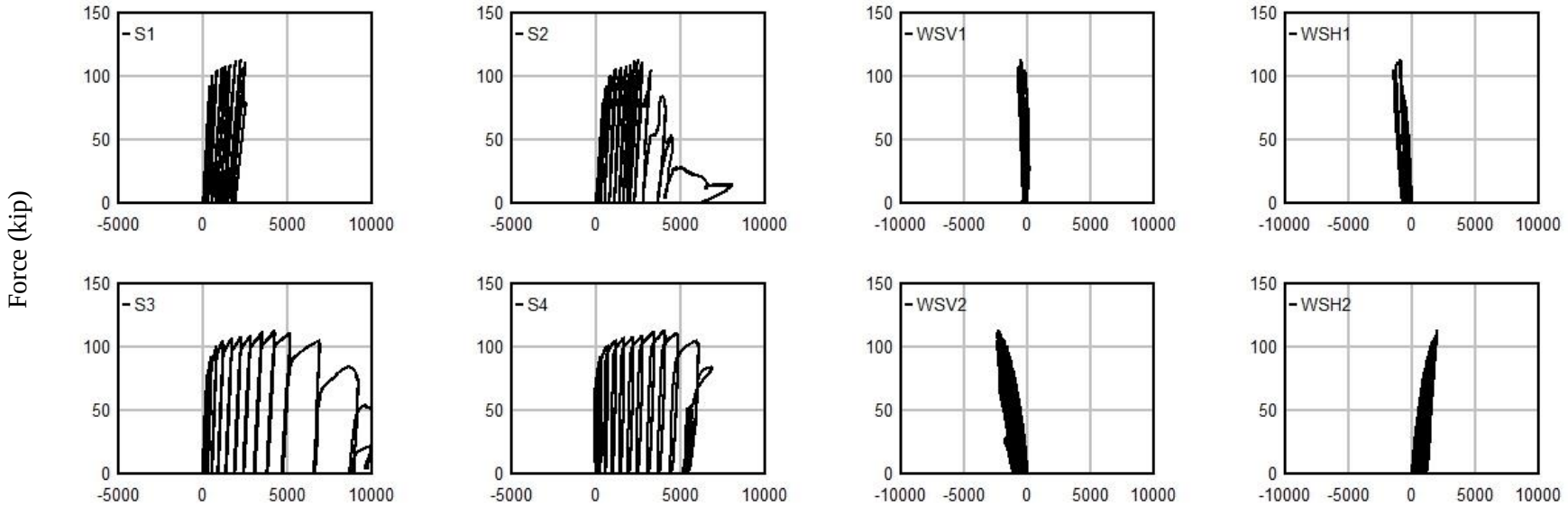

Test 25 – 2” Eccentricity – Displacements

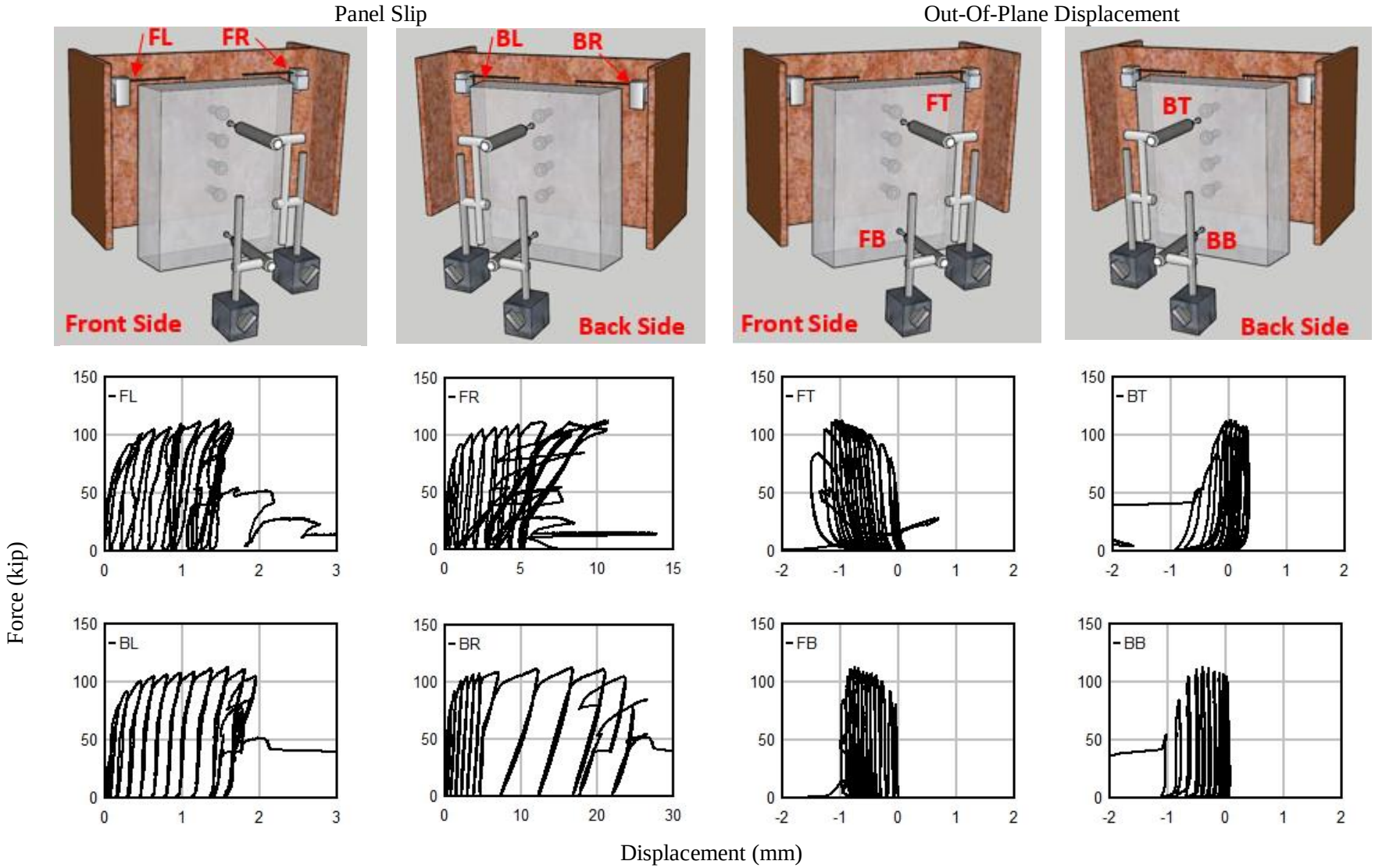

Test 26 – G8 Threaded Rods – Strains

Stud Strains

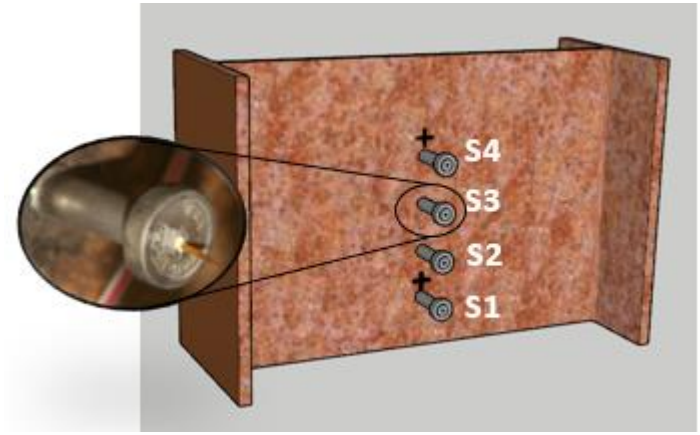

Web Strains

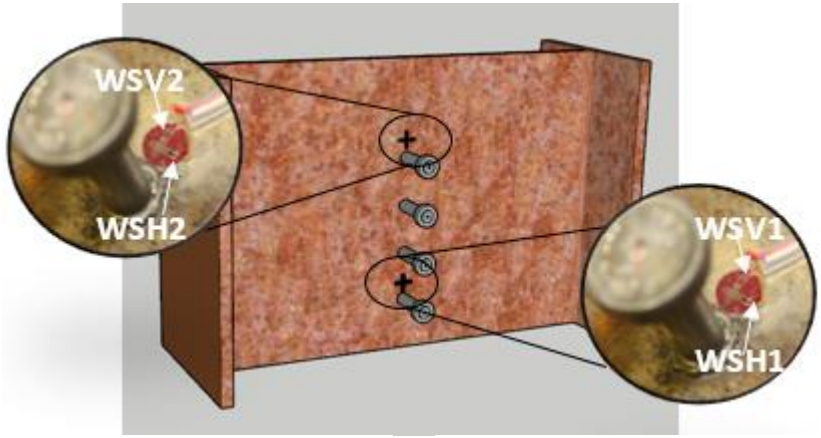

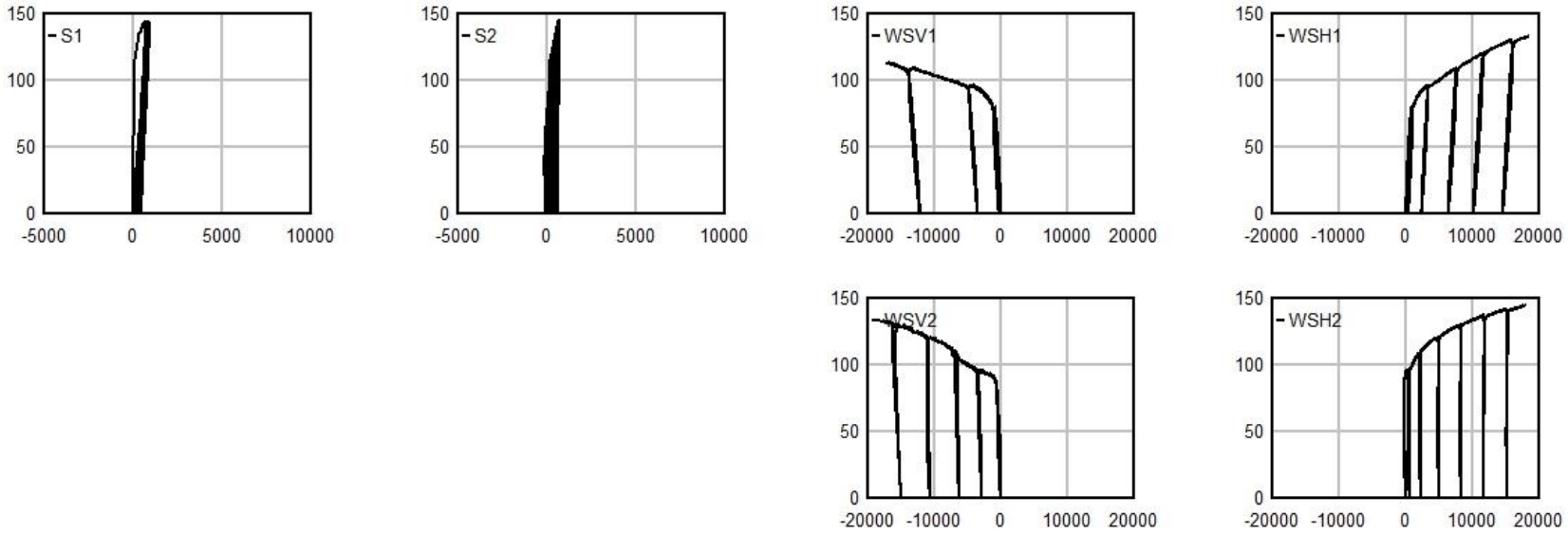

Test 26 – G8 Threaded Rods – Displacements

Panel Slip

Out-Of-Plane Displacement

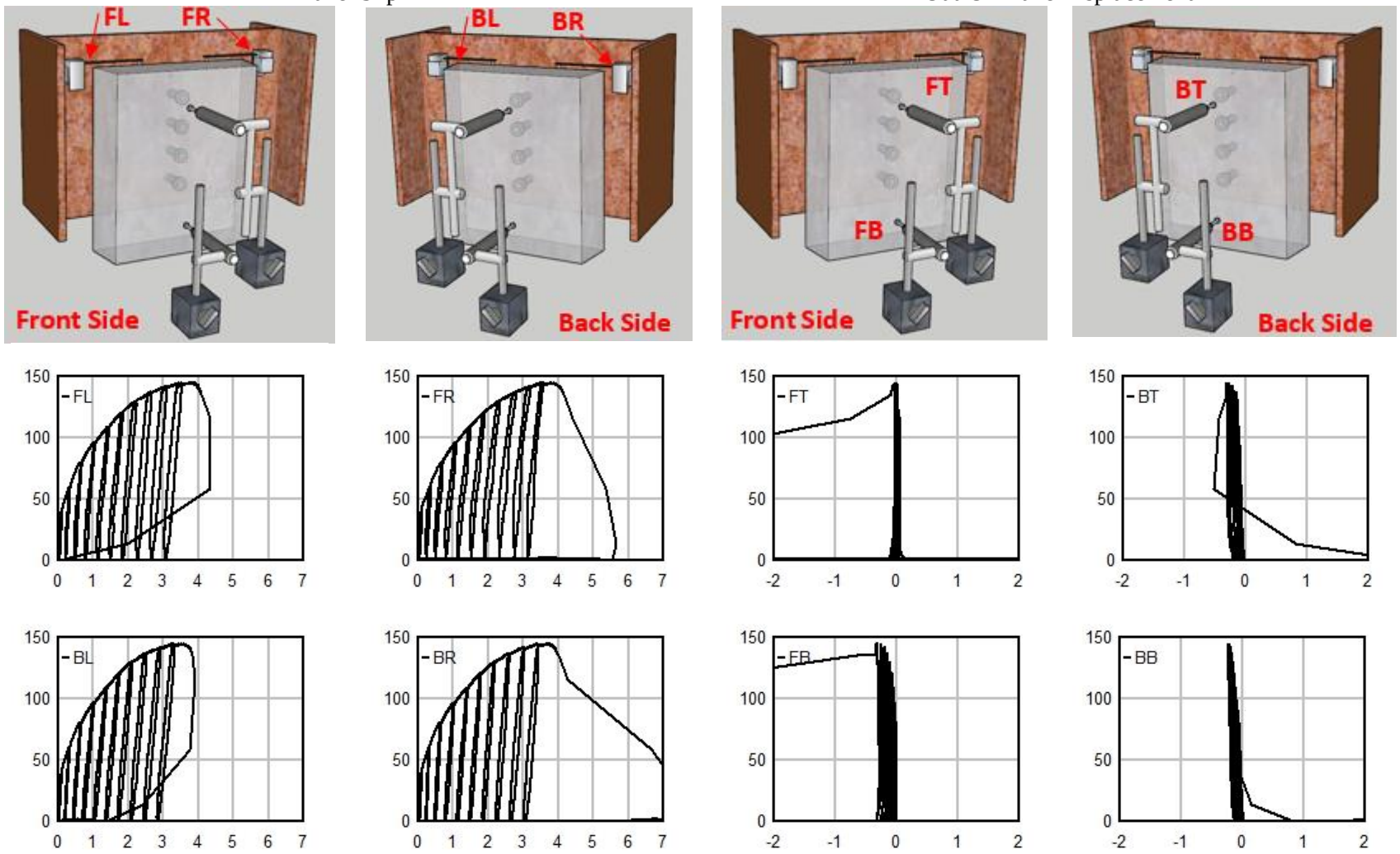

Test 27 – Corrosion 3 – Strains

Stud Strains

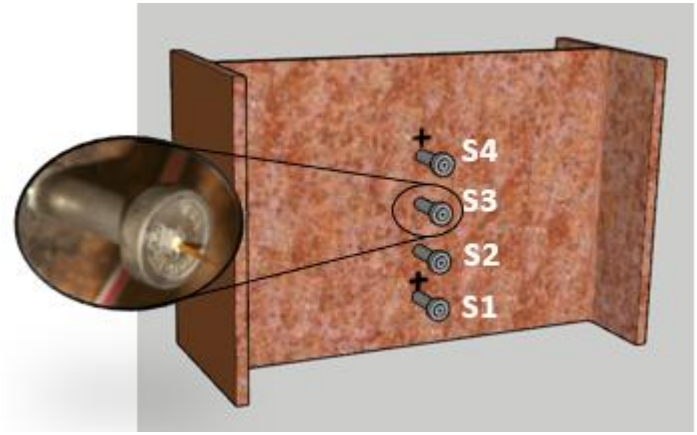

Web Strains

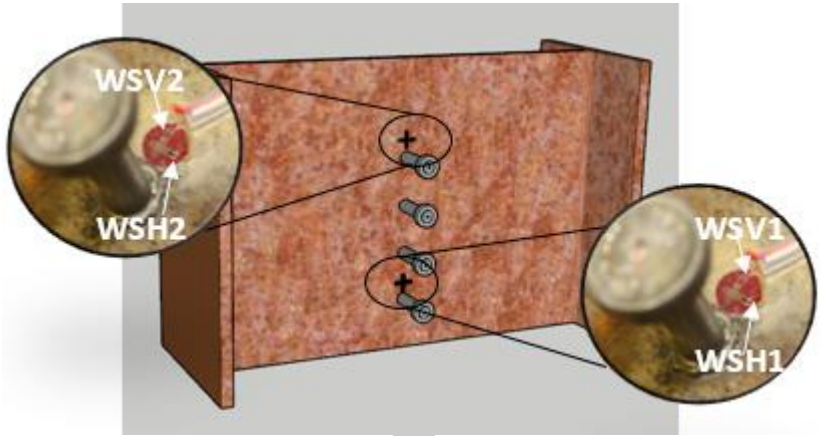

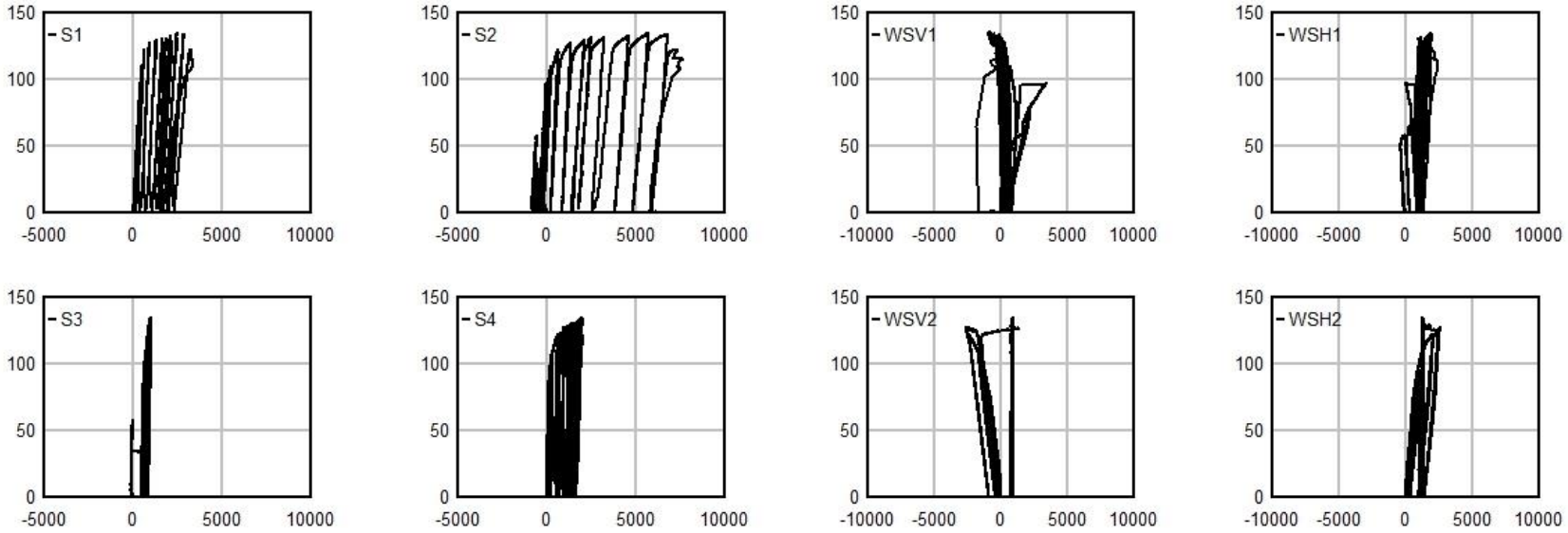

Test 27 – Corrosion 3 – Displacements

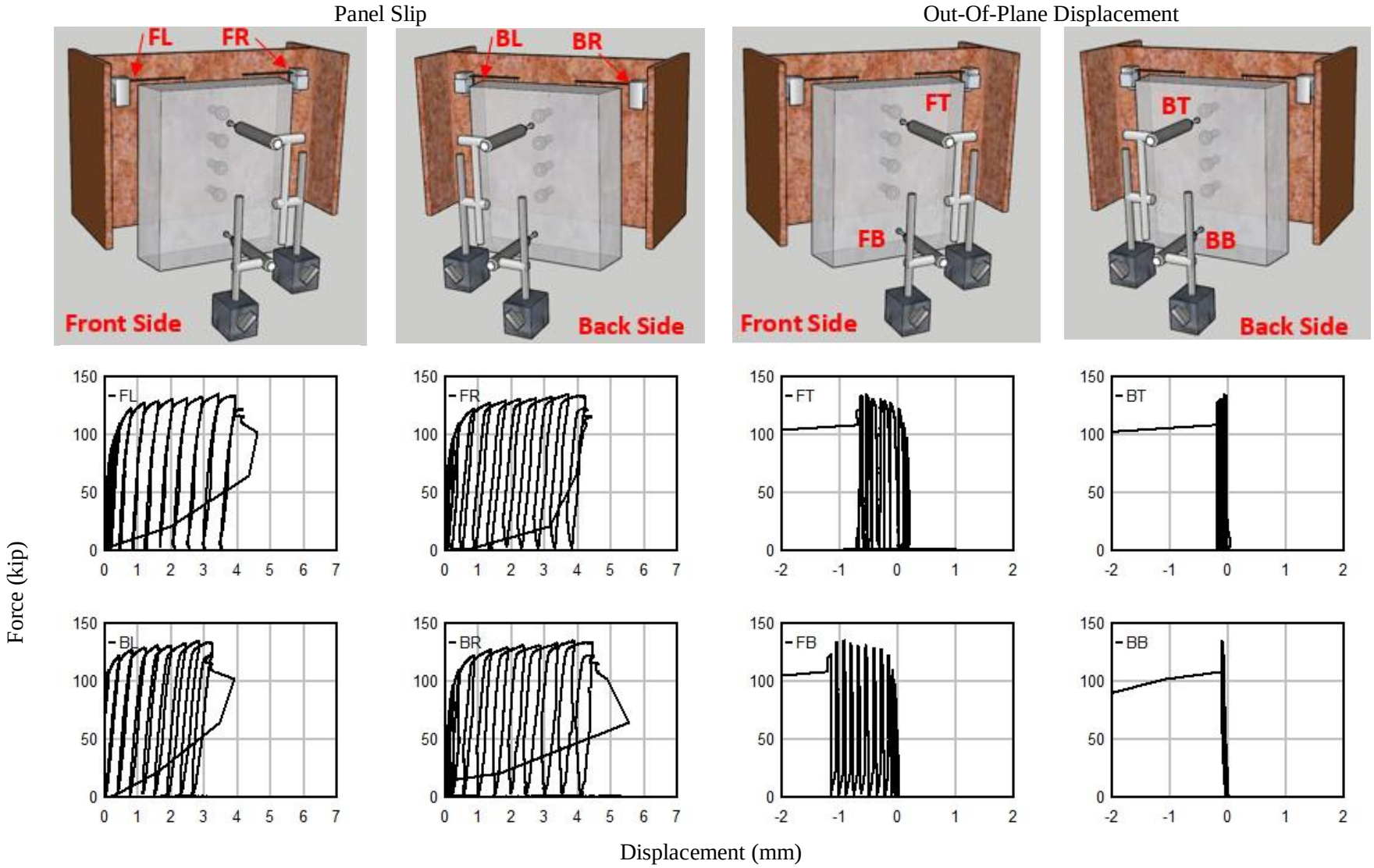

Test 28 – Truck Vibration – Displacements

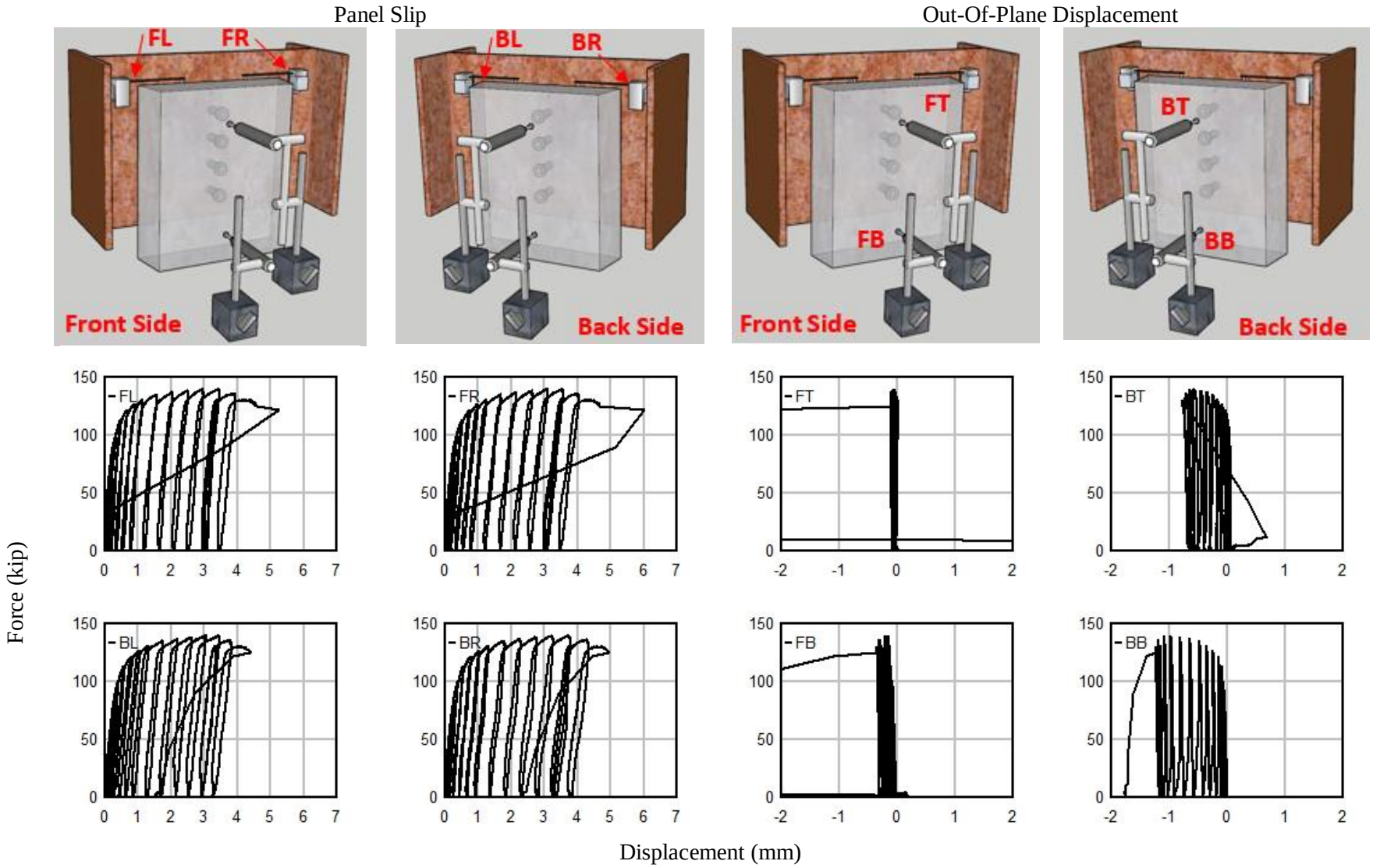

Test 29 – JS1000 – Displacements

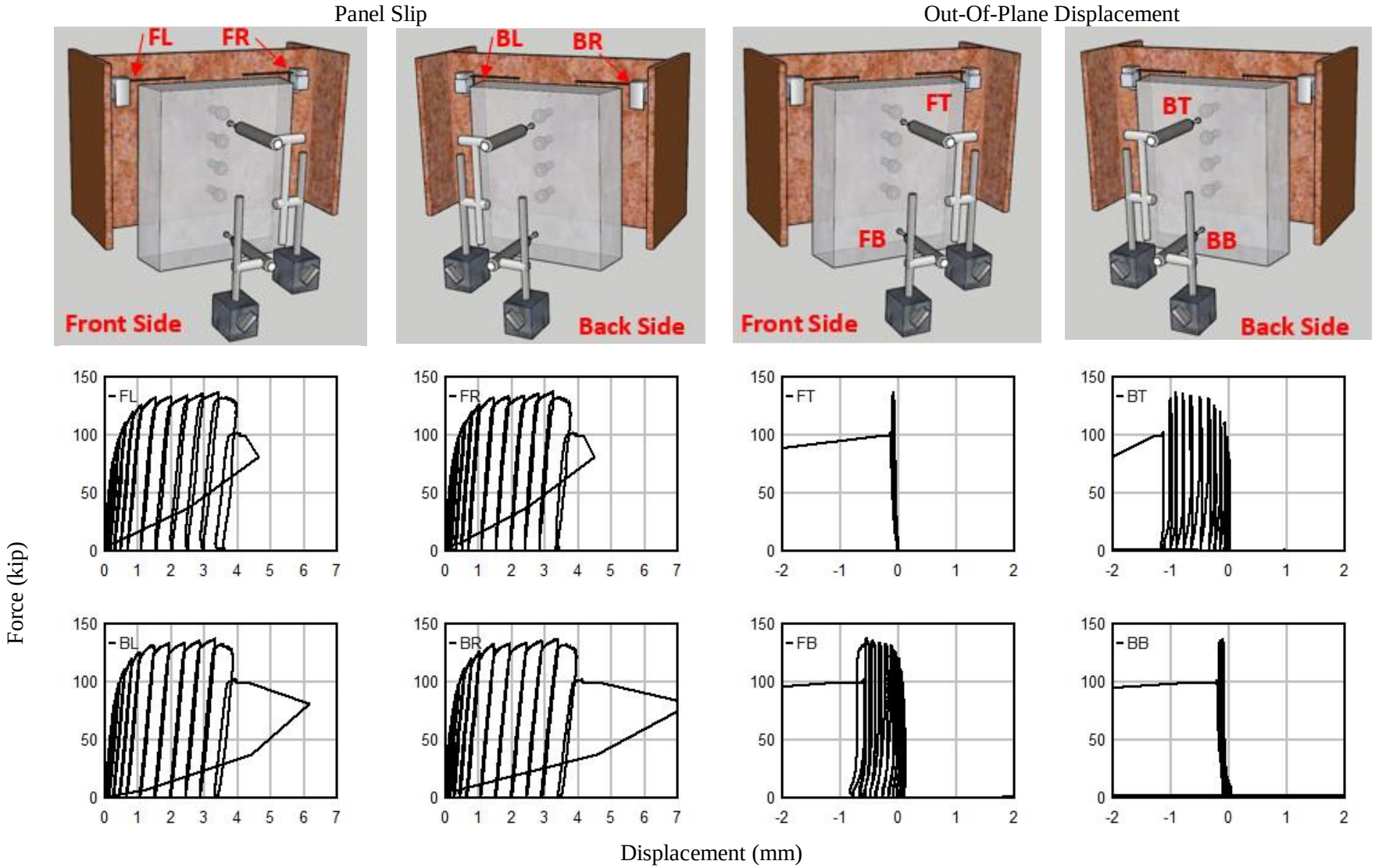

Test 30 – 2x2 HSC – Strains

Stud Strains

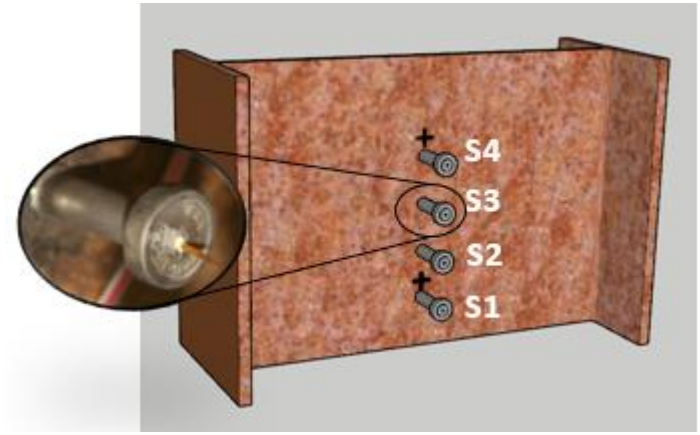

Web Strains

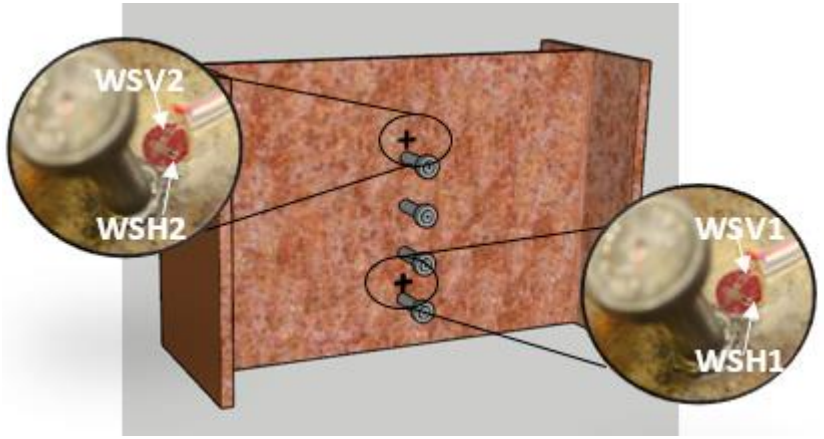

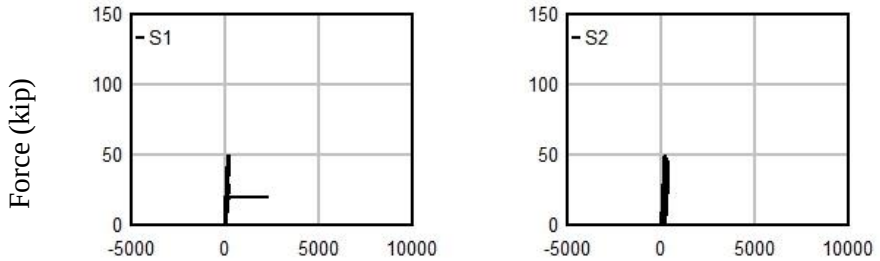

Test 30 – 2x2 HSC – Displacements

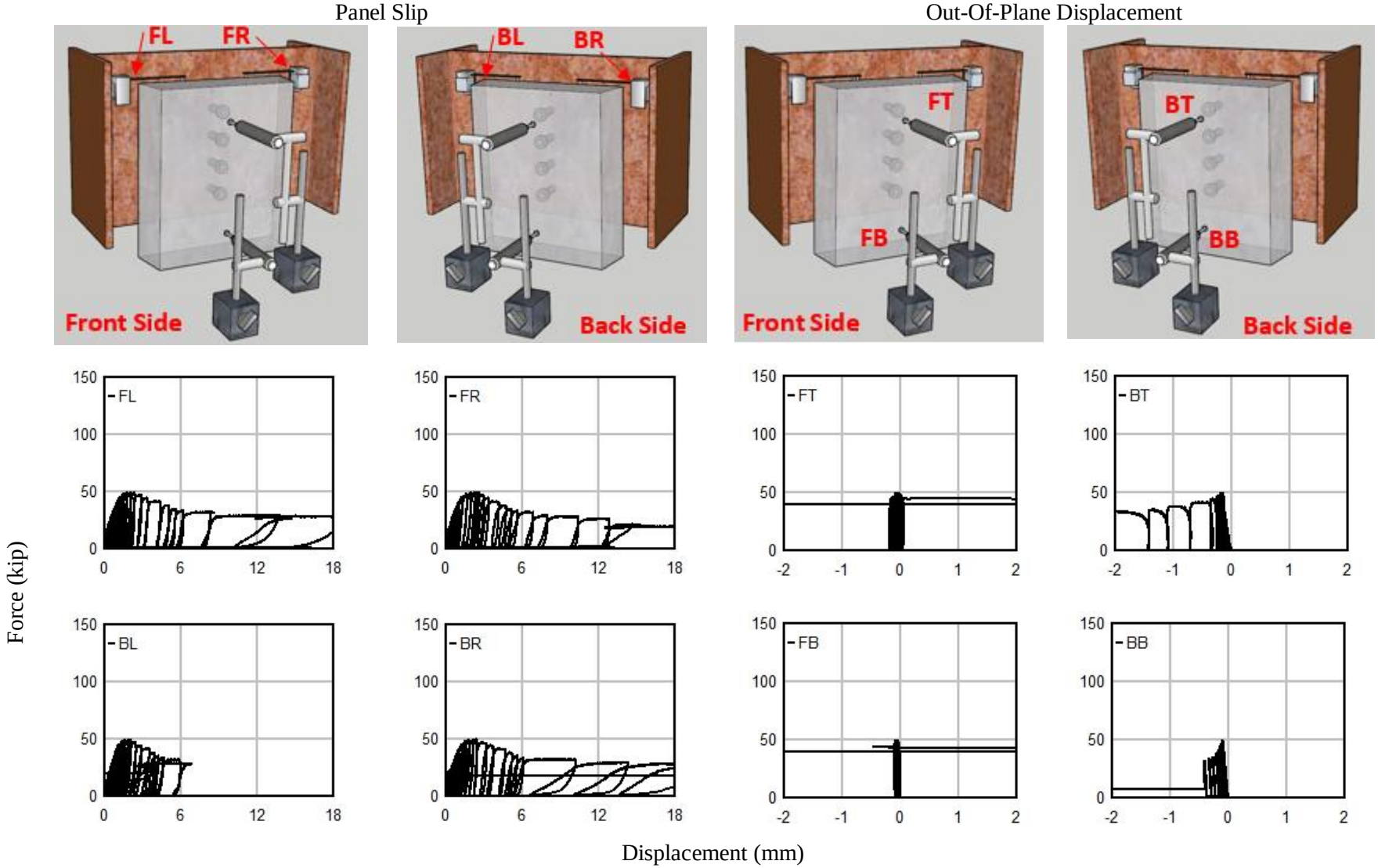

Test 31 – Reinforced HSC – Displacements

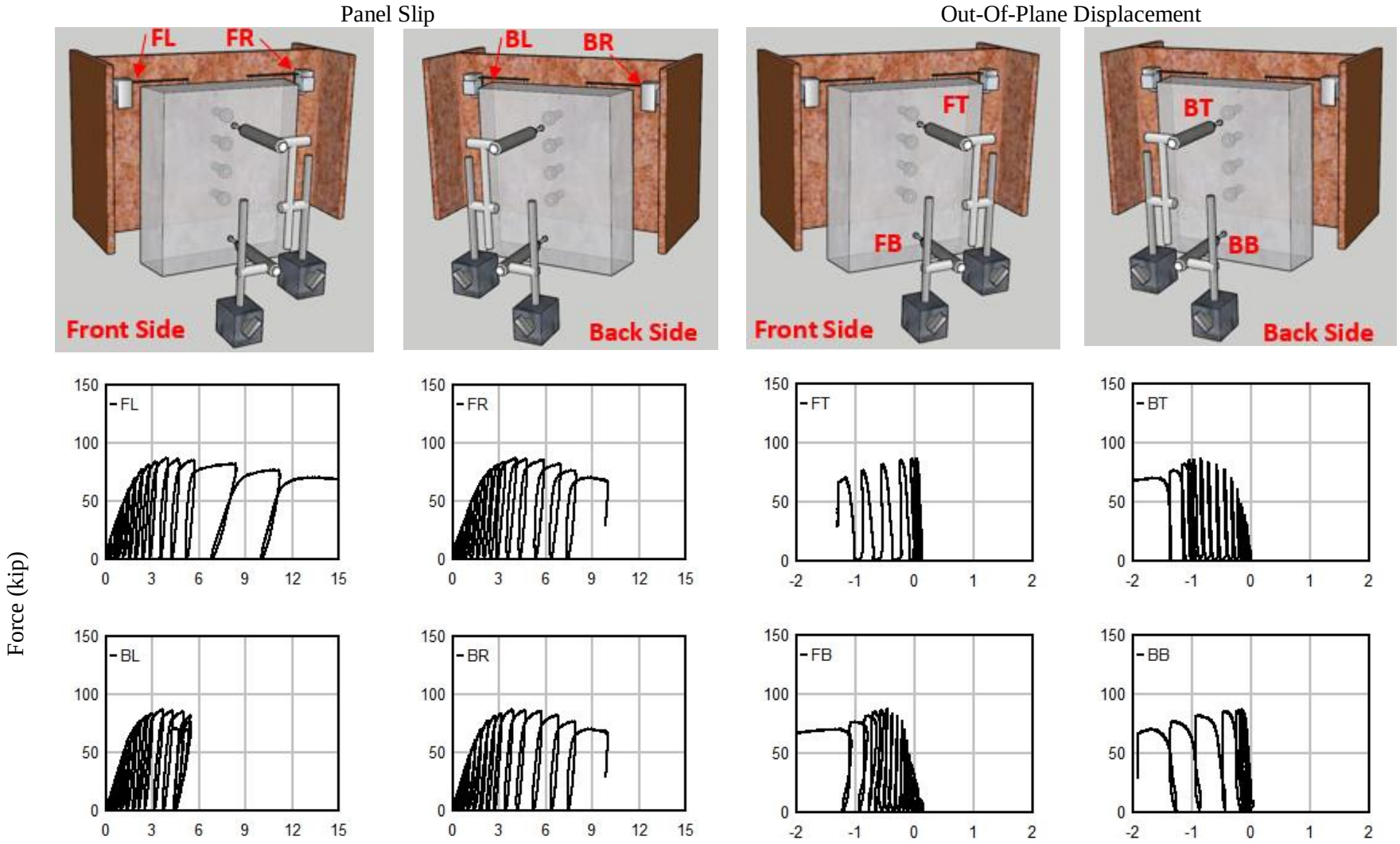

Test 32 – 1% Fiber Content – Displacements

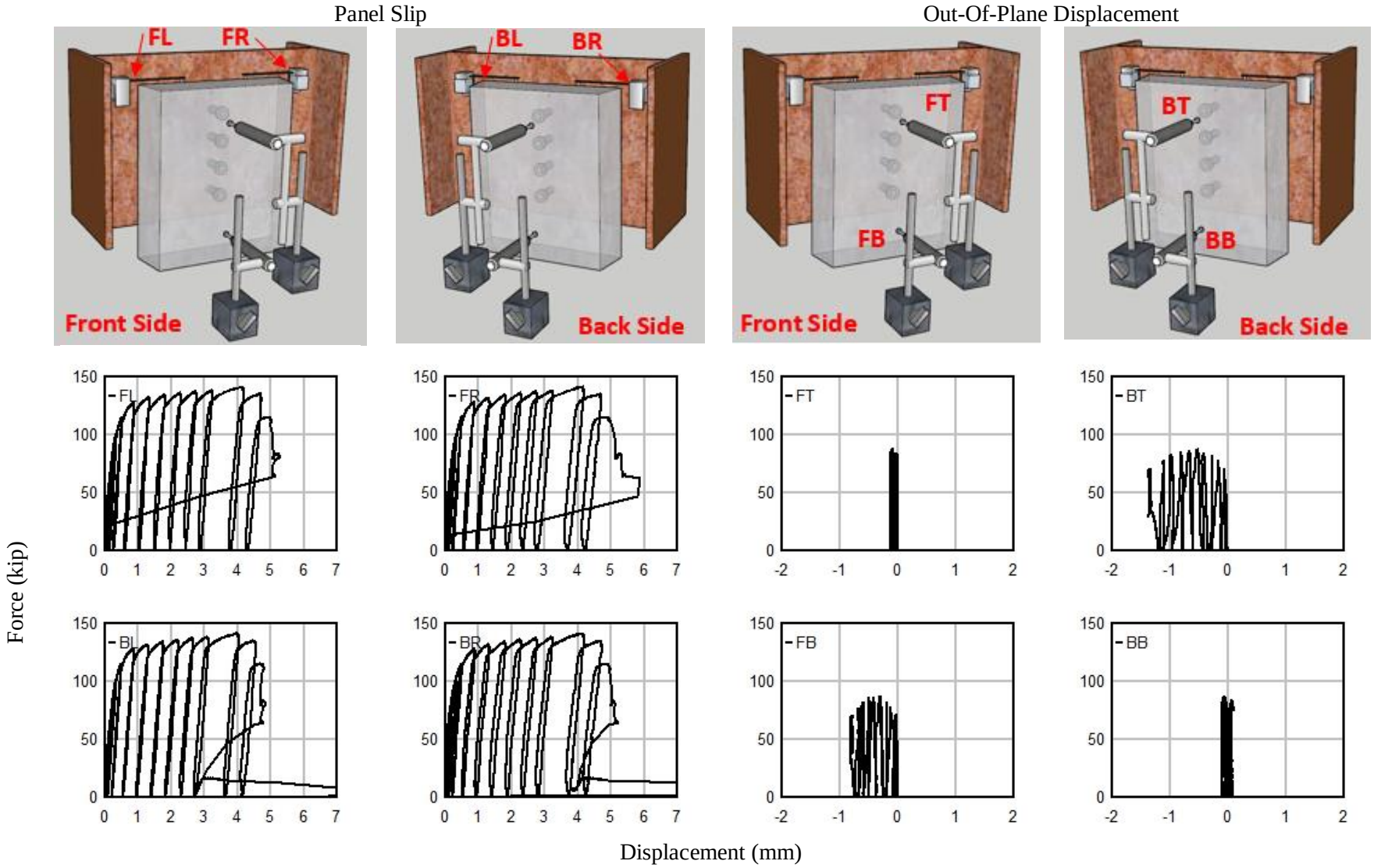

Test 33 – Unbonded Interface – Displacements

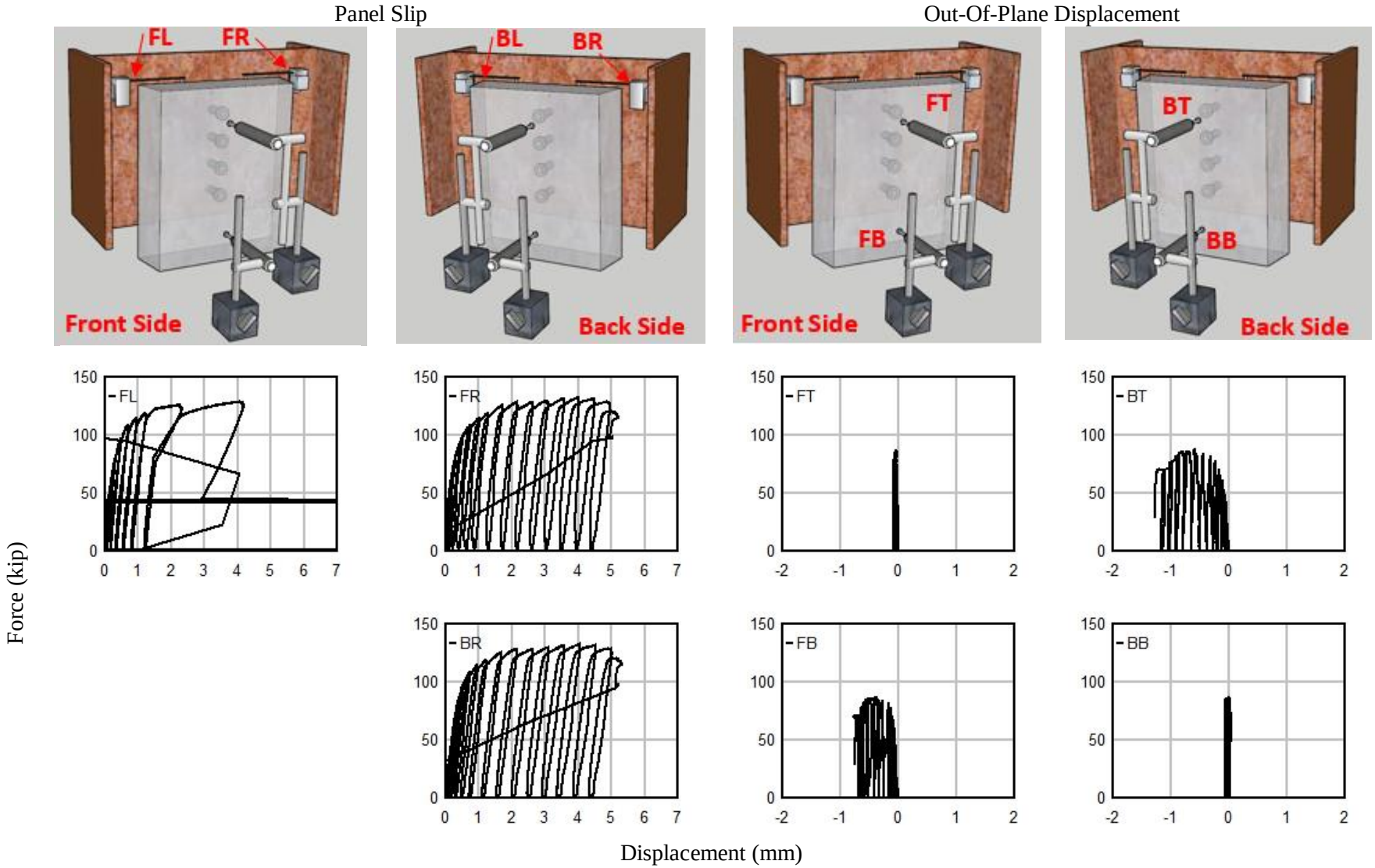

Test 34 – UHPC Dowel – 1.5” – 2% Fiber – Strains

Stud Strains

Web Strains

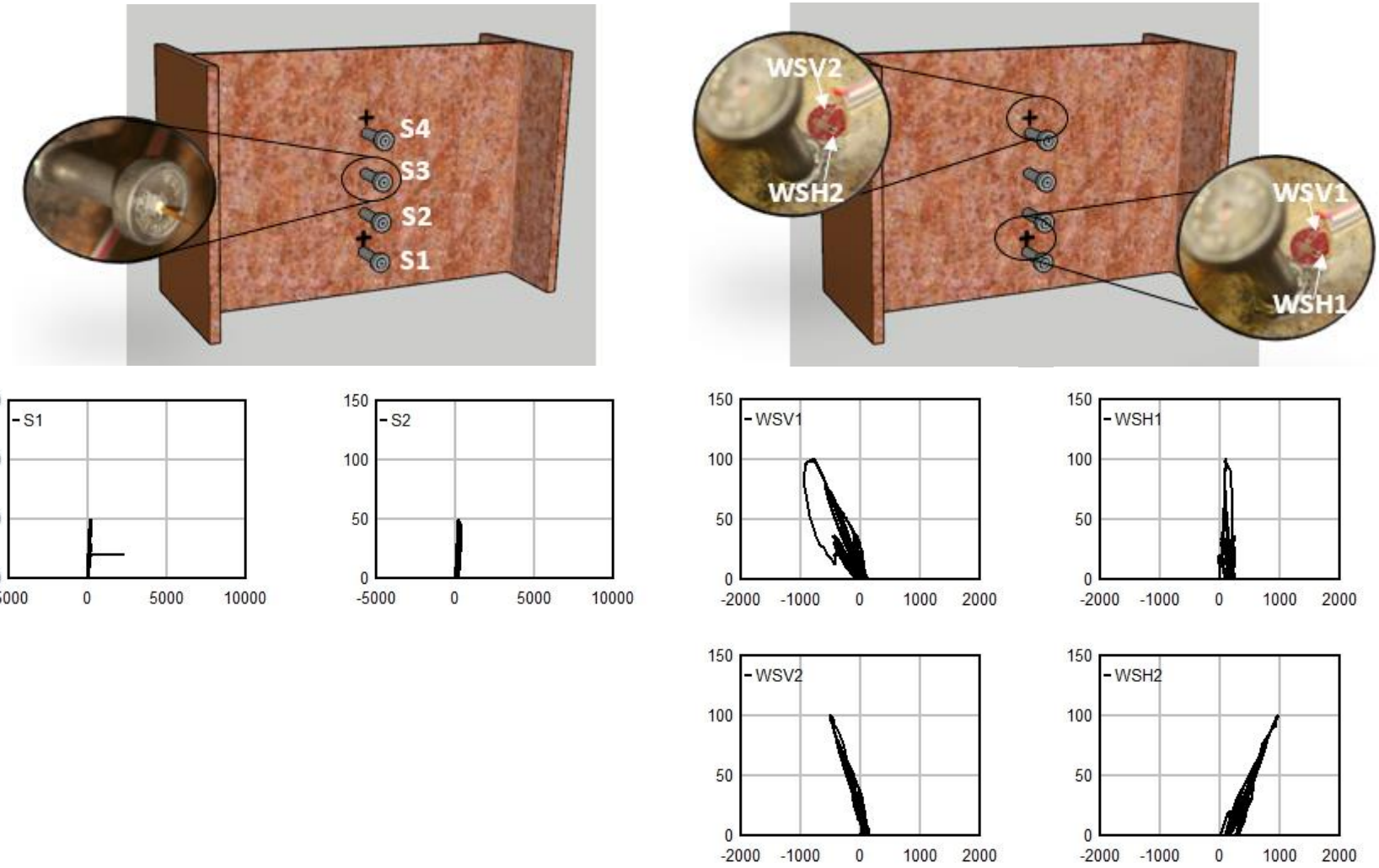

Test 34 – UHPC Dowel – 1.5” – 2% Fiber – Displacements

Panel Slip

Out-Of-Plane Displacement

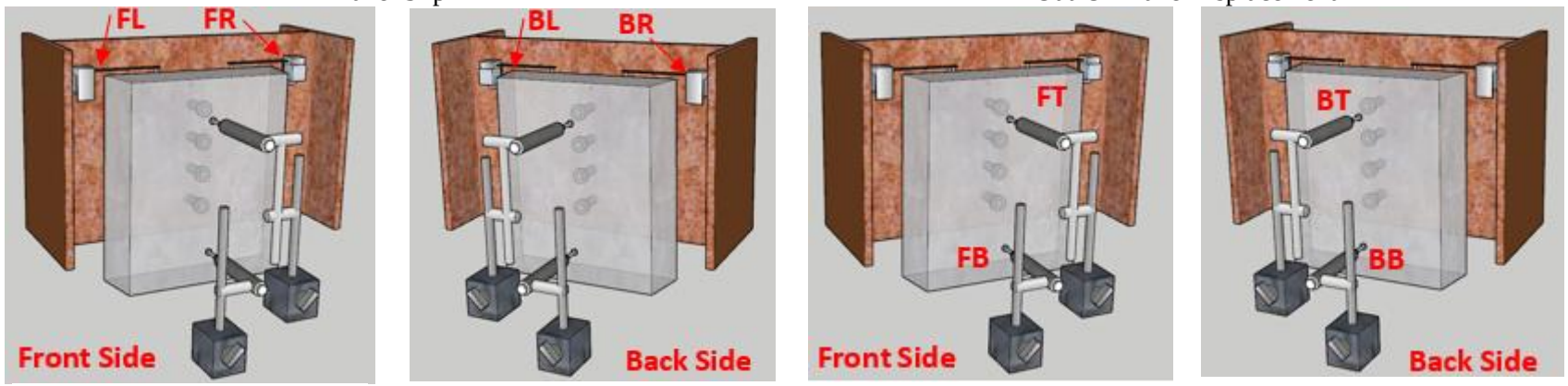

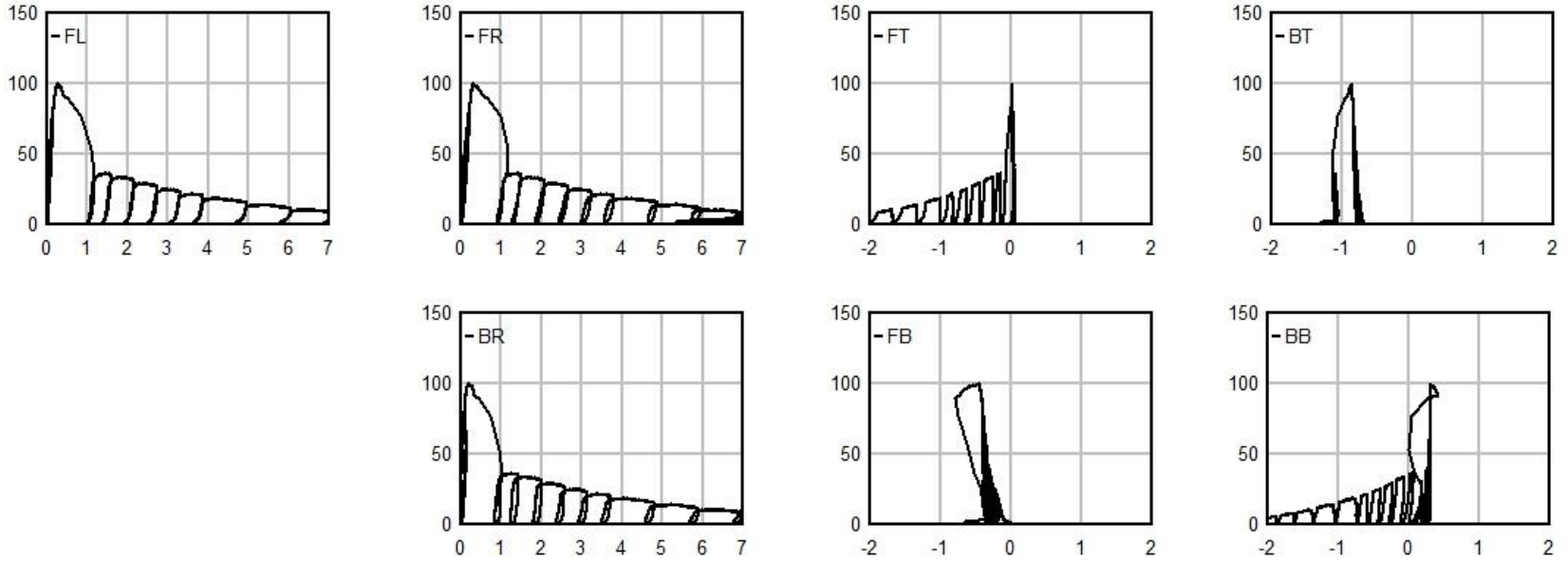

Force (kip)

Displacement (mm)

Test 35 – UHPC Dowel – 1.5” – 4% Fiber – Displacements

Panel Slip

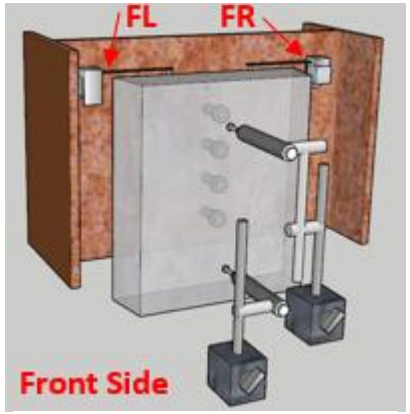

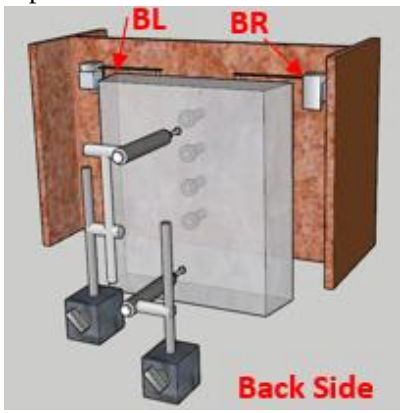

Out-Of-Plane Displacement

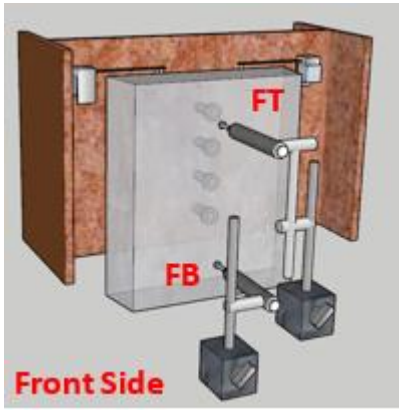

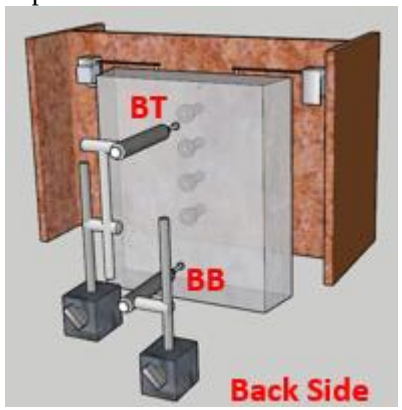

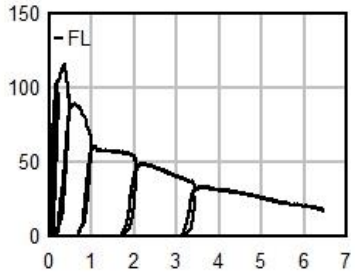

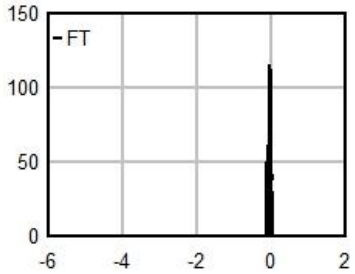

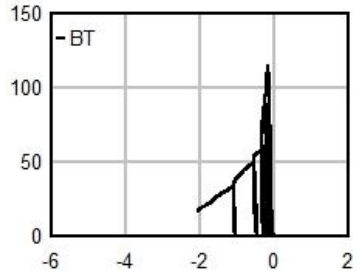

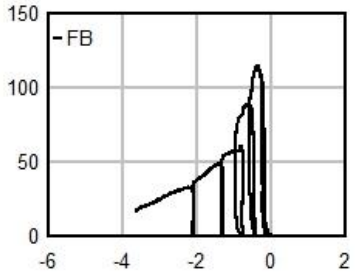

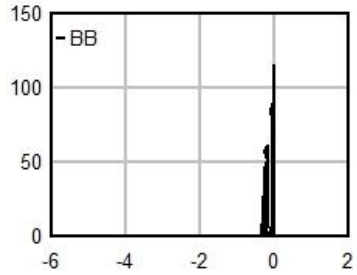

Force (kip)

Displacement (mm)

Test 36 – UHPC Dowel – 2.0” – 2% Fiber – Strains

Stud Strains

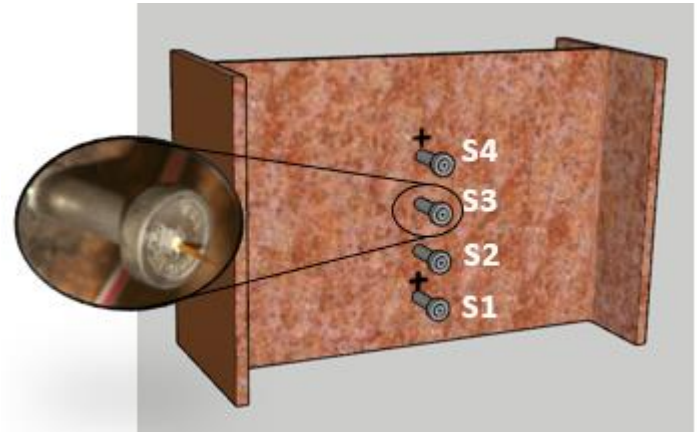

Web Strains

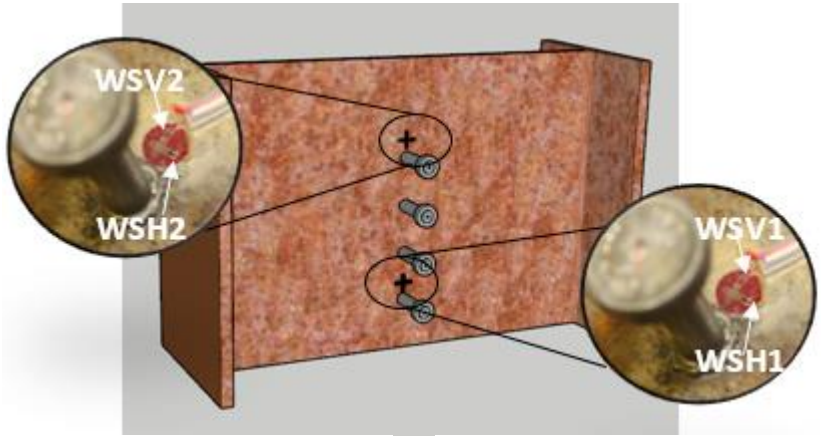

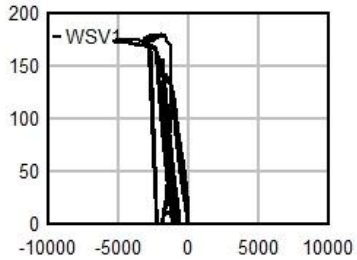

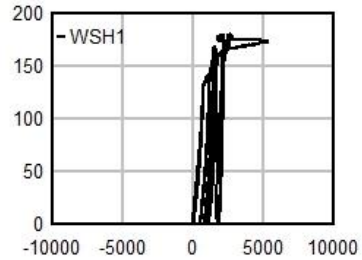

Force (kip)

Strain (με)

Test 36 – UHPC Dowel – 2.0” – 2% Fiber – Displacements

Panel Slip

Out-Of-Plane Displacement

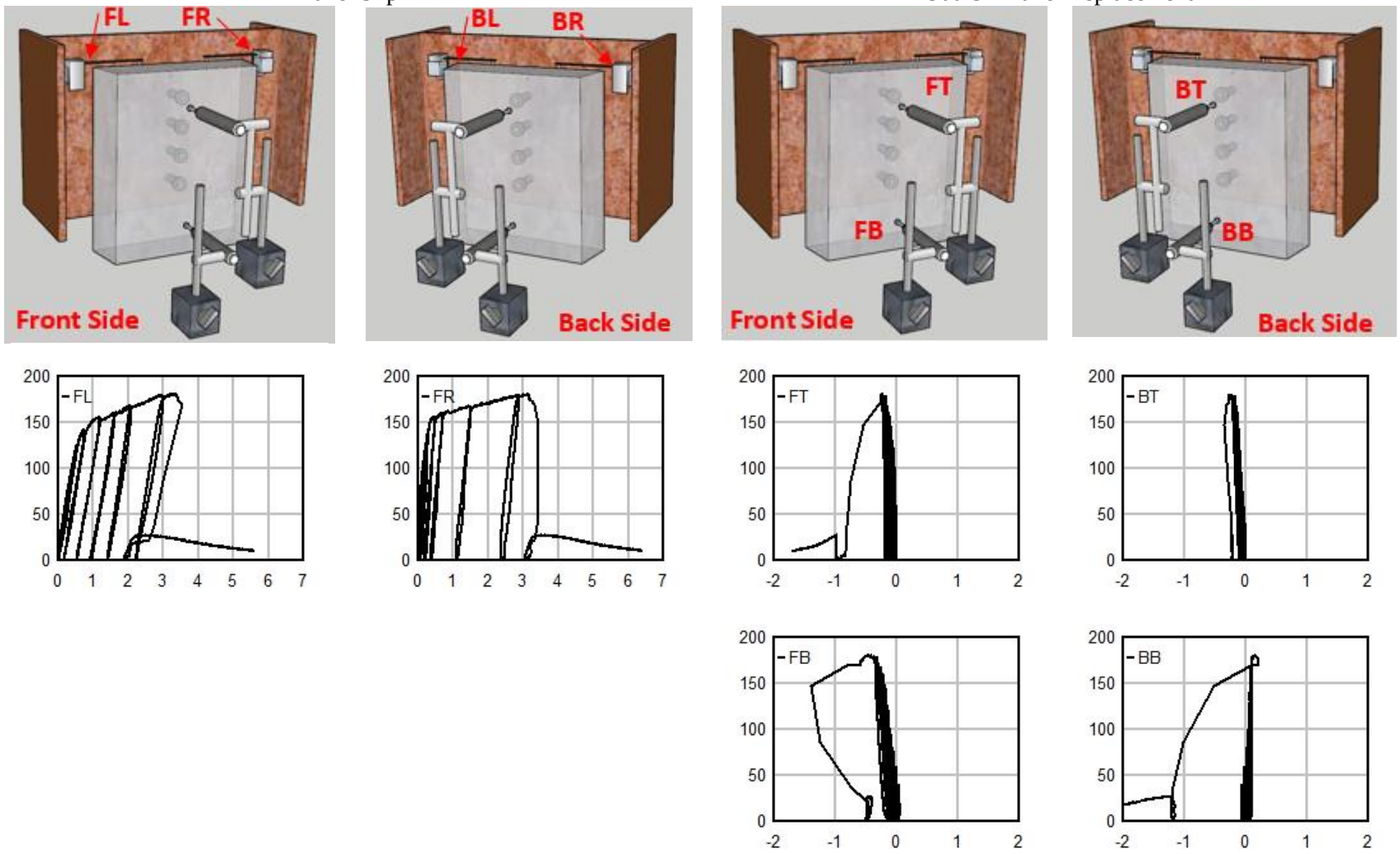

Test 37 – Threaded Bar #2 – Displacements

Panel Slip

Out-Of-Plane Displacement

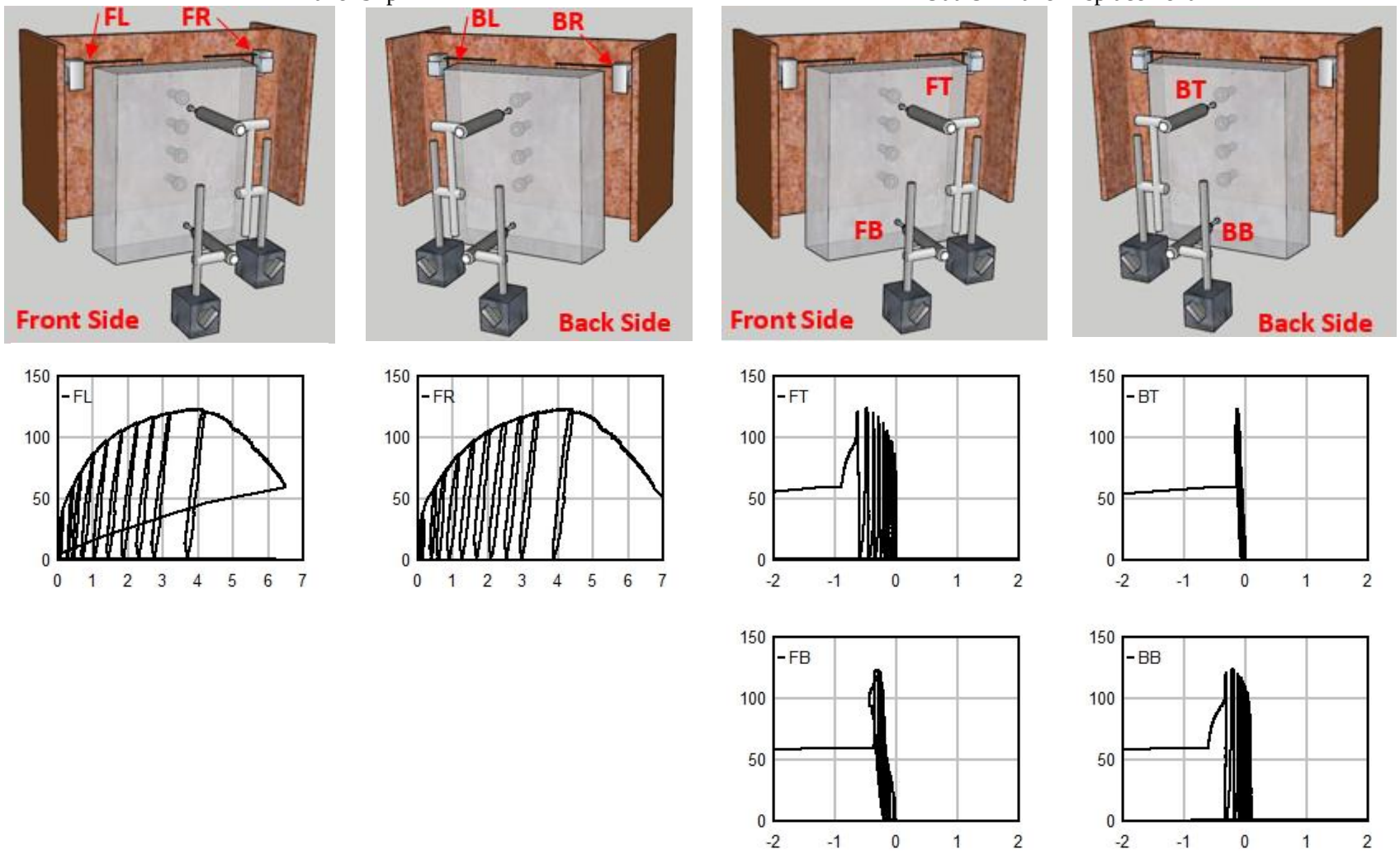

Test 38 – HSC Corrosion – Displacements

Panel Slip

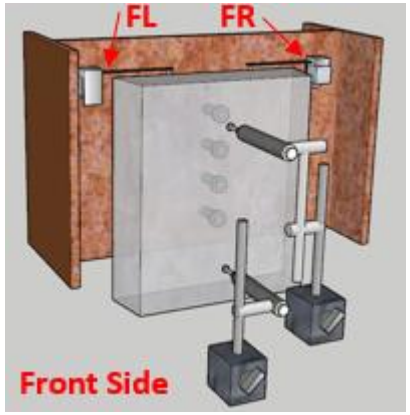

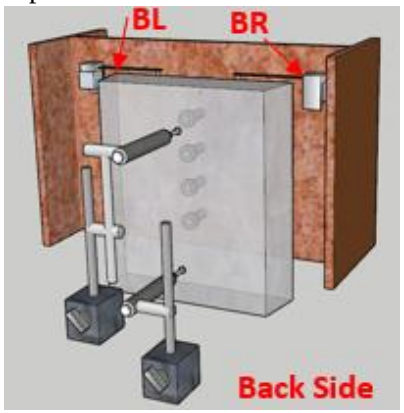

Out-Of-Plane Displacement

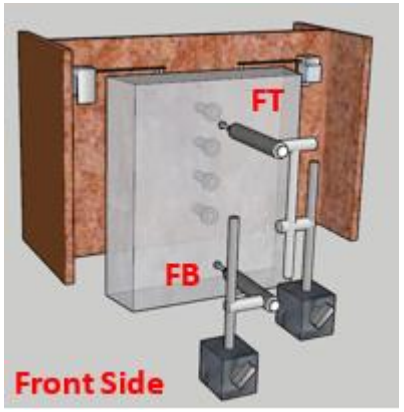

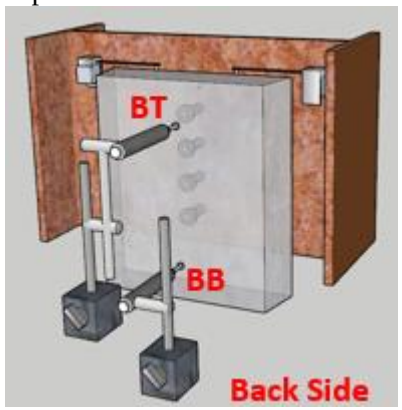

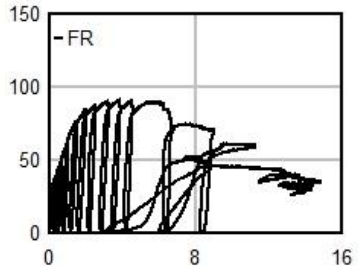

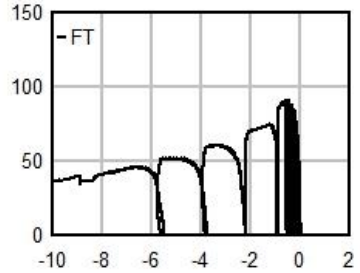

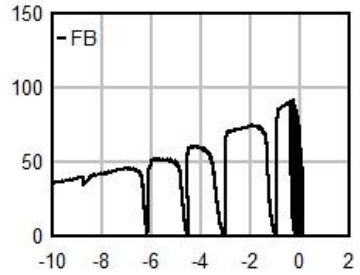

Force (kip)

Displacement (mm)

Appendix B: Failed Push-Out Specimen

Benchmark

Beam Section

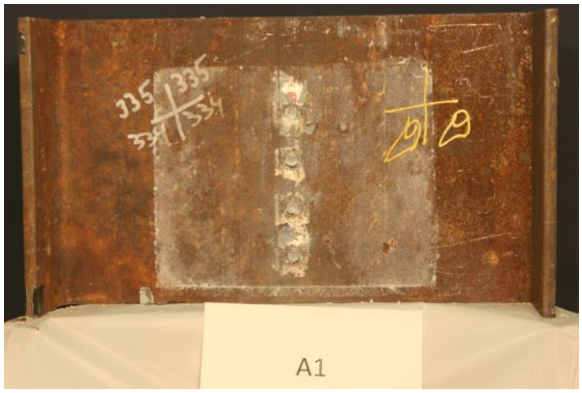

UHPC Panel

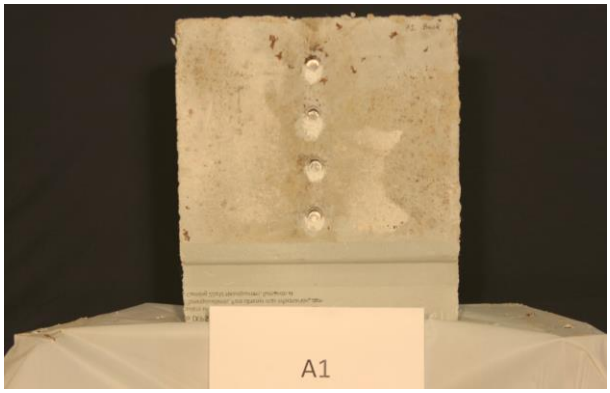

5/8” Diameter Studs

Beam Section

UHPC Panel

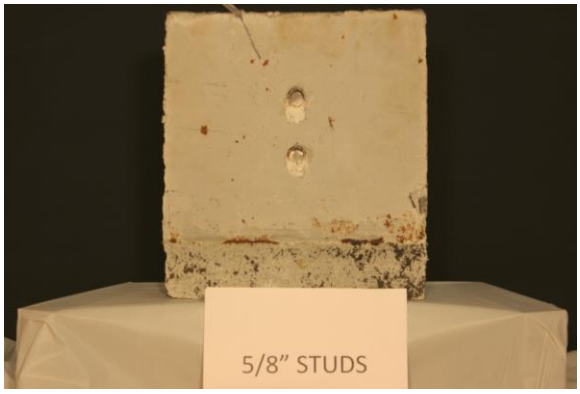

3db Stud Spacing

Beam Section

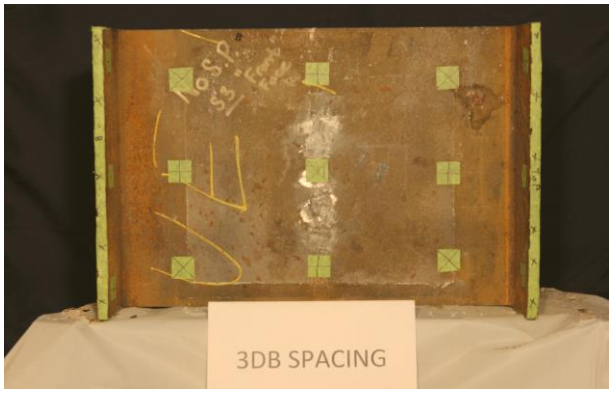

UHPC Panel

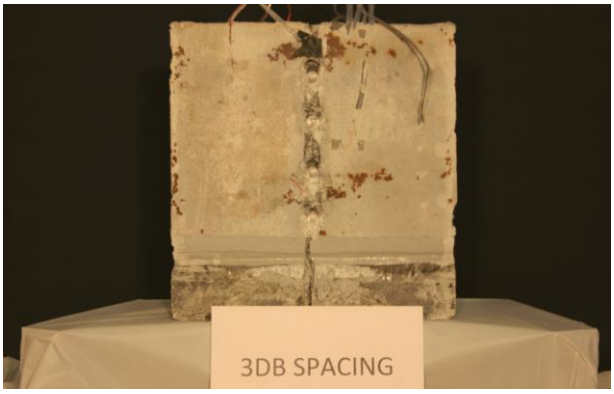

Vertical Stagger

Beam Section

UHPC Panel

Vertical and Horizontal Stagger

Beam Section

UHPC Panel

High-Strength Concrete

Beam Section

UHPC Panel

28 ksi

Beam Section

UHPC Panel

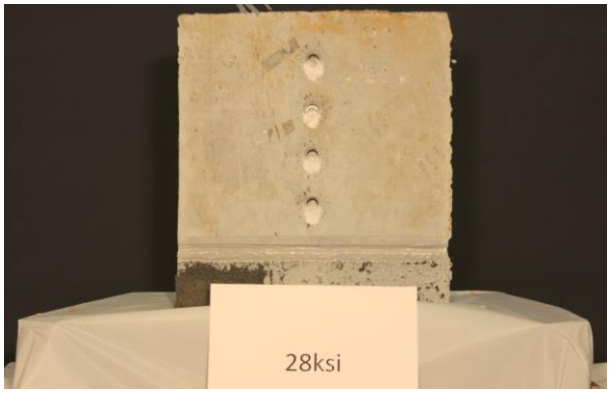

No Fibers

Beam Section

UHPC Panel

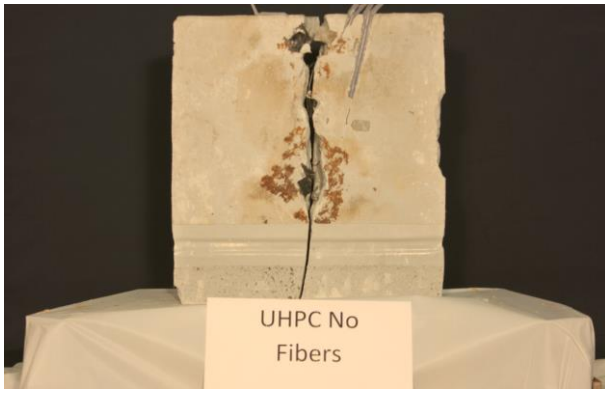

One-Sided Repair

Beam Section

UHPC Panel

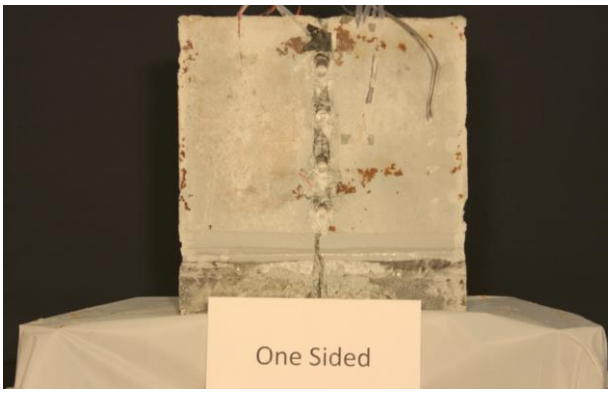

¾” Studs - Short

Beam Section

UHPC Panel

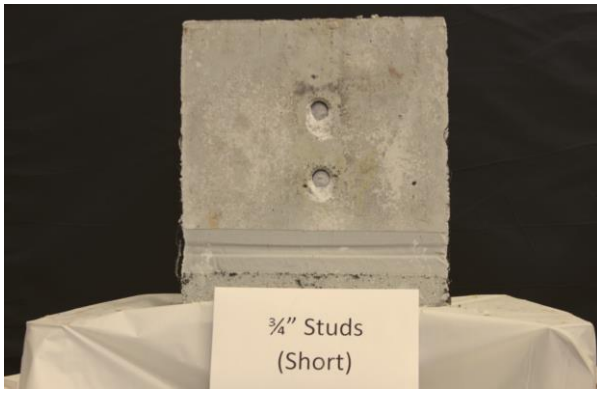

¾” Studs - Long

Beam Section

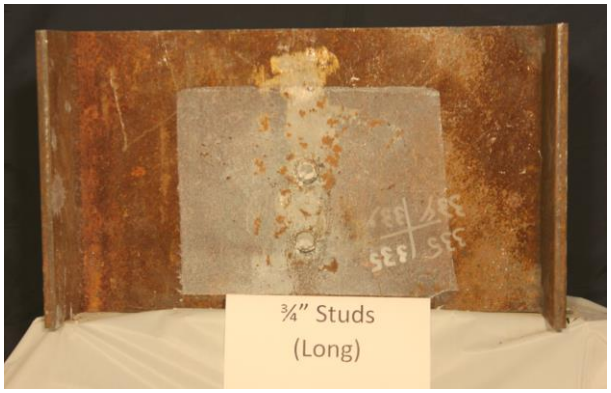

UHPC Panel

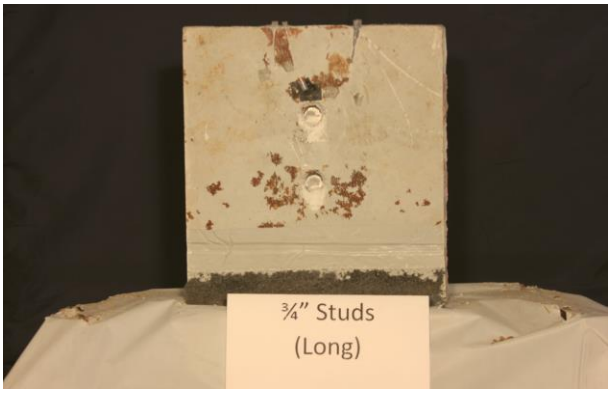

2x2 UHPC

Beam Section

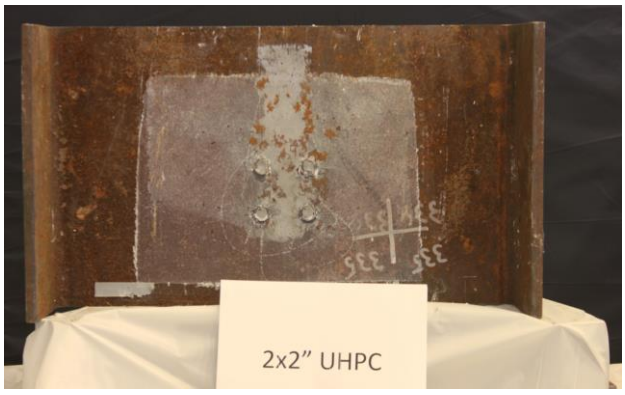

UHPC Panel

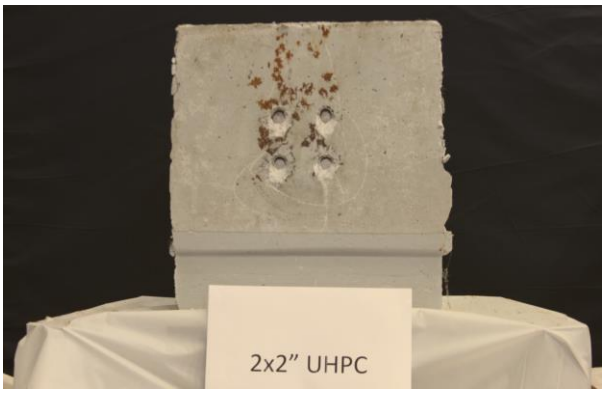

Precast Panel (2x2")

Beam Section

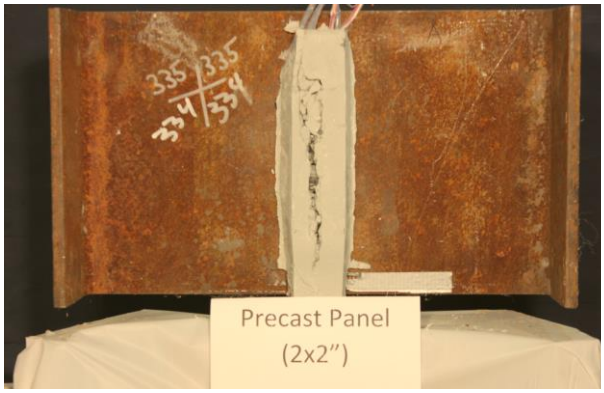

UHPC Panel

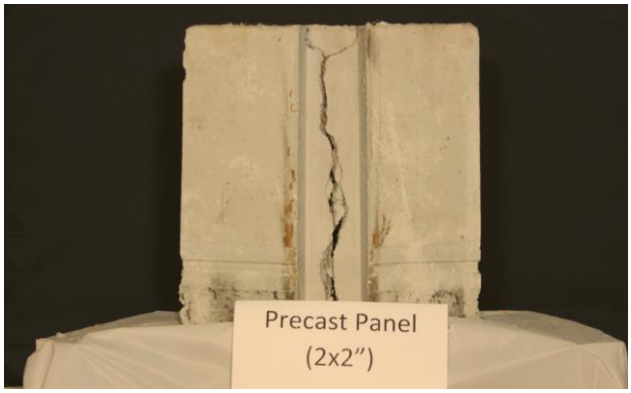

Corrosion 1

Beam Section

UHPC Panel

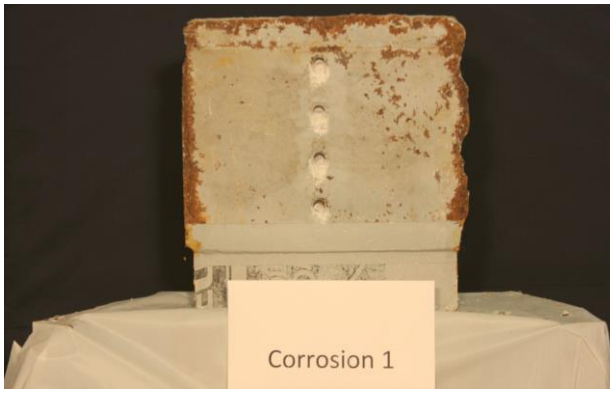

12 Hour Heat Cure

Beam Section

UHPC Panel

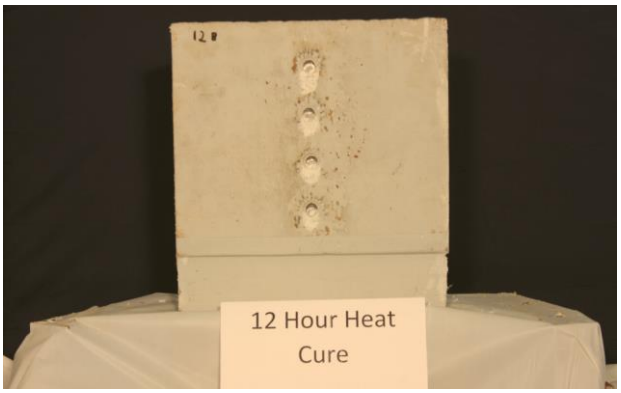

Precast Panel (2x4")

Beam Section

UHPC Panel

Benchmark #2

Beam Section

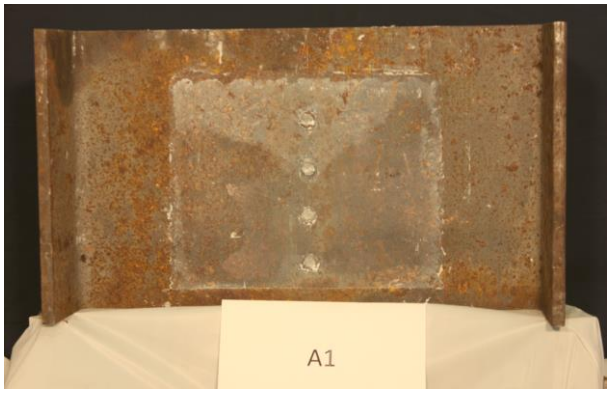

UHPC Panel

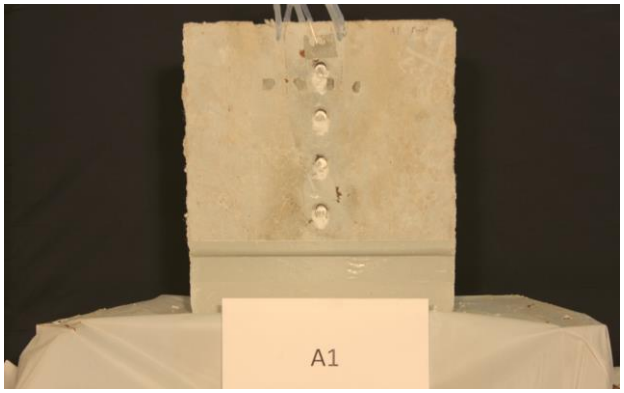

Benchmark #3

Beam Section

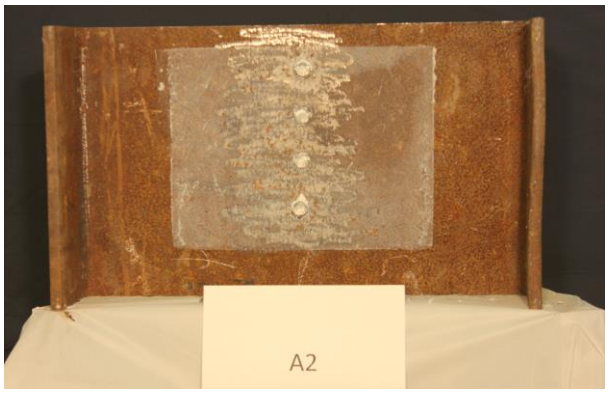

UHPC Panel

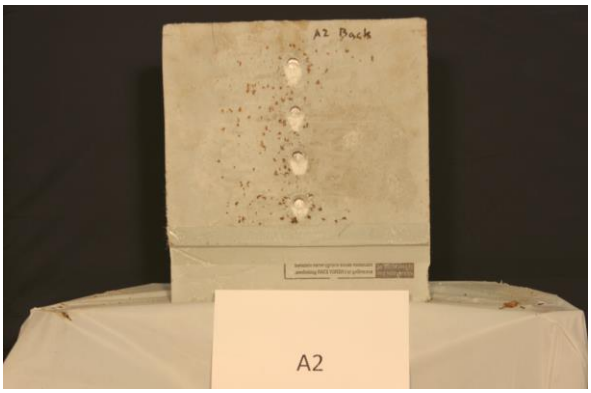

Corrosion #2

Beam Section

UHPC Panel

Painted Surface

Beam Section

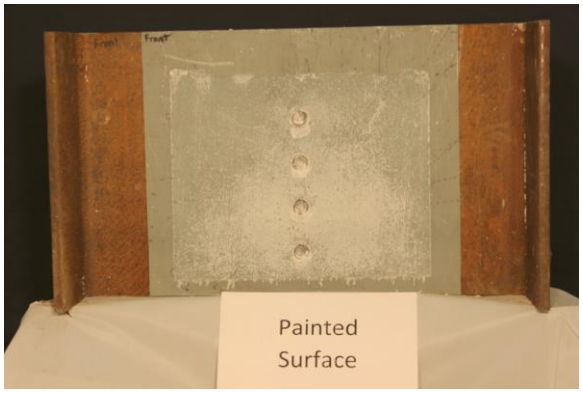

UHPC Panel

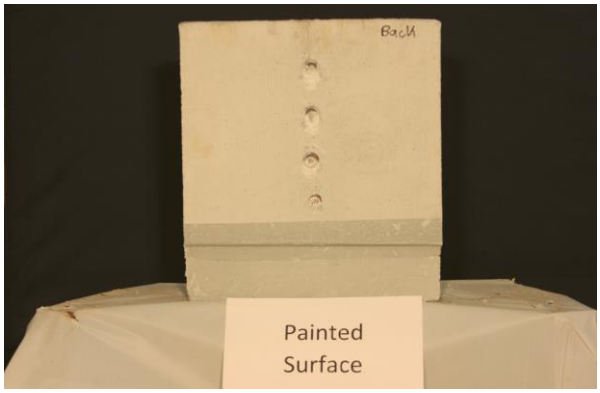

Vertical Ferrule

Beam Section

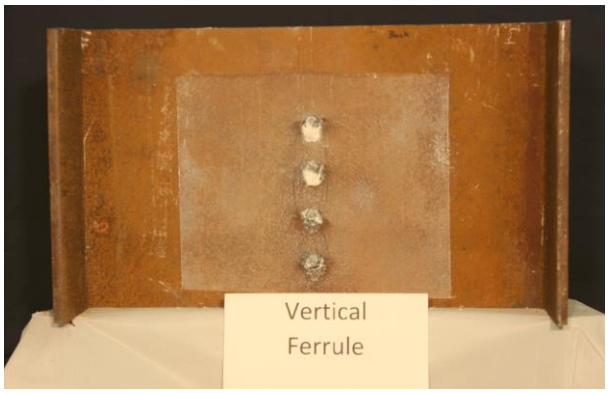

UHPC Panel

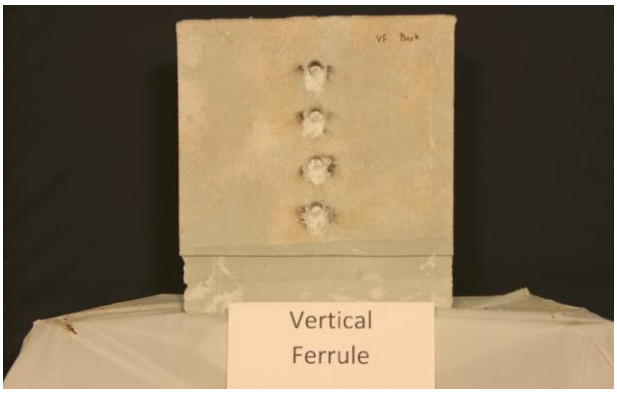

2” Eccentricity

Beam Section

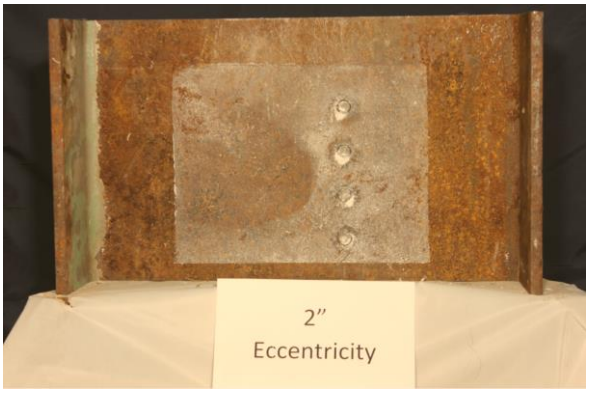

UHPC Panel

G8 Threaded Bars

Beam Section

UHPC Panel

Corrosion #3

Beam Section

UHPC Panel

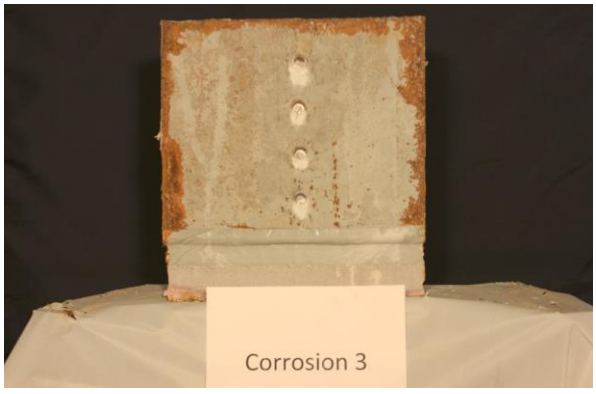

JS1000

Beam Section

UHPC Panel

2x2 HSC

Beam Section

UHPC Panel

N/A

1% Fiber Content

Beam Section

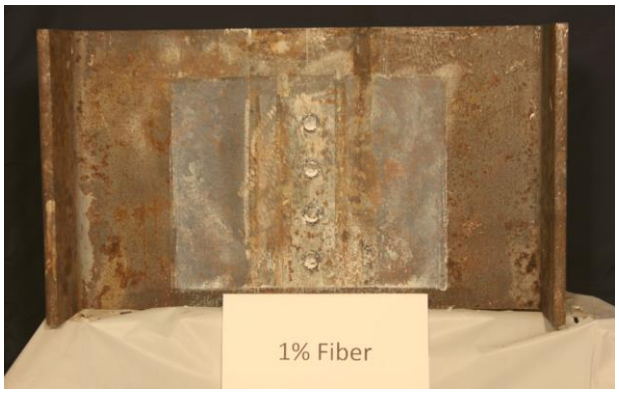

UHPC Panel

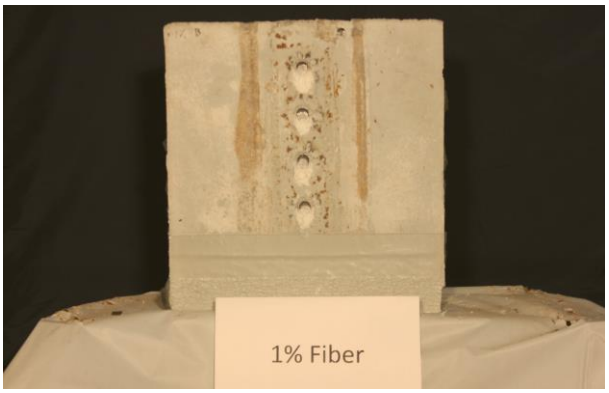

Unbonded Interface

Beam Section

UHPC Panel

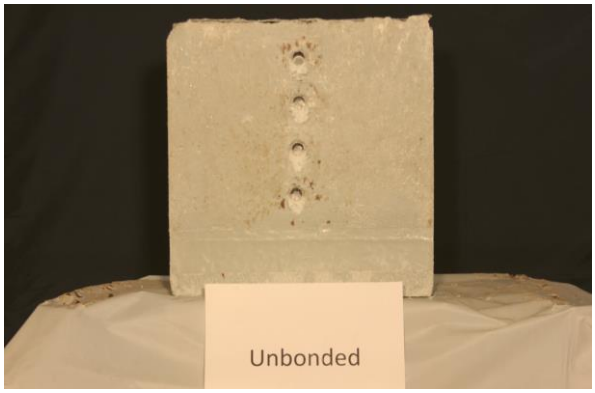

UHPC Dowel – 1.5 in – 2% Fiber

Beam Section

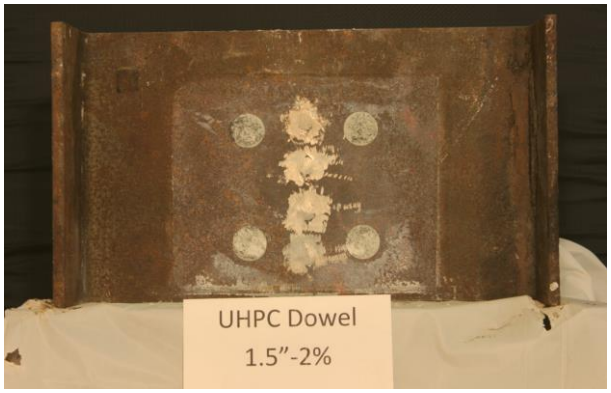

UHPC Panel

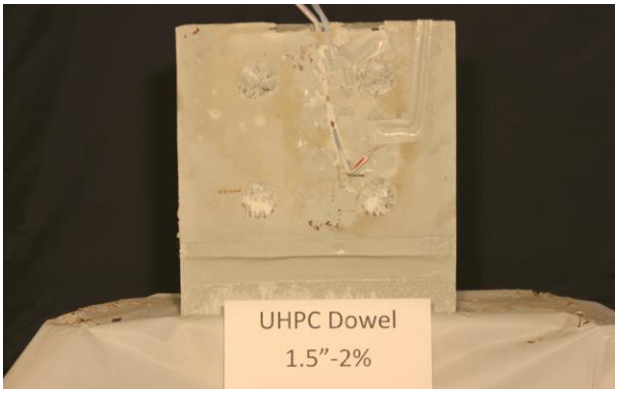

UHPC Dowel – 1.5 in – 4% Fiber

Beam Section

UHPC Panel

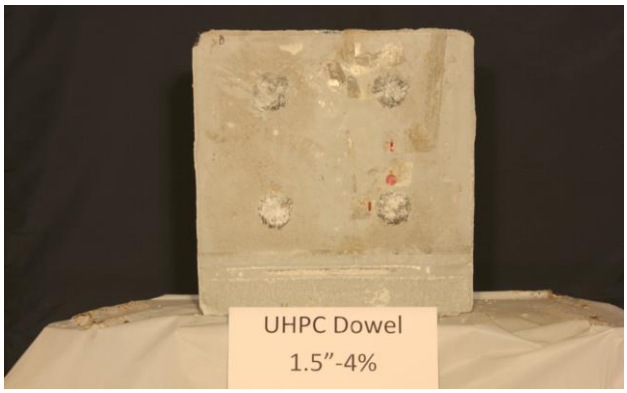

UHPC Dowel – 2.0 in – 2% Fiber

Beam Section

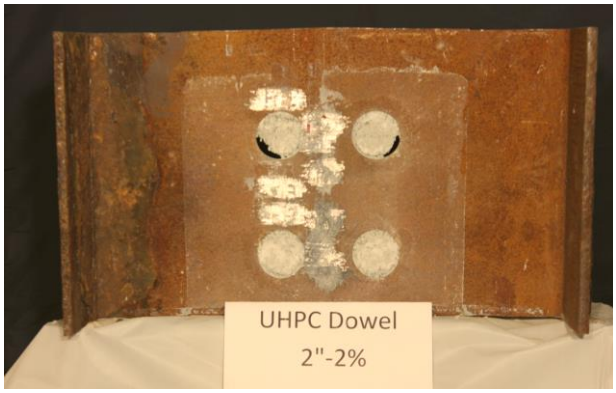

UHPC Panel

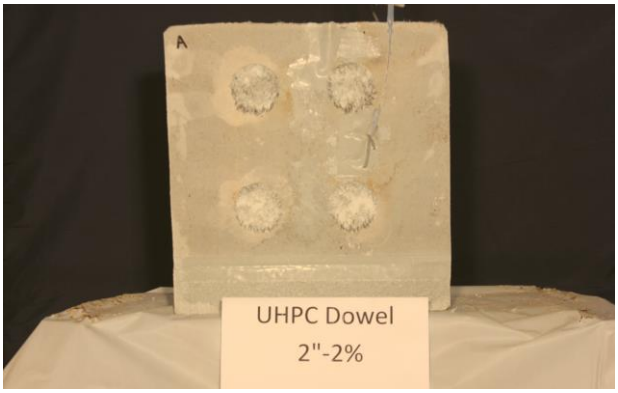

Threaded Bars #2

Beam Section

UHPC Panel